Synthesis and pharmacological characterization of bivalent ligands for the D_1-H_3 receptor heteromer and fluorescent ligands for the D_1 and H_3 receptors

Dissertation

zur Erlangung des Doktorgrades der Naturwissenschaften (Dr. rer. nat.)

an der Fakultät für Chemie und Pharmazie

der Universität Regensburg

vorgelegt von

Niklas Rosier

aus Norderstedt

im Jahr 2022

Die vorliegende Arbeit entstand im Zeitraum von Januar 2019 bis November 2022 unter der Anleitung von Dr. Steffen Pockes an der Fakultät für Chemie und Pharmazie der Universität Regensburg.

Das Promotionsgesuch wurde eingereicht im November 2022.

Vorsitzender des Prüfungsausschusses:	Prof. Dr. Jens Schlossmann
Erstgutachter:	Dr. Steffen Pockes
Zweitgutachter:	Prof. Dr. Pierre Koch
Drittprüfer:	Prof. Dr. Joachim Wegener

Acknowledgements

An dieser Stelle möchte ich allen Personen danken, die zur Entstehung und Fertigstellung dieser Arbeit beigetragen haben und mich in den letzten vier Jahren begleitet haben. Insbesondere möchte ich mich bei folgenden Personen bedanken:

An erster Stelle möchte ich mich bei Herrn Dr. Steffen Pockes für die Vergabe des herausfordernden und spannenden Themas bedanken, das Vertrauen mich als erstes Mitglied in seine Gruppe aufzunehmen, die stets freundschaftliche Betreuung meiner Arbeit, dafür dass ich meine Ideen stets einbringen und umsetzen durfte und für die vielen spaßigen Konferenzen und außeruniversitären Arbeitsgruppenaktivitäten;

bei Herrn Prof. Dr. Sigurd Elz für die Aufnahme an seinen Lehrstuhl und für die Bereitstellung von Laboren und Arbeitsmaterialien;

bei Herrn Prof. Dr. Pierre Koch für Bereitschaft das Zweitgutachten dieser Arbeit zu erstellen und als Zweitprüfer an der Promotionsprüfung teilzunehmen;

bei Herrn Prof. Dr. Joachim Wegener für die Bereitschaft als Drittprüfer an der Promotionsprüfung teilzunehmen;

bei Herrn Prof. Dr. Jens Schlossmann für Bereitschaft als Vorsitzender an der Promotionsprüfung teilzunehmen;

bei Herrn Prof. Dr. Rafael Franco und Frau Prof. Dr. Gemma Navarro für ihre stete Unterstützung bei biochemischen und pharmakologischen Fragen und für die Möglichkeit, meinen Auslandsaufenthalt in ihrer Arbeitsgruppe an der Universität Barcelona zu absolvieren. In diesem Zusammenhang möchte ich mich auch bei allen Mitgliedern ihrer Arbeitsgruppe für die nette Aufnahme in die Gruppe und die stete Hilfe bei praktischen Fragestellungen bedanken;

allen Co-Autoren möchte ich für die produktive und angenehme Zusammenarbeit danken, die die Publikation von zwei Beiträgen in Fachzeitschriften möglich gemacht haben: insbesondere bei Dr. Lukas Grätz, Dr. Hannes Schihada, Dr. Jan Möller, Dr. Ali Isbilir, Dr. Laura J. Humphrys und Dr. Katarzyna Szczepanska;

dem Elite-Netzwerk-Bayern für die finanzielle Unterstützung während meiner Promotion im Rahmen des Graduiertenkollegs „Receptor Dynamics: Emerging Paradigms of Novel Drugs“ und in diesem Zusammenhang allen Mitgliedern für die interessanten Workshops und Retreats;

bei Martin Nagl für vier Jahre Seite an Seite arbeiten im Labor, für die Hilfe bei diversen Problemen, für geteilte Frustrationen und Erfolge, das stete Aufmuntern mit entsprechenden Videos oder Scherzen und die schöne Zeit in Barcelona;

bei Denise Mönnich für ihre Unterstützung in der Zellkultur und bei allen Assays, für die Implementierung von neuen Assays und für ihre stets ansteckende gute Laune und die gute Zusammenarbeit;

bei allen Mitgliedern des Lehrstuhls Elz (Lukas Wirth, Simon Scheuerer, Sebastian Pitzl, Alexander Hubmann, Merlin Bresinsky, Vivien Czipper, Dr. Herwig Pongratz und Julia Blüml) für die überragende Arbeitsatmosphäre, gemeinsame Mittagessen, abendliche Aktivitäten, Kicker-Managerspiele und fachliche Fußballdiskussionen und für die Unterstützung bei fachlichen Problemen;

bei Frau Uta Hasselmann für die Unterstützung bei allen formalen und bürokratischen Angelegenheiten der Universität;

bei den Mitgliedern des Lehrstuhls von Prof. Dr. Koch (ehemals Prof. Dr. Buschauer) für die nette und konstruktive Zusammenarbeit und gemeinsamen Feierabendaktivitäten;

bei Prof. Dr. Jörg Heilmann für die Möglichkeit die Zellkultur an seinem Lehrstuhl zu benutzen und den Mitgliedern seines Lehrstuhls für die Unterstützung und Einarbeitung;

bei meinen Eltern die mich durch mein Studium und auch während meiner Promotion immer unterstützt haben.

Zu guter Letzt möchte ich mich bei meiner Frau Mariangel bedanken, dafür dass sie seit Jahren an meiner Seite ist, mich immer wieder aufbaut, wenn es mal schlecht läuft und mich immer in allem unterstützt hat während der Fertigstellung dieser Arbeit.

Publications, presentations and professional training

Publications (peer-reviewed articles published prior the submission of this thesis)

Rosier, N., Grätz, L., Schihada, H., Möller, J., Isbilir, A., Humphrys, L. J., Nagl, M., Seibel, U., Lohse M. J., Pockes, S. (2021). A Versatile Sub-Nanomolar Fluorescent Ligand Enables NanoBRET Binding Studies and Single-Molecule Microscopy at the Histamine H_3 Receptor. *Journal of Medicinal Chemistry*, *64*(15), 11695-11708.

Szczepańska, K., Podlewska, S., Dichiara, M., Gentile, D., Patamia, V., Rosier, N., Mönnich, D., Ruiz Canter, M., Karcz, T., Lazewska, D., Siwek, A., Pockes, S., Cobos E., Marrazzo, A., Stark, H., Rescifina, A., Bojarski, A., Amata, E. & Kieć-Kononowicz, K. (2021). Structural and Molecular Insight into Piperazine and Piperidine Derivatives as Histamine H3 and Sigma-1 Receptor Antagonists with Promising Antinociceptive Properties. *ACS chemical neuroscience*, *13*(1), 1-15.

Poster Presentations

N. Rosier, M. Nagl, L. Grätz, H. Schihada, M. Decker, R. Franco, S. Pockes. Bivalent Ligands for the D_1-H_3-receptor heteromer: Synthesis and pharmacology. *Frontiers in Medicinal Chemistry (GDCh)* (2019, Würzburg, Germany)

N. Rosier, M. Nagl, L. Grätz, H. Schihada, M. Decker, R. Franco, S. Pockes. Synthesis of bivalent ligands and development of pharmacological assay for D_1-H_3 receptor heteromers. *48th Meeting of the European Histamine Research Society* (2019, Krakow, Poland)

N. Rosier, M. Nagl[a], L. Grätz, H. Schihada, R. Franco, S. Pockes. Bivalent Ligands for the D_1-H_3-Receptor Heteromer, a Target with Neuroprotective Potential. *Conference of the German Pharmaceutical Society (DPhG)* (2019, Heidelberg, Germany)

Niklas Rosier, Lukas Grätz, Hannes Schihada, Jan Möller, Ali Isbilir, Laura J. Humphrys, Martin Nagl, Ulla Seibel, Martin J. Lohse, and Steffen Pockes. UR-NR266: A Subnanomolar Fluorescent Ligand Enables Single-Molecule Microscopy and NanoBRET Binding Studies at the Histamine H_3 Receptor. *Conference of the German Pharmaceutical Society (DPhG)* (2019, virtual meeting)

Niklas Rosier, Denise Mönnich, Martin Nagl, Gemma Navarro, Marc Gomez, Leonardo Pardo Carrasco, Rafael Franco, Steffen Pockes. Bivalent Ligands Targeting the D_1R-H_3R-heteromer: A Potential Target to Reduce β-Amyloid Induced Cell Death. *AD/PD conference* (2022, Barcelona, Spain).

Niklas Rosier, Denise Mönnich, Martin Nagl, Gemma Navarro, Marc Gomez, Leonardo Pardo Carrasco, Rafael Franco, Steffen Pockes. Bivalent Ligands for the D_1R-H_3R-Heteromer Reduce β-Amyloid-Induced Cell Death. *4GPCRnet international symposium* (2022, Leipzig, Germany).

Professional training

Since 01/2019	Fellowship Member of the graduate school “Receptor Dynamics: Emerging Paradigms for Novel Drugs” of the Elite-Network of Bavaria (ENB).

Abbreviations

5-TAMRA	5-carboxytetramethylrhodamine
Aβ	amyloid β protein
AcOH	acetic acid
APCI	atmospheric pressure chemical ionization
aq.	aqueous
AU	arbitrary units
BnOH	benzyl alcohol
Boc	*tert*-butoxycarbonyl
BSA	bovine serum albumine
^{t}BuOH	*tert*-butanol
BRET	bioluminescence resonance energy transfer
c	concentration
celite	celite 535®
cmpd	compound
CuAAC	copper-catalyzed azide alkyne click
d	doublet
DA	dopamine
DCM	dichloromethane
DIPEA	diisopropylethylamine
DMAP	dimehtylaminopyridine
DMEM	Dulbecco's Modified Eagle's Medium
DMF	dimethylformamide
DMSO	dimethylsulfoxide
DPM	decays per minute
D_xR	dopamine receptor of subtype x
EC_{50}	concentration of an agonist that induces 50 % of its maximal response
EDC*HCl	*N*-(3-Dimethylaminopropyl)-*N*' ethylcarbodiimide hydrochloride
EDTA	ethylenediaminetetraacetic acid
EI	electron impact
eq	equivalents

ESI	electron spray ionisation
Et_2O	diethyl ether
EtOAc	ethyl acetate
EtOH	ethanol
FCS	fetal calf serum
FDA	food and drug administration (USA)
FRET	Förster resonance energy transfer
G418	geniticin
h	hour; human
HATU	O-(7-Azabenzotriazole-1-yl)-N,N,N′,N′-tetramethyluronium-hexafluorphosphate
HEK293T	human embryonal kidney cells
HEPES	2-[4-(2-hydroxyethyl)-1-piperazin-1-yl]ethanesulfonic acid
HPLC	high performance liquid chromatography
HRMS	high resolution mass spectrometry
H_xR	histamine receptor of subtype x
IC_{50}	inhibitor (antagonist) concentration which displaces 50 % of labeled compound from the binding site (suppresses 50 % of agonist induces effect)
J	coupling constant
k	retention factor
K_b	equilibrium dissociation constant of a ligand determined in a functional assay
K_d	equilibrium dissociation constant of a ligand determined in saturation binding experiments,
K_i	equilibrium dissociation constant of a ligand determined in competition binding experiments
k_{obs}	observed association rate constant
k_{off}	dissociation rate constant
k_{on}	association rate constant
kin	kinetic
λ	wavelength
L-15	Leibovitz' L-15 medium
M	mol/l
m	multiplet
MeCN	acetonitrile

MeOH	methanol
min	minutes
m/z	mass/charge
n.d.	not determined
NEt_3	triethylamine
NLuc	NanoLuc® luciferase
NMR	nuclear magnetic resonance
PBS	phosphate buffered saline
Pd/C	palladium on charcoal (10 %)
PE	petroleum ether
PEI	polyethylene imine
PPh_3	triphenylphosphine
PTFE	polytetrafluoroethylene
pTsOH	*para*-toluenesulfonic acid
q	quartet
rt	room temperature
s	singlet, seconds
SD	standard deviation
SEM	standard error of the mean
t	triplet
t_0	dead time
t_R	retention time
TFA	trifluoroacetic acid
THF	tetrahydrofuran
UV	ultraviolet
wt %	weight percentage

Contents

1. General introduction

1.1 G protein-coupled receptors (GPCRs)

The superfamily of G protein-coupled receptors (GPCRs) with over 800 members represents the largest family of membrane proteins in the human genome.[1] All GPCRs share the common structural motif of seven transmembrane helices (TM), that are connected by three intra- (IL) and three extracellular loops (EL).[2] The highest structural homology between GPCRs is found in the transmembrane region.[3] Whereas the intracellular carboxyl terminus, the IL connecting TM5 and TM6, and especially the extracellular amino terminus are the most diverse fragments of GCPRs.[4] Based on phylogenetical analyses, vertebrate GPCRs are divided into five families; the glutamate, rhodopsin, adhesion, frizzled/taste2, and secretin family (GRAFS system).[1] Among these, the rhodopsin family is by far the largest and most diverse with a total of 701 members divided into 13 sub-branches.[1]

GPCRs mediate the cellular response to a wide range of external stimuli, including neurotransmitters, odorants, growth factors, lipids, ions, and even photons.[2] Despite the fact, that half of the GPCRs are part of the olfactory system, they are involved in a plethora of (patho)physiological processes.[5,6] Therefore, they represent an important therapeutical target class for the treatment of many disorders and diseases,[5,6] with 35 % of all FDA-approved small molecule drugs targeting GPCRs in 2017.[7] Despite the extensive GPCR research, the endogenous ligands of approximately 30 % of the non-olfactory GPCRs are still unknown.[8,9] These so-called “orphan-receptors” were in the center of research in the past decade, as they could be the key to novel drugs and therapies.[10]

1.1.1 GPCR signaling

In the most basic sense, GPCRs are communicators, which trigger a cellular response to an external stimulus.[11] To induce signaling, GPCRs couple and interact with different transducer proteins, for example G proteins.[12] These G proteins were long believed to be the only way in which GPCRs exert signaling, and therefore are responsible for the name of G protein-coupled receptors.[13,14] GPCR research in the past decades however, powered by advances in cloning, sequencing and the first crystal structures, revealed that GPCR signaling is far more complex and diverse as initially thought.[12,15,16] Instead of a two-state model, in which the GPCR is either in an active state or inactive state, it is clear now, that GPCRs can exist in a variety of different conformations.[17,18] In these different conformations they can couple and interact with distinct transducer and scaffold proteins, leading to diverse biological effects in the cell.[12,16] Beside the G proteins, GPCRs interact with regulatory and scaffold proteins, e.g. arrestins, GPCR kinases (GRK), PDZ-domain-containing scaffolds and non-PDZ scaffolds, for example A kinase anchor proteins (AKAPs).[12,16,19–22]

1.1.1.1 G protein-dependent signaling

The "classical" GPCR signaling pathway is mediated by the receptor-induced activation of heterotrimeric G proteins.[16] These G proteins, short for guanidine nucleotide binding proteins, consist of three subunits, Gα, Gβ, and Gγ.[23] The activation of a GPCR leads to an outward movement of TM helices 5 and 6, which enables the association of a G protein (Figure 1.1).[24] The activated receptor acts as a guanidine nucleotide exchange factor at the Gα subunit of the G protein, leading to the loss of GDP and binding of GTP.[25] This exchange causes a structural change at the Gα subunit, which results in the dissociation of the Gα and Gβγ subunits, which then interact with effector proteins.[15] Due to the intrinsic GTPase activity of the Gα subunit GTP is hydrolyzed to GDP, which leads to the reassembly of the heterotrimeric G protein and terminates the cellular response.[16] This activation cycle is however just the first step in a signal cascade leading to the biological response of the cell. The G protein subunits regulate different effector proteins, leading to the modulation of the concentration of so called "second-messengers", which then influence other proteins and subsequently the gene-expression.[26]

There are 16 different Gα, 5 Gβ, and 13 Gγ subunits and the G proteins are divided into four families (G_s, $G_{i/o}$, G_q, and $G_{12/13}$) based on the subtype of the Gα-subunit.[12,27] Each family of Gα subtype has different target effector proteins that they regulate (Figure 1.1). $G\alpha_s$ subunits activate the adenylyl cyclases (AC) 1-9, which leads to an increase of the second messenger cyclic adenosine monophosphate (cAMP).[28] cAMP activates the protein kinase A (PKA) as well as mitogen-activated protein kinases (MAPK) leading to a change in gene expression.[28] $G\alpha_{i/o}$ subunits inhibit the ACs and have the contrary effect of $G\alpha_s$ subunits on the cell.[29] $G\alpha_q$ subunits mainly activate the phospholipase C (PLC) which cleaves phosphatidyl-inositol-4,5-bisphosphate, resulting in the formation of the two second messengers diacyl glycerol (DAG) and inositol trisphosphate (IP_3).[29,30] IP_3 activates Ca^{2+} channels at the sarcoplasmic reticulum leading to an Ca^{2+} influx to the cytosol, whereas DAG in combination with Ca^{2+} activates the Protein kinase C (PKC).[30] $G\alpha_{12/13}$ mainly interact with RhoGEFs (ras homology guanosine nucleotide exchange factors), inducing an GDP/GTP exchange at the small G protein Rho, activating the MAPK signal cascade.[28] While these are the main effector proteins of the different G protein families, different isoforms of each family can interact with other effector proteins as well, leading to a more complex biological response of the cell.[28] The Gβγ subunit forms a constitutive heterodimer and effects and regulates a great variety of different proteins,[31] including inwardly rectifying K^+ channels (GIRK1/GIRK2, GIRK1/GIRK4),[32,33] GPCR kinases (GRK) 2 and 3,[34] adenylyl cylcases[35] and many more.[36]

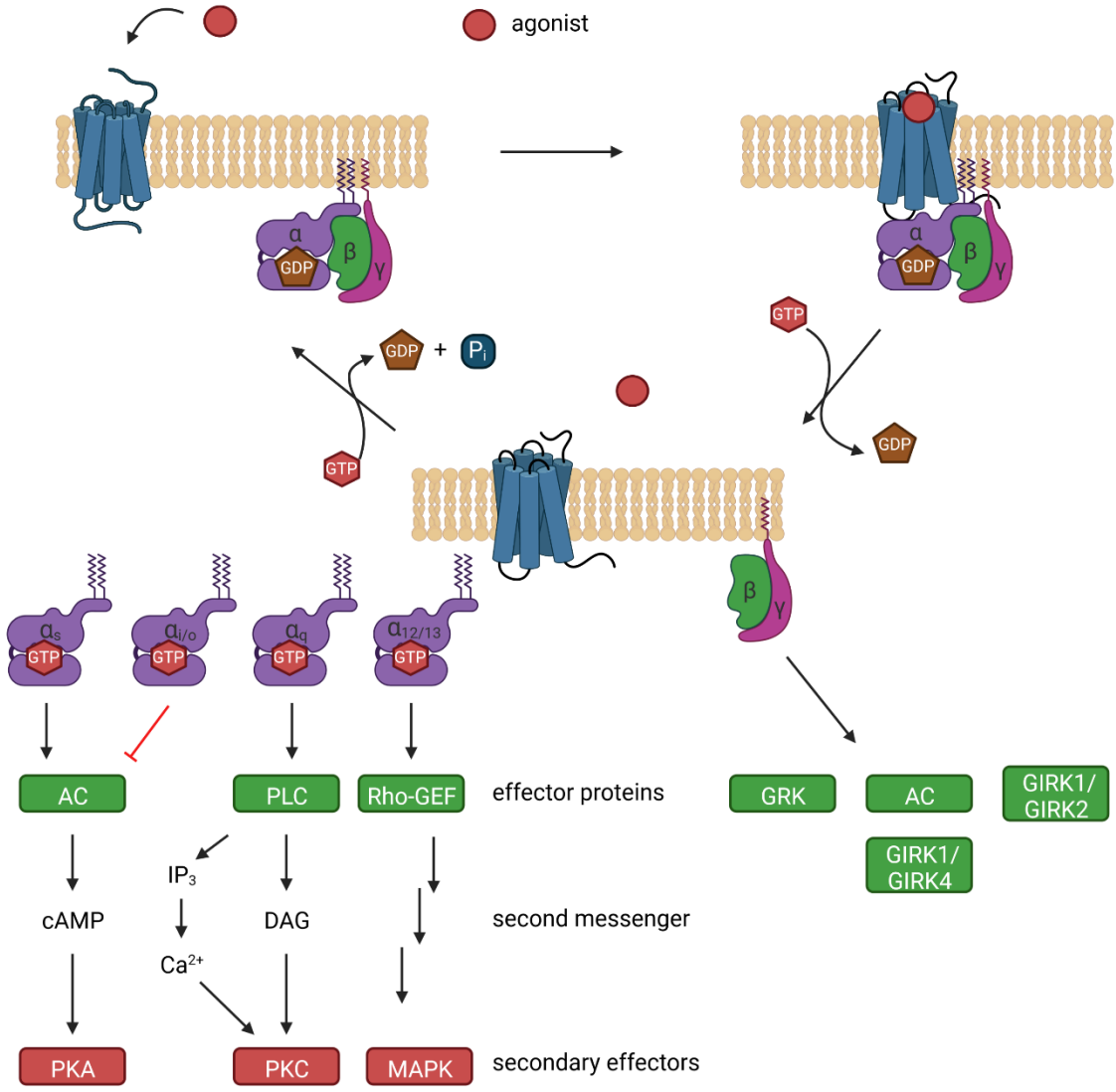

Figure 1.1: Schematic illustration of the G protein-activation cycle and signaling pathways: Activation of the GPCR leads to the recruitment of a heterotrimeric G protein. A GDP-GTP-exchange at the α-subunit leads to the dissociation of the Gα- and Gβγ-subunits, which then activate signal cascades. The α-subunit hydrolyzes GTP leading to the reassembly of the heterotrimeric G protein. Created with BioRender.com.

1.1.1.2 G protein-independent signaling

Besides the classical G protein activation cycle, GPCRs can exert biological effects independent of G proteins. The most extensively studied G protein-independent signaling pathway is that of β-arrestins.[37] Other proteins involved in GPCR signaling are regulators of G protein signaling (RGS), receptor activity modifying proteins (RAMPs) or calmudolin.[38]

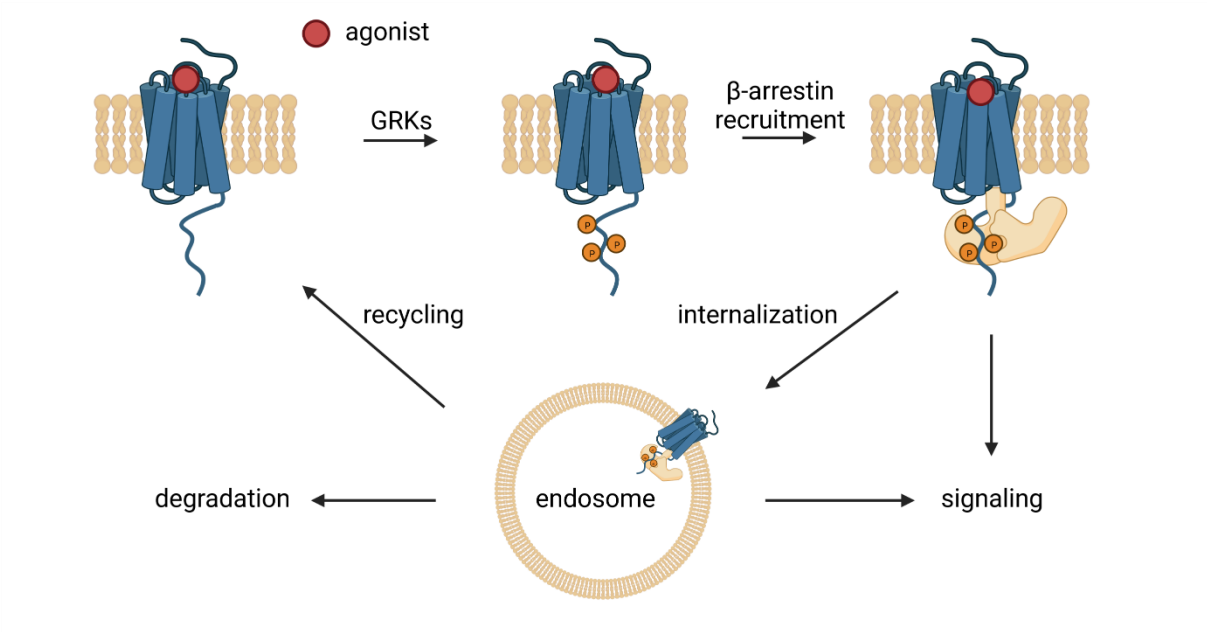

Figure 1.2: Schematic illustration of β-arrestin recruitment: Activation of the GPCR leads to intracellular phosphorylation by GRKs, followed by the recruitment of β-arrestin. Besides the regulation of internalization the β-arrestins can interact with different proteins, initiating signal cascades. Created with BioRender.com.

Receptor activation induces the intracellular phosphorylation of the GPCR by GRKs or second messenger-dependent kinases, leading to the association of β-arrestins to the GPCR (Figure 1.2).[37,39] When bound to a GPCR these β-arrestins can induce desensitization (inhibition of G protein binding to the receptor) depending on the way they are bound to the GPCR.[40] Furthermore they regulate the internalization of the receptor into clathrin-coated pits and its degradation.[41] Besides this negative regulating effect on G protein-dependent signaling, which prevents the cell from excessive stimulation, the β-arrestins can interact with a wide range of different proteins influencing many (patho)physiological processes.[42] For example, the β-arrestins couple the GPCR to the MAPK ERK1/2 pathway by interaction with tyrosine kinases of the Src family.[43] The extracellular signal-regulated kinase (ERK) MAPK pathway consists of multiple kinases and is associated with basic cellular functions such as proliferation, survival, differentiation, and motility.[44–46]

1.1.1.3 Biased agonism

The growing knowledge about the complex functionality of GPCRs also had an impact on the way ligands are viewed and characterized. While affinity (the ability to bind the receptor) and efficacy (the ability to trigger a cellular response) are still the most important properties of a receptor ligand, there are more parameters to consider.[47] In the classical way, ligands were classified as full agonists, partial

agonists, antagonists or inverse agonists (Figure 1.3A).[48] Full agonists bind the receptor and achieve 100 % efficacy, which is usually determined as the maximal biological response by the endogenous ligand. Partial agonists on the other hand activate the receptor, but do not achieve 100 % efficacy.[48] Antagonists don't have any effect on the receptor signaling, but they compete with other ligands for the binding site, hence block the receptor.[48] Inverse agonists lower the ligand-independent activity, also called constitutive activity,[49] of a receptor.[48] Given the fact that a GPCR can induce different signaling pathways, besides the classical G protein-dependent signaling, the concept of biased agonism or functional selectivity has gained in importance.[50–52]

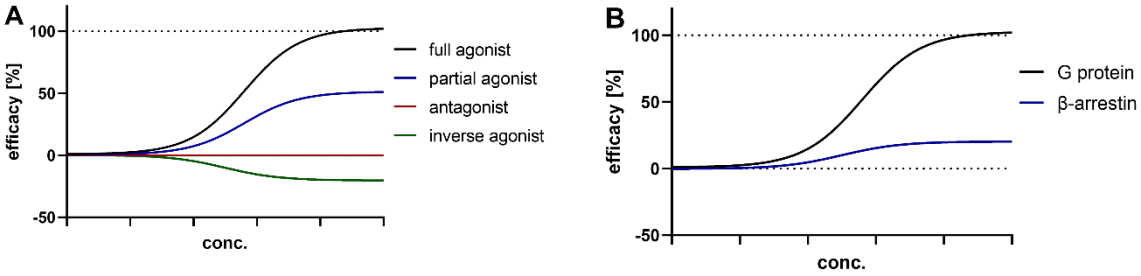

Figure 1.3: Exemplary dose-response curves of an agonist, partial agonist, antagonist, and inverse agonist (**A**). Exemplary dose-response curve of a G protein-biased ligand (**B**).

Biased agonism describes the ability of a ligand to selectively stabilize one conformation of a receptor and thereby activate one specific of multiple possible signaling pathways of the receptor (Figure 1.3B).[53] Driven by the promise of finding drugs that specifically activate therapeutic pathways and do not lead to undesirable side effects, great efforts have been made to find biased agonists.[54] However, until now only one biased GPCR-ligand gained FDA approval, while many others failed in clinical trials.[54,55] The reason for this may be the great focus on finding biased ligands for either the G protein- or the β-arrestin-dependent pathway.[54] These are by far the most extensively studied signaling pathways (see chapters 1.1.1.1 and 1.1.1.2) but a biased biological response is caused by more than just a biased ligand.[54] For example, "receptor-bias" describes the preferential signaling of a receptor through one pathway.[56] An unbiased ligand can lead to a biased response in different cell types, which is called "system-bias".[57] Other aspects of biased signaling are different protein conformations[58] or isoforms,[59] location of the receptor,[60] kinetic aspects,[51] or GPCR di- and oligomerization[61,62] (see chapter 1.1.2).

Conclusively GPCRs are more than simple "on-off" switches, but instead receive and process external stimuli and induce a specific biological response through a vast network of interactions with a plethora of different modulating, transducer, and effector proteins.

1.1.2 GPCR di- and oligomerization

For a long time class A GPCRs were believed to exist and signal exclusively as monomers.[63] Although it's proven that they do exist and are fully functional as monomers, in the last two decades the formation of class A GPCR homo- and heterodimers, as well as oligomers of a higher order, were described for many different receptors.[64] Nevertheless, there is still controversy about the validity of the proven dimers and there actual biological relevance.[63]

A great variety of different GPCR homo- and heteromers has been proven to exist in heterologous cell systems, but only some of them have also been validated *in vivo* (for overview see *Gomes et al*.).[64] Receptors can be forced to interact with each other by overexpression in artificial cell systems, which may not represent the biological reality.[65] Therefore, especially the *in vivo* existence of GPCR heteromers (Hets) is of biological and pharmaceutical relevance. To prove the existence of a GPCR Het *in vivo*, three criteria have been established, that should be fulfilled.[64] First, the protomers of the Het must colocalize and physically interact in native tissue, which is often shown by co-immunoprecipitation, proximity-based fluorescence techniques (FRET/BRET), or proximity ligation assays (PLA).[64] The second criteria is the exhibition of different properties from those of the protomers, for example changes in ligand binding, signaling, or receptor trafficking.[64] Examples for these changes are the ability of a Het to bind a different G protein than its protomers,[66] the influence of one receptor ligand on the efficacy of the other ligand,[67] cross-antagonism and others.[68] The third criteria is that this unique biochemical fingerprint is reversed by the interruption of the receptor heteromer.[64] For this purpose, in recent years disruptor proteins have been developed and applied.[68] These proteins mimic a TM helix of one receptor. If this domain is required for receptor dimerization, they can interfere the interaction of both receptors and inhibit the formation of a dimer.[69,70] These proteins can help to identify the interface between both receptors, which is useful for molecular modelling studies of GPCR dimers.[68] Moreover, they're being investigated as a possible drug themselves, inhibiting potential pathological GPCR dimerization.[68]

Advances in recent years in fluorescence microscopy, especially in single-molecule imaging, enabled a more direct way of detecting GPCR di- and oligomers in native tissue.[71] Single-molecule microscopy revealed a complex behavior of GPCRs at the membrane, including the formation of 'hot spots' for GPCR signaling and interactions.[71] It also proved the transient formations of GPCR di- and oligomers and for some receptors even a ratio of dimer to monomer could be determined.[72,73] Nevertheless, these studies only proof the existence of a dimer, but reveal nothing about its functional behavior.[63] Therefore, a combination of different techniques is needed for the detailed investigation of a receptor dimer and its potential use as a novel pharmacological target.

1.2 Dopamine receptors

The biogenic catecholamine dopamine (DA) acts as a neurotransmitter in the central nervous system (CNS) and in the periphery.[74] It's produced in the cytosol by a two-step biosynthesis starting from *L*-tyrosine (Scheme 1.1).[75] First the tyrosine hydroxylase (TYH) converts *L*-tyrosine into levodopa (*L*-DOPA) which is then decarboxylated by the aromatic *L*-amino acid decarboxylase (AADC) yielding dopamine.[76] Dopamine is then released from dopaminergic neurons, which are expressed in different areas of the brain, but mostly in the substantia nigra.[74]

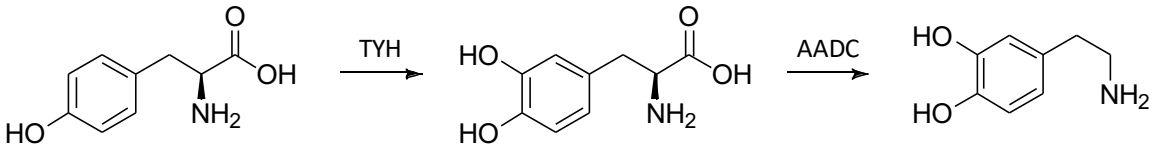

L-tyrosine levodopa dopamine

Scheme 1.1: Biosynthesis of dopamine.

Dopamine mediates its biological effects via five different GPCRs. These dopamine receptors are divided into two groups, D_1-like (D_1 and D_5) and D_2-like receptors (D_2, D_3, and D_4).[77] The D_1-like receptors are mainly coupled to $G\alpha_s$ proteins, thus activating the AC and leading to an increase in cytosolic cAMP. The D_2-like receptors mainly couple to $G\alpha_{i/o}$ proteins and therefore have the contrary effect on the cell.[77] The dopamine receptors are abundantly expressed in the CNS, but are also found in the periphery.[74] They are involved in almost all physiological processes in the brain[74] and dopaminergic impairment is associated to many diseases and disorders, for example Parkinson's Disease (PD),[78] schizophrenia,[79] hyperprolactinaemia, Tourette syndrome,[80] attention deficit/hyperactivity disorder (ADHD),[81] Huntington's disease,[82] and addiction.[83] The dopaminergic system and signaling is very complex because of the many interactions the dopamine receptors engage among each other or with different proteins.[74] For example, it has been reported that the D_1R and D_2R receptor can form a dimer which is then able to bind and signal via a $G\alpha_q$ protein.[84] Although there are many drugs on the market for the treatment of different diseases targeting the dopamine receptors, their complex signaling and network is not completely understood and requires more research.[85]

1.2.1 D_1-like receptors

The D_1R is the most abundant receptor of the dopamine receptor family in the CNS. It's expressed exclusively postsynaptic in multiple regions of the CNS, with the highest expression in nigrostriatal, mesolimbic, and mesocortical areas, including the striatum, frontal cortex, nucleus accumbens and the

olfactory bulb.[86] The D_5R is expressed at low levels in different brain regions, such as pyramidal neurons in the prefrontal cortex, the premotor cortex, the cingulated cortex, substantia nigra, hypothalamus and hippocampus.[86] In contrast to the D_2-like receptors, there are no introns in the coding regions for the D_1-like receptors, so there are no splice variants.[86] The D_1R plays an important role in synaptic plasticity,[87] the reward system,[75] locomotor activity,[88] and the process of learning and memory.[87] Therefore, it's implicated in different diseases such as PD, Alzheimer's disease (AD), and mild cognitive impairment.[85,87,89]

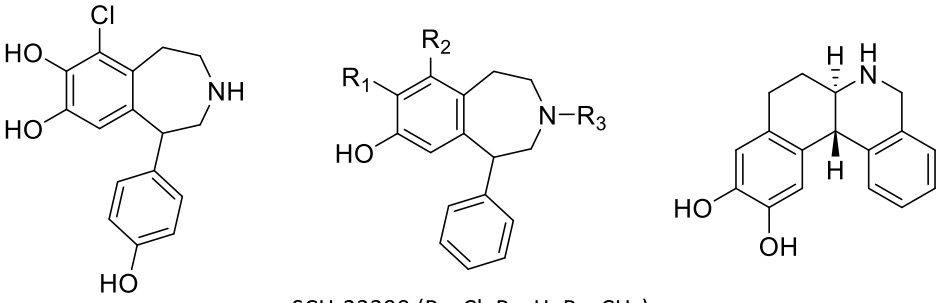

fenoldopam

SCH-23390 (R_1=Cl, R_2=H, R_3=CH_3)
SKF-81297 (R_1=OH, R_2=Cl, R_3=H)
SKF-38393 (R_1=OH, R_2=H, R_3=H)

dihydrexidine

Figure 1.4: Chemical structures of fenoldopam, SCH-23390, SKF-81297, SKF-38393 and dihydrexidine.

Beside the $G\alpha_s$ signaling the D_1R can activate different signal cascades, mostly by interacting with other receptors.[75] For example, the D_1R can induce Ca^{2+}-release in the cytosol by activating the PLC which leads to a modulation of neurotransmitter release.[90] Furthermore, multiple studies revealed the interaction between the D_1R and NMDA-receptors, coupling the D_1R to the MAPK/ERK signal pathway.[91,92] The D_1R is only able to activate this signaling in the presence of glutamate, but not in the absence.[93] The complex interactions between these receptors are described in Klein, M. O. *et al.* and will not be explained in detail in this thesis.[75]

Despite the long-known existence of the D_1R, there is only one drug on the market targeting selectively the D_1-like receptors: Fenoldopam as emergency treatment for hypertensive crisis (Figure 1.4).[87,94,95] For a long time, selective D_1R agonists were thought to be a suitable drug for the treatment of PD,[87] but the first benzazepine based agonists (e.g. SKF-38393; Figure 1.4) had poor intrinsic activity and therefore failed for the treatment.[96] The search led however to the discovery of compound SCH-23390 (Figure 1.4) by Schering-Plough, which is the most commonly used reference ligand for the D_1R and is also used as a [^{3}H]-radiolabeled ligand.[87,97,98] The first central active, selective, full D_1R agonist was dihydrexidine (DHX),[99] but failed in clinical phase IIa studies due to severe side effects.[100] Since then, the focus shifted to non-catechol compounds targeting the orthosteric binding sites[87] and positive allosteric modulators (PAMs), targeting an allosteric binding site at the IL-2 of the

receptor.[87,101,102] Nevertheless, no new candidate entered the market highlighting the need for further research and better understanding of the complex D_1R mediated signaling to develop more efficient and secure drugs.

1.3 Histamine receptors

The biogenic amine histamine (Figure 1.5) has been detected over a century ago and acts as a neurotransmitter and tissue hormone.[103–105] It's formed by decarboxylation of the amino acid *L*-histidine by the histidine decarboxylase (HDC).[106] Histamine is expressed ubiquitously in the human body with especially high concentrations in the lungs, skin and gastrointestinal tract.[105] Histamine mediates its biological effects by the activation of four different GPCRs, the histamine receptors.[107] The histamine H_1 receptor (H_1R) was first described in 1937, is coupled to $G\alpha_{q/11}$ proteins and is the target of the classical antihistamines for the treatment of allergic reactions.[105,108] Furthermore, CNS-penetrant H_1R antagonists have a sedative effect and are used as sleeping drugs (for example doxylamine).[109] The H_2R was described in 1972, is $G\alpha_s$-coupled and mainly expressed in the stomach and CNS.[110,111] Its antagonists revolutionized the treatment of gastric ulcers in the 1970s, but are now mostly replaced by proton-pump-inhibitors, like omeprazole or pantoprazole.[105] The H_3R (in 1983) and H_4R (in 2000), both mainly $G\alpha_{i/o}$-coupled, are the most recently found histamine receptors and revived the histamine research.[112,113] The H_4R is mostly related to inflammatory and immunological processes, but there's no drug on the market yet targeting specifically the H_4R.[105]

1.3.1 The histamine H_3 receptor (H_3R)

The H_3R was first pharmacologically characterized in 1983 as an autoreceptor, inhibiting the histamine release into the synaptic cleft.[112] The discovery of the selective agonist *R*-α-methylhistamine (RAMH) and the selective antagonist thioperamide confirmed the existence of the new histamine receptor subtype (Figure 1.5).[114] In 1999 the H_3R was successfully cloned.[115] Multiple introns in the encoding region lead to over 20 different functional isoforms of the receptor.[105,116] The largest one containing 445 amino acids is also the most dominant one.[117]

The H_3R is expressed pre- and postsynaptic in the peripheral nervous system and extensively in the CNS, especially in the cerebral cortex, the thalamus, the basal ganglia, the striatum, and the substantia nigra.[118] Due to the high expression in the CNS the H_3R is being related to multiple neuropsychiatric diseases, for example AD,[119] PD,[120] sleep disorders,[121] tic disorders,[122] ADHD,[123] and others.[124] Until now, the only FDA-approved drug is pitolisant (Figure 1.5)[124] for the treatment of narcolepsy, which is also in clinical studies for the treatment of the Prader-Willi-syndrome.[125]

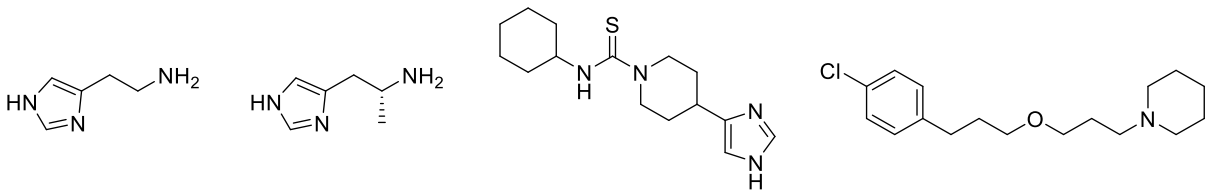

Figure 1.5: Chemical structures of histamine, RAMH, thioperamide, and pitolisant.

The H_3R has a high constitutive activity and binds a pertussis toxin-sensitive $G\alpha_{i/o}$ protein, leading to a decrease in cytosolic cAMP upon activation.[105] Beside the G protein-dependent signaling, the H_3R mediates the release of different neurotransmitters, e.g. biogenic amines, acetylcholine, γ-amino butyric acid (GABA), and glutamate.[105] Furthermore, activation of the H_3R leads to the activation of MAPK pathways,[126] the activation of the phosphatidylinositol 3-kinases (PI3K)[105] or modulation of the Na^+/H^+ exchange (NHE) system.[127] Interactions and dimerization with different GPCRs[105] and biased signaling by different isoforms[128] further broaden the signaling portfolio of the H_3R. Therefore, the modulation of the H_3R leads to a complex biological response and despite decades of research its complex network is not yet completely understood.

1.4 The D_1-H_3 receptor heteromer (D_1-H_3 Het)

The formation of the D_1-H_3 Het was first described by the group of Rafael Franco in 2009.[129] In this work they proved a close proximity of both receptors in transfected HEK-293T cells via a bioluminescence energy transfer (BRET) assay and a crosstalk between both receptors. The activation of the H_3R with RAMH led to a decrease in affinity for D_1R agonist binding in transfected human blastoma cells (SK-N-MC cells). They also showed that the selective H_3R agonist RAMH is only able to induce ERK1/2 phosphorylation in D_1R-H_3R co-expressing cells, but not in the absence of the D_1R. This activation could be blocked by the selective D_1R antagonist SCH-23390, as well as the SKF-81297-induced (D_1R agonist; Figure 1.4) ERK1/2 phosphorylation could be blocked by the H_3R antagonist thioperamide. This phenomenon is called cross-antagonism (Figure 1.6). At last, they showed that in D_1R-H_3R co-expressing cells D_1R activation led to a decrease in forskolin induced cAMP production, indicating a dimer-induced $G\alpha_{i/o}$ protein dependent signaling. This pharmacological fingerprint (cross-antagonism and H_3R agonist-induced ERK1/2 phosphorylation) was then used to prove the existence of D_1-H_3 Het *in vivo* in the rat striatum.[130] In the same publication the authors showed the colocalization of both receptors by co-immunostaining and co-immunoprecipitation in the GABAergic neurons of the direct striatal pathway in rat tissue.

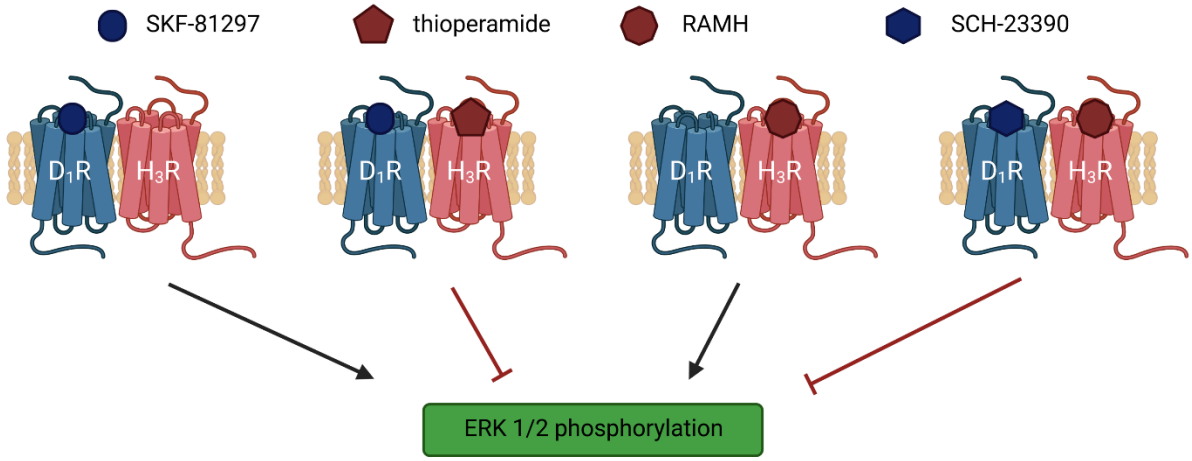

Figure 1.6: Schematic illustration of the cross-antagonism at the D_1-H_3 Het. Created with BioRender.com.

In 2017, the existence of the D_1-H_3 Het in the rat cortex was published.[131] In the same work the authors describe the formation of a macromolecular complex formed by the D_1R, H_3R, and NR1A and NR2B subunits of the NMDA receptor in transfected HEK-293T cells. To show the formation of this complex they used a combination of BRET and bimolecular fluorescence complementation (BiFC) techniques. Proximity ligation assays (PLA) suggested the formation of this complex in the rat cortex.

Furthermore, they showed, that NMDA-, dopamine-, or amyloid-β protein-induced cell death could be decreased by the selective H_3R antagonist thioperamide (Figure 1.7). This phenomenon was observed in wild type mice as well as in mice, that exhibit an accelerated AD phenotype (APP/PS1 mice), and probably is mediated by the formation of a D_1-H_3-NMDA heteromeric complex. Because of these neuroprotective properties this complex could be an attractive target in the treatment of neurodegenerative diseases such as AD.

Furthermore, the D_1-H_3 Het is reported to form a complex with the σ_1-receptor[132] and is proposed as a target for the treatment of Huntington's disease.[133] The complex biological functions of GPCR heteromers in general and the D_1-H_3 Het in specific are yet not fully understood. Selective pharmacological tools and new assay systems are needed to further elucidate their biological relevance and their suitability as a drug target.

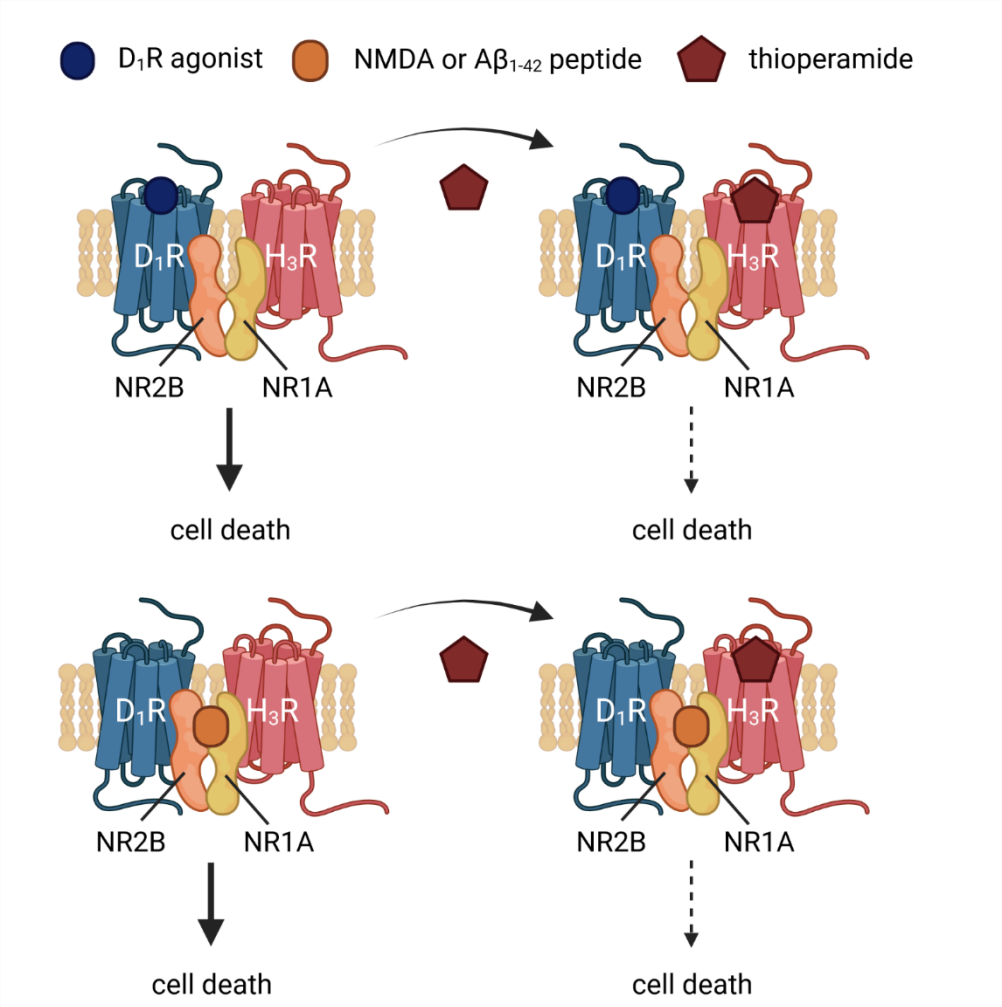

Figure 1.7: Schematic illustration of the neuroprotective effects of thioperamide mediated by the D_1-H_3-NMDA receptor complex. Adapted from Rodriguez-Ruiz, M. *et al*.[131] Created with BioRender.com.

1.5 Bivalent ligands

Bivalent ligands are a prominent pharmacological tool for the investigation of GPCR dimers. The concept of bivalent ligands was first introduced by Philip S. Portoghese in 1982. [134,135] A bivalent ligand consists of two recognition units, also called pharmacophores (e.g. receptor ligands), that are connected by a spacer.[136] Both pharmacophores can be identical (homo-bivalent ligand) or different (hetero-bivalent ligands). If the spacer allows the simultaneous binding of two adjacent binding sites, the bivalent ligand can show an increased affinity towards a receptor dimer, leading to a selectivity over the respective protomers.[136] The enhanced affinity is based on the model that after the first pharmacophore is bound to one receptor the second one is pushed in the vicinity of the second binding site.[136] Thus, there is an increased local concentration of the second recognition unit in close proximity to its respective binding site leading to a higher affinity (Figure 1.8).[136] This model explains the successful use of bivalent ligands but does not reflect the whole picture of bivalent binding. Other aspects must be considered as well, such as cooperativity between both receptors of the dimer and the different kinetics of bivalent ligands.[137] The ligand binding of one receptor of a dimer can lead to a decrease in affinity of the second receptor for its ligand. Due to this negative cooperativity the overall affinity of the bivalent ligand for the second receptor can be lower or equal, although it's bound in a bivalent manner.[137]

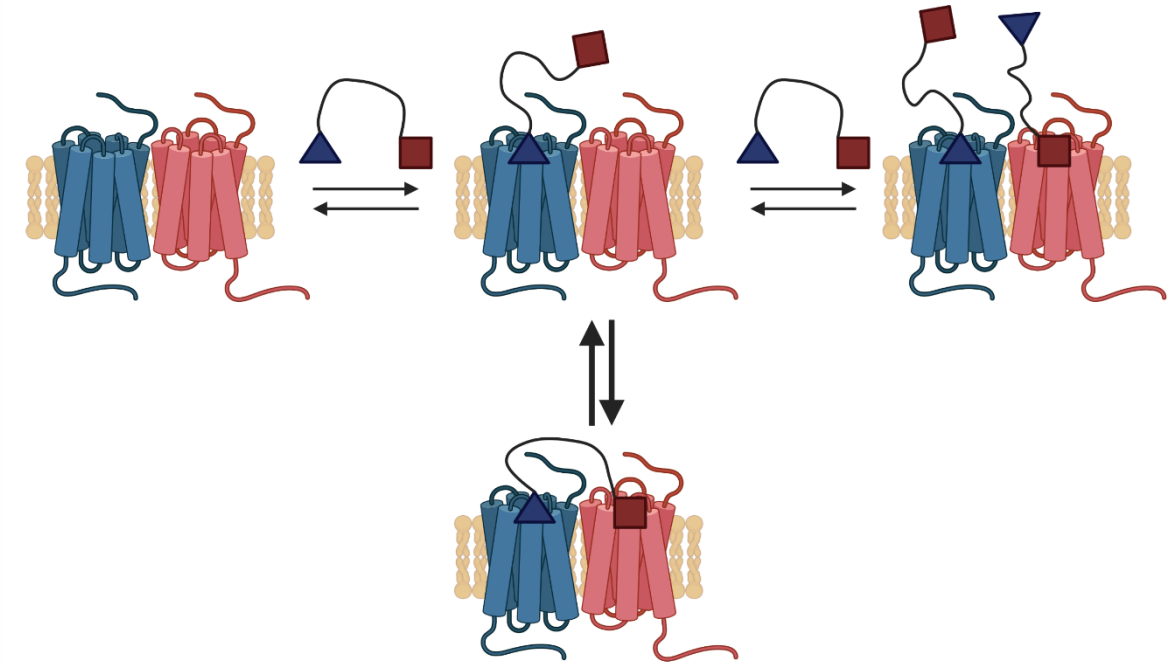

Figure 1.8: Schematic illustration of the sequential binding steps of a bivalent ligand to a receptor dimer (bivalent binding mode on the bottom). Created with BioRender.com.

Nevertheless, the bivalent ligand approach has been successfully applied to target selectively a variety of GPCR dimers, as shown in several reviews.[138–140] These bivalent ligands include structures targeting two orthosteric binding sites of the same or different receptors or the orthosteric and the allosteric binding sites of the same receptor (often called bitopic ligands).[140] Bivalent ligands are mostly used as pharmacological tools to investigate the biological behavior of a specific GPCR dimer, but have not made it to the market yet.[138] The nature of the bivalent ligands, especially their large size and high molecular weight, results in different adsorption, distribution, metabolism and excretion (ADME) problems impeding their *in vivo* use for now.[140] Especially, the plasma life-time, their ability to cross the blood brain barrier (BBB), and the complicated synthesis are to mention here.[140] Fortunately, the spacer region can be easily modified and adjusted to tackle some of this specific issues, since its main purpose is the connection of both pharmacophores. Promising attempts in this direction have been made including reports of BBB-penetrating bivalent ligands.[141,142] Nevertheless, there is still a long way to go towards a clinical applicable bivalent ligand.

1.6 Fluorescent ligands

Technological advances in the last two decades opened up a wide field of fluorescent-based approaches to study different aspects of GPCRs, such as ligand-binding and kinetics, receptor mobilization, trafficking and degradation as well as protein-protein interactions.[143,144] Fluorescent ligands are the key to many of these approaches.[145] They consist of a pharmacophore, a selective antagonist or agonist for the receptor of interest, which is labeled with a fluorescent dye.[146] This dye can be attached directly to the pharmacophore or separated from the pharmacophore by the insertion of a linker region.[145] The latter approach tends to have less influence on the binding behavior of the fluorescent ligand.[147] Although the aim of every fluorescent ligand is to retain the affinity, selectivity and efficacy of the parent ligand, a fluorescent labeled ligand constitutes a novel pharmacological entity.[144] All those parameters have to be determined again, as they can differ significantly from those of the parent ligand caused by the modification of the pharmacophore and the addition of the fluorophore.[148,149]

A multitude of fluorescent ligands for many different receptors have been published, that contain a great variety of different fluorescent dyes.[143–145] Based on the intended use of the fluorescent ligand its fluorescence properties can be tailor-made by choosing one of the hundreds of commercially available fluorescent dyes.[144,145,150] Once a fluorescent ligand was successfully synthesized, it can be used for many different approaches to elucidate GPCRs, for example to study ligand-binding to the receptor of interest.[144,151] In recent years, fluorescence-based techniques such as flow cytometry, fluorescence polarization, fluorescence anisotropy, and Förster resonance energy transfer- (FRET) or BRET-based techniques, have substituted many radioligand binding assays.[151,152] These techniques avoid the use of radioisotopes and their implicated costs and effort for radioactive authorization and disposal.[145] Especially the NanoBRET assay is a popular method for competitive ligand binding assays.[152] For this technique the Nano luciferase (NLuc), a genetically engineered, bright, and small luciferase, is fused to the extracellular site of the receptor.[153] After addition of a substrate the NLuc catalyzes an oxidation reaction which leads to the emission of blue light ($\lambda_{em.\ max} \approx 460$ nm).[153,154] If the fluorescent ligand is in close proximity, has the correct orientation and a spectral overlap with the NLuc, the fluorophore is excited by BRET and emits light of a higher wavelength (Figure 1.9).[152] Since BRET is highly distance dependent it only takes place when the fluorescent ligand is bound to the receptor. Therefore, the BRET efficiency correlates with the amount of bound ligand and can be used as a read out in competitive binding assays.[152] This method yields a very high signal-to-noise ratio because nonspecific binding events of the fluorescent ligands are usually not detected due to the larger distance to the NLuc.[152] Furthermore, this assay allows the detection of the ligand-binding in real-time

providing kinetic information and has no need to separate bound from unbound ligand as it's the case in radioligand binding assays.[152]

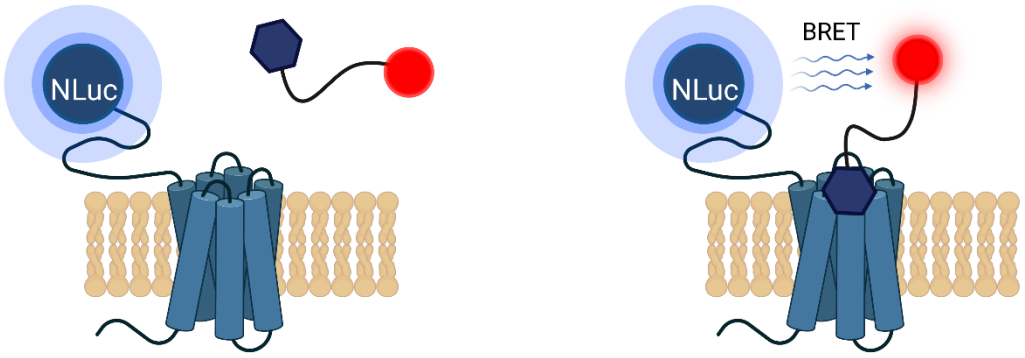

Figure 1.9: Schematic illustration of the NanoBRET principle. Created with BioRender.com.

Next to the use as a tracer in binding assays, fluorescent ligands can be used for fluorescent microscopy.[144] They allow the fluorescent labeling of receptors *in vitro* and *in vivo* without the need to genetically modify the receptor.[150,150] Using advanced techniques such as laser scanning confocal microscopy (LSCM) or total internal reflection microscopy (TIRF) the localization, mobilization, trafficking and degradation of receptors can be visualized and studied with the use of fluorescent ligands.[155,156] Especially, TIRF microscopy was successfully used for single-molecule imaging of receptors labeled with a fluorescent ligand.[157,158]

Because of their diverse applications ranging from single-molecule imaging to high-throughput screening fluorescent ligands are powerful tools for the investigation of GPCRs *in vitro* and *in vivo*.[144]

1.7 Alzheimer's disease (AD)

Alzheimer's disease is named after Alois Alzheimer, a german psychiatrist, who was the first to discover the disease in a patient over a century ago.[159] He documented the progressive illness in a patient showing increasing paranoia, sleep disorders, aggressiveness, and memory loss.[159] After the death of the patient an autopsy of the brain showed major histological alterations later known as plaques and neurofibrillary tangles, which he related to the symptoms prior to the death.[159]

Today, AD is the most common cause of dementia with over 55 million people worldwide suffering from this disease.[160] AD is most prevalent in people over 65 years and women are statistically more affected than men.[160] With approximately 10 million new cases every year the number of total cases is expected to rise up to 139 million by 2050.[160] Apart from the enormous impact the disease has on the quality of life of the patients and their families AD poses a major challenge for the medicinal and care systems. In 2019, the estimated global societal cost of dementia was 1.3 trillion US dollars and is expected to rise over 2.8 trillion US dollars by 2030.[160]

AD is a progressing, neurodegenerative disease. Early symptoms are usually forgetfulness and confusion in familiar places, which get worse in time leading to behavioral changes, loss of memory, cognitive impairment and loss of functional abilities.[160,161] Ultimately, these symptoms lead to the inability of living an independent life and the need for full time care.[160] The pathogenesis and mechanism of the progression of AD is still not fully understood but the formation of extracellular amyloid β (Aβ) plaques and intracellular neurofibrillary tangles (NFT) are considered as neuropathological indicators of AD.[161,162] While the pathological origin of AD is not known yet, there are general risk factors that increase the probability of obtaining AD.[160] Besides age and genetic implications a healthy lifestyle can help to lower the risk of obtaining AD, especially physical exercise, no smoking and excessive drinking, healthy blood pressure, blood sugar, and cholesterol levels.[160]

Treatment of AD was mostly symptomatic with four different approved drugs, three acetylcholine esterase inhibitors and one NMDA antagonist.[163] These drugs only achieve a modest improvement of the symptoms but do not cure AD or prevent neuronal degeneration.[161] In 1992, the so-called amyloid-hypothesis was published, which is the assumption that the main symptoms of AD are caused by the aggregation of Aβ.[164] This led to enormous effort of the scientific community and pharmaceutical industry to develop drugs that could reduce the Aβ-levels in the brain. Despite many promising candidates all of them failed in clinical studies mostly due to lack of clinical efficacy.[165] Finally in 2021 aducanumab, a monoclonal antibody for the Aβ protein, was approved by the FDA.[166] Aducanumab is the first Aβ-targeting drug entering the market, which successfully clears the brain of Aβ. Nevertheless, there is controversy about its clinical efficacy highlighted by the rejection of aducanumab by the European Medicines Agency (EMA) due to efficacy and safety concerns.[167]

While the scientific community is divided on the subject of the Aβ hypothesis the lack of success targeting Aβ led to a shift of focus towards other potential targets, for example tau-proteins[161] and to the detection of biomarkers.[168] The belief that the Aβ targeting drugs would have efficacy but are just administered too late in the disease led to an increasing effort to detect AD before the patient show any symptoms.[169] Much effort was invested to find universally applicable biomarkers and to standardize the diagnosis of AD.[168] There are several well-established central spinal fluid (CSF) biomarkers, e.g. $A\beta_{42}$ and the ratio of total tau and phosphorylated tau proteins, that are used to diagnose and classify AD.[170] Nevertheless, the research is still ongoing for biomarkers that can better predict the progression of the disease, for example synaptic biomarkers.[171] In recent years the detection of blood biomarkers is gaining more attention since they would have the advantage of avoiding a lumbar puncture and would facilitate continuous screenings during clinical trials.[168]

Conclusively, AD is one of the most urgent medical challenges in our time. The controversy about the Aβ hypothesis indicates that AD is a multicausal disease and many different factors and proteins play a role in its pathogenesis.[172] Nevertheless, recent advancements in drug design and especially in the detection of biomarkers give hope. Maybe an early detection of the disease long before the patients display clinical symptoms and better predictions of its progression with novel biomarkers allow individual therapies for each patient. However, there is still a long way to go to reach that point and understand the complex pathology of AD.

1.8 Scope of the thesis

The investigation and elucidation of the biological behavior of GPCR dimers poses a great challenge in modern pharmacology. Because there are no assay systems available that measure exclusively signaling by a GPCR dimer most of the results published about the functionality of GPCR complexes were obtained by indirect approaches. The most commonly used method is the detection of differences in signaling or ligand binding behavior of one receptor in the presence and absence of the second one.[64] These results are usually supported by evidence for co-localization and physical interaction of both receptors.[64] Bivalent ligands with a higher affinity towards the receptor dimer, compared to its protomers, can help to target receptor complexes selectively and further elucidate their functional behavior. Therefore, they are an important pharmacological tool in GPCR research.

The primary aim of this thesis was the synthesis and pharmacological characterization of bivalent ligands for the D_1-H_3 Het. Before the start of the synthesis, the design of the bivalent ligands had to be planned carefully. High affinity and selective ligands for both receptors had to be selected as lead structures for the pharmacophores. Based on structure activity relationships and molecular modelling results, suitable attachment points for the spacers had to be chosen as well as synthetically accessible ways of connecting the pharmacophores to the spacer. Furthermore, the spacers had to be designed as they highly influence the molecular weight and solubility of the final bivalent ligands. Molecular modelling of the D_1-H_3 Het by cooperation partners (Leonardo Pardo, Universitat Autònoma de Barcelona) gave insights into the appropriate length of the spacer but nevertheless spacers of different length and chemical composition had to be synthesized. Finally, a protocol for the effective synthesis of a set of different bivalent ligands had to established (see chapters 2.1 and 2.2).

Once the bivalent ligands were successfully synthesized, they had to be characterized pharmacologically. The first step in this process had to be the determination of the affinity towards both receptor protomers, using already established competitive radioligand or NanoBRET binding assays. The next step was the functional characterization of the bivalent ligands using a cAMP detection assay. Finally, the most promising ligand was analyzed for its neuroprotective properties at primary mouse cortex cells (see chapter 2.3).

The second part of the thesis was the synthesis of fluorescently labeled ligands for the D_1R and H_3R. These structures had to be designed carefully as well. The same pharmacophores that were synthesized for the bivalent ligands could be used as lead structures for the fluorescent ligands. Especially, the choice of the fluorescent dye is crucial for the design of a fluorescent ligand and depends mainly on the intended use of the final compound. After the successful synthesis the fluorescent ligands had to be characterized pharmacologically and regarding their fluorescence properties. For the determination of the affinity of the fluorescence ligands NanoBRET and radioligand binding assays

were used. After the determination of the excitation and emission spectra and the quantum yield, the fluorescent ligands could be used in different experimental setups including competitive NanoBRET binding assays, confocal microscopy, and single molecule TIRF imaging (see chapters 3 and 4).

2. Bivalent ligands for the D_1-H_3 receptor heteromer

The following experimental work was performed by co-authors:

preparation of primary mouse embryonal cortex cells:	Iu Raich, Jaume Lillo (Universidad de Barcelona)

2.1 Design of the bivalent ligands

Bivalent ligands are an entity of three parts: the two pharmacophores, one for each binding site, and the spacer. [138,140,173] To obtain the desired result of a functional bivalent ligand all three parts as well as their connection must be designed carefully before starting with the synthesis.

The first step is the choice of the pharmacophores. The lead structures should be high-affinity and selective compounds with the desired intrinsic activity. Once the lead structure has been selected the right position and structural moiety for the connection of the pharmacophore and the spacer must be chosen. Structure-activity relationships (SAR) or docking results can help to find the best attachment point in order to retain affinity, selectivity, and biological activity of the parent ligand.[140,173]

Agonistic and antagonistic pharmacophores were chosen for both receptors, in order to synthesize bivalent ligands with different combinations of intrinsic activities at both receptors. These ligands could be tools for investigation of the functional behavior of the D_1-H_3 Het, as they would allow the activation or inhibition of both receptors as well as selective activation of one and simultaneous inhibition of the other receptor.

As a lead structure for the D_1R pharmacophore SCH-23390 (SCH; Figure 2.1), a high-affinity and selective D_1-like receptor antagonist, was chosen.[97,174] SARs showed that the introduction of structural diverse groups at the 4'-position is well tolerated, whereas modifications at the tertiary amine or the phenolic hydroxy group can lead to significant changes in activity and affinity.[175] Furthermore, the introduction of a sulfonamide group at the 4'-position seemed to be beneficial for receptor binding and was therefore chosen as connecting functional group for the linker to the pharmacophore (Figure 2.1). [176] SKF-75760 (SKF) is structurally similar to SCH, but has a second phenolic hydroxy-group instead of the chlor-substituent at the aromatic moiety of the benzazepine.[177] In contrast to SCH, SKF acts as an agonist at the D_1R and was therefore used as a agonistic lead structure for the bivalent ligand using the same attachment point and mode as for SCH-23390 (Figure 2.1).[177]

For the H_3R pharmacophore JNJ-5207852 (JNJ) was chosen as the lead structure. This compound displays sub-nanomolar affinity towards the H_3R and exhibits an outstanding selectivity within the histamine receptor family and towards other GPCRs. [157,178] SARs showed that the introduction of an additional functional group at the *para*-position of the benzylic piperidine moiety is well tolerated.[157,179] Therefore, an amide group was inserted at this position to couple the pharmacophore to the linker (Figure 2.1). As an agonistic lead structure immepip was chosen, a high affinity and potent H_3R agonist.[116] For connection to the spacer the secondary amine was chosen due to the synthetic accessibility and the importance of the imidazole structure for receptor binding.

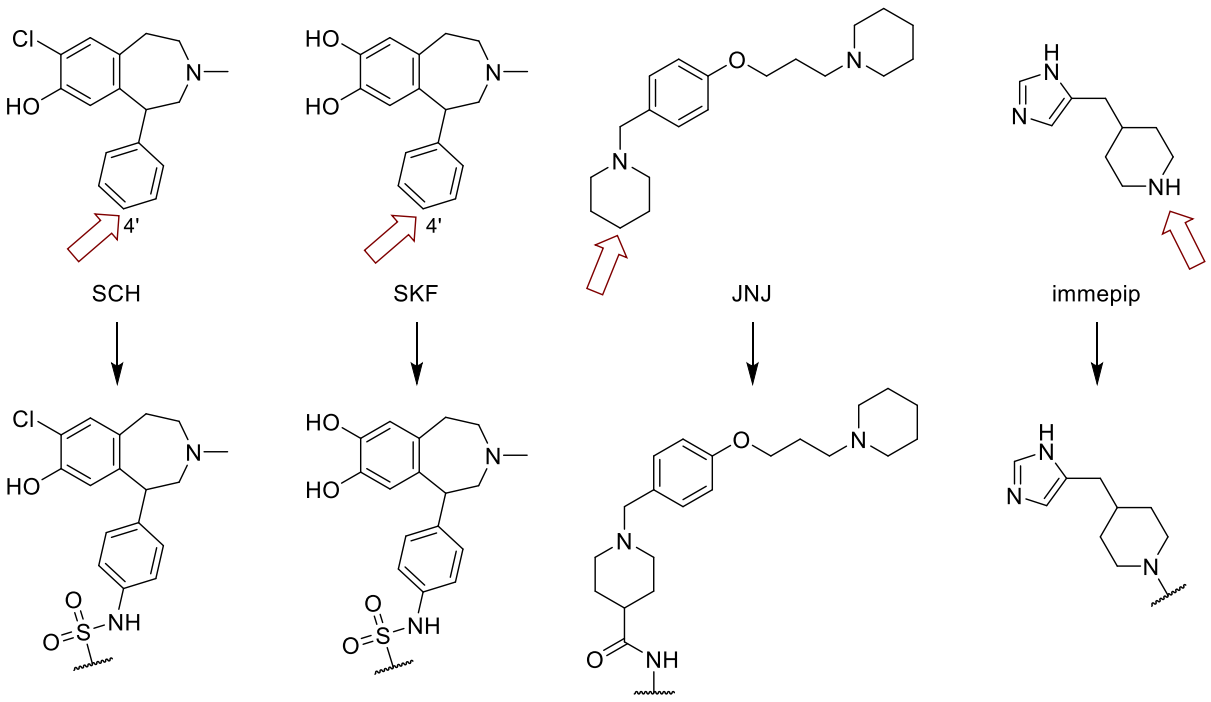

Figure 2.1: Lead structures for the pharmacophores with the chosen attachment points and the connecting functional groups to the linkers.

Regarding the spacer, length, flexibility, and solubility are among the most important criteria designing a bivalent ligand.[140,173] There is no general rule for the optimal length of a spacer for bivalent ligands because it depends mainly on the targeted receptor dimer. Therefore, a series of polyethylene glycol-based (PEG-based) spacers with different lengths was synthesized. The final distance between both pharmacophores was in the range from 39 to 57 atoms. PEG-based spacers are often used for bivalent ligands because they are chemically stable, increase the water solubility and are very flexible allowing the pharmacophores to turn into the right position for receptor binding.[140,180–183] Additionally, two spacers based on aliphatic carbon chains were synthesized as hydrophobic counterparts.

All spacers were terminally functionalized with azide groups. On the other hand, small aliphatic linkers with terminal C-C triple bonds were added to all pharmacophores (Figure 2.2). This combination of functional groups allows the final connection of spacer and pharmacophores by a cupper catalyzed azide-alkyne click (CuAAC) reaction. This reaction is a prime example for click-chemistry because of its high yields, regiospecificity, tolerance of additional functional groups, and the cheap and accessible catalyst.[184] For these reasons, it's a commonly used reaction in many different research areas and was chosen to connect all three parts of the bivalent ligand.[184]

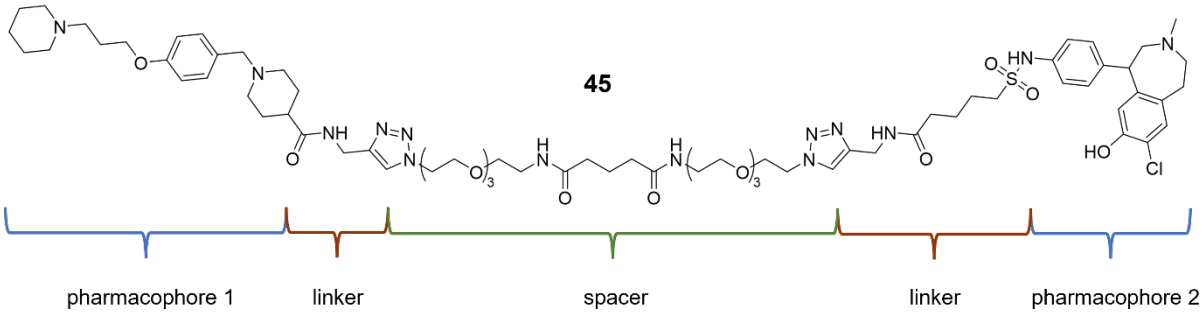

Figure 2.2: Chemical structure of **45** as an example for the schematic design of a bivalent ligand.

Docking experiments of the proposed SKF- and JNJ-based lead structures at both receptors confirmed the chosen attachment points as well suited as they are perfectly pointing out of the binding pockets. For these experiments homology models of both receptors based on the crystal structures of the H_1R (3RZE) and D_2R (6CM4) were used. Modelling experiments by the group of Prof. Leonardo Pardo (Universitat Autònoma de Barcelona) of the D_1-H_3 Het with a TM5-6 interface suggested a minimal necessary spacer length of 32 atoms to cover the shortest distance between both binding sites. However, additional length would increase the flexibility and allow a better connection of both binding sites. Therefore, the main focus was set on spacers with a total length of 39 to 47 atoms between both pharmacophores.

2.2 Synthesis of bivalent ligands for the D_1-H_3 Het

For the synthesis of the bivalent ligands, the pharmacophores and the spacers were synthesized separately and then connected by a CuAAC reaction. Based on previously published literature and retrosynthetic approaches, considering availability of the starting materials, yields, and the number of reaction steps, a synthetic route for each pharmacophore and spacer was developed and executed. The detailed experimental procedures, the analytical data, and the literature, if the structures were previously published, are presented in chapter 6.1.

2.2.1 Synthesis of the D_1R building blocks

The synthesis of the D_1R pharmacophores **13** and **15** was carried out following the synthetic route of 1-phenyl-2,3,4,5-tetrahydro-benzazepines by Neumayer *et al*. and Shen *et al.* (Scheme 2.1).[185,186] The epoxide **3** was synthesized in a three-step synthesis starting from the commercially available 4-nitroacetophenone.[186] An acid-catalyzed α-bromination reaction using *N*-bromosuccinimide (NBS) yielded **1** followed by a reduction of the carbonyl moiety with sodium borohydride affording the α-bromo alcohol **2**. This product was transformed via a base-catalyzed intramolecular S_N2 reaction into the epoxide **3** in excellent yields.

An aromatic chlorination of commercially available 4-methoxybenzaldehyde using sulfuryl chloride resulted in product **4** in high yields. A Henry-type reaction (**5**) followed by a reduction with $LiAlH_4$ yielded the primary amine **6**. For the selective mono-methylation of the amine, a Boc-protecting group was introduced (**7**), followed by the reduction with $LiAlH_4$. This reaction sequence selectively afforded the mono-methylated amine **8a** in excellent yields. **8a** as well as the commercially available 2-(3,4-Dimethoxyphenyl)-*N*-methylethylamine (**8b**) were coupled to the epoxide **3** in a S_N2 reaction generating α-amino alcohols **9a**,**b** in high yields. The key step in the synthesis is an acid catalyzed ring-closure using polyphosphoric acid (PPA) or Eaton`s reagent affording the 1-phenylbenzazepine derivatives **10a** and **10b**. The dimethoxy-substituted structure **9b** could be converted into **10b** with PPA at 100 °C in one hour. Applying the same reaction conditions for **9a** only resulted in a partial conversion of the starting material, whereas an increase in reaction time led to a deprotection of the methoxy-group. The purification of the free phenol derivative from the pure PPA resulted to be very complex because of the amphoteric nature of the molecule, which made it very difficult to extract it from the aqueous to the organic phase. The low conversion was probably caused by the chlorine substituent which deactivates the aromatic ring for electrophilic substitution reactions. Therefore, regarding the conversion of **9a** a different synthetic approach was chosen. 72 h at room temperature in Eaton's Reagent (10 wt % phosphoric pentoxide in methanesulfonic acid) generated **10a** in moderate

yields but without the cleavage of the methoxy group. Demethylation of the phenolic methoxy groups using boron tribromide (BBr_3; **11a**,**b**) followed by the protection with triisopropylsilyl (TIPS) chloride and *tert*-butyldimethylsilyl (TBS) chloride, respectively, afforded structures **12** and **14**. Reductive hydrogenation of the nitro group using palladium on charcoal as a catalyst yielded the anilines **13** and **15**.

Scheme 2.1: Synthesis of 1-phenylbenzazepine derivatives **13** and **15** as D_1R pharmacophores.

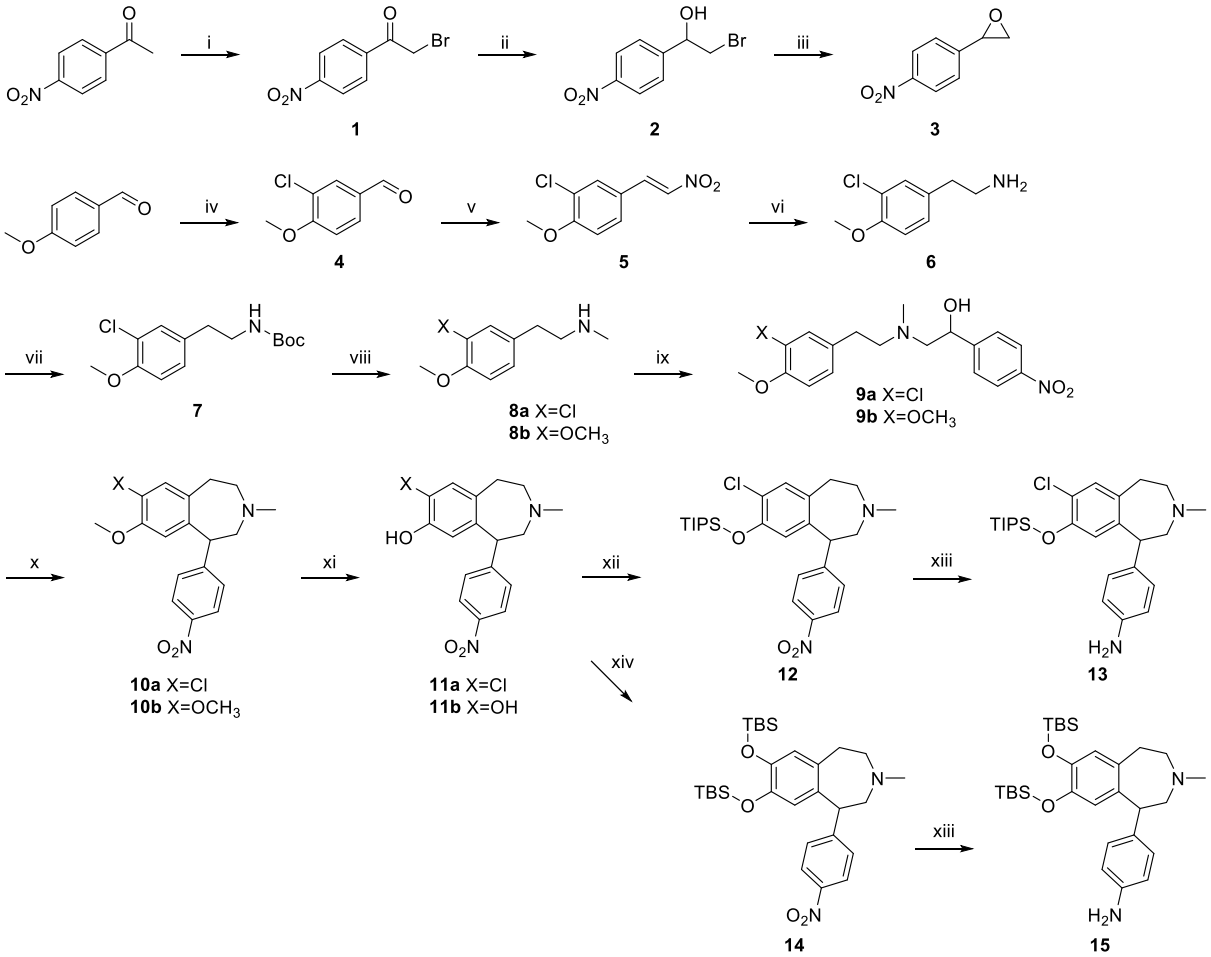

[a] Reagents and conditions: i) NBS, pTsOH, DCM, reflux, overnight, 64 %; ii) $NaBH_4$, MeOH, rt, 1 h, 66 %; iii) K_2CO_3, THF, reflux, overnight, 87 %; iv) SO_2Cl_2, AcOH, rt, overnight, 86 %; v) $MeNO_2$, NH_4OAc, AcOH, reflux, 4 h, 68 %; vi) $LiAlH_4$, THF, reflux, 3 h, 94 %; vii) Boc_2O, DCM, rt, overnight, 98 %; viii) $LiAlH_4$, THF, reflux, 3 h, 90 %; ix) **3**, MeCN, reflux, overnight, 90 %; x) a) **9a**, Eaton's reagent, rt, 72 h, 45 %, b) **9b**, PPA, 100 °C, 1 h, 69 %; xi) BBr_3, DCM, -78 °C, overnight, 84 %; xii) TIPSCl, imidazole, NEt_3, DMF, rt, overnight, 90 %; xiii) H_2, Pd/C, THF/MeOH, rt, overnight, 95 %; xiv) **11b,** TBSCl, DMAP, NEt_3, DCM/DMF, rt, overnight, 57 %.

To couple the pharmacophore with the spacer via a CuAAC reaction an alkyne group needed to be added. In a first attempt, propargyl amine was added to succinic anhydride and the product was connected to the aniline **11a** using HATU as a peptide coupling reagent to afford the alkyne-functionalized building block **18** (Scheme 2.2B). The insertion of a sulfonamide moiety instead of a

peptide group at the 4'-position of the 1-phenyl-2,3,4,5-tetrahydro-benzazepines was reported to increase affinity at the D_1R.[176] To achieve this goal two different sulfonyl chlorides were required (**17a**,**b**; Scheme 2.2A), which were synthesized from the respective alkyl bromides using thiourea and *N*-chlorosuccinimide (NCS).[187] The reaction of sulfonyl chloride **17a** to **13** in the presence of pyridine afforded structure **19**. Ester hydrolysis in basic conditions followed by a peptide coupling reaction using HATU with propargylamine yielded the final building block **20** (Scheme 2.2B). The reaction of **15** with **17b** afforded structure **21**. Hydrogenolytic ester cleavage using palladium on charcoal as a catalyst followed by a peptide coupling with propargylamine using HATU allowed the insertion of the alkyne group while retaining the *tert*-butyl-dimethyl silyl (TBS) protecting groups (**22**; Scheme 2.2C).

Scheme 2.2: Synthesis of final alkyne-functionalized D_1R building blocks **18**, **20,** and **22**.[a]

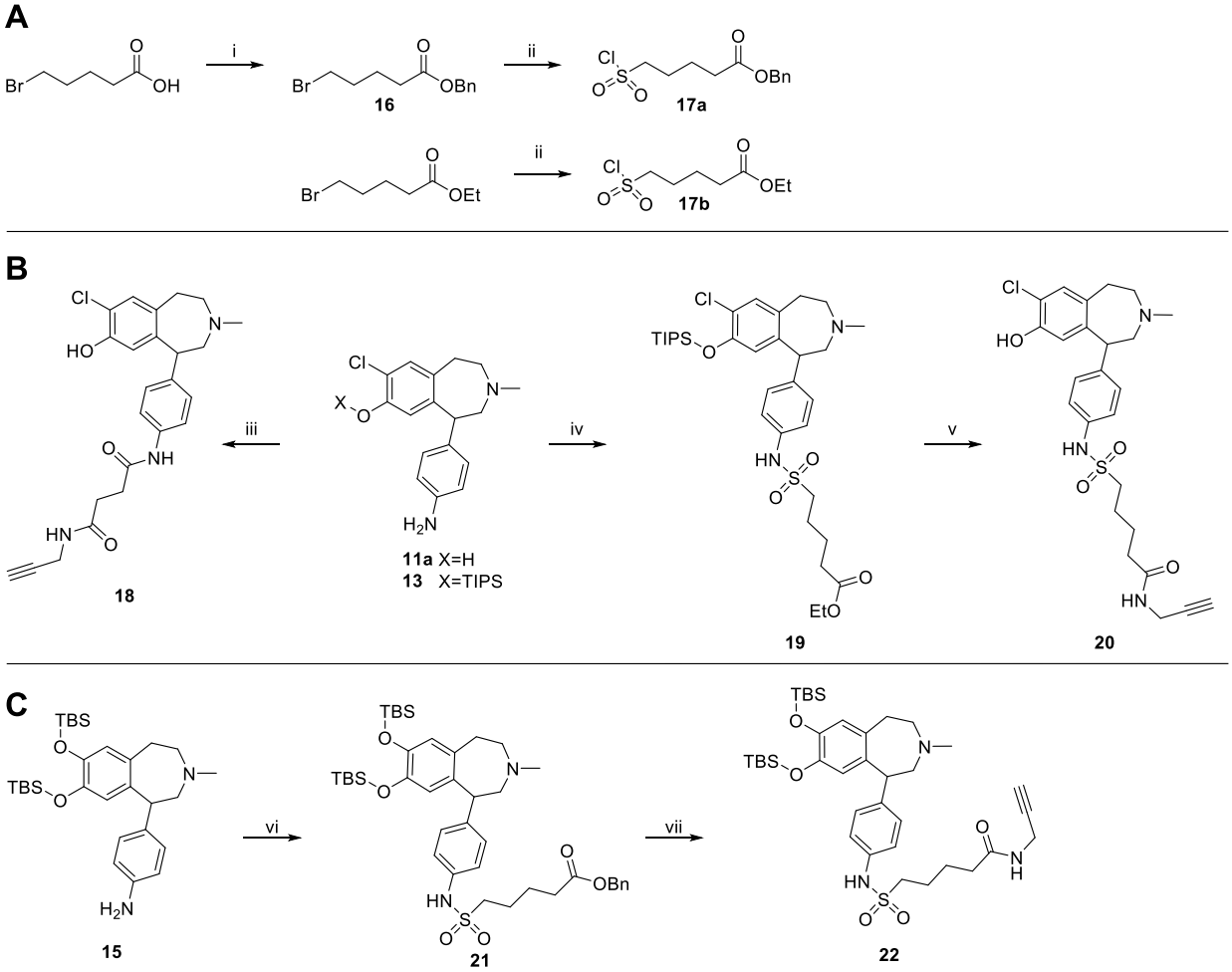

[a] Reagents and conditions: i) BnOH, DMAP, DCC, DCM, rt, overnight, 89 %; ii) 1. Thiourea, EtOH, overnight, reflux, 2. NCS, MeCN, 2N HCl, 30 min, 5 °C, 87 %; iii) 1. succinic anhydride, propargyl amine, DMF, rt, 3h; 2. **11a**, HATU, DIPEA, DMF, rt, overnight, 48 % ; iv) **17b**, pyridine, $CHCl_3$, 50 °C, overnight, 56 %; v) 1. LiOH, H_2O/THF, rt, overnight, 2. propargylamine, HATU, DIPEA, DMF, rt, overnight, 92 %; vi) **17a**, pyridine, $CHCl_3$, 50 °C, overnight, 59 %; vii) 1. Pd/C, H_2, MeOH, 60 °C, 3h; 2. propargylamine, HATU, DIPEA, DMF, rt, overnight, 62 %.

2.2.2 Synthesis of the H_3R building blocks

The synthesis of the antagonistic H_3R building block **27** was performed following previously described protocols by Apodaca *et al*. and Wingen *et al*.[178,188] The commercially available 4-hydroxybenzaldehyde was converted in a S_N2 reaction with 1-bromo-3-chloropropane to produce **23** (Scheme 2.3A). A second S_N2 reaction with piperidine afforded compound **24**, which was converted to **25** by a reductive amination with sodium triacetoxyborohydride. Acid catalyzed ester hydrolyzation (**26**) followed by a HATU catalyzed peptide coupling to propargyl amine generated the final JNJ-based building block **27** in good yields.

Immepip (**29**) was synthesized following the procedures of Kitbunnadaj *et al*.[189] *N*-Boc-4-piperidineacetaldehyde was converted to the imidazole in a Van Leusen reaction.[190] First the aldehyde was stirred with toluenesulfonyl methyl isocyanide and NaCN for 2 h at room temperature. The resulted product was heated in a microwave in saturated ammonia in ethanol to 120 °C (approx. 10 bar) affording the imidazole **28** in moderate yields (Scheme 2.3B). Deprotection of the Boc-protecting group followed by a nucleophilic substitution with commercially available propargyl bromide yielded structure **30**. As an alternative building block a longer alkyl linker was introduced (**32**). Therefore, 5-hexyn-1-ol was converted to the bromide (**31**) in an Appel-reaction using triphenylphosphine and carbon tetrabromide as a brominating agent.[191] Nucleophilic substitution of **31** with immepip (**29**) yielded the building block **32** (Scheme 2.3B).

Scheme 2.3: Synthesis of the alkyne-functionalized H_3R building blocks **27**, **30**, and **32**.[a]

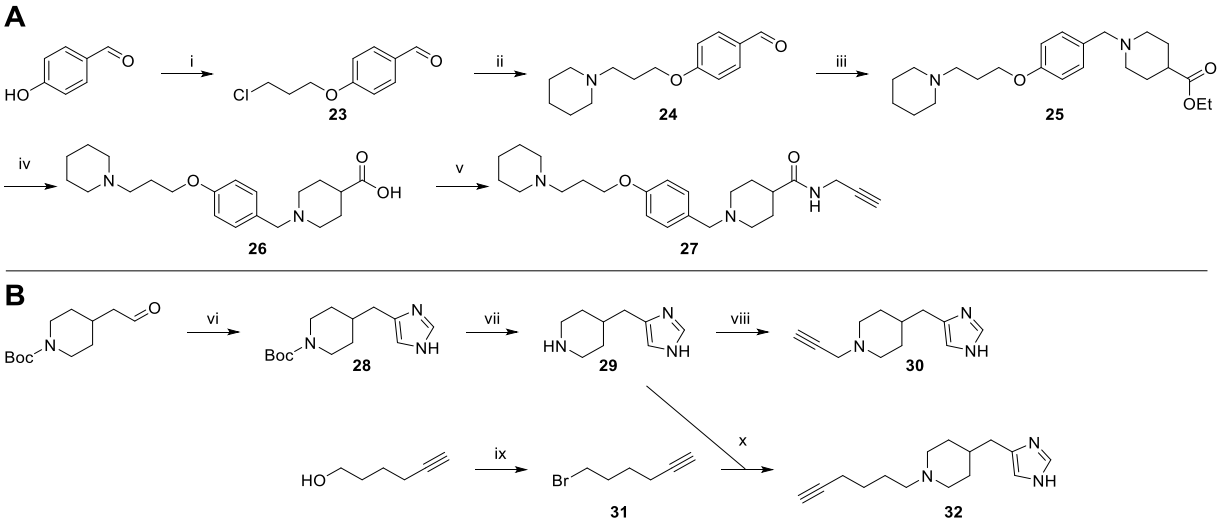

[a] Reagents and conditions: i) 1-Br-3-Cl-propane, K_2CO_3, MeCN, reflux, 18 h, 89 %; ii) piperidine, Na_2CO_3, KI, MeCN, reflux, 20 h, 76 %; iii) ethyl isonipecotate, $NaBH(OAc)_3$, $CHCl_3$, rt, overnight, 95 %; iv) 2 N aq. HCl, THF, rt, overnight, 92 %; v) EDC*HCl, HOBt, DIPEA, propargylamine, 30 min, 100 °C, MW, 72 %; vi) 1. *p*-toluenesulfonylmethyl isocyanide, NaCN, EtOH, rt, 2h; 2. NH_3, EtOH, 120 °C, MW, 2 h, 60 %; vii) TFA, DCM, rt, overnight; viii) Na_2CO_3, propargyl bromide, EtOH, rt, overnight, 35 %; ix) PPh_3, CBr_4, DCM, rt, 2 h, 88 %; x) K_2CO_3, EtOH, rt, overnight, 80 %.

The nucleophilic substitution reaction of the alkylic bromides with **29** could theoretically occur at the imidazole moiety or at the secondary aliphatic amine. The latter should be more reactive due to its higher basicity and nucleophilicity. To prevent substitutions at the imidazole moiety as a side product, the reaction was carried out at room temperature. Although it was expected that the reaction would take place exclusively at the secondary aliphatic amine 2D NMR analysis was performed to assure the correct product formation. A $^1H/^1H$ Nuclear Overhauser Effect Spectroscopy (NOESY) spectrum of structure **30** was recorded. This 2D NMR spectroscopy method enables the detection of non-scalar correlations between protons that are in close proximity to each other by measuring the $^1H/^1H$ Nuclear Overhauser Effect (NOE).[192] On both axis a ^1H-spectrum is shown (Figure 2.3).[193] The red signals on the diagonal depict cross-signals between the same cores and are not evaluated.[193] The blue signals represent the NOE between two different cores.[193] In this spectrum no signal was detected indicating a close proximity between the aromatic hydrogens of the imidazole and those of the propargylic side chain. However, after assigning the different signals to their respective hydrogens based on their ^1H NMR shifts and coupling constants, a proximity between the hydrogen atoms of carbon atom 13 and the hydrogen atoms of carbons 1 and 3 could be detected. The hydrogens of the carbons 1 and 3 respectively split into two different signals (1,3 and 1'3') due to the different confirmations of the ring system.[194] These results confirm the structural identity of **30**. For structure **32** the same results were obtained but are not shown in this thesis.

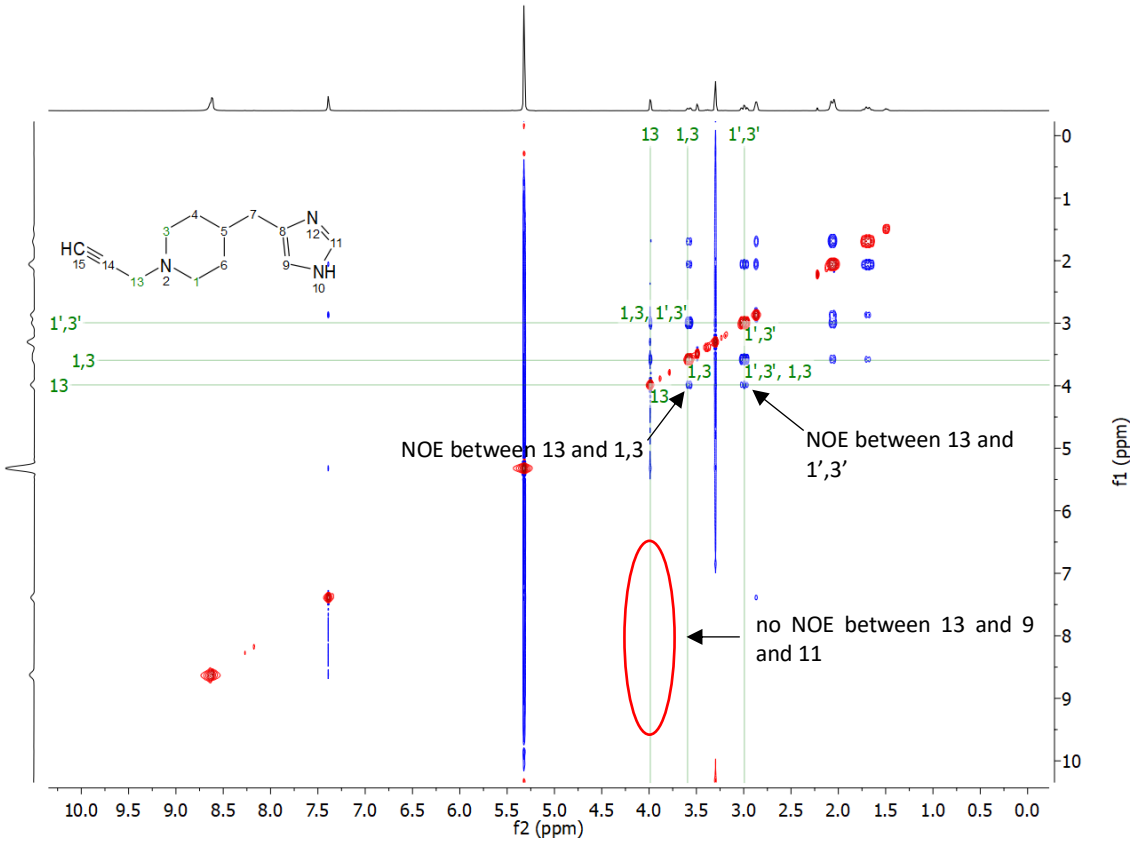

Figure 2.3: NOESY spectrum of **30**. The cross signals of the protons are depicted in red, whereas NOE interactions are depicted in blue. The different signals were assigned to the respective hydrogens based on the ^{1}H NMR shifts and coupling constants. The blue dots at the crossing of the lines from 13 and 1,3 or 1',3' respectively indicate a close proximity between the hydrogens.

2.2.3 Synthesis of the spacers

The polyethylene glycol spacers were synthesized starting from the commercially available tri-, tetra-, penta- and hexaethylene glycol following the reaction protocol published by Iyer, S. *et al*. (Scheme 2.4A).[195] After the introduction of the mesylate moieties (**33a-d**) as good leaving groups the terminal azide groups were inserted under S_N2 conditions (**34a-d**). A selective Staudinger-type reduction of one azide group in a heterogenous mixture of 1 N aqueous HCl and ethyl acetate yielded the primary amines (**35a-d**). This reaction allows the selective reduction of one azide group without using an excess of the diazides. Once the amine is formed in the reaction mixture it is directly protonated by the hydrochloric acid and transferred into the aqueous phase. Therefore, the second azide group is not available in the organic phase for a second reduction step. After the reaction of these amines with glutaryl chloride the final spacers **36a-d** with terminal azide groups were obtained in good yields.

Scheme 2.4: Synthesis of the spacers **36a**-**d** and **39a**,**b**.[a]

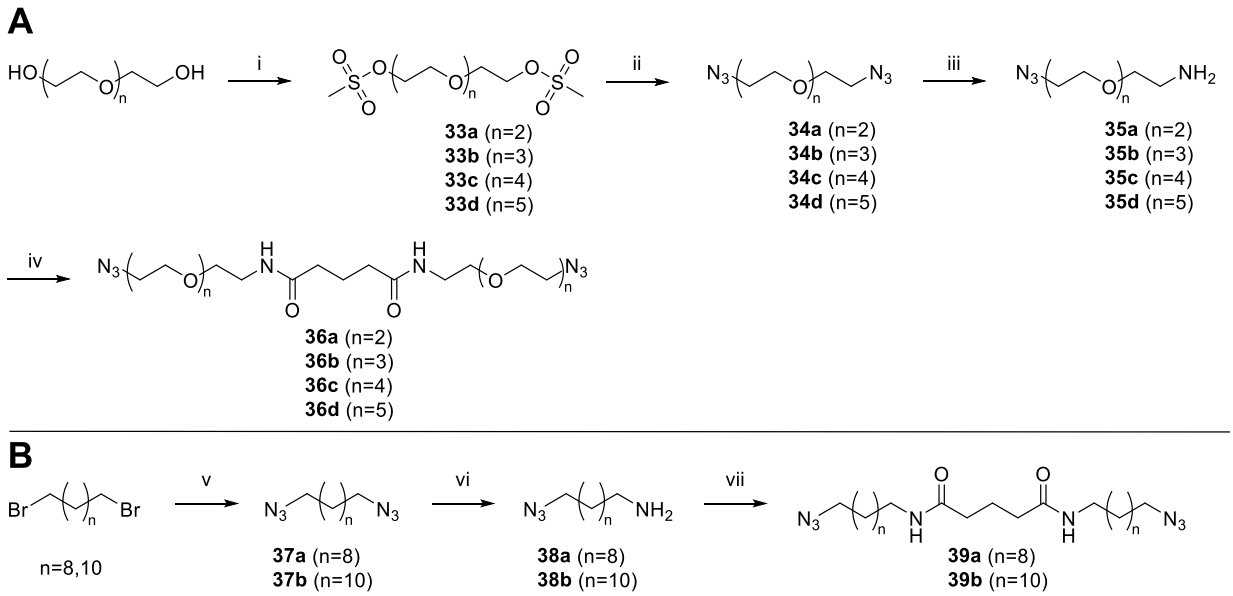

[a] Reagents and conditions: i) methanesulfonyl chloride, NEt_3, DCM, rt, overnight, 78-97 %; ii) NaN_3, EtOH/DMF (4:1), reflux, overnight, 92-99 %; iii) PPh_3, 1 N HCl/THF/EtOAc (5:1:5), rt, overnight, 47-77 %; iv) glutaryl chloride, NEt_3, DCM, rt, overnight; 34-92 %; v) NaN_3, EtOH/DMF (4:1), reflux, overnight, 93-97 %; vi) PPh_3, THF, rt, overnight, 33-38 %; vii) glutaryl chloride, NEt_3, DCM, rt, overnight; 54-81 %.

The alkylic spacers (**39a**,**b**) were synthesized following the same synthetic route starting from the commercially available 1,10-dibromodecane and 1,12-dibromododecane (Scheme 2.4B). The selective Staudinger type reduction of one azide group resulted in very low yields (< 10 %), most likely because of the poor water solubility of the protonated alkylic amines (**38a**,**b**). Therefore, this reaction was performed in THF with an excess (3 eq) of the diazides (**37a**,**b**) and slow addition of PPh_3. By using this synthetic approach the yield was improved to 33 % and 38 %, respectively. The last step could then be performed in the same manner as for the PEG-based counterparts affording the final alkylic spacers **39a**,**b** in good yields.

2.2.4 Synthesis of bivalent ligands in a one-pot reaction

The synthesis of the final bivalent ligands was achieved by a one-pot CuAAC reaction. For this reaction equimolar amounts of both building blocks and the spacer were dissolved in a mixture of DCM and MeOH (1:1). Copper(II)sulfate pentahydrate in combination with ascorbic acid to form the reactive copper(I)-species in situ were used as catalyst. Using the one-pot approach lowered the expected maximum yield of the reaction but had the advantage of a single purification step. Furthermore, it allowed the accessible synthesis of a set of different bivalent ligands by interchanging just one of the three components. For example, bivalent ligands **40**-**43** could all be synthesized with the same building

blocks by adding a different spacer (Scheme 2.5A). This synthetic approach avoided the need for an individual building block for each bivalent ligand making the synthesis of a broad variety of final compounds more accessible. As side products the homo-bivalent ligands containing two D_1R or two H_3R pharmacophores were formed. Isolation and purification of the desired products was achieved by preparative HPLC. Because of the similar chemical structure of the different products in the reaction mixture the purification of the desired hetero-bivalent ligands was difficult in some cases. This led to lower yields despite high conversion rates of the starting compounds.

Scheme 2.5: Synthesis of bivalent ligands **40**-**47**.[a]

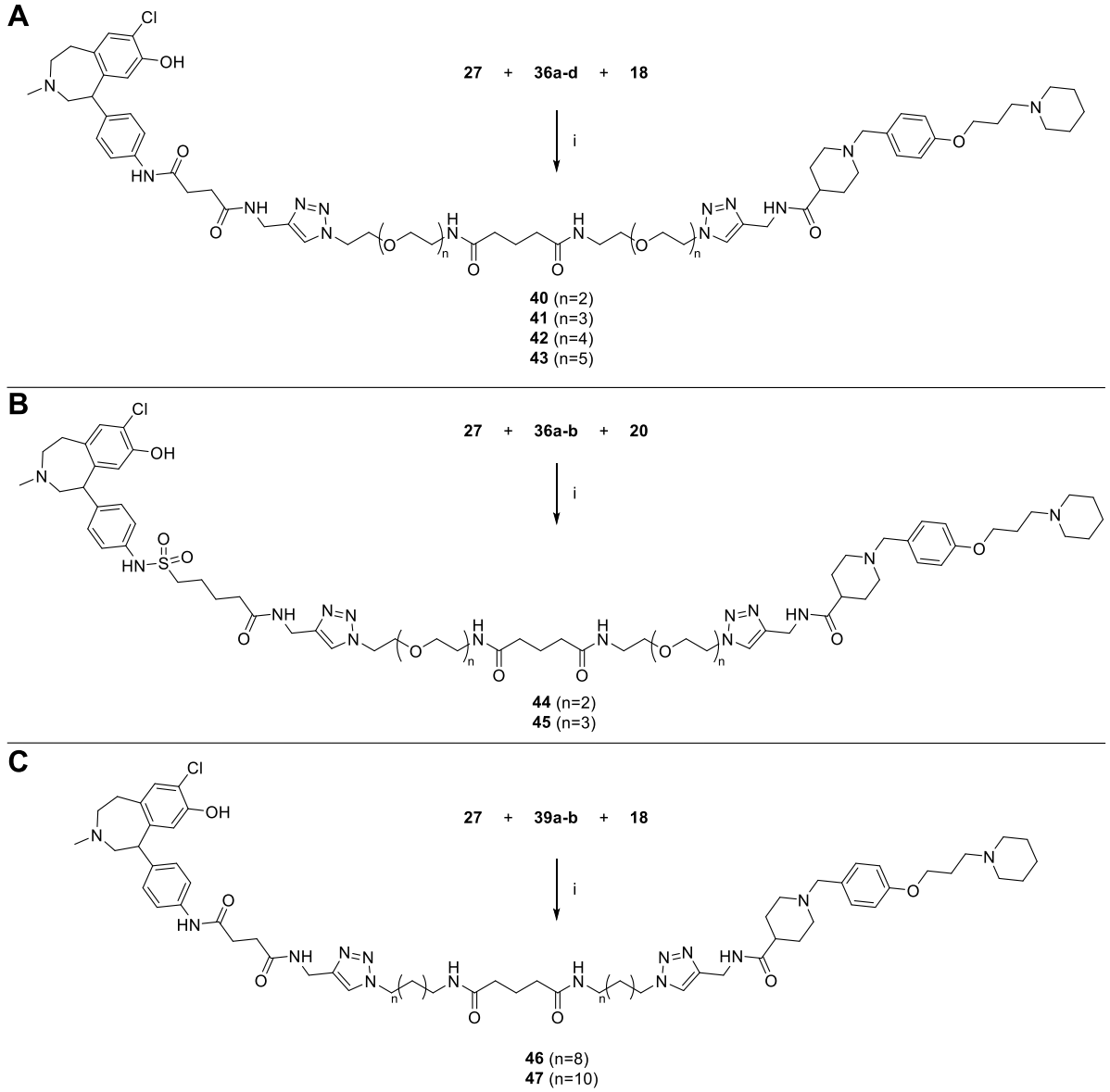

[a] Reagents and conditions: i) $CuSO_4$, ascorbic acid, DCM/MeOH (1:1), rt, 72 h, 4-25 %.

The antagonistic building blocks **27** (H_3R) and **18** (D_1R) were combined with the spacers **36a-d** to form bivalent ligands **40**-**43** with a linker range from 39 to 57 atoms between both pharmacophores (Scheme 2.5A). The same reaction was performed with the modified D_1R building block **20** and the linkers **36a** and **36b** to yield structures **44** and **45** (Scheme 2.5B). Only these two spacers were chosen because they yielded bivalent ligands with a distance between both pharmacophores of 41 and 47 atoms, respectively. These lengths should suffice to allow simultaneous binding based on the modeling results of the D_1-H_3 Het. Bivalent ligands **44** and **45** containing the alkylic linkers were synthesized in the same way using compounds **27**, **18**, and **39a**,**b** (Scheme 2.5C).

2.2.5 Sequential synthesis of bivalent ligands

The one-pot approach turned out to be unsuccessful for the synthesis of the SKF-based bivalent ligands. A one-pot synthesis with a SKF-based building block with deprotected phenolic hydroxy groups afforded a mixture of the homo- and hetero-bivalent ligands that could not be separated by preparative HPLC. As an alternative the reaction was performed with the TBS-protected D_1R building block **22**. This approach was expected to facilitate the separation of the different products because the bulky, aliphatic silyl groups increase the difference in lipophilicity of the homo- and hetero-bivalent ligands. Unfortunately, this approach yielded almost exclusively homo-bivalent ligands. A reason for this could be different reaction velocities of both pharmacophores due to different solubility profiles. Structure **53** with an immepip-based H_3R-pharmacophore was also synthesized in a one-pot reaction but afforded a very low yield of 3 % (Scheme 2.6B).

Therefore, a different synthetic approach for the other immepip-based (**54**-**56**) and the SKF-based bivalent ligands (**49**,**50**) had to be applied. The first step was the connection of one building block to the spacer followed by the coupling of the purified product to the second building block. To reduce the formation of homo-bivalent ligands in the first reaction a fivefold excess of the spacer was used, which could be recovered after the reaction. The JNJ-based building block **27** was coupled to spacers **36a** and **36b** resulting in compounds **48a**,**b** (Scheme 2.6A). In a second CuAAC reaction with SKF-based building block **22**, **48a**,**b** were converted into the final bivalent ligands **49** and **50**. Prior to the purification by preparative HPLC the TBS protecting groups were removed by the addition of 10 % aq. TFA.

The immepip-based building block **30** was coupled to the spacer **36b** affording product **51**, which was converted to the bivalent ligand **54** (Scheme 2.6B)**. 54** is the equivalent, with a longer spacer (**36b** instead of **36a**), to bivalent ligand **53**, which was synthesized in a one-pot reaction.

The reaction of SCH-based pharmacophore **20** with spacers **36a** and **36b** afforded products **52a** and **52b**, which were then coupled to the immepip-based building block with a longer alkylic linker (**32**)

yielding bivalent ligands **55** and **56** (Scheme 2.6B). All of these CuAAC reactions were performed in a mixture of *tert*-butanol and water (1:1) using copper sulfate pentahydrate and ascorbic acid as catalyst and *tris*-(benzyltriazolylmethyl)-amine (TBTA) as a copper(I)-chelating ligand. This synthetic protocol accelerated the reaction time from 72 h to an overnight reaction.

Scheme 2.6: Synthesis of bivalent ligands **49**, **50**, and **53**-**56** in a two-step synthesis.[a]

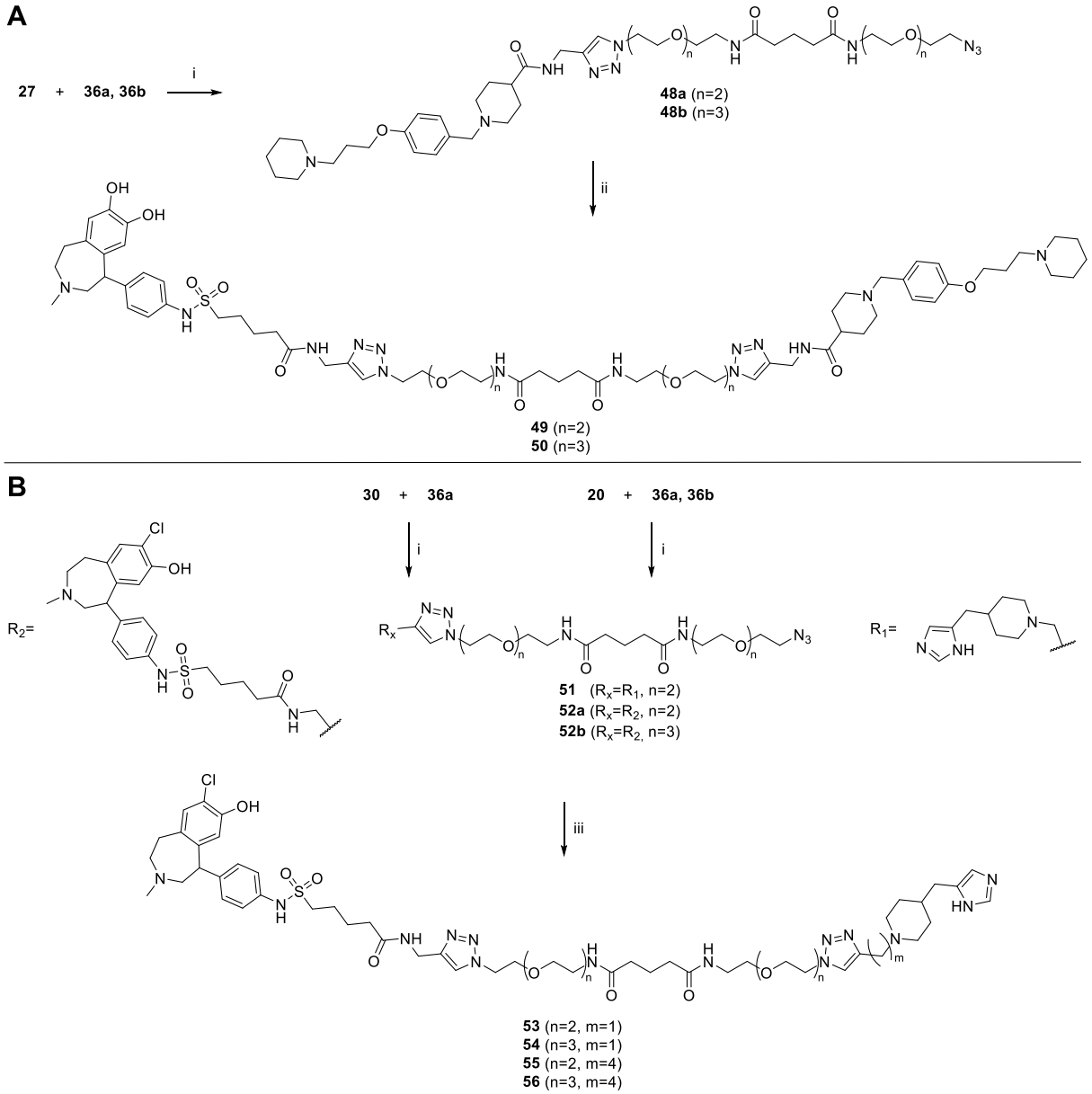

[a] Reagents and conditions: i) 5 eq of **36a**,**b**, $CuSO_4$, ascorbic acid, TBTA, $H_2O/^tBuOH$ (1:1), rt, 15 h, 27-53 %; ii) 1. $CuSO_4$, ascorbic acid, TBTA, $H_2O/^tBuOH$ (1:1), rt, 15 h; 2. 10 % aq. TFA, MeCN/H_2O, rt, 1 h, 12-69 %; iii) for product **53**: **51**, **20**, $CuSO_4$, ascorbic acid, TBTA, $H_2O/^tBuOH$ (1:1), rt, 15 h, 12 %; for product **54** (one-pot reaction): **20**, **30**, **36b**, $CuSO_4$, ascorbic acid, DCM/MeOH, rt, 72 h, 3 %; for product **55**: **52a**, **32**, $CuSO_4$, ascorbic acid, TBTA, $H_2O/^tBuOH$ (1:1), rt, 15 h, 16 %; for product **56**: **52b**, **32**, $CuSO_4$, ascorbic acid, TBTA, $H_2O/^tBuOH$ (1:1), rt, 15 h, 12 %.

2.2.6 Synthesis of the endcapped ligands

As a negative control, to prove that a possible change in binding behavior of a bivalent ligand is indeed caused by a bivalent binding mode, so-called endcapped ligands were synthesized. These ligands consist of just one pharmacophore, which is attached to the same spacer as the bivalent ligand but without the second pharmacophore. In order to achieve this, propargyl amine was acetylated (**57**) and subsequently coupled to the spacer **36a** yielding product **58** (Scheme 2.7). For the synthesis of the final endcapped ligands **59**-**62** the different building blocks were attached to **58** in a CuAAC reaction.

Scheme 2.7: Synthesis of the endcapped ligands **59**-**62**.[a]

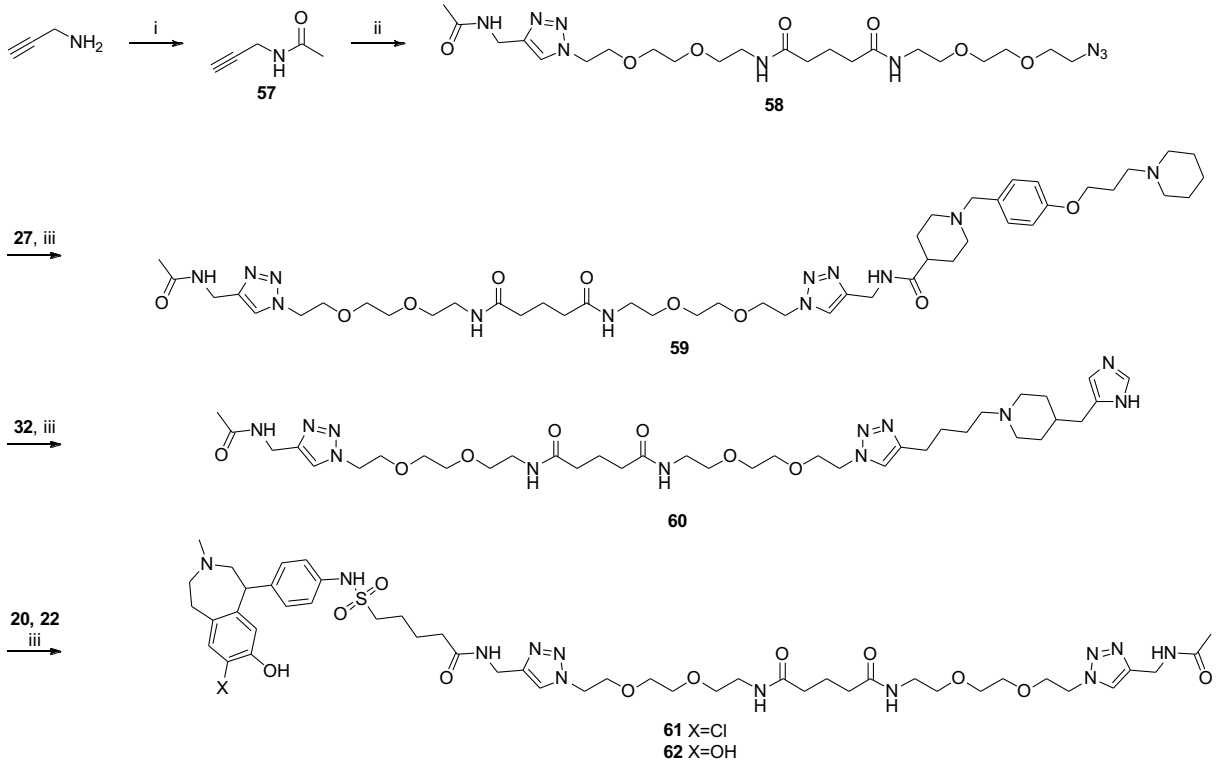

[a] Reagents and conditions: i) acetyl chloride, NEt_3, DCM, rt, overnight, 80 %; ii) **36a**, $CuSO_4$, ascorbic acid, TBTA, H_2O/^{t}BuOH (1:1), rt, overnight, 83 %; iii) $CuSO_4$, ascorbic acid, TBTA, H_2O/^{t}BuOH (1:1), rt, overnight, 20-30 %.

2.2.7 Synthesis of D_1R ligands

As an additional control the SCH- and SKF-based pharmacophores were synthesized without the spacers, with only a mesylate group. These compounds can be used as reference compounds to determine the effect on the binding behavior caused by the attachment of the spacer. For this purpose, methanesulfonyl chloride was added to compounds **13** and **15** to add a methanesulfonyl group at the aromatic amino moiety (Scheme 2.8). Deprotection of the silyl protecting groups using tetrabutylammonium fluoride and purification by preparative HPLC afforded the final products **63** and

64. For the H_3R pharmacophores the ethyl ester (**25**) was used as a reference for the JNJ-based bivalent ligands. The pharmacological properties of immepip are well established,[189,196,197] therefore no additional reference compound was synthesized and tested.

An overview of all synthesized bivalent, endcapped, and reference ligands with their respective spacer length and pharmacophore combination is given in Table 2.1 together with the results of competition binding experiments at the D_1R and H_3R (chapter 2.3.1).

Scheme 2.8: Synthesis of D_1R ligands **63** and **64** as reference compounds.[a]

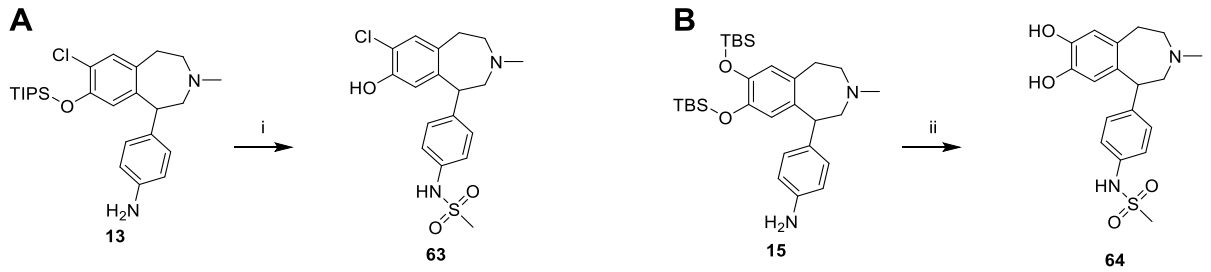

[a] Reagents and conditions: i) 1. MsCl, NEt_3, DCM, rt, overnight; 2. TBAF, THF, rt, 30 min, 33 %; ii) 1. MsCl, pyridine, CHCl3, rt, overnight; 2. TBAF, THF, rt, 30 min, 26 %.

The purity and stability of all bivalent, endcapped, and reference ligands was determined by HPLC (HPLC runs are presented in the Appendix; chapter 8.1). The chemical structure of all synthesized compounds was proven by ^1H and ^{13}C NMR as well as HRMS. The chemical structures and ^1H NMR spectra of the bivalent, endcapped, and reference ligands are presented in the Appendix (chapter 8.2).

2.2.8 ^1H NMR spectra of 1-phenyl-2,3,4,5-tetrahydro-1*H*-benzazepines

Analyzing the ^1H NMR spectra of the synthesized compounds, a peculiarity was observed for the compounds containing the 1-phenyl-2,3,4,5,tetrahydro-1*H*-benzazepine partial structure of the D_1R pharmacophore. In Figure 2.4 cutouts of two NMR spectra of compound **18** are presented. The upper spectrum (black) was recorded after purification of **18** by flash chromatography resulting in the free base of **18**. The singlet peak at 6.16 ppm was assigned to the hydrogen atom bound to carbon 3 (see chemical structure in Figure 2.4) based on its chemical shift and multiplicity. The lower spectrum (blue) was recorded of structure **18** after purification by preparative HPLC yielding the TFA salt of **18** (protonated at the tertiary amine). The peak at 6.16 ppm of this spectrum integrates to only 0.72 hydrogens in reference to the other aromatic peaks. An additional peak at 6.71 ppm was detected with an integral of 0.28 hydrogens. Therefore, it was suspected, that both signals can be assigned to the same nucleus (hydrogen bound to carbon 3).

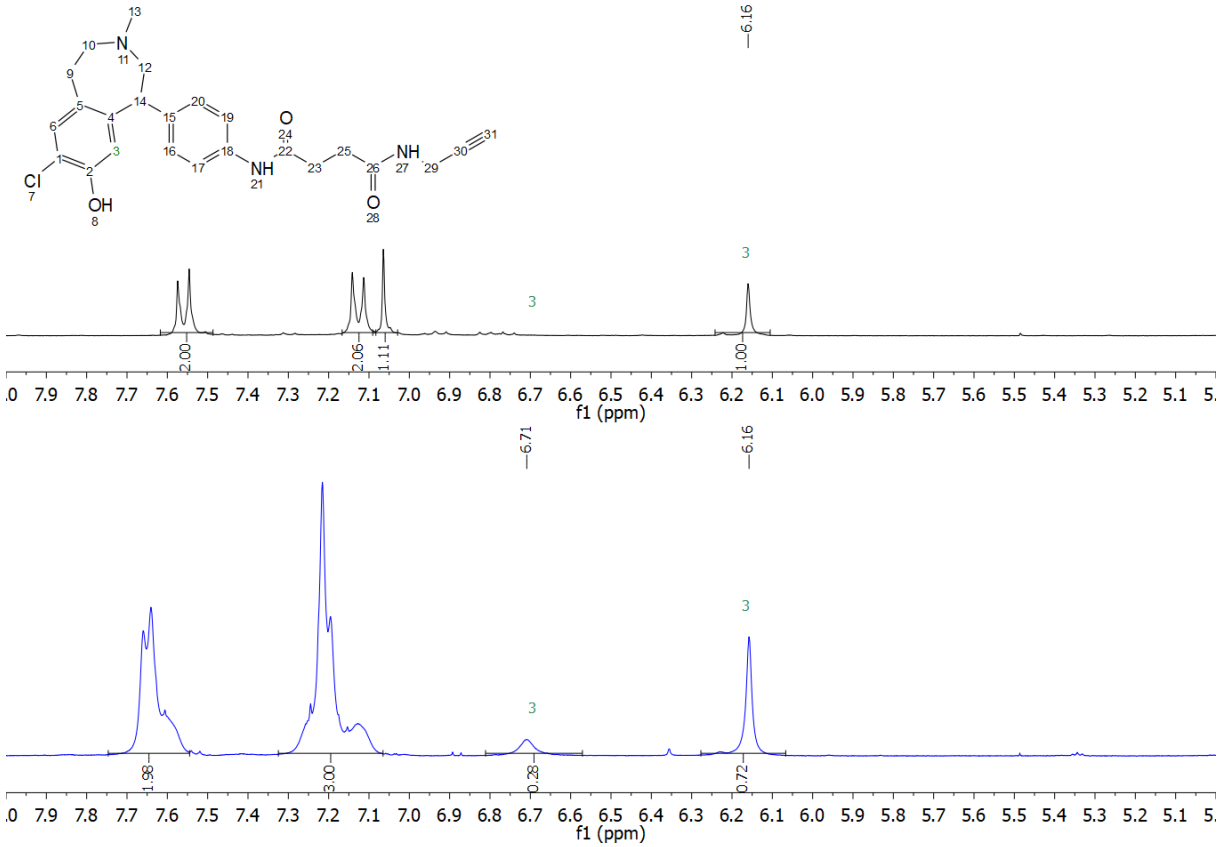

Figure 2.4: Chemical structure and aromatic region of the ^{1}H NMR spectrum of **18** (free base) in CD_3OD (top, black). Aromatic region of the ^{1}H NMR spectrum of **18** (TFA salt) in CD_3OD (bottom, blue).

In order to validate this hypothesis an additional ^{1}H-^{1}H rotating frame overhauser enhancement specroscopy (ROESY) spectrum was recorded. Similar to NOESY this NMR method allows the detection of the proximity of protons by detecting an NOE in a rotating frame[198]. The aromatic region of the ^{1}H-^{1}H ROESY spectrum of the TFA salt of **18** is presented in Figure 2.5. Similar to NOESY spectra along the diagonal the cross signals of the distinct protons are visible in red and have always a positive phase (red) in ROESY spectra.[198,199] ROE dipolar relaxation signals of two protons in close proximity are indicated by blue signals (negative phase).[198] For the signals of interest at 6.16 and 6.71 ppm cross peaks could be detected in the ROESY spectrum. Because these cross-peaks are in the same phase as the diagonal (red), they don't represent ROE cross relaxation between two distinct nuclei but are cross peaks due to chemical exchange of the same nucleus.[198] Chemical exchange means that a nucleus is changing between two different environments leading to a change in the chemical shift.[200] In the case of **18** the different environments can be caused by different enantiomers and/or ring conformations of the seven membered heterocycle.

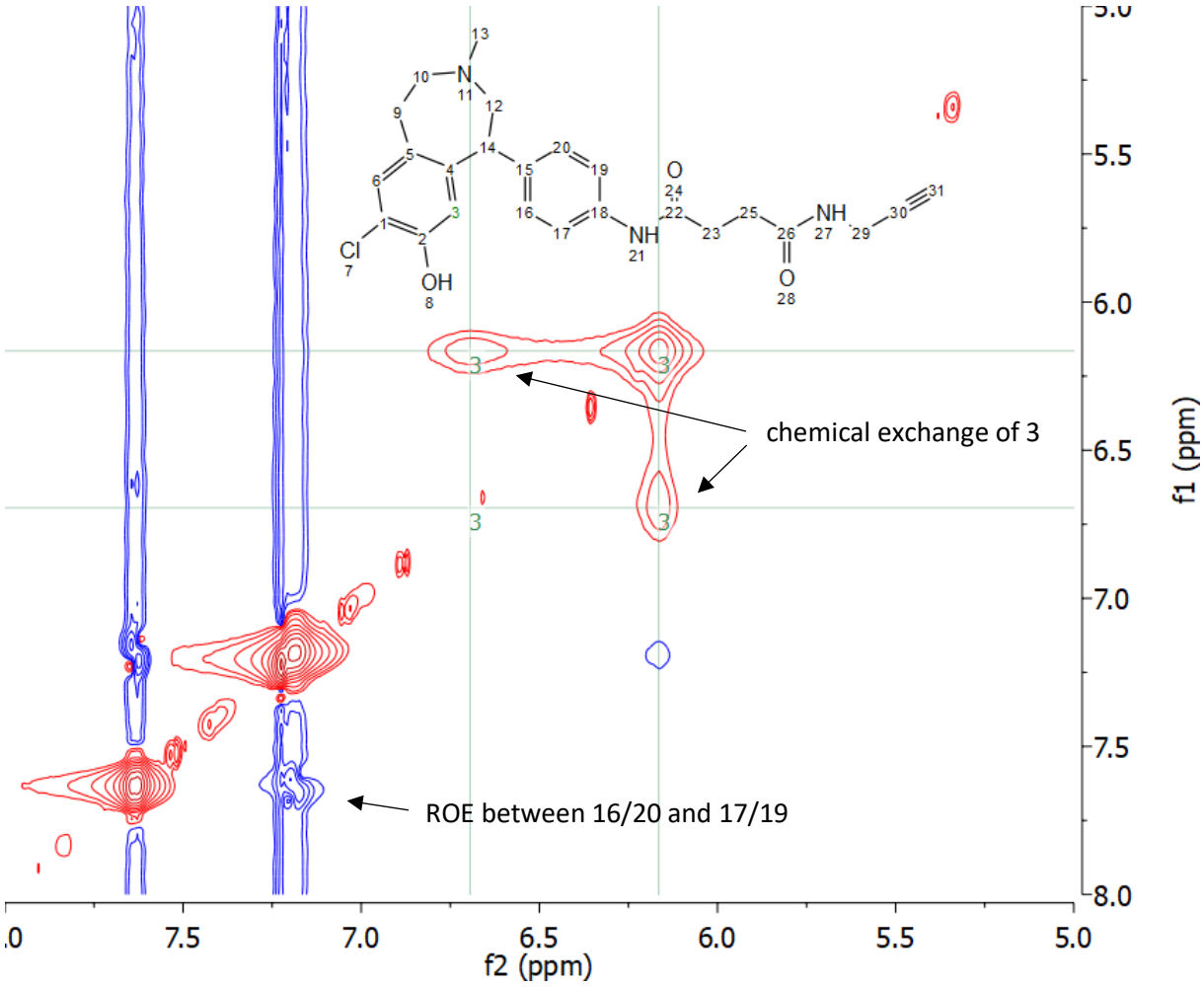

Figure 2.5: Aromatic region of the ^{1}H-^{1}H ROESY spectrum of **18** (TFA salt).

The phenomena of the split-up signal could be observed for all compounds containing this structural motif if they were purified by preparative HPLC, hence the tertiary amine was protonated. The split of one signal into two distinct signals and the broadening of the other aromatic peaks indicate a dynamic process, probably the interchange between two distinct conformations. However, no further efforts were made to determine the exact conformations of the compounds that cause the different signals in the ^{1}H NMR spectra or why this phenomenom can only be observed after protonation, because the focus was to prove the general chemical structure of the compounds. This was achieved with NMR spectra in combination with HRMS. Whenever this split-up peak pattern was observed for a compound it was denoted as d* in the chemical experimental section (chapter 6.1.2) with the coupling constant *J*.

It has to be noted that the NMR signals of the aliphatic hydrogens of the seven-membered ring are most likely also affected by the protonation and different conformations. However, a separation of one signal into two could not be detected as easily because of the already complex and overlapping signals of the different nuclei. The complex scalar coupling between the different hydrogens of the ring

system, as well as the high density of signals in that area of the spectrum, make it very difficult to assign distinct peaks to specific hydrogens.

2.3 Pharmacological characterization

All of the bivalent ligands, endcapped ligands, and reference ligands mentioned in chapter 2.2. were characterized pharmacologically for their binding properties at the D_1R and H_3R. For the determination of pK_i values at the D_1R, radioligand binding assays at homogenates of HEK-293T cells stably expressing the human (h) D_1R were performed.[201] Radioligand binding assays (RLBs) are a well-established method to determine the affinity of an unlabeled ligand towards a receptor. In these assays the decrease in receptor-bound radioactivity, caused by the displacement of a constant concentration of the radioligand by an unlabeled ligand, is measured. For the determination of the affinity towards the H_3R the newly established NanoBRET binding assay was used (see chapter 1.6 and 4).[157] This fluorescence-based alternative avoids the use of radioisotopes, which makes the handling of the assay easier and safer. The assay was performed using live HEK-293T cells stably expressing the NLuc-hH_3R.[202] To prove the validity of this assay a set of seven bivalent ligands was additionally tested in a standard radioligand binding assay for the H_3R using live HEK-293T cells stably expressing the hH_3R.[157] Furthermore, some selected bivalent ligands were tested for their selectivity within the dopamine and histamine receptor families, as well as for their intrinsic activity using a commercially available cAMP detection kit from PerkinElmer. The most promising compound **45** was additionally analyzed for its neuroprotective effect in primary mouse embryonal cortex cells. All data were analyzed using Prism GraphPad (version 9.4.0). The detailed experimental procedures and cell biological methods are described in chapter 6.2.

2.3.1 Competition binding experiments at the D_1R and H_3R

The first step of the pharmacological characterization of the novel bivalent ligands was the determination of their binding affinity towards their primary targets, the D_1R and H_3R. The results of these assays as well as the composition of the bivalent ligands are presented in Table 2.1.

The first set of ligands (**40**-**43**) possesses the same pharmacophores but have increasingly longer spacers (39-57 atoms). Therefore, this set is well suited for the analysis of the influence of the spacer on the receptor binding. Notably an increasing spacer length decreases the affinity of the bivalent ligand towards both receptors (pK_i (D_1R): from 8.10 to 7.39; pK_i (H_3R): from10.08 to 9.71). This was to be expected and is reported for a variety of bivalent ligands, but nevertheless **40-43** show an exceptional affinity in the low nanomolar range at the D_1R and sub-nanomolar range at the H_3R.[140] Because of the increasing size and molecular weight of these compounds, they are sterically more hindered, making it more difficult for the pharmacophores to obtain the right conformation for the receptor binding.

For the bivalent ligands with alkylic spacers **46** and **47** a big difference in binding affinity at both receptors was observed. The pK_i values of **46** (pK_i (D_1R) = 8.41; pK_i (H_3R) = 10.09) at both receptors are in the same range as those of **40** (pK_i (D_1R) = 8.10; pK_i (H_3R) = 10.08) and **41** (pK_i (D_1R) = 7.77; pK_i (H_3R) = 9.97), including a higher affinity at the D_1R. These compounds have PEG-based spacers of similar lengths. Surprisingly, **47** (pK_i (D_1R) = 6.59; pK_i (H_3R) = 7.16), which only differs structurally from **46** by two more carbon atoms in both aliphatic chains of the spacer, loses up to 100-fold affinity at both receptors compared to **46**. This huge loss of affinity is not likely to be caused by the slightly increased size of the bivalent ligand. Especially when **46** and **47** are compared to **40**-**43**, which have a larger difference in size but a smaller change in affinity. Possible reasons for this drastic change in receptor binding could be, that, due to the longer aliphatic chain, **47** has a higher lipophilicity. This could lead to adhesion at the plastic of the assay plate or the plastic cups that are used for the preparation of the dilutions leading to a decrease of the actual free ligand concentration in the well. Another problem could be a higher unspecific binding at cell membranes or other proteins. However, no further experiments were conducted to determine the reasons of this phenomenon because the other bivalent ligands showed more promising binding data. Moreover, the PEG-based bivalent ligands are better water-soluble making them more suitable for *in vitro* and *in vivo* assays.

Comparing the binding data at the D_1R of **40** (pK_i (D_1R) = 8.10; pK_i (H_3R) = 10.16) and **41** (pK_i (D_1R) = 7.77; pK_i (H_3R) = 9.97) to those of **44** (pK_i (D_1R) = 8.88; pK_i (H_3R) = 10.21) and **45** (pK_i (D_1R) = 8.67; pK_i (H_3R) = 10.00) it can be noted that the insertion of the sulfonamide group led to an increase in D_1R affinity and had, as expected, no influence on H_3R binding affinity. Despite their size **44** and **45** show exceptional K_i-values in the one-digit nanomolar range for the D_1R and sub-nanomolar range at the H_3R. Comparing the pK_i-values to those of the reference compound **63** (pK_i (D_1R) = 8.99) and JNJ (pK_i (H_3R) = 10.22)[157] there is only a small loss in affinity towards both receptors (less than 10-fold), despite the addition of the large spacers and the second pharmacophore. Compounds **49** (pK_i (D_1R) = 8.39; pK_i (H_3R) = 10.02) and **50** (pK_i (D_1R) = 7.83; pK_i (H_3R) = 9.99) with the SKF-based D_1R pharmacophores showed a lower affinity towards the D_1R than **44** and **45**, which was expected since the reference compound **64** (pK_i (D_1R) = 8.33) also has a lower pK_i value than **63**.

Compounds **40**-**43** and **45**-**47** were additionally tested in a H_3R radioligand binding assay to validate the results of the newly established NanoBRET binding assay. All values are in good agreement with those from the NanoBRET assay confirming that the addition of the NLuc to the receptor does not interfere with the binding of large ligands.

Table 2.1: Composition of the bivalent ligands and binding data at the D_1R and H_3R.

cmpd	D_1R building block[a]	H_3R building block[b]	linker length (atoms)[c]	pK_i ± SEM					
				D_1R (RLB)[d]	*N*	H_3R (NanoBRET)[e]	*N*	H_3R (RLB)[f]	*N*
40	SCH-1	JNJ	39	8.10 ± 0.06	3	10.08 ± 0.04	3	10.16 ± 0.01	2
41	SCH-1	JNJ	45	7.77 ± 0.06	3	9.97 ± 0.13	3	9.87 ± 0.11	2
42	SCH-1	JNJ	51	7.69 ± 0.09	3	9.84 ± 0.03	3	9.98 ± 0.06	2
43	SCH-1	JNJ	57	7.39 ± 0.02	3	9.71 ± 0.06	3	9.67 ± 0.08	2
44	SCH-2	JNJ	41	8.88 ± 0.07	3	10.21 ± 0.08	3	n.d.	---
45	SCH-2	JNJ	47	8.67 ± 0.10	4	10.00 ± 0.03	3	10.11 ± 0.10	2
46	SCH-1	JNJ	43 (alkyl)	8.41 ± 0.07	3	10.09 ± 0.04	3	10.03 ± 0.02	2
47	SCH-1	JNJ	47 (alkyl)	6.59 ± 0.02	3	7.16 ± 0.19	3	7.74 ± 0.06	2
49	SKF	JNJ	41	8.39 ± 0.01	3	10.02 ± 0.08	4	n.d.	---
50	SKF	JNJ	47	7.83 ± 0.05	3	9.99 ± 0.11	3	n.d.	---
53	SCH-2	immepip short	38	8.58 ± 0.06	3	5.89± 0.03	3	n.d.	---
54	SCH-2	immepip short	44	8.39 ± 0.12	3	5.66 ± 0.00	2	n.d.	---
55	SCH-2	immepip long	41	8.45 ± 0.11	3	6.09 ± 0.17	3	n.d.	---

56	SCH-2	immepip long	47	8.28 ± 0.03	3	6.07 ± 0.10	4	n.d.	---
59	endcapped	JNJ	---	< 5	3	9.99 ± 0.04	3	n.d.	---
60	endcapped	immepip long	---	5.42 ± 0.08	3	6.02 ± 0.06	3	n.d.	---
61	SCH-2	endcapped	---	7.91 ± 0.09	3	6.30 ± 0.06	3	n.d.	---
62	SKF	endcapped	---	7.26 ± 0.13	3	5.88 ± 0.08	3	n.d.	---
63	SCH-2	D_1R reference compound	---	8.99 ± 0.10	3	5.54 ± 0.05	3	n.d.	---
64	SKF	D_1R reference compound	---	8.33 ± 0.15	4	< 5	3	n.d.	---

[a]SCH-1: SCH-based building block with amide linkage to the linker (**18**), SCH-2: SCH-based building block with sulfonamide linkage to the linker (**20**), SKF: SKF-based building block (**22**). [b]JNJ: JNJ-based building block (**27**), immepip short: immepip-based building block with short alkylic linker (**30**), immepip long: immepip-based building block with long alkylic linker (**32**). [c]Number of atoms between both pharmacophores. [d]Competition binding experiments at HEK-293T cell homogenates stably expressing the hD_1R[201]; displacement of 0.2 nM, 0.4 nM or 1 nM [^{3}H]*N*-Methyl-SCH-23390 (K_d = 0.4 nM). [e]Competition binding experiments at HEK-293T cells stably expressing NLuc-hH_3R[202]; displacement of 0.5 nM UR-NR266[157] (K_d = 0.16 nM). [f]Comepetition binding assays at HEK293T-SP-FLAG-hH_3R cells[157]; displacement of [^{3}H]UR-PI294[203] (K_d = 3 nM). Data shown are mean values ± SEM of *N* independent experiments, each performed in triplicate. Data were analyzed by nonlinear regression and were best fitted to four parameter sigmoidal concentration-response curves.

Unfortunately, the compounds **53** (pK_i (D_1R) = 8.58; pK_i (H_3R) = 5.89) and **54** (pK_i (D_1R) = 8.39; pK_i (H_3R) = 5.66) with the immepip-based H_3R pharmacophores lost affinity towards the H_3R receptor. This indicates that the addition of the spacer interferes heavily with the receptor binding. It was suggested that due to the short aliphatic linker the basic triazole moiety was too close to the secondary amine and maybe inhibited ligand binding to the receptor. Therefore, two derivatives with longer aliphatic linkers **55** (pK_i (D_1R) = 8.45; pK_i (H_3R) = 6.09) and **56** (pK_i (D_1R) = 8.28; pK_i (H_3R) = 6.07) were synthesized and tested. Although, this led to a small increase in affinity towards the H_3R, there was still a huge loss in affinity compared to immepip (pK_i (H_3R)= 9.32).[190] These results suggest that the secondary amine is not a well-suited attachment point for the connection to a linker. An alternative would be the coupling of the linker to the carbon atom that connects the imidazole and piperidine rings. Efforts in this direction were not made due to the lack of time to design and execute a new synthesis.

Surprisingly, the endcapped ligands with the SCH and SKF pharmacophore **61** (pK_i (D_1R) = 7.91; pK_i (H_3R) = 6.30) and **62** (pK_i (D_1R) = 7.26; pK_i (H_3R) = 5.88) showed lower affinities towards their respective receptors than their bivalent counterparts, despite their lower molecular weight and size. A reason could be their lower water-solubility or negative influencing interactions with the cell-membrane or other proteins. Nevertheless, they possess a sufficiently high affinity towards the receptors to be used as negative controls. Furthermore, they displayed some moderate binding affinity towards the H_3R, including a higher affinity than the reference compounds **63** (pK_i (H_3R) = 5.54) and **64** (pK_i (H_3R) = < 5). Apparently, the addition of the linkers and spacer increase the affinity of these compounds towards the H_3R. Nevertheless, they are still selective for the D_1R. The endcapped ligands with the JNJ and immepip pharmacophores **59** (pK_i (H_3R) = 9.99) and **60** (pK_i (H_3R) = 6.02) possess pK_i values in the same range as the bivalent ligands.

2.3.2 Selectivity within the dopamine and histamine receptor families

Besides the affinity towards a specific receptor the selectivity of a ligand for a specific target is of great importance. Especially inside a receptor family many ligands don't discriminate between the different receptor subtypes, for example the endogenous ligands. Although highly selective compounds were chosen as lead structures the selectivity profile must be determined for the bivalent ligands, because of the structural modification and the addition of a second pharmacophore. Due to the structural similarity of the different compounds not all the bivalent ligands were tested. **44** and **45** as most promising structures were tested at both receptor families. Additionally, **49** and **50** were analyzed as SKF-based bivalent ligands for their selectivity inside the dopamine receptor family. Because of the limited access to D_4R-expressing cells, only **45** and **50** could be tested at this receptor. Furthermore,

no bivalent ligand with an immepip-based pharmacophore was evaluated for the selectivity inside the histamine receptor family, because of the already low affinity towards the H_3R. The results of these binding studies are represented in Table 2.2 and Figure 2.6.

All four compounds showed at least a 1,000-fold selectivity for the D_1-like receptors compared to the D_2R and D_4R receptors (Table 2.2; Figure 2.6A-D). The affinity of these compounds for the D_3R (pK_i (D_3R) = 5.15-5.60) is higher than for the D_2R (pK_i (D_2R) < 5) and D_4R (pK_i (D_4R) < 5), but they still have at least a 300-fold selectivity for the D_1R. As expected, none of the ligands showed a significant difference (two-tailed t-test; p-value > 0.05) within the D_1-like receptors (Table 2.2), except **44** (pK_i (D_1R) = 8.88; pK_i (D_5R) = 7.80; p-value < 0.05) which has a 10-fold higher affinity towards the D_1R. In general, there are no compounds published, that possess a high selectivity for the D_1R over the D_5R. As SCH is not selective for the D_1R over the D_5R and SKF hasn't been tested at the D_5R no preference for one of those receptors was expected for any of the bivalent ligands.[204]

Table 2.2: Selectivity of compounds **44**, **45**, **49** and **50**.

cmpd	pK_i ± SEM[a]										D_1R selectivity		pK_i ± SEM[b]								H_3R selectivity
	D_1R[c]	*N*	D_2R[d]	*N*	D_3R[e]	*N*	D_4R[f]	*N*	D_5R[g]	*N*	$K_i(D_{2,4}R)$ / $K_i(D_1R)$	$K_i(D_3R)$ / $K_i(D_1R)$	H_1R[h]	*N*	H_2R[i]	*N*	H_3R[k]	*N*	H_4R[l]	*N*	$K_i(H_{1,2,4}R)$ / $K_i(H_3R)$
44	8.88 ± 0.07	3	< 5	3	5.15 ± 0.18	3	n.d.	---	7.80 ± 0.08	3	> 40,000	> 6,000	< 5	3	< 5	3	10.21 ± 0.08	3	< 5	3	> 100,000
45	8.67 ± 0.10	4	< 5	3	5.60 ± 0.03	3	< 5	3	8.32 ± 0.09	3	> 4,500	> 950	< 5	3	< 5	3	10.00 ± 0.03	3	< 5	3	> 100,000
49	8.58 ± 0.06	3	< 5	3	5.30 ± 0.19	3	n.d.	---	8.25 ± 0.17	3	> 7,500	> 1,500	n.d.	---	n.d.	---	n.d.	---	n.d.	---	
50	8.39 ± 0.12	3	< 5	3	5.46 ± 0.19	3	<5	3	7.66 ± 0.07	3	> 2,000	> 300	n.d.	---	n.d.	---	n.d.	---	n.d.	---	

[a]Competition binding experiments at HEK-293T cell homogenates stably expressing the hD_1R, $hD_{2long}R$, hD_3R, $hD_{4.4}R$, or hD_5R.[201,205] [b]Competition binding assay at HEK293-SP-FLAG-hH_1R, HEK293-SP-FLAG-hH_2R, HEK293-SP-FLAG-hH_3R or HEK293-SP-FLAG-hH_4R cells.[4,157,202] [c]Displacement of 0.2 nM, 0.4 nM or 1 nM [^{3}H]SCH-23390 (K_d = 0.4 nM). [d]Displacement of 0.05 nM [^{3}H]*N*-Methylspiperone (K_d = 0.014 nM). [e]Displacement of 0.05 nM [^{3}H]*N*-Methylspiperone (K_d = 0.014 nM). [f]Displacement of 0.10 nM [^{3}H]*N*-Methylspiperone (K_d = 0.078 nM). [g]Displacement of 1 nM [^{3}H]-SCH-23390 (K_d = 0.4 nM). [h]Displacement of 5 nM [^{3}H]mepyramine (K_d = 3 nM). [i]Displacement of 50 nM [^{3}H]UR-DE-257[206] (K_d = 66.9 nM). [k]Displacement of 4 nM [^{3}H]UR-PI-294[203] (K_d = 5 nM). [l]Displacement of 4 nM [^{3}H]UR-PI-294 (K_d = 5 nM). Data shown are mean values ± SEM of *N* independent experiments, each performed in triplicate. Data were analyzed by nonlinear regression and were best fitted to a four parameter sigmoidal concentration-response curves.

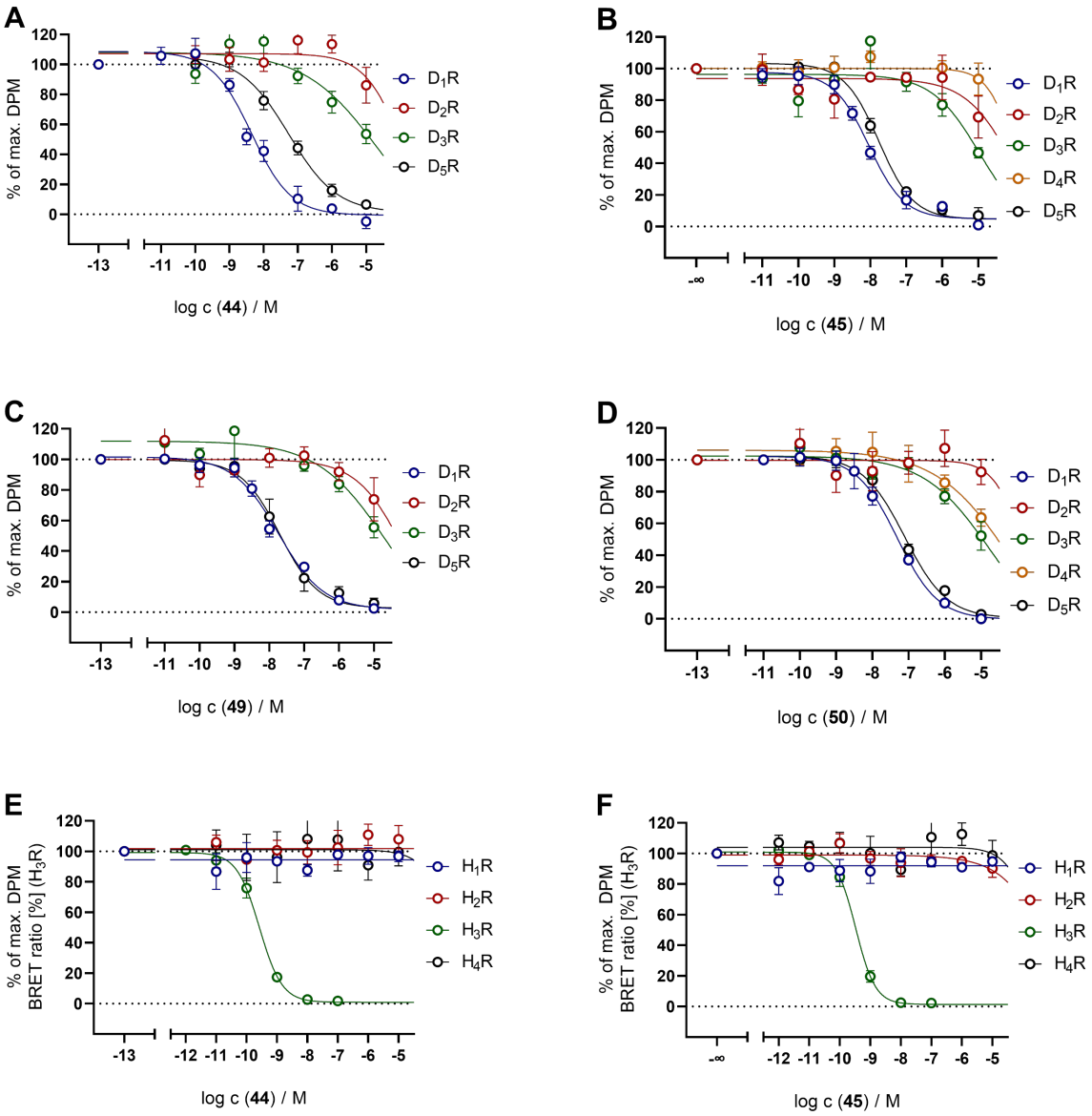

Figure 2.6: Representative competition binding curves of **44** (**A**), **45** (**B**), **49** (**C**) and **50** (**D**) at the dopamine receptors. Representative competition binding curves of **44** (**E**) and **45** (**F**) at the histamine receptors.

44 and **45** were chosen as JNJ-based compounds to test the affinity inside the histamine receptor family, because they show the best overall binding profile at both receptors. Fortunately, both compounds retained the extraordinary selectivity of the JNJ lead compound. As no affinity towards any of the other histamine receptors could be detected (Figure 2.6E, F) they are at least 100,000-fold selective towards the H_3R compared to the H_1R, H_2R, and H_4R.

These results prove the compounds, especially **44** and **45**, to be selective and high-affinity bivalent ligands for the D_1R and H_3R.

2.3.3 Functional characterization of selected bivalent ligands

After determining the affinity and selectivity of the bivalent ligands it was important to verify their biological mode of action (efficacy). The structural changes caused by the addition of the large spacers can lead to a change in biological activity, even if the affinity towards a receptor is maintained.[140,173] Because of the structural similarity regarding the pharmacophores and their linkers not all the compounds were tested, but only those with the highest affinity to the receptor of each pharmacophore using the LANCE *Ultra* cAMP detection kit (PerkinElmer).

2.3.3.1 LANCE *Ultra* cAMP detection assay

Activation or inhibition of $G\alpha_s$- or $G\alpha_i$-coupled GPCRs modulates the intracellular cAMP levels by the activation or inhibition of the ACs. Therefore, the cAMP concentration is a suitable marker for the distinction between GPCR agonists and antagonists.

The LANCE *Ultra* cAMP detection kit (PerkinElmer, Germany) allows the detection of intracellular cAMP concentrations by time-resolved fluorescence resonance energy transfer (TR-FRET). The FRET between Europium-labelled cAMP (FRET donor) and cAMP-specific monoclonal antibodies labelled with the U*Light*™ dye (FRET-acceptor) is measured. After addition and incubation with the agonist or antagonist both FRET-components are added to the cells. The biogenic cAMP from the cells competes with the Eu-labelled cAMP for the binding sites at the antibody (Figure 2.7). Therefore, the cAMP concentration correlates with the FRET intensity (the higher the cAMP concentration the lower the FRET intensity).

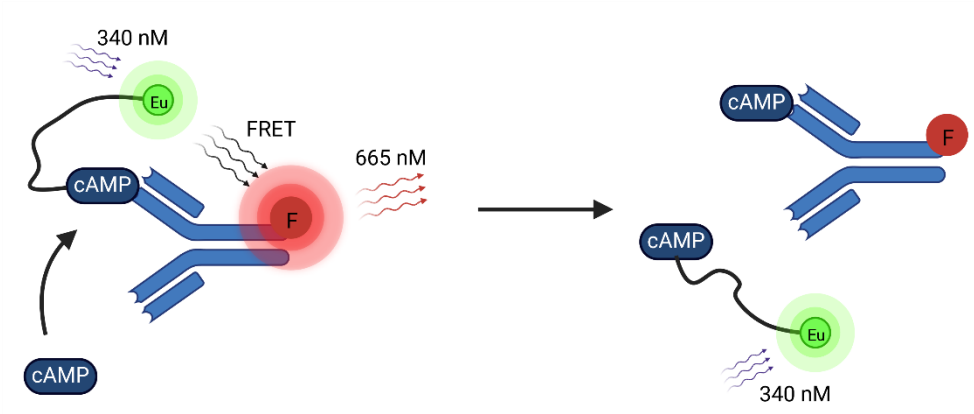

Figure 2.7: Schematic principle of the LANCE Ultra cAMP detection kit. On the left side FRET takes place between the antibody-bound Eu-labelled cAMP and the fluorophore of the antibody. At the right unlabelled cAMP displaced the Eu-labelled cAMP, therefore no FRET takes place. Created with BioRender.com.

2.3.3.2 Results of the cAMP detection assay

The easiest setup for this assay is the agonist mode at a $G\alpha_s$-coupled GPCR (e.g. D_1R). The addition of an agonist leads to an increase of intracellular cAMP levels, which can be measured and transformed into a dose-response curve. To perform the assay in the antagonist mode the cells are treated with a constant concentration of an agonist and increasing concentrations of the antagonist, to measure the decrease of the cAMP levels.

First the bivalent ligands with SKF-based pharmacophores (**49** and **50**), the endcapped ligand **62**, and the reference compound **64** were tested. Unfortunately, none of the compounds showed a pronounced agonistic effect at the D_1R (Figure 2.8A). Only at high concentrations of 10 µM an efficacy of 20 % was observed. The effect caused by 500 nM of the full agonist SKF-81297 (Figure 1.4)[177] was set as 100 % efficacy. Surprisingly, the reference compound **64** didn't act as an agonist as well, despite only small modifications compared to the lead structure SKF-75760. These results indicate that the chosen lead structure is not suited for the synthesis of a bivalent ligand with an agonistic pharmacophore for the D_1R. The same experiments were conducted at D_1R and H_3R co-expressing cells. The total levels of cAMP upon activation with 500 nM of SKF-81297 were lower than in cells only expressing the D_1R. This suggests a negative cross-talk between both receptors, which was previously described.[61] Nevertheless, no difference in the ligands mode of action was observed (Figure 2.8B).

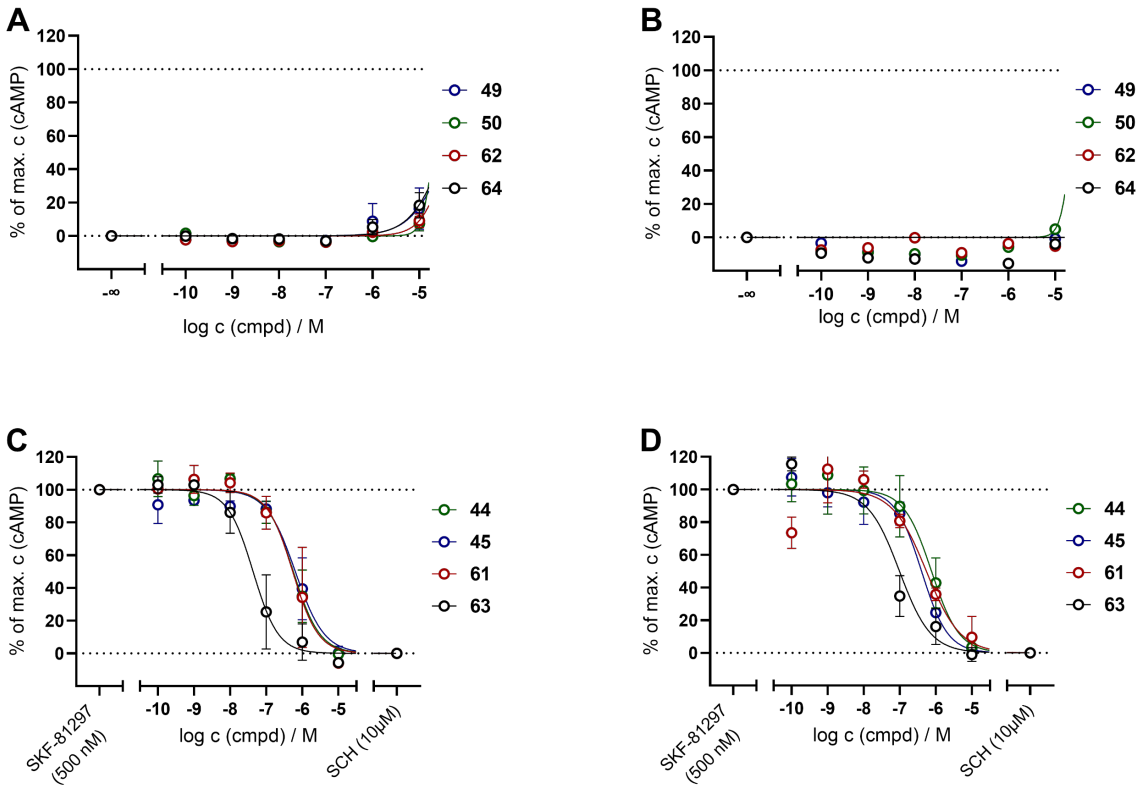

Figure 2.8: Dose-response curves of **44**, **45**, **49**, **50**, **61**, **62**, **63**, and **64** in the functional cAMP assays. **A**: Dose-response curves at HEK-293T cells transiently expressing the hD_1R (agonist mode). **B**: Dose-response curve at HEK-293T cells transiently expressing the hD_1R and hH_3R (agonist mode). **C**: Dose-response curves at HEK-293T cells transiently expressing the hD_1R. Inhibition of 500nM SKF-81297 (antagonist mode). **D**: Dose-response curves at HEK-293T cells transiently expressing the hD_1R and hH_3R. Inhibition of 500nM SKF-81297 (antagonist mode). The cAMP concentration induced by 500 nM of SKF-81297 is set as 100 %. Graphs represent the means of three independent experiments each performed in triplicate. Data were analyzed by nonlinear regression and were best fitted to four parameter sigmoidal concentration-response curves.

The next step was the analysis of the bivalent ligands with a SCH-based D_1R pharmacophore (**44** and **45**), the respective endcapped ligand **61**, and the reference ligand **63**. To measure the antagonistic effect of these compounds, the D_1R was activated with 500 nM of SKF-81297 (100 % efficacy). All four compounds could completely inhibit the activation of the receptor at high concentrations at both D_1R and D_1R-H_3R co-expressing cells (Figure 2.8A,B). The pIC_{50} values are presented in Table 2.3. As expected, because of the higher binding affinity, the reference compound **64** has a higher pIC_{50} value than the bivalent and endcapped ligands. Furthermore, for **45** a significantly higher pIC_{50} value at the D_1R-H_3R co-expressing cells was measured compared to the D_1R expressing cells (two-tailed t-test, $p = 0.047$). This could be an indication for a higher binding affinity of **45** at D_1-H_3 Hets. For compounds **44**, **62**, and **64** no significant difference between both cell types was observed.

Table 2.3: Functional data of compounds **44**, **45**, **49**, **50**, **55**, **59**, **61**, **62**, **63, 64** and imetit.

cmpd	p*IC*$_{50}$						p*EC*$_{50}$					
	D_1R[a]	*N*	D_1R H_3R[b]	*N*	H_3R[c]	*N*	H_3R[d]	α [%][e] (H_3R)	*N*	D_1R[f]	α [%][e] (D_1R)	*N*
44	6.23 ± 0.19	3	6.24 ± 0.22	3	7.84 ± 0.44	3	n.d.	n.d.	---	n.d.	n.d.	---
45	5.83 ± 0.04	3	6.36 ± 0.11	3	8.08 ± 0.16	3	n.d.	n.d.	---	n.d.	n.d.	---
49	n.d.	---	n.d.	---	n.d.	---	n.d.	n.d.	---	n.a.	n.a.	3
50	n.d.	---	n.d.	---	n.d.	---	n.d.	n.d.	---	n.a.	n.a.	3
55	n.d.	---	n.d.	---	n.d.	---	7.36 ± 0.32	72.4 ± 9.0	3	n.d.	n.d.	---
59	n.d.	---	n.d	---	7.21 ± 0.53	3	n.d.	n.d.	---	n.d.	n.d.	---
61	6.24 ± 0.30	2	6.29± 0.06	2	n.d.	---	n.d.	n.d.	---	n.d.	n.d.	---
62	n.d.	---	n.d.	---	n.d.	---	n.d.	n.d.	---	n.a.	n.a.	3
63	7.27 ± 0.32	3	7.22 ± 0.17	2	n.d.	---	n.d.	n.d.	---	n.d.	n.d.	---
64	n.d.	---	n.d.	---	n.d.	---	n.d.	n.d.	---	n.a.	n.a.	3
imetit	n.d.	---	n.d.	---	n.d.	---	8.62 - 9.90[207,208]	100	---	n.d.	n.d.	---

[a]cAMP assay performed at HEK-293T cells transiently expressing the hD_1R; inhibition of 500 nM SKF-81297. [b]cAMP assay performed at HEK-293T cells transiently expressing the hD_1R and the hH_3R; inhibition of 500 nM SKF-81297. [c]cAMP assay performed at HEK-293T cells transiently expressing the hH_3R; cAMP production was stimulated with forskolin; inhibition of 500 nM imetit. [d]cAMP assay performed at HEK-293T cells transiently expressing the hH_3R; cAMP production was stimulated with forskolin; pEC_{50} values of imetit were taken from literature. [e]Intrinsic activity α; effect of 500 nM imetit (H_3R) or SKF-81297 (D_1R) was set as 100 %. [f]cAMP assay performed at HEK-293T cells transiently expressing the hD_1R. Data shown are mean values ± SEM of *N* independent experiments, each performed in triplicate. Data were analyzed by nonlinear regression and were best fitted to four parameter sigmoidal concentration-response curves. n.d. = not determined: n.a. = not active.

The same experiments were performed activating the H_3R instead of the D_1R. Because the H_3R is $G\alpha_i$-coupled, the activation of this receptor with an agonist does not lead to a detectable change in intracellular cAMP levels. Therefore, forskolin, an agonist for the ACs, is used to induce intracellular cAMP production. The agonistic effect at the H_3R could then be determined by measuring the decrease in intracellular cAMP levels, thus the inhibition of the forskolin-activated ACs by the activated $G\alpha_i$ protein. This leads to an inversion of the dose-response curves compared to the D_1R. While agonists lower the cAMP levels, antagonists counteract this effect, leading to an increase of the cAMP concentrations.

Bivalent ligands **44** and **45**, as well as the endcapped ligand **59** were tested in the antagonist mode. All three ligands could completely inhibit the agonistic effect of the H_3R selective full agonist imetit[209] (c = 500 nM; Figure 2.9A). In accordance with the binding data, the pIC_{50} values of **44** and **45** are higher compared to the endcapped ligand **59** (Table 2.3). Additionally, the immepip-based bivalent ligand **55** was tested for an agonistic effect at the H_3R. A concentration-dependent decrease of the intracellular cAMP levels could be observed (Figure 2.9B). **55** was characterized as a partial agonist with an intrinisic activity α of 72 % compared to imetit and a pEC_{50} value of 7.36. The higher pEC_{50} value compared to the the pK_i value (6.09) can be explained by the different assay systems, which can lead to an amplification of the signal because of measuring further downstream.

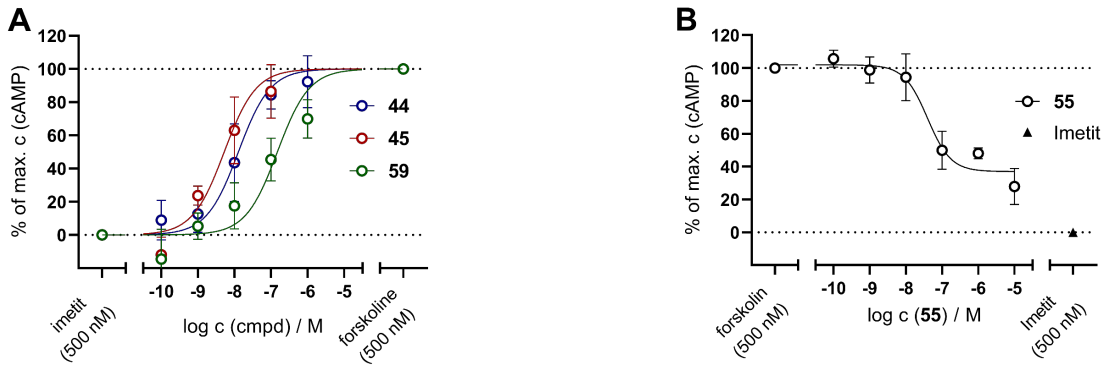

Figure 2.9: Dose-response curves of **44**, **45**, **55**, and **59** in the functional cAMP assays. **A**: Dose-response curves at HEK-293T cells transiently expressing the hH_3R; inhibition of 500nM Imetit (antagonist mode). **B**: Dose-response curve at HEK-293T cells transiently expressing the hH_3R (agonist mode). The cAMP concentration induced by 500 nM forskolin was set as 100 % and the concentration with imetit (500 nM) added was set as 0 %. Graphs represent the means of three independent experiments each performed in triplicate. Data were analyzed by nonlinear regression and were best fitted to three parameter sigmoidal concentration-response curves.

Unfortunately, the selective full H_3R agonist imetit (pEC_{50} = 8.62-9.90)[207,208] could only reduce the forskolin-induced cAMP generation by a small margin, which made the determination of pIC_{50} values for the JNJ-based bivalent ligands more difficult and increased the errors. One reason for the small effect of imetit could be a low receptor expression leading to a weak cellular response, not strong enough to efficiently antagonize forskolin. Additionally, forskolin activates all of the transmembrane adenylyl cyclases (AC 1-8)[210,211] except AC9,[212,213] whereas $G\alpha_i$-subunits mainly inhibit AC1, AC5, and AC6.[214,215] This selective inhibition could also lead to a lower inhibitory response upon H_3R activation. Using D_1R and H_3R co-expressing cells imetit could not reduce the cAMP levels in a significant manner, again indicating a negative cross-talk between both receptors.[61] Therefore, no dose-response curves could be recorded using these cells activating the H_3R.

2.3.4 *In vitro* neuroprotection of **45**

The D_1-H_3 Het was reported to have neuroprotective properties and its inhibition by H_3R antagonists led to a reduction of excitotoxic cell death (see chapter 1.4).[131] Based on these results, the antagonistic bivalent ligands should be able to reduce the Aβ-induced cell death in neurons. To test this hypothesis, cortex cells from mice embryos were extracted and cultivated. After seven days Aβ (c = 500 nM) and the respective compounds were added. After an additional seven days the cells were detached from the culture plate and the percentage of live cells versus total cells was determined by trypan blue staining. The results are depicted in (Figure 2.10). Because of the limited number of available cells only the most promising compound **45** was tested. Additionally, the endcapped ligands **59** and **61** were used as negative controls to determine if the bivalent ligand has a more pronounced neuroprotective effect, due to a possible higher affinity towards the receptor dimer.

All three compounds were able to reduce the Aβ-induced cell death, with **45** showing the most pronounced effect at concentrations of 10 and 100 nM (Figure 2.10A). Focusing on **45**, a concentration-dependent neuroprotective effect was observed with a significant reduction in cell death at concentrations of 10 and 100 nM compared to the addition of Aβ alone (Figure 2.10B). The strongest neuroprotective effect was observed at 100 nM, significantly higher compared to the lower concentrations of 10 and 100 pM. An increase of the concentration up to 1 µM led to a lower percentage of live cells. This is probably caused by an overdose effect, a neurotoxic effect of the compound itself at high concentrations. This was observed for all three compounds and confirmed by the fact that the addition of 1 µM of the compounds alone without Aβ had a neurotoxic effect compared to the blank control. Comparing the three compounds at the concentration of 100 nM a stronger neuroprotective effect of **45** was observed, although only compared to **59** the difference was statistically significant (Figure 2.10C).

Overall, this data supports the hypothesis of a neuroprotective potential for the D_1-H_3 Het and indicates a higher binding affinity and stronger neuroprotective effect of the bivalent ligands compared to the endcapped controls.

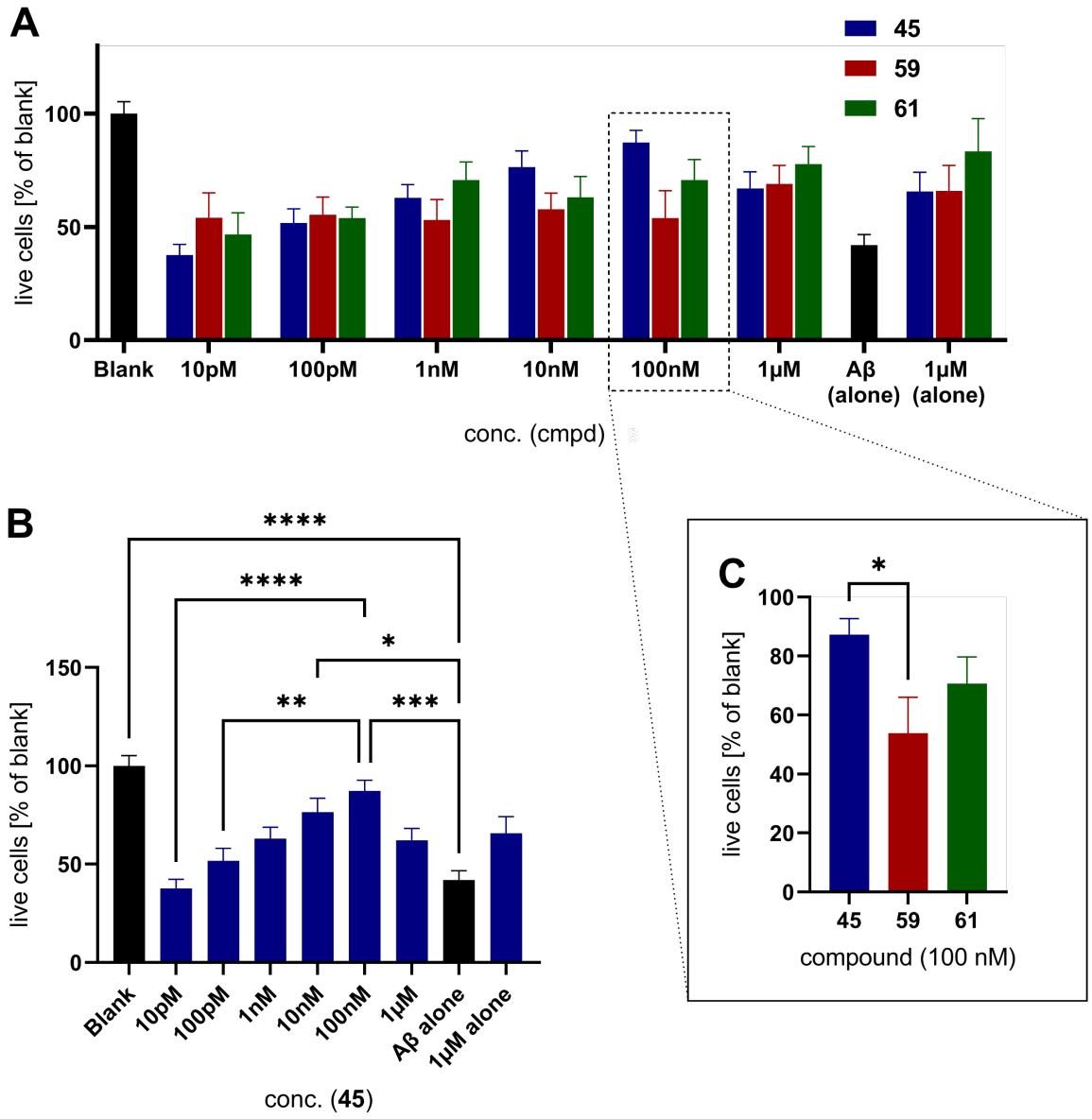

Figure 2.10: Cell death assay at mouse embryonal cortex cells. **A**: Results of compounds **45**, **59** and **61**. **B**: Isolated results of **45**. **C**: Comparison of the three compounds at a concentration of 100 nM. Data represent mean values ± SEM of two (**59** and **61**) or four (**45**) different experiments on two different days, each performed in triplicate or quadruplicate. One-way ANOVA followed by Bonferroni's post hoc test showed significant effects between different concentrations (* $p < 0.5$; ** $p < 0.01$; *** $p < 0.001$; **** $p < 0.0001$).

2.4 Conclusion

The project of the bivalent ligands started by designing them on paper. Based on SAR and modeling results connection points and functional groups were chosen to attach the linkers to the pharmacophores. After designing the ligands, the synthesis had to be developed and executed. All pharmacophores could be synthesized with the desired linker that added a C-C triple bond, forming building blocks for the final bivalent ligands. Additionally, a set of spacers with different lengths with terminal azide-groups was synthesized. This allowed the connection of the building blocks and spacers by the CuAAC reaction. The synthetic approach of connecting all parts at the end allowed a synthesis of 16 bivalent and four endcapped ligands without the need for an individual pharmacophore for each target structure. Bivalent ligands with the same pharmacophores but different spacer lengths were synthesized because the needed length for a bivalent binding mode was unknown.

All final compounds were tested in competition binding assays for their affinity towards the D_1R and H_3R and fortunately they retained a high affinity towards both receptors. Only for the immepip-based bivalent ligands a big loss in affinity was observed towards the H_3R. Especially compounds **44** and **45** showed exceptional high affinity at both receptors in the low nanomolar (D_1R) and sub-nanomolar (H_3R) range, which is remarkable for ligands of that size. Additionally, selected compounds were tested for their selectivity inside the dopamine and histamine receptor family. A high selectivity was achieved for all tested ligands, except for the D_5R. This was to be expected since the lead structures SCH and SKF aren't selective within the D_1-like receptor sub-family. Functional analysis of selected compounds revealed that all pharmacophores retained their mode of action, except the SKF-based ligands. Instead of activating the D_1R they acted as silent antagonists in a cAMP detection assay.

Finally, **45**, the most promising compound based on the previous results, was tested in an *in vitro* neuroprotection assay using primary cortex cells of mice embryos. A significant reduction in Aβ-induced cell death was observed, which was higher than the effect of the endcapped ligands **59** and **61**. These results highlight the neuroprotective properties of the D_1-H_3 Het and the potential of bivalent ligands to target this receptor complex with a higher affinity than monovalent ligands.

Radioligand competition binding assays at cells co-expressing the D_1R and H_3R, to prove a bivalent binding mode, are currently ongoing as part of the PhD project of Denise Mönnich. Preliminary results are very promising and indicate that the bivalent ligands are indeed able to bind simultaneously both receptors, but different control experiments are still needed to confirm this hypothesis.

3. Fluorescent ligands for the D_1R

The following experimental work was performed by co-authors:

NanoBRET studies:	Denise Mönnich (University of Regensburg, Germany)
G_{i2}-BRET sensor and assays:	Hannes Schihada (Phillips-University Marburg, Germany)
Confocal microscopy:	Steffen Pockes (University of Regensburg, Germany),
	Irene Reyes-Resina (University of Barcelona, Spain)

3.1 Design of the fluorescent ligands

Fluorescent ligands can be considered as an entity of three distinct parts: the pharmacophore, the linker, and the fluorescent dye (Figure 3.1). Each of the three parts must be chosen individually based on the intended use of the final fluorescent ligand.[143,145,216]

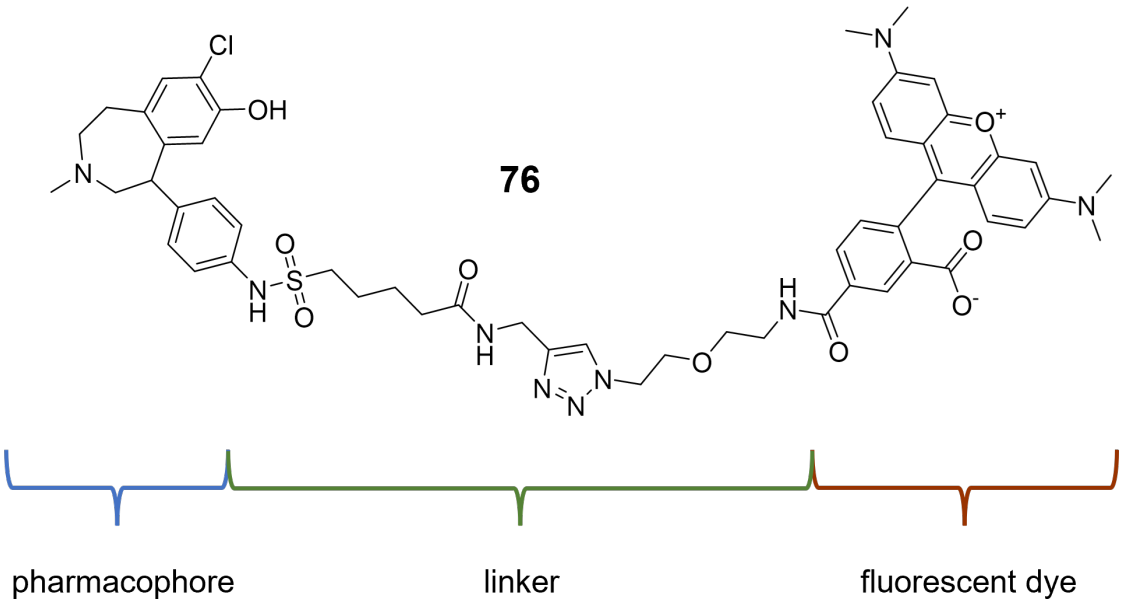

Figure 3.1: Chemical structure of **76** as an example for the schematic design of a fluorescent ligand.

The same lead structure that was chosen for the bivalent ligands was used for the fluorescent ligands (SCH-23390). Besides the high affinity and selectivity the antagonistic mode of action was important, because agonists can induce receptor internalization and degradation which could be disadvantageous for binding studies.[145,174] Furthermore, the same attachment point and functional connecting group, that proved to be successful for the bivalent ligands, were used for the connection of the pharmacophore to the linker.

Based on previously described D_1R fluorescent ligands, which had the fluorescent dye directly attached to the ligand, two compounds with a short alkylic linker were synthesized.[217] Additionally, fluorescent ligands with longer PEG-based linkers were prepared, which should allow the fluorophore to reach outside the binding pocket and therefore have less influence on the ligand binding. PEG-based linkers are commonly used in fluorescent ligands because they usually don't interact with cell membranes, are chemically stable and well soluble in water.[218] The connection of the pharmacophore with the PEG-unit was performed in three steps. First a short alkylic spacer was attached to the pharmacophore which was then connected via a peptide coupling reaction to propargylamine. This

product was coupled via a CuAAC reaction to a PEG-2 or PEG-3 unit, which were orthogonally functionalized with a primary amine and an azide group (**70**, **34a**).

The choice of the fluorescent dye is crucial and depends mainly on the intended use of the final fluorescent ligand. Important criteria to consider are spectral properties, quantum yield, solubility, solvatochromic effects, chemical stability, photostability, commercial availability, and an efficient coupling to the pharmacophore.[145] The 5-TAMRA fluorescent dye was chosen to label the ligands, because it is known to yield excellent results in the NanoBRET binding assay and is also suited for fluorescent microscopy and single-molecule TIRF imaging.[152,157,219–222] Additionally, DY549-P1 (Dyomics GmbH, Jena, Germany) was used, as it possesses similar spectral properties as 5-TAMRA and therefore should be suitable for the NanoBRET assay as well. Furthermore, it was reported to yield excellent results in single molecule microscopy.[223] Both dyes are hydrophilic, which makes them less prone to interactions with cell membranes than, for example, BODIPY fluorescent dyes, leading to lower nonspecific binding.[224]

3.2 Chemistry

The synthesis of the fluorescent ligands can be separated into three parts: the synthesis of the pharmacophore, the linkers and the connection of the different structures including labeling with a fluorescent dye.

The synthesis of the pharmacophore for the fluorescent ligands followed the same synthetic route as for the bivalent ligands. In order to synthesize the fluorescent ligands with the short alkylic linkers, an acetyl instead of a triisopropyl silyl protecting group was introduced at the phenolic hydroxy group of **11a** yielding **65** which was subsequently reduced by palladium catalyzed hydrogenation to afford the aniline **66** (Scheme 3.1A). To introduce the sulfonamide moiety the commercially available *N*-(3-bromopropyl)phthalimide was converted to the sulfonyl chloride **67** (Scheme 3.1B). Coupling of **67** with **66** in the presence of pyridine afforded **68** in good yields. Simultaneous deprotection of the acetyl and phthalimide groups with hydrazine in ethanol afforded the final precursor for the fluorescent ligands (**69**), which was purified by preparative HPLC.

Scheme 3.1: Synthesis of fluorescent ligand precursor **69**.[a]

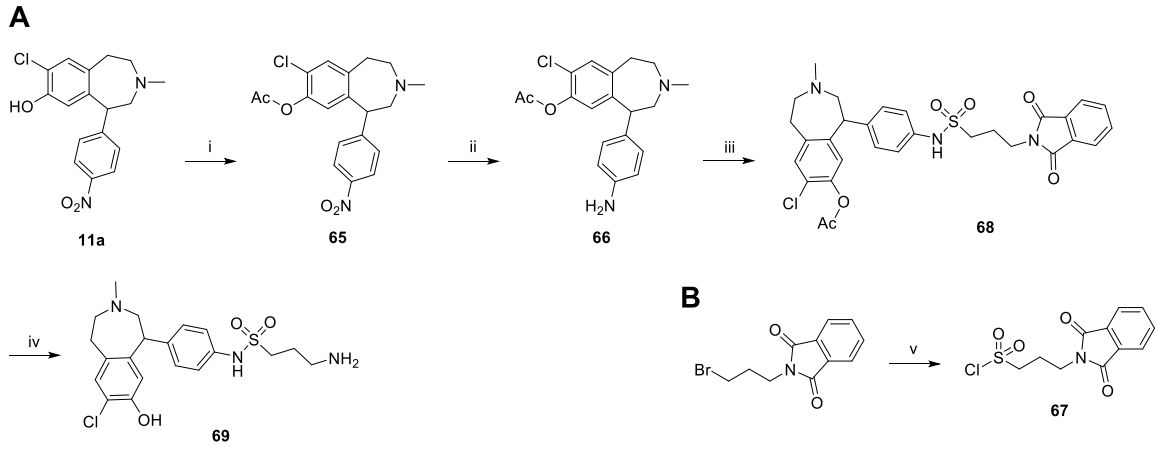

[a] Reagents and conditions: i) AcCl, NEt_3, DCM, rt, overnight, 77 %; ii) H_2, Pd/C, MeOH/DCM (1:1), rt, overnight, 95 %; iii) **67**, pyridine, $CHCl_3$, 50 °C overnight, 62 %; iv) hydrazine hydrate, EtOH, 80 °C, overnight, 23 %; v) 1. thiourea, EtOH, 80 °C, 1 h, 2. NCS, MeCN, HCl (2 N), 10 °C, 30 min, 89 %.

For the synthesis of the fluorescent ligands with the PEG-based linkers the same building block that was synthesized for the bivalent ligands (**20**) could be used, as well as the linker **35a**. An additional PEG-linker of shorter length was synthesized (**72** via **70** and **71**) using the same reaction protocol that was used previously for the bivalent ligands (Scheme 3.2A).[195] The linkers were connected to **20** using the CuAAC reaction, affording the fluorescent ligand precursor molecules **73a** and **73b** (Scheme 3.2B).

Scheme 3.2: Synthesis of precursor molecules **73a** and **73b**.[a]

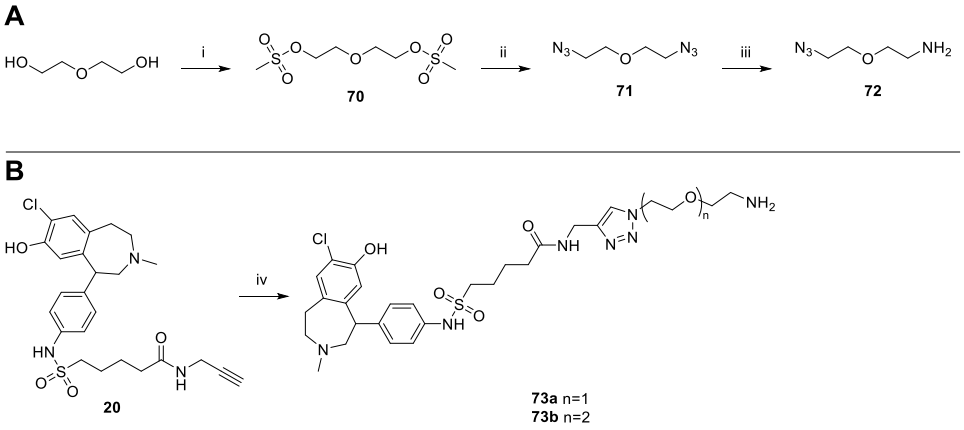

[a] Reagents and conditions: i) MsCl, NEt_3, DCM, rt, overnight, 96 %; ii) NaN_3, EtOH/DMF (4:1), reflux, overnight, 98 %; iii) PPh_3, EtOAc/THF/1N aq. HCL (5:1:5), rt, overnight, 60 %; iv) **72** or **35a**, $CuSO_4$*H2O, ascorbic acid, DCM/MeOH (4:1), rt, 72h, 8-14 %.

Most of the commercial fluorescent dyes are available as *N*-hydroxy succinimidyl (NHS) esters. These activated esters are ideally suited for labeling at primary amino groups. Therefore, the precursor molecules were designed and synthesized accordingly. To synthesize the final fluorescent ligands an excess of precursor and NEt_3 was dissolved in DMF. The fluorescent dye NHS ester was added and the reaction vessel was shaken at room temperature for 3 h under the exclusion of light. After quenching the reaction with aqueous TFA the fluorescent ligands could be purified by preparative HPLC. This reaction protocol allowed the synthesis of six different fluorescent ligands (**74**-**79**) in satisfactory yields (Scheme 3.3).

Scheme 3.3: Synthesis of fluorescent ligands **74**-**79**.[a]

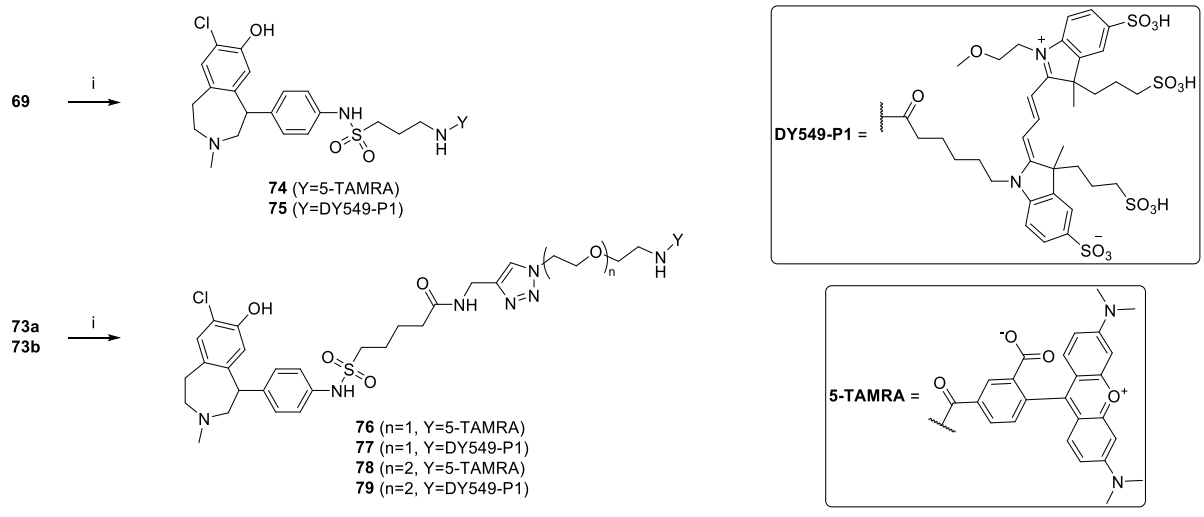

[a] Reagents and conditions: i) 5-TAMRA-NHS ester or DY549-P1-NHS ester, NEt_3, DMF, rt, 3 h, 39-89 %.

The purity and stability of all fluorescent ligands was determined by HPLC (HPLC runs are presented in the Appendix; chapter 8.1). The chemical structure of all synthesized compounds was proven by ^{1}H and ^{13}C NMR as well as HRMS. The final fluorescent ligands were only characterized by HRMS because of the small amount obtained from these compounds. The chemical structures of the fluorescent ligands are presented in the Appendix (chapter 8.3).

3.3 Fluorescence properties

The fluorescence properties are usually not affected heavily by the addition of a ligand, if the fluorophore is chemically not changed, as it's the case for the 5-TAMRA and DY549-P1 dye. Nevertheless, the absorption and emission spectra and the quantum yield should be determined for new fluorescent ligands. The knowledge of the excitation and emission spectra and a high quantum yield are essential for their use in pharmacological assays and fluorescence microscopy. Because of the similar fluorescent dyes emission and excitation spectra of only **76**-**79** were recorded, as they were thought to be the most affine ligands (Figure 3.2). The spectra were recorded in PBS buffer containing 1 % of BSA because most of the pharmacological assays and fluorescence microscopy experiments are performed in aqueous media. The excitation and emission maxima are presented in Table 3.1.

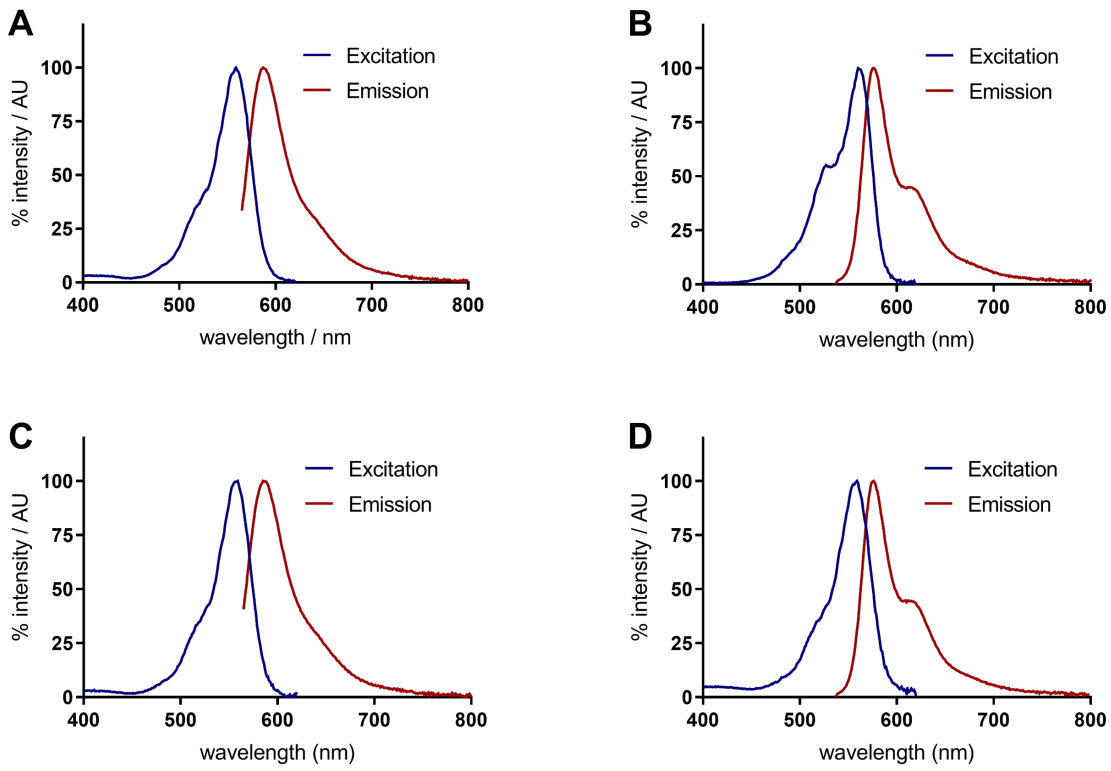

Figure 3.2: Excitation and emission spectra of **76** (**A**), **77** (**B**), **78** (**C**), and **79** (**D**).

The quantum yield of these compounds were determined in PBS buffer containing 1 % BSA for all four compounds and additionally in PBS buffer for compounds **77** and **78** following a previously published protocol.[225] **77** and **79** weren't analyzed in both media due to the limited amount of the DY549-P1-labeled fluorescent ligands. To determine the quantum yield of the novel ligands, the absorption at the maximal excitation wavelength ($\lambda_{exc,max}$) was determined. Afterwards, the emission

spectrum was recorded and corrected by the subtraction of the blank spectra and multiplication with a lamp correction factor. The quantum yield was then calculated by the following formula:[225]

$$\Phi_x = \frac{A_s}{A_x} \times \frac{F_x}{F_s} \times \left(\frac{\eta_x}{\eta_s}\right)^2 \times \Phi_s$$

with A being the absorption, F the integral of the emission spectra, η the refractive indices of the solvents, and Φ the quantum yield. The denominator s refers to the reference fluorescent dye cresyl violet perchlorate with a known quantum yield in ethanol of 54 %, whereas x refers to the unknown fluorescent ligand. The results are presented in Table 3.1. The 5-TAMRA-labeled compounds (**76** and **78**) have a higher quantum yield of approximately 36 % in PBS buffer compared to the DY549-P1-labeled ligands (**77** and **79**; approx. 19 %). Furthermore, it was observed that the addition of 1 % BSA led to a decrease in the quantum yield of the 5-TAMRA-labeled fluorescent ligands, but they still have a satisfactory quantum yield of 30 %.

Based on these results all four ligands, but especially **76** and **78**, should be suitable for the use in NanoBRET assays as well as in fluorescence microscopy.

Table 3.1: Fluorescence properties of compounds **76**-**79**.

cmpd	$\lambda_{exc,max}/\lambda_{em,max}$ (nm)	absorbance	Φ (%)[a]	
			PBS	PBS + 1 % BSA
76	559 / 586	0.20	36.77 ± 0.41	29.47 ± 0.35
77	561 / 575	0.16	n.d.	19.06 ± 0.26
78	559 / 585	0.14	36.52 ± 0.44	30.77 ± 0.43
79	560 / 574	0.15	n.d.	18.00 ± 0.33

[a] Data shown are mean values ± SEM three different slit adjustments (exc./em.): 5/5 nm, 5/10 nm, 10/10 nm.

3.4 Pharmacological characterization

Because of the structural modifications of the lead structure and the addition of the fluorescent dye the fluorescent ligand represents a new pharmacological entity and has to be analyzed carefully, before it can be used in different experimental setups. To test the affinity towards the D_1R and D_5R and the suitability for the NanoBRET assay, saturation binding assays at cells stably expressing the NLuc-hD_1R and NLuc-hD_5R-Nluc were performed. Additionally, competition radioligand binding studies at all wild type receptors of the dopamine receptor family were executed. Thereby, the influence of the genetical modification of the receptor on ligand binding at the D_1-like receptors and the selectivity towards the D_2-like receptors could be determined. The most promising compound was analyzed for its biological mode of action and suitability for confocal microscopy.

3.4.1 NanoBRET binding assays

The first step in the pharmacological characterization of a novel compound is the determination of its affinity towards the target protein. To achieve this and simultaneously assess the suitability of the fluorescent ligands for the NanoBRET assay, saturation binding experiments with all compounds were performed at cells stably expressing the NLuc-hD_1R fusion protein. If the ligand binds the receptor and the fluorophore is in the right orientation towards the NLuc it's excited by BRET and the BRET ratio can be determined (see chapter 1.6).

Preliminary results by Denise Mönnich showed a saturable BRET signal for all compounds except **75** and representative saturation binding curves could be recorded (Figure 3.3). Based on these saturation binding curves pK_d values were calculated (Table 3.2). Generally, the 5-TAMRA-labeled ligands (pK_d (D_1R) = 7.79-8.20) showed higher affinity and higher BRET ratios at the D_1R compared to the DY549-P1-labeled ligands (pK_d (D_1R) = 7.19-7.39), with **76** exhibiting the highest pK_d value of 8.20 and the highest BRET signal. Furthermore, for all ligands a low nonspecific binding was observed, which is usually the case in NanoBRET assays, because all binding events, that are not in close proximity to the NLuc, are not detected. The absence of a BRET signal using **75** as a fluorescent ligand can be caused by the lack of binding to the receptor or by an unfavorable orientation of the fluorophore towards the NLuc. Therefore, saturation binding experiments at higher concentration need to be performed to determine if the concentration of 50 nM is not sufficient for ligand binding. Additionally, radioligand binding assays should be performed at the same receptor to measure ligand binding even if no BRET signal can be detected due to an unfavorable orientation of the fluorophore and NLuc.

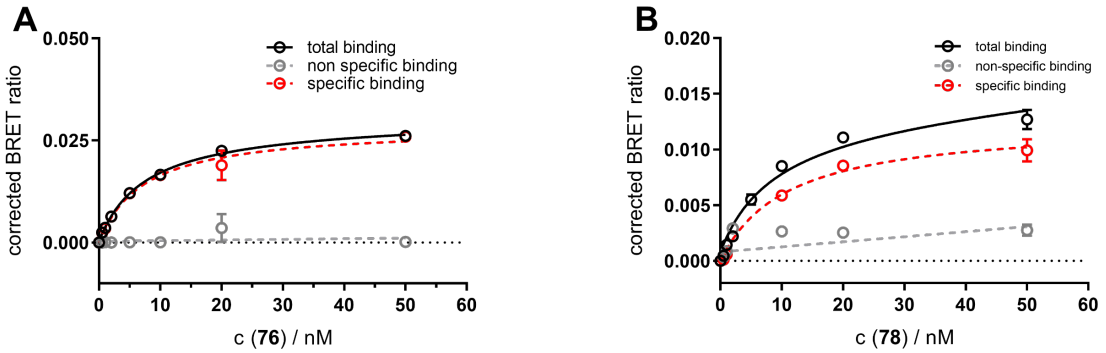

Figure 3.3: Representative isotherms from saturation binding experiments with **76** (**A**) and **78** (**B**) at the NLuc-hD$_1$R stably expressed in HEK293T cells.

Table 3.2: Binding data of **74**-**79** from NanoBRET saturation binding experiments at the D$_1$R.

cmpd	pK_d D$_1$R (NanoBRET)[a]	*N*
74	7.79 ± 0.05	2
75	no BRET signal	1
76	8.20 ± 0.04	2
77	7.19	1
78	7.96	1
79	7.33	1

[a]Experiments were performed at HEK293T cells stably expressing the NLuc-hD$_1$R. Data represent mean ± SEM of *N* independent experiments, each performed in triplicate. Data were analyzed by nonlinear regression and were best fitted to saturation binding curves.

3.4.2 Radioligand binding studies

The NanoBRET assay possesses various advantages over radioligand binding assays (see chapter 1.6) but a possible disadvantage is the genetical modification of the receptor by the addition of the NLuc. Radioligand binding studies at all five wild type dopamine receptors were performed to investigate a potential influence of the receptor modification and to determine the selectivity of the fluorescent ligands inside the dopamine receptor family (Figure 3.4). Comparing these results (Table

3.3) with the binding constants from the NanoBRET saturation binding experiments (Table 3.2) a big difference was observed for compound **74** (pK_i (D_1R) = 6.40; pK_d (D_1R) = 7.79). For the other 5-TAMRA labeled ligands **76** (pK_i (D_1R) = 8.34; pK_d (D_1R) = 8.20) and **78** (pK_i (D_1R) = 8.02; pK_d (D_1R) = 7.96) both experiments are in good agreement, whereas the DY549-P1-labeled ligands **77** (pK_i (D_1R) = 6.54; pK_d (D_1R) = 7.19) and **79** (pK_i (D_1R) = 6.85; pK_d (D_1R) = 7.33) show a higher affinity in the NanoBRET setup. Generally, it seems that the addition of the NLuc to the receptor only has a major effect on the binding of **74**. However, additional saturation and competition binding assays using the NanoBRET setup should confirm its validity as an alternative to radioligand binding studies. Additionally, the radioligand binding results confirm the fact that the 5-TAMRA labeled ligands show a higher affinity towards both the D_1R and D_5R comparing them to their DY549-P1-labeled counterparts.

The selectivity of the most affine ligands **76** (pK_i (D_1R) = 8.34; pK_i (D_5R) = 7.62) and **78** (pK_i (D_1R) = 8.02; pK_i (D_5R) = 7.65), compared to the D_2-like receptors, was determined (Figure 3.4C, D). Both compounds are over 1,000-fold selective compared to the D_2R and D_4R. Analogous to the bivalent ligands they display a lower selectivity comparing the D_1-like receptors to the D_3R but still have at least a 100-fold selectivity for the D_1R and D_5R.

Because of their high affinity, selectivity, and quantum yield **76** and **78** are promising structures for additional studies at the D_1-like receptors.

Table 3.3: Data from radioligand binding assays at the dopamine receptors.

cmpd	pK_i ± SEM[a]										$D_{1,5}R$ selectivity	
	D_1R[b]	*N*	D_2R[c]	*N*	D_3R[d]	*N*	D_4R[e]	*N*	D_5R[f]	*N*	K_i ($D_{2,4}R$) / K_i ($D_{1,5}R$)	K_i (D_3R) / K_i($D_{1,5}R$)
74	6.40 ± 0.39	3	n.d.	---	n.d.	---	n.d.	---	n.d.	---		
75	8.00 ± 0.18	4	n.d.	---	n.d.	---	n.d.	---	n.d.	---		
76	8.34 ± 0.21	3	< 5	3	5.67 ± 0.06	3	< 5	3	7.62 ± 0.03	3	> 1,000	> 100
77	6.54 ± 0.23	3	n.d.	---	n.d.	---	n.d.	---	6.03 ± 0.12	3		
78	8.02 ± 0.14	3	< 5	3	5.57 ± 0.03	3	< 5	3	7.65 ± 0.14	3	> 1,000	> 100
79	6.85 ± 0.07	3	n.d.	---	n.d.	---	n.d.	---	6.06 ± 0.10	3		

[a]Competition binding experiments at HEK-293T cell homogenates stably expressing the hD_1R, $hD_{2long}R$, hD_3R, $hD_{4.4}R$, or hD_5R. [b]Displacement of 1 nM [^{3}H]SCH-23390 (K_d = 0.4 nM). [c]Displacement of 0.05 nM [^{3}H]*N*-methylspiperone (K_d = 0.014 nM). [d]Displacement of 0.05 nM [^{3}H]*N*-methylspiperone (K_d = 0.014 nM). [e]Displacement of 0.10 nM [^{3}H]*N*-methylspiperone (K_d = 0.078 nM). [f]Displacement of 1 nM [^{3}H]SCH-23390 (K_d = 0.4 nM). Data shown are mean values ± SEM of *N* independent experiments, each performed in triplicate. Data were analyzed by nonlinear regression and were best fitted to sigmoidal concentration-response curves.

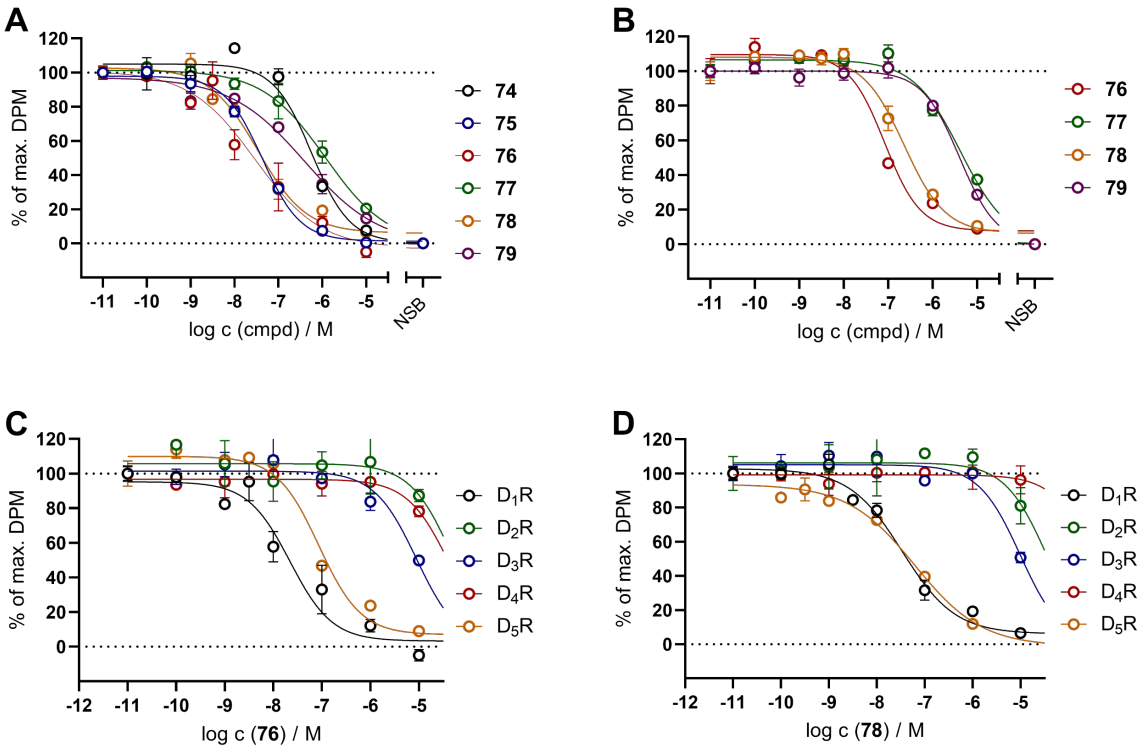

Figure 3.4: Representative competition binding curves of the fluorescent ligands at the D_1R (**A**) and D_5R (**B**). Representative displacement curves of **76** (**C**) and **78** (**D**) at the $D_{1\text{-}5}R$.

3.4.3 Functional characterization of the fluorescent ligands

The knowledge of the fluorescent ligand's mode of action is of utmost importance for the different possible applications. For example, as a tracer in the NanoBRET binding assay an antagonist is preferred because agonists can induce receptor internalization, which could alter the results and lead to wrong interpretations of the obtained data. To determine the functional activity of the novel fluorescent ligands, **76** was tested by Dr. Hannes Schihada (Phillips-University Marburg, Germany) in a previously published G protein biosensor assay.[226] For this assay, the $G\alpha_s$-subunits are tagged with the NLuc as BRET donor and the Gγ-subunits with the circulary permuted Venus (cpVenus[173]) yellow fluorescent protein as a BRET acceptor. If the G protein is in its heterotrimeric form a BRET signal can be detected. Activation of the GPCR of interest leads to the dissociation of the Gα-subunit from the Gβγ-subunit (see chapter 1.1.1.1.) and therefore to a decrease of the BRET signal.[226] Since all of the fluorescent ligands contain the same pharmacophore only **76** was analyzed as the most promising compound.

76 was tested in cells transiently expressing the D_1R or D_5R together with the $G\alpha_s$ NanoBRET biosensor. First, the experiments were performed in the agonist mode to analyze if the addition of the fluorescent ligand leads to a decrease in the BRET signal, thus activates the receptor (Figure 3.5A). Only

at high concentrations of 1 µM a slight decrease could be observed, which is most likely an optical artefact, because receptor binding should already take place at lower concentrations (see Table 3.3). Additionally, it was tested if **76** could counteract the dopamine-induced activation of the D_1R and D_5R (Figure 3.5B). For this purpose, both receptors were incubated with increasing concentrations of **76** and then 1 µM of dopamine was added. Indeed, **76** could completely inhibit the dopamine induced activation of both receptors (IC_{50} (D_1R) = 117 nM; IC_{50} (D_5R) = 11 nM). These results confirmed that **76** acts as a neutral antagonist at the D_1-like receptors and should therefore be suitable as a fluorescent tracer in the NanoBRET binding assay.

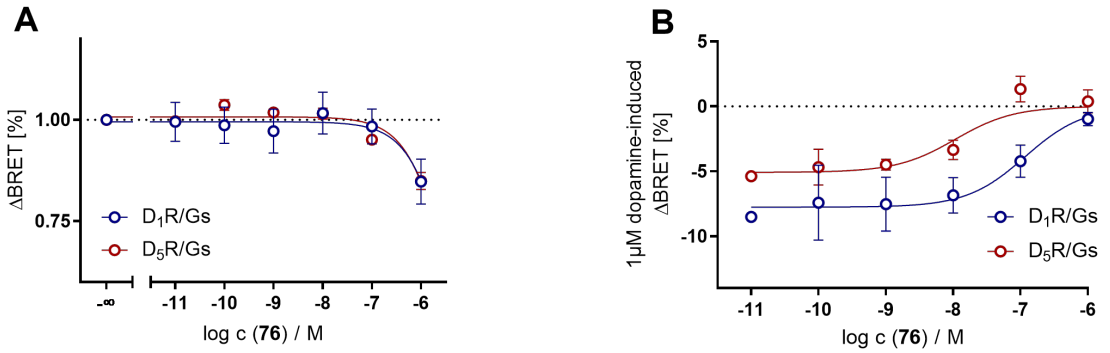

Figure 3.5: Dose-response curves of **76** at the $G\alpha_s$ biosensor assay. **A**: Dose-response curves of **76** in the agonist mode. **B**: Inhibition of 1 µM dopamine by **76**. Graphs represent the means of three independent experiments each performed in duplicate. Data were analyzed by nonlinear regression and were best fitted to sigmoidal concentration-response curves.

3.5 Fluorescence Microscopy

Fluorescence microscopy is a useful tool to detect and visualize the localization, trafficking, interaction, and degradation of fluorescently labeled proteins, membranes, or other parts of living cells. In its simplest way fluorescence microscopy detects fluorophores in a probe by exciting them with light of a specific wavelength and detecting the emitted light of a higher wavelength.[227] The proteins of interest can be labeled by genetical insertion of fluorescent proteins or with fluorescent ligands or antibodies.[157,228,229] The key feature of fluorescence microscopy is the selective detection of the emitted light separated from the excitation light, usually achieved by the use of transmission filters and or dichroic mirrors.[227] In these traditional wide-field fluorescence microscope the whole probe is excited at once and the fluorescence detected by the camera includes a lot of background and out of focus fluorescence leading to low contrast and spatial resolution.[230] Advanced fluorescence microscopy techniques such as laser scanning confocal microscopy (LSCM) and total internal reflection fluorescence (TIRF) microscopy tackle these disadvantages and lead to images of higher resolution and contrast.[230]

3.5.1 Laser scanning confocal microscopy

For LSCM a laser instead of a lamp is used to excite the fluorophores and the excitation light is focused by an objective lens on the cell or specimen of interest.[231] By using a pinhole in front of a light detector only the fluorescence of the confocal point is detected, while the background fluorescence is rejected. Since only one point of the sample is excited at a time the region of interest is then scanned systematically leading to a high resolution 2D image of the cell.[230] By scanning multiple planes at different depths of the cell so called z-stacks can be generated that can be transformed in a 3D image of the cell.[231]

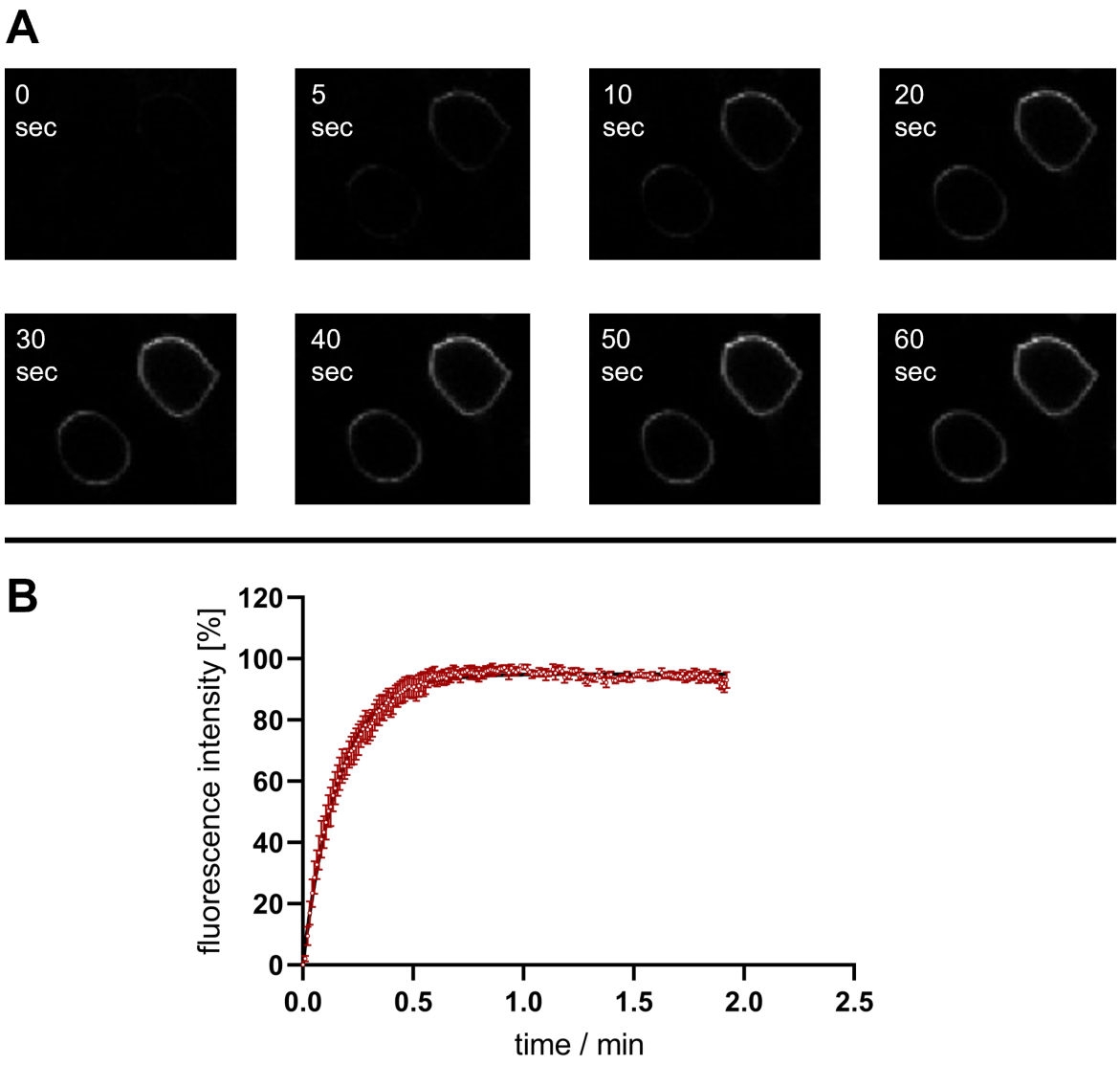

Figure 3.6: Association of **76** to the hD_1R at HEK-293T cells using LSCM. Time-lapse confocal microscopy images of **76** (c = 50 nM) at HEK-293T cells transiently expressing the hD_1R (**A**). Representative association curve of **76** (c = 50 nM) at HEK-293T cells transiently expressing the hD_1R (**B**). Data represent mean ± SEM of four independent cells of one experiment.

To test the suitability of **76** for LSCM and to visualize the binding of **76** to the D_1R, HEK-293T cells were transiently transfected with the hD_1R. 48 hours after transfection confocal microscopy images were recorded (Figure 3.6A). After addition of 50 nM of **76** a rapid accumulation of fluorescence at the cell surface was observed. This is caused by the fast association of **76** to the D_1Rs expressed on the cell membrane reaching saturation binding in less than one minute. Based on the fluorescence intensity of individual cells, a time-dependent association curve could be obtained illustrating the fast binding of **76** to the D_1R (Figure 3.6B). Based on the association and dissociation rates a kinetic pK_d

value of 8.07 was calculated (Table 3.4), which is in excellent agreement with the pK_d value of 8.20 obtained from the NanoBRET saturation binding assays (Table 3.2).

Table 3.4: Kinetic binding constants of **76** at the hD_1R in confocal microscopy.

cmpd	confocal microscopy					
	k_{obs}[a] (min^{-1})	τ_{ass}[b] (min)	k_{off}[c] (min^{-1})	τ_{diss}[d] (min)	k_{on}[e] (min^{-1})	pK_d (kin)[f]
76	5.24 ± 0.43	0.21 ± 0.03	0.76 ± 0.16	1.76 ± 0.88	0.09 ± 0.01	8.07 ± 0.01

[a]17 cells from four independent experiments were analyzed. Data represent mean values ± SEM. Experiments were performed at HEK293T cells transiently expressing the hD_1R. [b]Data represent mean values ± CI (95 %). Association time constant: $\tau_{ass} = 1/k_{obs}$. [c]5 cells from one experiment were analyzed. Data represent mean values ± SEM. Experiments were performed at HEK293T cells transiently expressing the hD_1R. [d] [b]Data represent mean values ± CI (95 %). Dissociation time constant: $\tau_{ass} = 1/k_{off}$. [e]Association rate constant: $k_{on} = (k_{obs} - k_{off}) / c$(**76**). Indicated errors were calculated according to the Gaussian law of error propagation. [f] K_d (kin) = k_{off}/k_{on}; pK_d (kin) = −log K_d (kin). Indicated errors were calculated according to the Gaussian law of error propagation.

These results demonstrate the suitability of **76** for the use in fluorescence microscopy as a labeling agent to visualize D_1R in live cells.

3.6 Conclusion

A set of six different fluorescent ligands, containing linkers of different lengths and chemical compositions and two different fluorescent dyes, was designed and synthesized. The previously designed and synthesized D_1R pharmacophore for the bivalent ligands could be used as a pharmacophore for the fluorescent ligands. Two fluorescent dyes, 5-TAMRA and DY549-P1, were chosen because of their proposed suitability as a fluorescent tracer for the NanoBRET assay. After the successful synthesis and purification of the ligands their fluorescent and pharmacological properties were determined. Saturation binding experiments using the NanoBRET setup confirmed their suitability for this assay as well as their affinity towards the D_1R, with **76** showing the highest BRET signal and affinity. In order to study the influence of the genetical modification of the receptor and the selectivity of the ligands, radioligand binding studies were performed revealing **76** and **78** as D_1-like receptor selective fluorescent ligands with binding affinity in the one-digit nanomolar range. As **76** showed the best overall results regarding affinity, selectivity, quantum yield, and BRET signal it was used as an exemplary compound to determine the mode of action. A G protein biosensor assay confirmed the suspected silent antagonism of **76**. These results make **76** a promising candidate for the use as a fluorescent tracer in NanoBRET competition binding assays, which will soon be performed by Denise Mönnich as part of her PhD project.

Furthermore, **76** was used successfully to label D_1Rs in live cells for LSCM demonstrating its suitability for fluorescence microscopy and can possibly be used as a labeling agent for TIRF single-molecule imaging of the D_1R as well.

All in all, the set of fluorescent ligands, especially **76**, represent a versatile tool for different experimental setups for further investigations at the D_1-like receptors.

4. Fluorescent ligand for the H_3R

Note: Prior to the submission of this thesis, the content of this chapter (with additional data) was published in collaboration with partners:

Rosier, N., Grätz, L., Schihada, H., Möller, J., Isbilir, A., Humphrys, L. J., Nagl, M., Seibel, U., Lohse M. J., Pockes, S. (2021). A Versatile Sub-Nanomolar Fluorescent Ligand Enables NanoBRET Binding Studies and Single-Molecule Microscopy at the Histamine H_3 Receptor. *Journal of Medicinal Chemistry*, *64*(15), 11695-11708.[157]

The following experimental work was performed by co-authors:

NanoBRET studies:	Lukas Grätz
G_{i2}-BRET sensor and assays:	Hannes Schihada
Confocal microscopy:	Ali Isbilir
TIRF microscopy:	Jan Möller
Off-target screening:	Lukas Grätz and Laura J. Humphrys
HEK293-SP-FLAG-hH_3R cell line:	Ulla Seibel
Radioligand binding assays:	Martin Nagl

4.1 Design

Similar to the D_1R fluorescent ligands the three parts of the H_3R bivalent ligand had to be designed carefully.[216]

The same lead structure that was used for the bivalent ligands was chosen as well for the fluorescent ligand. The H_3R antagonist JNJ-5207852 is one of the most affine H_3R ligands reported so far. Besides its high H_3R affinity it shows an excellent selectivity not only within the histamine receptor family but also with respect to 50 other different targets.[178] These properties combined with the synthetic accessibility and good water solubility make it an excellent pharmacophore for a fluorescent ligand. Structure activity relationships showed a high tolerance of the ligand towards structural changes at the para position of the benzylic piperidine moiety.[179] Thus, this position of the molecule has been chosen to attach the linker via an amide group.

In terms of the linker moiety, a flexible polyethyleneglycole-based (PEG-based) structure with a length of 13 atoms was used, which we assumed would be sufficient to reach outside the binding pocket, thus reducing the probability of a negative impact of the linker on ligand binding. PEG-based linkers are often used in fluorescent ligands, as they are chemically stable, show higher water solubility than alkylic structures and are less susceptible to interact with cell membranes.[218]

The choice of the fluorescent dye must be taken carefully for any fluorescent ligand and depends mainly on the intended application of the ligand. With the aim of a versatile fluorescent ligand for the use in the NanoBRET binding assay and fluorescence microscopy the 5-TAMRA fluorescent dye was chosen. The suitability of this dye for the NanoBRET binding has been shown for different receptors,[152,220] as it led to a better signal to noise ratio and less adhesion to the plastic vessel than, e.g. BODIPY labelled ligands at the H_2R.[219] Furthermore, 5-TAMRA was reported as a fluorescent dye for single-molecule imaging in TIRF microscopy[221,222] and, due to its hydrophilicity, it is less prone to interact with cell membranes than BODIPY[224], resulting in a lower nonspecific binding in fluorescence microscopy techniques.

4.2 Chemistry

The synthesis of the fluorescent ligands can be separated into three parts: the synthesis of the pharmacophore, the linkers and the connection of the different parts including labeling with a fluorescent dye. The syntheses of the H_3R pharmacophore (**26**) and the linker (**35b**) were performed analogous to the synthetic protocols described in chapters 2.2.2 . and 2.2.3 .

Scheme 4.1: Synthesis of the H_3R fluorescent ligand **82**.[a]

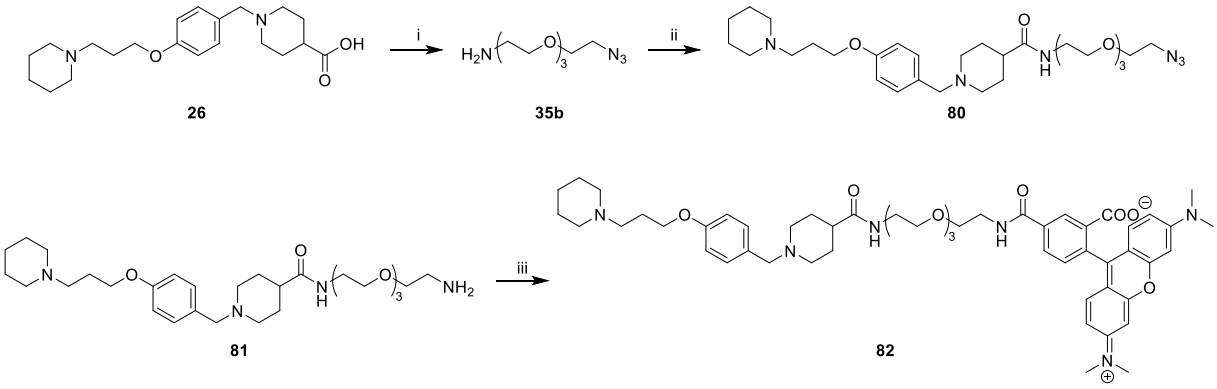

[a]Reagents and conditions: i) 1. **26**, EDC x HCl, HOBt, DIPEA, DCM/DMF (1:1), rt, 30 min; 2. **35b**, 100 °C MW, 30 min, 65 %; ii) 1. PPh_3, THF, 4 h, 45 °C; 2. H_2O, 2 h, 45 °C, 60 %; iii) 1. 5-TAMRA NHS ester, NEt_3, DMF, rt, 2.5 h; 2. 10 % aq. TFA, rt, 15 min, 82 %.

The H_3R pharmacophore **26** was coupled with **35b** using EDC/HOBt as coupling reagents under microwave irradiation to afford product **80**, which was reduced to the primary amine **81** by a "Staudinger" reaction (Scheme 4.1). In the final step, **81** was coupled with the 5-TAMRA-NHS ester in DMF to afford fluorescent ligand **82**.[219] After preparative HPLC purification, **82** was obtained with high purity (99 %) and yield (82 %). The fluorescent ligand was further examined for its chemical stability in aqueous solution and showed no decomposition within an incubation period of six months (HPLC purity controls are shown in the appendix, chapter 8.1).

The chemical structure of all synthesized compounds was proven by ^1H and ^{13}C NMR as well as HRMS. The chemical structure and ^1H NMR spectra of **82** are presented in the appendix (chapter 8.3).

4.3 Fluorescence properties of 82

Fluorescence properties of **82** (in PBS containing 1 % BSA) were ascertained by recording excitation and emission spectra shown in Figure 4.1. The 5-TAMRA-labeled ligand exhibited an excitation maximum at 555 nm and an emission maximum at 585 nm (Table 4.1). The quantum yield of **82** was determined as described in chapter 3.3. Analogous to the 5-TAMRA labeled D_1R fluorescent ligands **76** and **78**, **82** has a quantum yield in the same range (35 %) and the addition of BSA to the aqueous media led to a slight decrease of Φ.

Table 4.1: Fluorescence properties of compound **82**.

cmpd	$\lambda_{exc,max}/\lambda_{em,max}$ (nm)	absorbance	Φ[a] (%)	
			PBS	PBS + 1 % BSA
82	555 / 585	0.16	35.09 ± 0.35	33.31 ± 0.55

[a]Data shown are mean values ± SEM for three different slit adjustments (exc./em.): 5/5 nm, 5/10 nm, 10/10 nm.

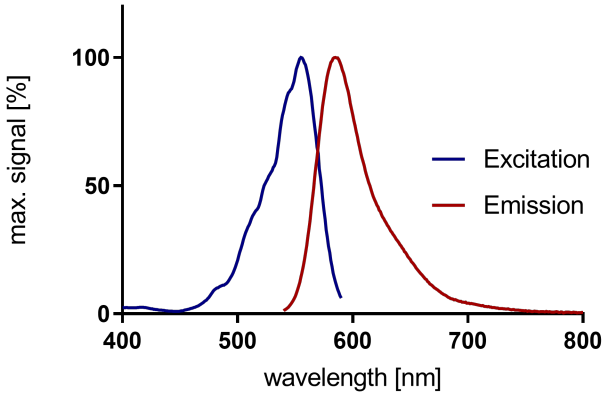

Figure 4.1: Excitation and emission spectra of **82**.

4.4 Pharmacological characterization

The first step in the pharmacological characterization of the fluorescent ligand **82**, structurally derived from the H_3R antagonist JNJ-5207852[178] (Figure 2.1), was the investigation of the binding behavior in different assays. To achieve one of our main goals the compound was tested for suitability in the NanoBRET binding assay at the NLuc-hH_3R stably expressed in HEK293 cells. BRET saturation binding experiments provided a binding constant for **82** in the sub-nanomolar range (pK_d = 9.80 ± 0.07, Figure 4.2A, Table 4.2) and very low nonspecific binding. In order to investigate a potential influence of the receptor modification on ligand binding, **82** was additionally examined in flow cytometry using wild-type hH_3R cells (HEK293-SP-FLAG-hH_3R) (Figure 4.2B).

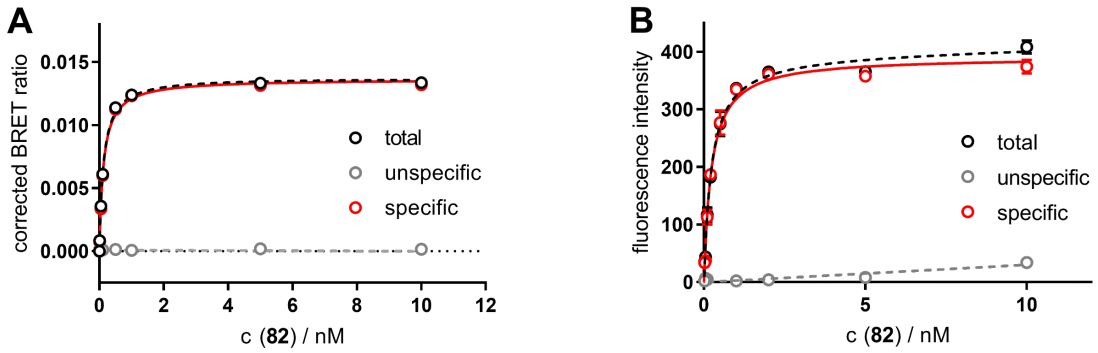

Figure 4.2: Representative isotherms from saturation binding experiments with **82** at the NLuc-hH_3R (**A**, NanoBRET) and at the wild-type hH_3R (**B**, flow cytometry), both stably expressed in HEK293 cells.

Table 4.2: Comparison of thermodynamic and kinetic binding constants of **82** at the wild-type hH_3R and the NLuc-hH_3R.

cmpd	Flow cytometry	NanoBRET binding						
	pK_d (sat)[a]	pK_d (sat)[b]	k_{obs}[c] / min^{-1}	τ_{ass}[d] / min	k_{off}[c] / min^{-1}	τ_{diss}[e] / min	k_{on}[f] / min^{-1} nM^{-1}	pK_d (kin)[g]
82	9.71 ± 0.04	9.80 ± 0.07	0.51 ± 0.02	1.97 ± 0.14	0.16 ± 0.01	6.45 ± 0.62	0.71 ± 0.04	9.66 ± 0.15

[a]Data represent mean values ± SEM from three independent experiments each performed in duplicate. Flow cytometric measurements performed with HEK293-SP-FLAG-hH_3R (wild-type hH_3R) cells. [b]Data represent mean values ± SEM from three independent experiments each performed in triplicate. NanoBRET binding experiments performed with live HEK293 cells stably expressing the NLuc-hH_3R. [c]Data represent mean values ± SEM or [d,e] ± CI (95 %) from four independent experiments. [d]Association time constant: $\tau_{ass} = 1/k_{obs}$. [e]Dissociation time constant: $\tau_{diss} = 1/k_{off}$. [f]Association rate constant: $k_{on} = (k_{obs}-k_{off})/c(\mathbf{12})$. [g]$K_d$ (kin) = k_{off}/k_{on}; pK_d (kin) = -log K_d (kin). [f,g]Indicated errors were calculated according to the Gaussian law of error propagation.

The receptor affinity of **82** to wild-type H_3Rs (pK_d = 9.71 ± 0.04, Table 1) was in the same range as for the NLuc-hH_3Rs showing no significant difference ($p < 0.05$, two-tailed t-test). Fortunately, this experimental setup further confirmed the minimal nonspecific binding of this ligand observed in the BRET assay.

To further characterize the fluorescent tracer radioligand competition binding experiments were performed at the $H_{1\text{-}4}$R providing information on receptor subtype selectivity within the histamine receptor family. The ligand exhibited receptor affinity to the H_3R in a sub-nanomolar range with a pK_i of 9.52 ± 0.08 and an outstanding selectivity profile being at least 100,000-fold selective towards the human H_1R, H_2R and H_4R (Figure 4.3; Table 4.3).

Table 4.3: Binding and functional data of **82** on human histamine receptor subtypes.

cmpd	Radioligand competition binding[a]								H_3R selectivity	G_{i2} activation[b]	
	pK_i								K_i ($H_{1,2,4}$R)/ K_i (H_3R)	pK_b	
	hH_1R[c]	*N*	hH_2R[d]	*N*	hH_3R[e]	*N*	hH_4R[f]	*N*	h$H_{1,2,4}$R	hH_3R[g]	*N*
82	< 4	3	< 4	3	9.52 ± 0.08	3	< 4	3	> 100.000	9.04 ± 0.03	3

[a]Competition binding assay at HEK293-SP-FLAG-hH_1R, HEK293-SP-FLAG-hH_2R, HEK293-SP-FLAG-hH_3R or HEK293-SP-FLAG-hH_4R cells. [b]Competition binding experiment at HEK293A cells stably expressing the G_{i2} BRET sensor with the wild-type hH_3R. [c]Displacement of 5 nM [^{3}H]mepyramine (K_d = 4.5 nM). [d]Displacement of 20 nM [^{3}H]UR-DE257[206] (K_d = 66.9 nM). [e]Displacement of 2 nM [^{3}H]UR-PI294[203] (K_d = 5 nM). [f]Displacement of 15 nM [^{3}H]histamine (K_d = 15.88 nM). [g]Inhibition of imetit-induced (c = 1 nM, EC_{50} = 0.85 nM) G_{i2} activation. Data shown are mean values ± SEM of *N* independent experiments, each performed in triplicate. Data were analyzed by nonlinear regression and were best fitted to sigmoidal concentration-response curves. Displacement curves are presented in Figure 4.3.

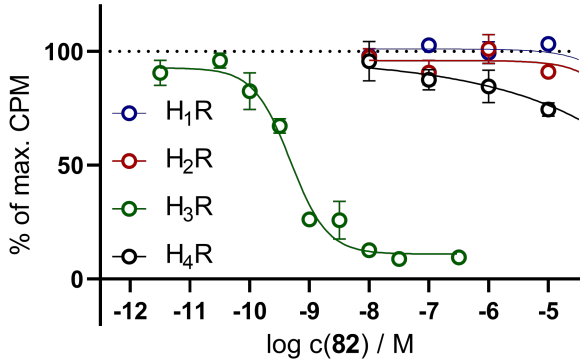

Figure 4.3: Displacement curves from radioligand competition binding experiments performed with compound **82** and the respective radioligands (Table 4.3 footnotes).

Being aware of the fact that the fluorescent ligand's pharmacological mode of action is crucial, e.g., since an agonist might distort apparent affinities of competitive ligands due to internalization processes and induction of ternary complex formation (ligand/H_3R/G-protein), we wanted to gain insights into the functional behavior of **82**. Therefore, we employed a recently developed BRET-based G_{i2} biosensor detecting G protein activation as a decrease in BRET between NLuc-tagged $G\alpha_{i2}$ and cpVenus-tagged $G\gamma_2$.[226] As a BRET acceptor we used cpVenus, which was fused C-terminally to $G\gamma_2$. After agonist stimulation, the receptor activation and subsequent dissociation of the heterotrimeric G protein results in a decrease in BRET (for details see Rosier, N. *et al*.[157]). As expected, **82** acted as a neutral antagonist (Figure 4.4A) revealing a pK_b value of 9.04 ± 0.03 in competition experiments with the selective H_3R agonist imetit (Figure 4.4B).

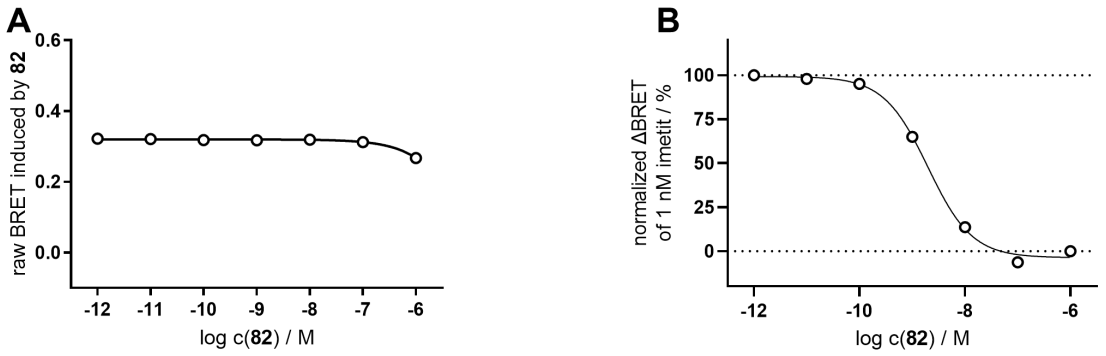

Figure 4.4: Concentration-response curves (CRCs) for G_i activation of **82** in the absence (**A**) and presence (**B**) of 1 nM imetit at HEK293A cells transiently expressing the G_{i2} BRET sensor along with the wild-type hH_3R.

However, before using **82** as a molecular tool to characterize other H_3R ligands the kinetic behavior of the fluorescent ligand should be determined first. The NanoBRET setup is ideally suited for this purpose due to its ability to perform real-time kinetic measurements. 500 pM of **82** were used to measure ligand association at the H_3R (Figure 4.5). Ligand binding to the receptor saturated after about 15 minutes (τ_{ass} = 1.97 ± 0.14) and the ligand fully dissociated with a tau (τ) value of 6.45 ± 0.62 min upon addition of an excess of clobenpropit (c = 250 nM, Figure 4.5; Table 4.2). All kinetic parameters describing the binding of **82** in the BRET binding assay are presented in Table 4.2.

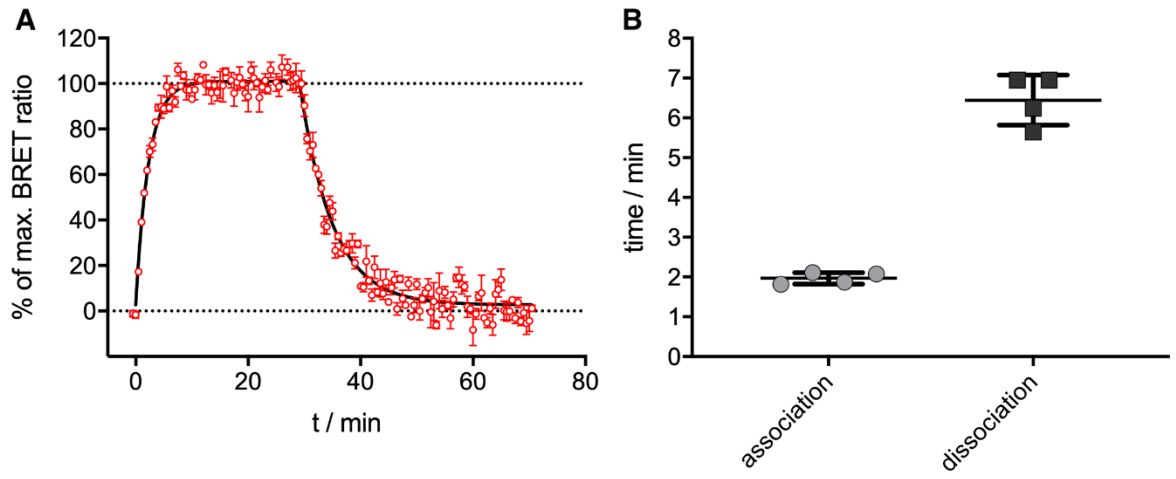

Figure 4.5: BRET-based specific binding kinetics of the fluorescent ligand **82** at the NLuc-hH_3R, stably expressed in HEK293 cells. (**A**) Graph shows association of **82** (c = 500 pM) to the receptor and dissociation of **82** induced by addition of clobenpropit (c = 250 nM, 500-fold excess) from a representative experiment. (**B**) Scatter dot plot displaying the quantification of tau (τ) values for association/dissociation of the fluorescent ligand. Data were analyzed from four independent experiments represented with mean ± SD.

The complete reversibility of receptor binding makes the fluorescent ligand a suitable tool for the use in competition binding studies, in our case performed with a selection of standard H_3R agonists and antagonists. We selected histamine (his),[232] imetit (imet),[233] (R)-(-)-α-methylhistamine (RAMH),[114] (S)-(+)-α-methylhistamine (SAMH)[114] as agonists and clobenpropit (clob),[234] Z27743747 (Z-cmpd),[235] thioperamide (thio),[114] pitolisant (pito)[236] and JNJ-5207852 (JNJ)[178] represented the inverse agonists/antagonists. For all ligands, total displacement could be determined with Hill slopes around 1 (Figure 4.6). Overall, our data are in good agreement with data from literature (Table 4.4), apart from RAMH and SAMH showing larger deviations. However, it is remarkable that the assay can distinguish between the two enantiomers RAMH and SAMH, a phenomenon that has been described several times at the hH_3R (Table 3).[114,237–239]

Table 4.4: Binding data (pK_i values) of standard H_3R ligands determined at the human H_3R in the NanoBRET binding assay.[a]

cmpd	NanoBRET (**82**)		references
	pK_i	*N*	pK_i
his	6.23 ± 0.08	4	6.3[240]; 6.5[202]; 7.6[241]; 8.0[239]
imet	7.90 ± 0.11	3	8.3[240]; 8.8[239]
RAMH	7.20 ± 0.02	3	8.4[238]; 8.2[239]; 8.3[237]
SAMH	5.79 ± 0.11	3	6.4[240]; 7.6[238]; 7.2[239]; 7.3[237]
clob	9.30 ± 0.08	3	9.6[240]; 9.5[202]; 8.6[239]
Z-cmpd	7.71 ± 0.01	3	7.4[235]; 7.3[237]
thio	7.28 ± 0.18	3	7.3[240]; 7.4[202]; 7.3[239]
pito	9.04 ± 0.12	3	8.6[240]; 8.6[236]
JNJ	10.22 ± 0.02	3	9.225

[a]Data represent mean values ± SEM from *N* independent experiments, each performed in triplicate. NanoBRET experiments were performed at live HEK293 cells stably expressing the NLuc-hH_3R as described in the Experimental Section. Used abbreviations: histamine (his), imetit (imet), (R)-(-)-α-methylhistamine (RAMH), (S)-(+)-α-methylhistamine (SAMH), clobenpropit (clob), Z27743747 (Z-cmpd), thioperamide (thio), pitolisant (pito) and JNJ-5207852 (JNJ).

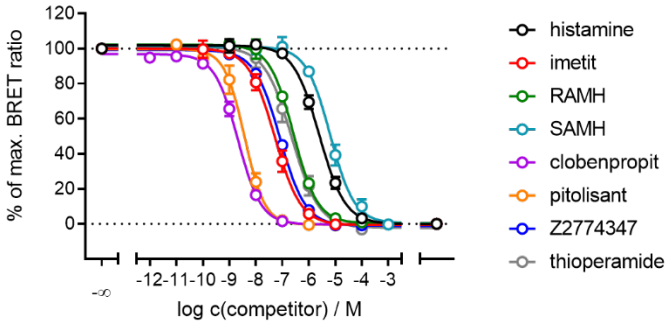

Figure 4.6: Displacement curves from BRET competition binding experiments of the fluorescent ligand **82** (c = 500 pM) and reported H_3 receptor ligands at HEK293 cells, stably expressing the NLuc-hH_3R. "Vehicle" denotes for the condition where the cells were not incubated with **82**. Used abbreviations: histamine (his), imetit (imet), (R)-(-)-α-methylhistamine (RAMH), (S)-(+)-α-methylhistamine (SAMH), clobenpropit (clob), Z27743747 (Z-cmpd), thioperamide (thio), pitolisant (pito) and JNJ-5207852 (JNJ).

4.5 Fluorescence microscopy

To visualize the binding and dissociation kinetics of the fluorescent ligand, we used confocal microscopy imaging. In this experiment, time-lapse images of HEK293-SP-FLAG-hH_3R cells were acquired (Figure 4.7).

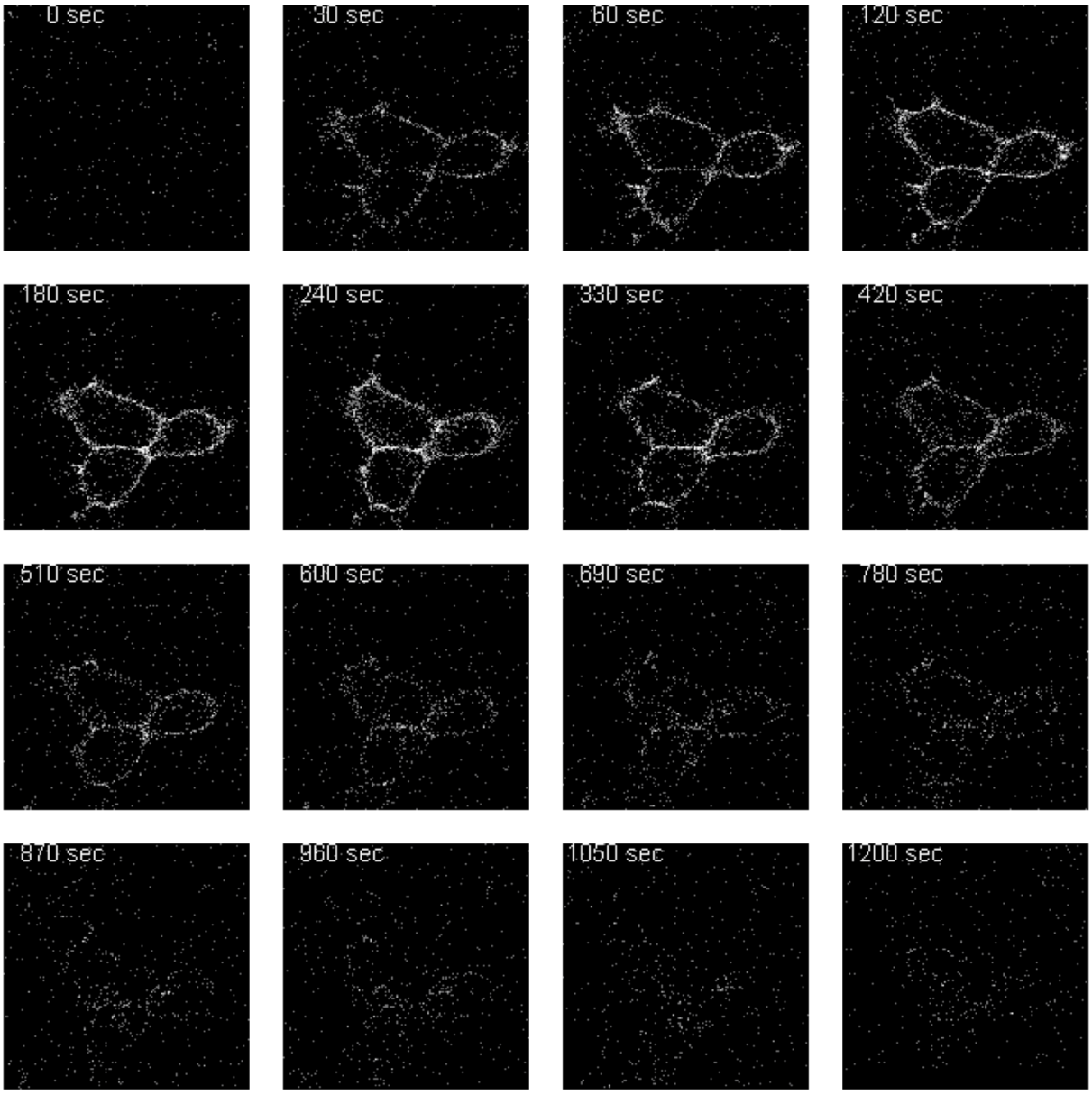

Figure 4.7: Time-lapse confocal microscopy images of the fluorescent ligand **82**: Imaging of the HEK293-SP-FLAG-hH_3R cells treated with 5 nM fluorescent ligand displayed a time-dependent increase of the fluorescence signal on the cell surface, indicating ligand binding to the H_3R. Competing **82** with the unlabeled H_3R antagonist clobenpropit decreased the fluorescence signal in a time-dependent manner (addition of clobenpropit after 220 seconds).

Compared to the kinetic NanoBRET experiments we used ten times higher concentrations of **82** to facilitate visualization with the confocal microscope. After the addition of **82** (c = 5 nM), the

fluorescence signal on the cell surface increased and reached a plateau within 4 minutes (Figure 4.8A). The fluorescent ligand's dissociation was initiated by the addition of 2.5 µM clobenpropit (500-fold excess). The addition of clobenpropit (after 220 seconds) decreased the fluorescent signal indicating the dissociation of **82** (Figure 4.8B). We observed a τ value of 0.48 ± 0.07 min for the association and 3.50 ± 0.46 min for the dissociation of the fluorescent ligand (Table 4.5).

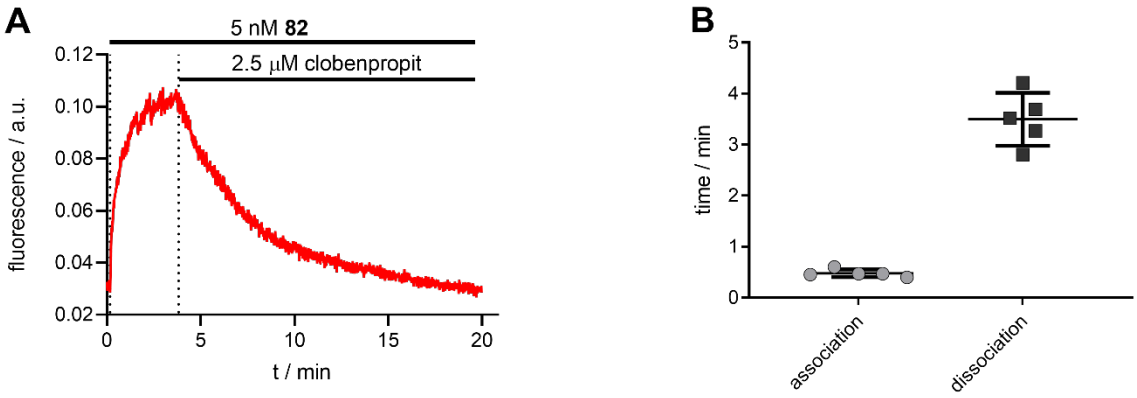

Figure 4.8: Association and dissociation kinetics of the fluorescent ligand: (**A**) Representative graph displaying the quantification of the fluorescence signal obtained from experiments as in Figure 4.2. The fluorescence signal (in arbitrary units) was plotted as a function of time and association/dissociation kinetics were calculated by fitting an exponential decay function on the signal (from baseline to saturation, and from saturation to decay to the baseline). Addition of the competitor clobenpropit after 220 seconds. (**B**) Scatter dot plot displaying the quantification of tau (τ) values for association/dissociation of the fluorescent ligand. Five cells from three independent experiments were analyzed. Data were represented with mean ± SD.

These experiments demonstrated that the binding of the fluorescent ligand to the H_3R occurs very rapidly and that the bound ligand can be displaced completely. Due to the use of different concentrations (see above) a difference in k_{obs} values was to be expected (Table 4.2 and Table 4.5). However, the k_{on} and k_{off} values, which would be expected to be the same, differ by a factor of nearly two (Table 4.2 and Table 4.5). This could be a result of the receptor's modification with the NanoLuc which maybe influence the binding kinetics. Consequently, the kinetic pK_d values from the NanoBRET (pK_d = 9.66 ± 0.15) and confocal experiments (pK_d = 9.10 ± 0.06) differ but are still in good agreement, so both assays can be considered complementary (Table 4.2 and Table 4.5). Additionally, we tested the photobleaching properties of **82** by immobilizing the fluorescent ligand in 0.5 % agarose film in 1µM final concentration. In these experiments the ligand shows a negligible photobleaching (4 %, N = 4) after 20 minutes which is unlikely to affect the observed association and dissociation kinetics of **82**.

Table 4.5: Kinetic binding constants of **82** at the wild-type hH_3R in confocal microscopy.

cmpd	Confocal microscopy					
	k_{obs}[a] / min^{-1}	τ_{ass}[b] / min	k_{off}[a] / min^{-1}	τ_{diss}[c] / min	k_{on}[d] / min^{-1} nM^{-1}	pK_d (kin)[e]
82	2.13 ± 0.14	0.48 ± 0.07	0.29 ± 0.02	3.50 ± 0.46	0.37 ± 0.03	9.10 ± 0.06

[a,b,c]Five cells from three independent experiments were analyzed. [a]Data represent mean values ± SEM or [b,c] ± CI (95 %). Confocal microscopy measurements performed at HEK293-SP-FLAG-hH_3R (wild-type hH_3R) cells. [b]Association time constant: $\tau_{ass} = 1/k_{obs}$. [c]Dissociation time constant: $\tau_{diss} = 1/k_{off}$. Association rate constant: $k_{on} = (k_{obs}-k_{off})/c$(**82**). [e]$K_d$ (kin) = k_{off}/k_{on}; pK_d (kin) = -log K_d (kin). [d,e]Indicated errors were calculated according to the Gaussian law of error propagation.

Due to the low nonspecific binding and the high affinity of our compound we wondered about its suitability for total internal reflection fluorescence (TIRF) single-molecule microscopy as shown previously for a few other fluorescent GPCR ligands.[158,242,243] Indeed, its favorable properties were confirmed in microscopy experiments and allowed the acquisition of single-molecule TIRF movies in the presence of 3 nM **82** in the imaging buffer with negligible background fluorescence (Figure 4.9A). We further tested the labeling efficiency under these conditions by using a H_3R control construct, which was C-terminally tagged with the photostable fluorescent protein mNeonGreen. Dual color acquisition revealed colocalization, a labeling efficiency of 96.1 ± 2.1 % and a nonspecific binding of 2.5 ± 0.8 under these conditions (Figure 4.9B). Single-particle tracking of the acquired TIRF movies and subsequent diffusion analysis of the receptor tracks (Figure 4.9C, D) showed similar receptor dynamics for the H_3R (diffusion coefficient of 0.085 ± 0,006 $\mu m^2/s$) as shown previously for other class A GPCRs.[242,243]

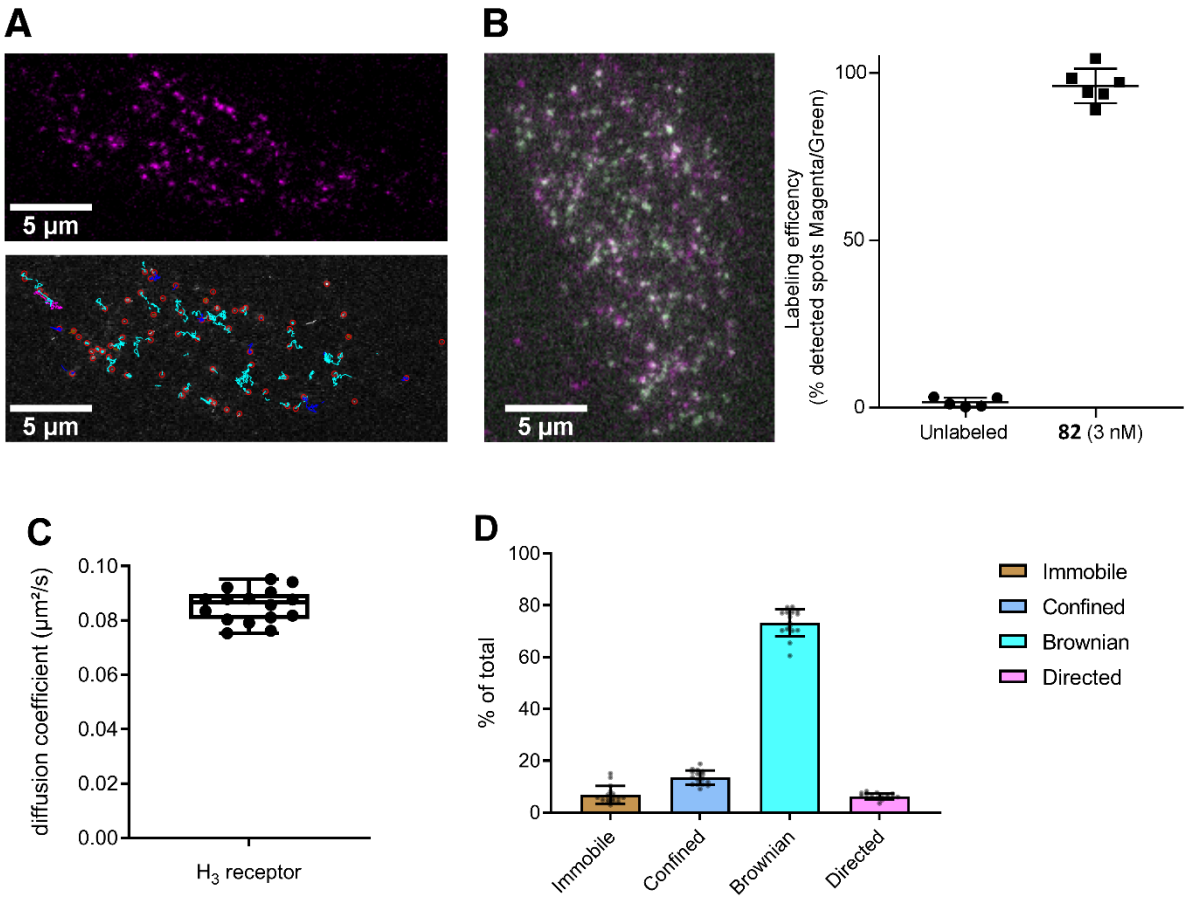

Figure 4.9: (**A**) Top panel: wild-type H_3 receptors labeled with 3 nM **82**; Bottom panel: Single particle tracking of individual wild-type H_3 receptors and classification of diffusion classes (magenta = directed diffusion, blue = confined diffusion, cyan = Brownian motion and brown = immobile). Shown images are representative of four independent experimental days. (**B**) Labeling efficiency measured by colocalization of the two colors in their corresponding detection channels (GFP/Cy3) as shown in the representative image. Labeling efficiencies are for the unlabeled control 2.5 ± 1.8 % and 96.1 ± 5.2 % at 3 nM of **82**, respectively. Data are mean ± SD and originate from three independent experiments. Each datapoint refers to one cell. (**C**) Diffusion analysis based on single-particle tracking gives a diffusion coefficient of 0.085 ± 0,006 $\mu m^2/s$. The diffusion type classification (**D**) is composed by 6.9 ± 0.8% immobile, 13.5 ± 0.7% confined, 73.3 ± 1.3% Brownian motion and 6.3 ± 0.3% directed tracks undergoing the corresponding type of diffusion. Data are mean ± SD and originate from three independent experiments. Each datapoint refers to one cell.

4.6 Off-target screening of 82

Once selectivity within the histamine receptor family was established we sought to identify any binding of **82** to other GPCR members. We performed an off-target screen using 14 different GPCRs. Therefore, we used the BRET-based binding assay with transient NLuc-receptor expression. Unfortunately, the capacity of the unpublished Nluc-receptor constructs to bind their endogenous ligands could not be thoroughly controlled given the lack of validated fluorescent ligands. Instead, it was only presumed based on sufficient surface expression of these constructs and based on the experience that N-terminal insertion of the nano luciferase usually does not affect the binding ability of class A GPCRs.[220,244–247] Receptor cell surface expression was confirmed by an ELISA using a NanoLuc antibody (Cat. No. MAB100261, Bio-Techne, Minneapolis, MN, USA; results see Rosier, N. *et al*.[157]). We determined that at 200 nM of **82** there was little off-target binding with only the muscarinic hM_2R and hM_4R displaying mild but significant affinity (13.2 ± 4.5 % and 6.7 ± 5.3 % of hH_3R response, respectively; Figure 4.10). Some ligand binding at the hM_2R and hM_4R was unsurprising as the binding sites of these receptors share features with the hH_3R and several characteristics of known H_3R ligands have proved useful in developing muscarinic antagonists.[248,249] It should be noted that BRET signals from binding experiments to different Nluc-GPCR constructs can only be compared with caution given the different N-terminal lengths and localisations of orthosteric binding pockets. Therefore, the low BRET signals observed at hM_2R and hM_4R (only ~ 10 % of the BRET signal detected with Nluc-hH_3R) do not provide a quantitative value but rather an estimate for the binding of **82** to the receptors. Nevertheless, we believe that the low BRET signals for the muscarinic receptors using a maximal concentration of 200 nM do not indicate any off-target issues as **82** has sub-nanomolar affinity for the target hH_3R.

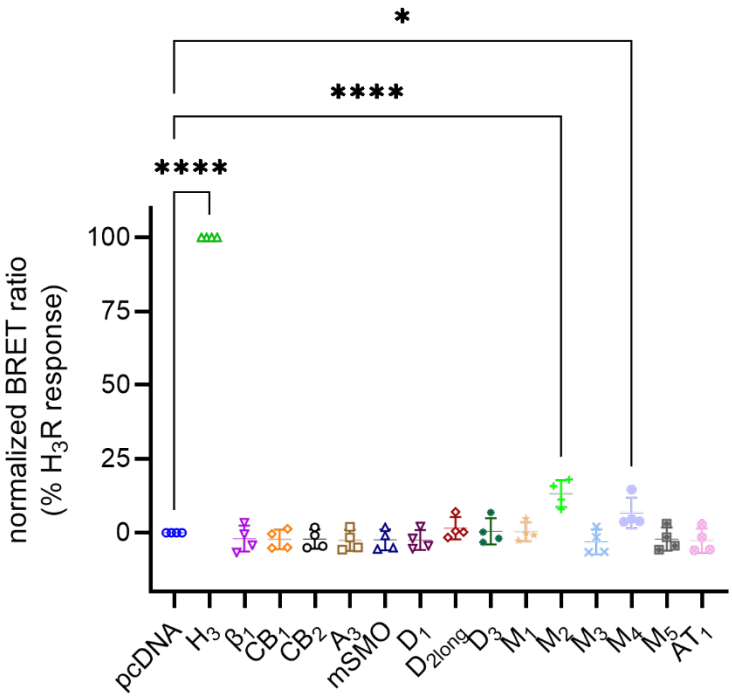

Figure 4.10: Off-target affinity in BRET binding experiments of the fluorescent ligand **82** (c = 200 nM) in HEK293T cells transiently expressing NLuc-receptor constructs. Data were normalized to the hH_3R (100%) and empty vector control (0%). Transfection with an empty pcDNA vector backbone is expressed as 'pcDNA'. Receptor abbreviations are as follows: H_3, histamine H_3; β_1, β_1 adrenoceptor; $CB_{1/2}$, cannabinoid receptor type 1/2; A_3, adenosine A_3; mSMO, mouse smoothened; $D_{1/2long/3}$, dopamine $D_{1/2long/3}$; $M_{1/2/3/4/5}$, muscarinic acetylcholine $M_{1/2/3/4/5}$; AT_1, angiotensin II type 1. All receptor sequences are human, save the smoothened receptor originating from mouse. Lines represent mean ± SD of four experiments, with each experimental condition performed in duplicate. Statistical significance was assessed by one-way ANOVA followed by Fisher's LSD post-hoc test against 'pcDNA'; *: $P < 0.05$; ****: $P < 0.0001$.

4.7 Conclusion

In **82**, we described a sub-nanomolar affinity fluorescent ligand at the H_3R with an outstanding selectivity profile within the histamine receptor family. The 5-TAMRA-labeled neutral antagonist was broadly characterized analytically, pharmacologically and showed excellent kinetic and fluorescence properties. These results ensure excellent suitability for the recently described NanoBRET assay. The successful use as a fluorescent probe in the NanoBRET binding assay highlights the versatility of **82** and its suitability as a powerful tool in the urgently needed research for new drug candidates at the H_3R. A comprehensive off-target screening at 14 different receptors reveals **82** as a selective compound.

Due to its high affinity, an exceptional receptor selectivity combined with a high brightness and the proven low nonspecific binding **82** shows remarkable results in fluorescent microscopy and is the first fluorescent ligand to enable single-molecule imaging of the H_3R. Furthermore, it allows the presence of saturating concentrations in the imaging buffer during single-molecule image acquisition. This accounts for the obvious advantage of continuous labeling of receptors in the course of the experiment and compensates fluorophore photobleaching. Thus, **82** is a versatile tool suitable for binding and also imaging studies at the H_3R. To the best of our knowledge this is unique within the panel of available H_3R fluorescent ligands lifting the study of H_3R-dependent disease-related functions onto another level. Especially the suitability in TIRF and confocal microscopy makes **82** a valuable tool to further investigate the role of the H_3R in the central nervous system as the H_3R was reported to form heteroreceptor complexes in combination with other GPCRs and ion channels.[61,131,133] This could be of great interest for neurodegenerative diseases, e.g. Alzheimer's disease, as these receptor complexes have arisen as promising targets to prevent neuronal cell death.[131]

5. Summary and outlook

Although G protein-coupled receptors (GPCRs) are already among the most targeted protein class by FDA-approved drugs there are still a lot of unsolved question about them. In recent years, with growing evidence for GPCR di- and oligomerization the conviction manifested in the research community that GPCR do not function exclusively as monomers. Many research groups described changes in ligand binding, signaling behavior, and receptor trafficking upon di- or oligomerization, raising the question of the pharmaceutical potential of GPCR di- and oligomers. Nevertheless, responding this question is far from easy and requires novel pharmacological assays system as well as pharmacological tool compounds, such as bivalent ligands. The concept of bivalent ligands has been introduced decades ago and consists of the idea of connecting two pharmacophores for two distinct binding sites in a way that both can bind their recognition site simultaneously. Due to this bivalent binding mode a higher affinity and selectivity for the receptor dimer, compared to the protomers, can be achieved.

The aim of this thesis was the synthesis and pharmacological characterization of bivalent ligands for the D_1-H_3 receptor heteromer (D_1-H_3 Het), which was published first in 2009 and was linked to neuronal cell death. Prior to starting the synthesis, the bivalent ligands had to be designed carefully choosing appropriate lead structures for the pharmacophores and suitable attachment points to connect them to the spacer. Molecular modeling studies gave an insight into the probable distance of both binding pockets and an indication of appropriate spacer lengths. Based on literature and retrosynthetic approaches a synthesis for the bivalent ligands was designed and executed. By introducing C-C triple bonds to all pharmacophores and azide groups to all spacers a variety of different bivalent ligands could be synthesized using CuAAC reaction from the same building blocks. This approach avoided the need of an individual pharmacophore or spacer for each bivalent ligand.

After the successful synthesis of 16 bivalent ligands, four endcapped ligands and two reference compounds all novel structures were analyzed for their affinity towards the D_1R and H_3R. Fortunately, most of the ligands maintained the affinity of the lead structures with **44** and **45** showing the highest binding affinities at both receptors in the sub-nanomolar range at the H_3R and one-digit nanomolar range at the D_1R. For compounds of that size such high binding affinities are remarkable. Therefore, these compounds were used to determine the selectivity of the bivalent ligands inside the histamine and dopamine receptor family as well as their mode of action. Both compounds proved to be selective and acted as silent antagonists at both receptors.

Finally, **45** was analyzed for its neuroprotective properties in primary mouse cortex cells upon Aβ-induced cell death. Indeed, a significant, concentration dependent neuroprotective effect was observed after the treatment of these cells with Aβ in the presence of different concentrations of **45**. Furthermore, a visibly higher reduction of cell death was observed for **45** compared to the endcapped ligands **59** and **61**. These results underlined the neuroprotective potential of the D_1-H_3 Het.

All these results demonstrate the high affinity of these ligands and indirectly indicate a bivalent binding mode. Modelling results support this hypothesis by confirming that the spacers should be of sufficient length. Nevertheless, to confirm a true bivalent binding mode additional competition binding studies at D_1R-H_3R co-expressing cells need to be performed. These experiments are currently in progress as part of the doctoral thesis of Denise Mönnich, but preliminary results are very promising. As previously shown for other bivalent ligands **45** afforded a biphasic binding curve demonstrating a high affinity and low affinity binding state in competitive radioligand binding experiments at the H_3R in D_1R-H_3R co-expressing cells. These results are indicating that **45** is indeed a bivalent ligand for the D_1-H_3 Het but these results have yet to be confirmed by additional experiments. Once a working assay system is established additional bivalent ligands with high affinity agonistic pharmacophores could be synthesized to study the effect they have on the D_1-H_3 Het. Therefore, a new agonistic lead structure for the D_1R should be chosen, as well as a different attachment point for the linker to the immepip-base pharmacophore (H_3R) in order to retain the high affinity of immepip.

In addition to the bivalent ligands, fluorescent ligands for both the D_1-like and the H_3 receptor were designed and synthesized. For this purpose, the same pharmacophores and linkers that were already synthesized for the bivalent ligands were used. Two different red fluorescent dyes (5-TAMRA and DY549-P1) were used to label the ligands. A set of six different fluorescent ligands for the D_1R and one fluorescent ligand for the H_3R were successfully synthesized. For the D_1R especially **76** showed a high affinity and BRET signal in NanoBRET saturation binding studies performed by Denise Mönnich. The high affinity and selectivity of **76** for the D_1-like receptors was confirmed by radioligand competition binding assays. Additionally, **76** was successfully used to label the D_1R for laser scanning confocal microscopy highlighting its diverse possible applications to study the D_1R. Currently ongoing experiments by Denise Mönnich are determining the suitability of **76** as a fluorescent tracer for NanoBRET competition binding studies for the screening of novel ligands at the D_1-like receptors. Furthermore, single-molecule TIRF imaging experiments of the D_1R by labeling the receptor with **76** are currently ongoing by a cooperation partner.

The H_3R fluorescent ligand **82** possesses a high affinity in the sub-nanomolar range and an exceptional selectivity for the H_3R inside the histamine receptor family. An additional off-target screening confirmed its selectivity towards 14 different GPCRs. Furthermore, **82** can be used as a fluorescent tracer for the competition NanoBRET binding assay and for the visualization of receptor binding by LSCM and even single-molecule studies using TIRF microscpopy. Due to the high affinity and diverse applications these fluorescent ligands represent powerful tools for further investigations at their respective receptors.

6. Experimental section

6.1 Chemistry

The following sections describe the experimental and analytical procedures and data for all compounds mentioned in this work.

6.1.1 General conditions

The references for all previously published compounds are cited at the synthetic procedures. All commercially available compounds (not labeled with a number) and solvents were purchased from the following commercial suppliers: Merck (Darmstadt, Germany), Sigma-Aldrich (Munich, Germany), Acros Organics (Geel, Belgium), Alfa Aesar (Karlsruhe, Germany), abcr (Karlsruhe, Germany), or TCI Europe (Zwijndrecht, Belgium). All compounds were used as received. All solvents were of analytical grade, except for column and flash chromatography. Dry sovlents were generated by the addition of 4 Å molecular sieve. All reactions with dry solvents were carried out under argon atmosphere. Microwave assisted reactions were performed on an Initiator 2.0 synthesizer (Biotage, Uppsala, Sweden). Reactions were monitored by thin layer chromatography (TLC) on Merck silica gel 60 F254 aluminum sheets and spots were visualized under UV light at 254 nm, by potassium permanganate, or ninhydrin staining. Column chromatography was accomplished using Merck Silica gel Geduran 60 (0.063-0.200 mm). Flash chromatography was performed with a 971-FP Flash Purification System (Agilent Technologies, Santa Clara, USA) using PF-30SIHP-F0012, PF-30SIHP-F0024, or PF-30SIHP-F0120 columns (Interchim, Montluçon Cedex, France). Composition of the mobile phase (column chromatography) or gradient (flash chromatography) is specified for each compound in the synthetic protocol. Preparative HPLC was performed with a system from Waters (Milford, Massachusetts, USA) consisting of a 2524 binary gradient module, a 2489 detector, a prep inject injector, and a fraction collector III. A YMC-Triart C18 (150 x 20 mm, 5 µm; YMC Co. Ltd., Kyoto, Japan) or a Gemini 5 µm NX-C18 110 Å LC column (250 x 21.2 mm; Phenomenex Ltd. Aschaffenburg, Germany) was used. As a mobile phase 0.1 % TFA or NH_3 in Millipore water and acetonitrile was used. The temperature was 25 °C, the flow rate 20 ml/min, and UV detection was performed at 220 nm. Lyophilization was done with a Christ alpha 2-4 LD equipped with a Vacuubrand RZ 6 rotary vane vacuum pump. Deuterated solvents for nuclear magnetic resonance (^{1}H NMR and ^{13}C NMR) spectra were purchased from Deutero GmbH (Kastellaun, Germany). Nuclear magnetic resonance (^{1}H NMR and ^{13}C NMR) spectra were recorded on a Bruker (Karlsruhe, Germany) Avance 300 (^{1}H: 300 MHz, ^{13}C: 75 MHz), 400 (^{1}H: 400 MHz, ^{13}C: 101 MHz), or 600 (^{1}H: 600 MHz,). The chemical shift δ is given in parts per million (ppm). Multiplicities were specified with the following abbreviations: s (singlet), d (doublet), t (triplet), q (quartet), m (multiplet) and br (broad signal). d* is used for compounds were one proton is split into two separate singlets with a large coupling constant (*J*; see chapter2.2.8 . NMR spectra were processed

with Mestre Nova 11.0 (Mestrelab Research, Compostela, Spain). ^{1}H NMR and ^{13}C NMR spectra of final compounds are presented in the appendix. Analytical HPLC experiments were performed on a 1100 HPLC system from Agilent Technologies equipped with Instant Pilot controller, a G1312A Bin Pump, a G1329A ALS autosampler, a G1379A vacuum degasser, a G1316A column compartment and a G1315B DAD detector. The column was a Phenomenex Kinetex XB-C18 column (250 x 4.6 mm, 5 µm; Phenomenex Ltd. Aschaffenburg, Germany) or a Phenomenex Gemini 5 µm NX-C18 110 Å LC column (250 x 4.6 mm), tempered at 30 °C. As mobile phase, mixtures of MeCN and aqueous TFA or NH_3 were used (linear gradient: MeCN/TFA (0.1 %) (v/v) 0 min: 10:90, 25-35 min: 95:5, 36-45 min: 10:90; flow rate = 1.00 mL/min, t_0 = 3.21 min). Capacity factors were calculated according to $k = (t_R - t_0)/t_0$. Detection was performed at 220 nm. Furthermore, a filtration of the stock solutions with PTFE filters (25 mm, 0.2 µm, Phenomenex Ltd., Aschaffenburg, Germany) was carried out before testing. Compound purities determined by HPLC were calculated as the peak area of the analyzed compound in % relative to the total peak area (UV detection at 220 nm). The HPLC purity and stability analysis of final compounds are presented in the appendix. High-resolution mass spectrometry (HRMS) was performed on an Agilent 6540 UHD Accurate-Mass Q-TOF LC/MS system (Agilent Technologies, Santa Clara, CA) using an ESI or APCI source or on a Jeol AccuTOF GCX LC/MS system (Jeol, Akishima, Japan) using an EI source. Chemical structures and names were generated with ChemBioDraw 20.0 (Cambridgesoft). Figures 1.1, 1.2, 1.6, 1.7, 1.8, 1.9, and 2.7 were created with BioRender.com.

6.1.2 Synthesis and analytical data

2-Bromo-1-(4-nitrophenyl)ethan-1-one (1)[250]

4-Nitroacetophenone (10.00 g, 60.54 mmol, 1 eq) was dissolved in DCM and added to a suspension of *N*-bromosuccinimide (12.92 g, 72.64 mmol, 1.2 eq) and *p*-toluenesulfonic acid (1.14 g, 6.06 mmol, 0.1 eq) in DCM at room temperature. The reaction was heated to reflux overnight. The reaction was poured on water and the organic phase was separated. The aqueous phase was extracted with DCM, the combined organic phases washed with saturated bicarbonate solution and brine, dried over Na_2SO_4 and the solvent was removed under reduced pressure. The crude product was purified by column chromatography (DCM/PE 1:1). A pale-yellow solid was obtained (9.41 g, 64 %). R_f = 0.61 (PE/DCM 4:6). ^{1}H NMR (300 MHz, $CDCl_3$) δ 8.48 – 8.26 (m, 2H), 8.21 – 8.07 (m, 2H), 4.47 (s, 2H). ^{13}C NMR (75 MHz, $CDCl_3$) δ 189.92, 150.71, 138.37, 130.11, 124.08, 30.18. HRMS (EI-MS): m/z $M^{\bullet+}$ calculated for $C_8H_6NO_3Br^{\bullet+}$: 242.9526, found 242.9522; $C_8H_6NO_3Br$ (244.04).

2-Bromo-1-(4-nitrophenyl)ethan-1-ol (2)[251]

1 (3.34 g, 13.70 mmol, 1 eq) was dissolved in MeOH. $NaBH_4$ (0.18 g, 4.80 mmol, 0.35 eq) was added in portions at 0 °C. The reaction was stirred for 1 h at room temperature. The solvent was removed under reduced pressure and the crude product was dissolved in water. The aqueous phase was extracted with diethyl ether. The combined organic phases were washed with saturated ammonium chloride solution and brine, dried over Na_2SO_4 and the solvent was removed under reduced pressure. A slightly yellow solid was obtained (2.23 g, 66 %). The product was used without further purification.

2-(4-Nitrophenyl)oxirane (3)[252]

2 (0.5 g, 2.03 mmol, 1 eq) and K_2CO_3 (0.56 g, 4.06 mmol, 2 eq) were dissolved in THF and heated to reflux overnight. The solid was filtered off and the solvent was removed under reduced pressure. The crude product was purified by column chromatography (PE/EtOAc 8:2). A yellow solid was obtained (0.29 g, 87 %). R_f = 0.78 (PE/EtOAc 7:3). ^{1}H NMR (300 MHz, $CDCl_3$) δ 8.29 – 8.13 (m, 2H), 7.56 – 7.36 (m, 2H), 3.96 (dd, *J* = 4.1, 2.5 Hz, 1H), 3.23 (dd, *J* = 5.5, 4.1 Hz, 1H), 2.78 (dd, *J* = 5.5, 2.5 Hz, 1H). ^{13}C NMR (75 MHz, $CDCl_3$) δ 145.26, 126.24, 123.85, 51.71, 51.48. HRMS (EI-MS): m/z $M^{\bullet+}$ calculated for $C_8H_7NO_3^{\bullet+}$: 164.0342, found 164.0339; $C_8H_7NO_3$ (165.15).

3-Chloro-4-methoxybenzaldehyde (4)[253]

Sulfuryl chloride (2.41 ml, 29.38 mmol, 2 eq) was added to a solution of 4-methoxybenzaldehyde (2.00 g, 14.69 mmol, 1 eq) in acetic acid. The reaction was stirred overnight at room temperature and poured onto a mixture of ice and water. The white solid was filtered off, washed with ice cold water and hexanes and dried *in vacuo*. A white solid was obtained (2,15 g, 86 %). R_f = 0.68 (PE/EtOAc 7:3). ^{1}H NMR (300 MHz, $CDCl_3$) δ 9.85 (s, 1H), 7.91 (d, *J* = 2.0 Hz, 1H), 7.78 (dd, *J* = 8.5, 2.0 Hz, 1H), 7.05 (d, *J* = 8.5 Hz, 1H), 3.99 (s, 3H). ^{13}C NMR (75 MHz, $CDCl_3$) δ 189.8, 159.9, 131.3, 130.6, 130.3, 123.7, 111.7, 56.5. HRMS (APCI-MS): m/z $[M+H]^+$ calculated for $C_8H_8ClO_2^+$: 171.0207, found 171.0207; $C_8H_7ClO_2$ (170.59).

2-Chloro-1-methoxy-4-(2-nitrovinyl)benzene (5)[254]

4 (6.40 g, 37.52 mmol, 1 eq), nitromethane (6.03 ml, 112.56 mmol, 3 eq) and ammonium acetate (2.40 g, 93.80 mmol, 2.5 eq) were dissolved in acetic acid and heated to reflux for 4 h. Water was added and the reaction was extracted with DCM. The combined organic phases were washed with 1 N aq. NaOH solution and brine, dried over Na_2SO_4 and the solvent removed under reduced pressure. The crude product was purified via column chromatography (PE/EtOAc 8:2). A yellow solid was obtained (5.49 g, 68 %). R_f = 0.67 (PE/EtOAc 7:3). ^{1}H NMR (300 MHz, $CDCl_3$) δ 7.90 (d, *J* = 13.6 Hz, 1H),

7.58 (d, *J* = 2.2 Hz, 1H), 7.50 (d, *J* = 13.6 Hz, 1H), 7.44 (dd, *J* = 8.7, 2.3 Hz, 1H), 6.98 (d, *J* = 8.6 Hz, 1H), 3.97 (s, 3H). ^{13}C NMR (75 MHz, $CDCl_3$) δ 158.08, 137.69, 136.02, 130.48, 129.83, 123.83, 123.33, 112.36, 56.46. HRMS (EI-MS): m/z $M^{\bullet+}$ calculated for $C_9H_8ClNO_3^{\bullet+}$: 213.0180, found 213.0187; $C_9H_8ClNO_3$ (213.67).

2-(3-Chloro-4-methoxyphenyl)ethan-1-amine (6)[254]

5 (5.43 g, 25.42 mmol, 1 eq) was dissolved in THF and added slowly to a suspension of $LiAlH_4$ (2.89 g, 76.26 mmol, 3 eq) in THF at room temperature. The reaction was heated to reflux for 3 h. After cooling to room temperature water (10 ml) and 20 % aq. KOH-solution were added carefully at 0 °C and the reaction was stirred for 30 min at room temperature. The white solid was filtered off and the filtrate was dried under reduced pressure. The crude product was dried *in vacuo*. A yellow oil was obtained (4.44 g, 94 %). R_f = 0.05 (DCM/MeOH 98:2). ^{1}H NMR (300 MHz, $CDCl_3$) δ 7.20 (d, *J* = 2.1 Hz, 1H), 7.05 (dd, *J* = 8.3, 2.2 Hz, 1H), 6.86 (d, *J* = 8.4 Hz, 1H), 3.87 (s, 3H), 2.92 (t, *J* = 6.8 Hz, 2H), 2.66 (t, *J* = 6.8 Hz, 2H), 1.49 (bs, 2H). ^{13}C NMR (75 MHz, $CDCl_3$) δ 153.45, 132.98, 130.47, 128.03, 122.26, 112.13, 56.20, 43.46, 38.78. HRMS (ESI-MS): m/z $[M+H]^+$ calculated for $C_9H_{13}ClNO^+$: 186.0680, found 186.0679; $C_9H_{12}ClNO$ (185,65).

***tert*-Butyl (3-chloro-4-methoxyphenethyl)carbamate (7)**

Di-*tert*-butyldicarbonate (3.23 g, 14.82 mmol, 1.1 eq) was dissolved in DCM and added slowly to a solution of **6** (2.50 g, 13.47 mmol, 1 eq) in DCM at room temperature. The reaction was stirred at room temperature overnight. The solvent was removed under reduced pressure and the crude product was dried *in vacuo*. A slightly yellow solid was obtained (3.79 g, 98 %). R_f = 0.48 (PE/EtOAc 8:2). ^{1}H NMR (400 MHz, $CDCl_3$) δ 7.19 (d, *J* = 2.1 Hz, 1H), 7.03 (dd, *J* = 8.4, 2.1 Hz, 1H), 6.85 (d, *J* = 8.4 Hz, 1H), 3.87 (s, 3H), 3.31 (t, *J* = 7.0 Hz, 2H), 2.70 (t, *J* = 7.0 Hz, 2H), 1.42 (s, 9H). ^{13}C NMR (101 MHz, $CDCl_3$) δ 155.90, 153.61, 132.15, 130.49, 127.98, 122.33, 112.22, 56.18, 40.89, 35.11, 28.39, 23.86. HRMS (ESI-MS): m/z $[M+H]^+$ calculated for $C_{14}H_{21}ClNO_3^+$: 286.1204, found 286.1204; $C_{14}H_{20}ClNO_3$ (285.77).

2-(3-Chloro-4-methoxyphenyl)-*N*-methylethan-1-amine (8a)[255]

7 (6.2 g, 21.70 mmol, 1 eq) was dissolved in THF and added slowly to a suspension of $LiAlH_4$ (2.47 g, 65.10 mmol, 3 eq) in THF at room temperature. The reaction was heated to reflux for 3 h. After cooling to room temperature water (10 ml) and 20 % aq. KOH-solution were added carefully at 0 °C and the reaction was stirred for 30 min at room temperature. The white solid was filtered off and the filtrate was dried under reduced pressure. The crude product was dried *in vacuo*. A yellow oil was obtained (3.88 g, 90 %). R_f = 0.16 (DCM/MeOH + 1 % NH_3 95:5). ^{1}H NMR (300 MHz, $CDCl_3$) δ 7.21 (d, *J* = 2.1 Hz, 1H), 7.05 (dd, *J* = 8.4, 2.2 Hz, 1H), 6.85 (d, *J* = 8.4 Hz, 1H), 3.87 (s, *J* = 3.9 Hz, 3H), 2.84 – 2.76

(m, 2H), 2.76 – 2.68 (m, 2H), 2.43 (s, 3H). ^{13}C NMR (75 MHz, $CDCl_3$) δ 153.42, 133.24, 130.34, 127.92, 122.27, 112.13, 77.48, 77.06, 76.63, 56.20, 53.13, 36.38, 35.03. HRMS (ESI-MS): m/z $[M+H]^+$ calculated for $C_{10}H_{15}ClNO^+$: 200.0837, found 200.0839; $C_{10}H_{14}ClNO$ (199.69).

2-((3-Chloro-4-methoxyphenethyl)(methyl)amino)-1-(4-nitrophenyl)ethan-1-ol (9a)[186]

8a (2.44 g, 12.22 mmol, 1 eq) and **3** (2.02 g, 12.22 mmol, 1 eq) were dissolved in acetonitrile and heated to reflux overnight. The solvent was removed under reduced pressure and the crude product was purified by column chromatography (DCM/MeOH + 1 % NH_3 98:2). A brown oil was obtained (4.00 g, 90 %). R_f = 0.16 (DCM/MeOH + 1 % NH_3 98:2). ^{1}H NMR (300 MHz, $CDCl_3$) δ 8.23 – 8.12 (m, 2H), 7.57 – 7.47 (m, 2H), 7.20 (d, *J* = 2.2 Hz, 1H), 7.05 (dd, *J* = 8.4, 2.2 Hz, 1H), 6.86 (d, *J* = 8.4 Hz, 1H), 4.78 (dd, *J* = 10.4, 3.5 Hz, 1H), 4.19 (bs, 1H), 3.87 (s, 3H), 2.90 – 2.57 (m, 5H), 2.52 – 2.41 (m, 4H). ^{13}C NMR (75 MHz, $CDCl_3$) δ 153.54, 149.73, 147.33, 132.59, 130.34, 127.85, 126.52, 123.64, 122.32, 112.16, 68.56, 65.26, 59.18, 56.19, 41.73, 32.47. HRMS (ESI-MS): m/z $[M+H]^+$ calculated for $C_{18}H_{22}ClN_2O_4^+$: 365.1263, found 365.1268; $C_{18}H_{21}ClN_2O_4$ (364.83).

2-((3,4-Dimethoxyphenethyl)(methyl)amino)-1-(4-nitrophenyl)ethan-1-ol (9b)[256]

3 (6.70 g, 40.57 mmol, 1 eq) and 2-(3,4-dimethoxyphenyl)-*N*-methylethan-1-amine (**8b**; 7.92 g, 40.57 mmol, 1 eq) were dissolved in acetonitrile and the reaction was heated to reflux overnight. The solvent was evaporated under reduced pressure and the crude product was purified by column chromatography (DCM/MeOH + 1 % NH_3 98:2). A brown oil was obtained (12.60 g, 90 %). R_f = 0.60 (DCM/MeOH + 1 % NH_3 95:5). ^{1}H NMR (300 MHz, $CDCl_3$) δ 8.25 – 8.12 (m, 2H), 7.58 – 7.44 (m, 2H), 6.83 – 6.78 (m, 1H), 6.76 – 6.68 (m, 2H), 4.74 (dd, *J* = 10.4, 3.6 Hz, 1H), 3.88 (s, 3H), 3.86 (s, 3H), 2.85 – 2.56 (m, 5H), 2.52 – 2.36 (m, 4H). ^{13}C NMR (75 MHz, $CDCl_3$) δ 149.99, 148.94, 147.52, 147.29, 132.28, 126.47, 123.62, 120.56, 111.92, 111.30, 68.61, 65.33, 59.46, 55.93, 55.90, 41.74, 33.47. HRMS (ESI-MS): m/z $[M+H]^+$ calculated for $C_{19}H_{25}N_2O_5^+$: 361.1758, found 361.1757; $C_{19}H_{24}N_2O_5$ (360.17).

7-Chloro-8-methoxy-3-methyl-1-(4-nitrophenyl)-2,3,4,5-tetrahydro-1*H*-benzo[*d*]azepine (10a)

9a (2.49 g, 7.65 mmol, 1 eq) was dissolved in Eaton's reagent (40 ml) and stirred for 72 h at room temperature. The reaction was poured onto ice water and basified with 20 % aqueous KOH-solution. The aqueous phase was extracted with DCM. The combined organic phases were washed with water, dried over Na_2SO_4 and the solvent was removed under reduced pressure. The crude product was purified by column chromatography (DCM/MeOH + 1 % NH_3 98:2). A red solid was obtained (1.20 g, 45 %). R_f = 0.18 (DCM/MeOH + 1 % NH_3 98:2). ^{1}H NMR (300 MHz, $CDCl_3$) δ 8.22 – 8.10 (m, 2H), 7.37 – 7.28 (m, 2H), 7.14 (s, 1H), 6.39 (s, 1H), 4.42 – 4.27 (m, 1H), 3.71 (s, 3H), 3.26 – 3.13 (m, 1H), 2.96 – 2.75 (m, 2H), 2.73 – 2.52 (m, 3H), 2.38 (s, 3H). ^{13}C NMR (75 MHz, $CDCl_3$) δ 153.29, 149.94,

146.48, 141.87, 134.37, 131.64, 129.06, 123.72, 120.27, 113.44, 61.34, 57.29, 56.15, 50.27, 47.93, 34.98. HRMS (ESI-MS): m/z $[M+H]^+$ calculated for $C_{18}H_{20}ClN_2O_3^+$: 347.1157, found 347.1162; $C_{18}H_{19}ClN_2O_3$ (346.81).

7,8-Dimethoxy-3-methyl-1-(4-nitrophenyl)-2,3,4,5-tetrahydro-1*H*-benzo[*d*]azepine (10b)

9b (9.48 g, 27.53 mmol, 1 eq) was dissolved in polyphosphoric acid (50 ml) and stirred at 100 °C for 3 h. After cooling to room temperature, the reaction was poured onto water and basified. The aqueous phase was extracted with DCM, the combined organic phases were washed with brine, dried over Na_2SO_4 and the solvent was removed under reduced pressure. The crude product was purified by column chromatography (DCM/MeOH + 1 % NH_3 98:2). A brown solid was obtained (6.51 g, 69 %). R_f = 0.32 (DCM/MeOH + 1 % NH_3 98:2). ^{1}H NMR (300 MHz, $CDCl_3$) δ 8.24 – 8.10 (m, 2H), 7.40 – 7.27 (m, 2H), 6.69 (s, 1H), 6.35 (s, 1H), 4.30 (d, *J* = 6.9 Hz, 1H), 3.88 (s, 3H), 3.71 (s, 3H), 3.29 – 3.13 (m, 1H), 2.96 – 2.47 (m, 5H), 2.38 (s, 3H). ^{13}C NMR (75 MHz, $CDCl_3$) δ 150.84, 147.42, 146.99, 146.35, 134.09, 133.70, 129.04, 123.64, 113.81, 113.19, 61.71, 57.51, 56.00, 50.16, 48.10, 35.91. HRMS (EI-MS): m/z $M^{\bullet+}$ calculated for $C_{19}H_{22}N_2O_4^{\bullet+}$: 342.1574, found 342.1577; $C_{19}H_{22}N_2O_4$ (342.40).

8-Chloro-3-methyl-5-(4-nitrophenyl)-2,3,4,5-tetrahydro-1*H*-benzo[*d*]azepin-7-ol (11a)[186]

10a (0.80 g, 2.31 mmol, 1 eq) was dissolved in DCM and cooled to -78 °C under Ar-atmosphere. BBr_3 (0.33 ml, 3.45 mmol, 1.5 eq) dissolved in DCM was added at -78 °C and the reaction was stirred for 1 h at this temperature. Subsequently, the reaction was stirred at room temperature overnight. MeOH (5 ml) was added at -78 °C and the reaction was stirred for 1 h at room temperature. The solvent was removed under reduced pressure and the product was dried *in vacuo*. A brown solid was obtained (0.80 g, 84 %). The product was used without further purification. HRMS (ESI-MS): m/z $[M+H]^+$ calculated for $C_{17}H_{18}ClN_2O_3^+$: 333.1000, found 333.1004; $C_{17}H_{17}ClN_2O_3$*HBr (413.70).

3-Methyl-1-(4-nitrophenyl)-2,3,4,5-tetrahydro-1*H*-benzo[*d*]azepine-7,8-diol (11b)

10b (2.00 g, 5.84 mmol, 1 eq) was dissolved in DCM and cooled to -78 °C under Ar-atmosphere. BBr_3 (1.66 ml, 17.52 mmol, 3 eq) was added slowly and the reaction was stirred for 30 min at -78 °C and afterwards overnight at room temperature. The reaction was cooled to -78 °C and quenched with methanol. The reaction was stirred at room temperature for 1 h and the solvent was evaporated under reduced pressure. A brown solid was obtained (1.80 g, 78 %). The product was used without further purification. HRMS (ESI-MS): m/z $[M+H]^+$ calculated for $C_{17}H_{19}N_2O_4^+$: 315.1339, found 315.1345; $C_{17}H_{18}N_2O_4$*HBr (395.25).

7-Chloro-3-methyl-1-(4-nitrophenyl)-8-((triisopropylsilyl)oxy)-2,3,4,5-tetrahydro-1*H*-benzo[*d*]azepine (12)

Triisopropylsilyl chloride (309 µl, 1.46 mmol, 2 eq) and imidazole (0.10g, 1.46 mmol, 2 eq) were dissolved in DMF. **11a** (0.30 g, 0.73 mmol, 1 eq) and NEt_3 (513 µl, 3.65 mmol, 5 eq) dissolved in DMF were added at room temperature under Ar-atmosphere. The reaction was stirred overnight at room temperature and subsequently poured onto water. The aqueous phase was extracted with diethyl ether. The combined organic phases were washed with saturated ammonium chloride solution and brine, dried over Na_2SO_4 and the solvent was removed under reduced pressure. The crude product was purified by flash chromatography (SiO_2, 0 min to 20 min, 100:0 to 95:5 DCM/MeOH). R_f = 0.40 (DCM/MeOH 95:5). A slightly yellow solid was obtained (0.32 g, 90 %). ^{1}H NMR (300 MHz, $CDCl_3$) δ 8.29 – 8.15 (m, 2H), 7.38 – 7.28 (m, 1H), 7.12 (s, 1H), 6.06 (s, 1H), 4.53 – 4.28 (m, 1H), 3.13 – 2.83 (m, 4H), 2.78 – 2.63 (m, 1H), 2.50 – 2.35 (m, 4H), 1.05 – 0.88 (m, 21H). ^{13}C NMR (75 MHz, $CDCl_3$) δ 150.35, 150.15, 146.69, 142.27, 134.19, 131.25, 129.22, 123.85, 122.65, 120.20, 61.91, 57.25, 49.02, 47.66, 34.92, 17.77, 12.71. HRMS (ESI-MS): m/z $[M+H]^+$ calculated for $C_{26}H_{38}ClN_2O_3Si^+$: 489.2335, found 489.2342; $C_{26}H_{37}ClN_2O_3Si$ (488.23).

4-(7-Chloro-3-methyl-8-((triisopropylsilyl)oxy)-2,3,4,5-tetrahydro-1*H*-benzo[*d*]azepin-1-yl)aniline (13)

12 (0.42 g, 0.86 mmol, 1 eq) and Pd/C (10 %) (0.04 g, 10 wt %) were dissolved in a mixture of THF and MeOH (1:1) and the reaction was stirred overnight under H_2-atmosphere. The reaction was filtered over celite and the solvent was removed under reduced pressure. The crude product was dried *in vacuo.* A brown oil was obtained (0.38 g, 96 %). The product was used without further purification. HRMS (ESI-MS): m/z $[M+H]^+$ calculated for $C_{26}H_{40}ClN_2OSi^+$: 459.2593, found 459.2598; $C_{26}H_{39}ClN_2OSi$ (459.15).

7,8-Bis((*tert*-butyldimethylsilyl)oxy)-3-methyl-1-(4-nitrophenyl)-2,3,4,5-tetrahydro-1*H*-benzo[*d*]azepine (14)

11b (1.27 g, 2.40 mmol, 1 eq), NEt_3 (1.69 ml, 12.00 mmol, 5 eq) and *N,N*-dimethylaminopyridine (DMAP) (29 mg, 0.24 mmol, 0.1 eq) were dissolved in DCM/DMF (9:1). *tert*-Butyldimethylsilyl chloride (1.81 g, 12.00 mmol, 5 eq) was added at room temperature and the reaction was stirred overnight. The solvents were removed under reduced pressure and the residue was dissolved in Et_2O. The organic phase was washed with water, saturated NH_4Cl solution and brine, dried over Na_2SO_4 and the solvent was removed under reduced pressure. The crude product was purified by column chromatography (DCM/MeOH 98:2). A white solid was obtained (0.74 g, 57 %). R_f = 0.34 (DCM/MeOH 98:2). ^{1}H NMR (300 MHz, $CDCl_3$) δ 8.28 – 8.16 (m, 2H), 7.42 – 7.31 (m, 2H), 6.63 (s, 1H), 6.02 (s, 1H), 4.48 (bs, 1H), 3.32

– 2.98 (m, 3H), 2.82 – 2.27 (m, 6H), 0.99 – 0.93 (m, 9H), 0.87 – 0.77 (m, 9H), 0.21 – 0.13 (m, 6H), 0.04 – -0.08 (m, 6H). ^{13}C NMR (75 MHz, $CDCl_3$) δ 148.17, 147.38, 146.25, 146.02, 132.45, 129.46, 124.49, 122.72, 59.57, 57.78, 42.81, 25.81, 25.73, 18.38. HRMS (ESI-MS): m/z $[M+H]^+$ calculated for $C_{29}H_{47}N_2O_4Si_2^+$: 543.3069, found 543.3082; $C_{29}H_{46}N_2O_4Si_2$ (542.87).

4-(7,8-Bis((*tert*-butyldimethylsilyl)oxy)-3-methyl-2,3,4,5-tetrahydro-1*H*-benzo[*d*]azepin-1-yl)aniline (15)

14 (0.30 g, 0.55 mmol, 1 eq) was dissolved in THF/MeOH (1:1). Pd/C (10 %; 0.03 g, 10wt %) was added and the reaction was stirred overnight under H_2-atmosphere. The reaction was filtered through celite and the solvent was removed under reduced pressure. The crude product was purified by column chromatography (DCM/MeOH 98:2). A white solid was obtained (0.26 g, 93 %). R_f = 0.26 (DCM/MeOH 98:2). ^{1}H NMR (300 MHz, $CDCl_3$) δ 7.03 – 6.89 (m, 2H), 6.73 – 6.62 (m, 2H), 6.58 (s, 1H), 6.12 (s, 1H), 4.15 (d, *J* = 8.8 Hz, 1H), 3.88 – 3.48 (m, 2H), 3.18 – 2.90 (m, 3H), 2.75 – 2.61 (m, 2H), 2.42 – 2.23 (m, 4H), 1.02 – 0.95 (m, 10H), 0.89 – 0.80 (m, 9H), 0.20 – 0.13 (m, 7H), 0.04 – -0.10 (m, 6H). ^{13}C NMR (75 MHz, $CDCl_3$) δ 144.74, 144.34, 143.81, 138.18, 133.79, 133.63, 129.19, 122.21, 121.02, 115.33, 63.71, 57.53, 47.97, 47.64, 35.60, 25.91, 18.42, 18.36. HRMS (ESI-MS): m/z $[M+H]^+$ calculated for $C_{29}H_{49}N_2O_2Si_2^+$: 513.3327, found 513.3336; $C_{29}H_{48}N_2O_2Si_2$ (512.89).

Benzyl 5-bromopentanoate (16) [257]

5-Bromopentanoic acid (1.50 g, 8.29 mmol, 1.1 eq), benzyl alcohol (784µl, 7.54 mmol, 1 eq) and DMAP (0.09 g, 0.75 mmol, 0.1 eq) were dissolved in DCM. Dicyclohexylcarbodiimide (1.87 g, 9.05 mmol, 1.2 eq) dissolved in DCM was added slowly at room temperature and the reaction was stirred overnight. The white solid was filtered off and the filtrate was concentrated under reduced pressure. The crude product was purified by column chromatography (PE/EtOAc 9:1). A clear oil was obtained (2.00 g, 89 %). R_f = 0.74 (PE/EtOAc 8:2). ^{1}H NMR (300 MHz, $CDCl_3$) δ 7.46 – 7.27 (m, 5H), 5.12 (s, 2H), 3.40 (t, *J* = 6.4 Hz, 2H), 2.40 (t, *J* = 7.1 Hz, 2H), 1.97 – 1.72 (m, 4H). ^{13}C NMR (75 MHz, $CDCl_3$) δ 172.98, 135.93, 128.62, 128.31, 128.27, 66.33, 33.30, 33.04, 31.97, 23.50. HRMS (APCI-MS): m/z $[M+H]^+$ calculated for $C_{12}H_{16}BrO_2^+$: 271.0328, found 271.0324; $C_{12}H_{15}BrO_2$ (271.15).

Benzyl 5-(chlorosulfonyl)pentanoate (17a)[187,258]

16 (0.50 g, 1.84 mmol, 1 eq) and thiourea (0.14 g, 1.84 mmol, 1 eq) were heated in MeCN to reflux overnight. The solvent was removed under reduced pressure and the remaining white solid was added at 5 °C to a suspension of *N*-chlorosuccinimide (1.23 g, 9.20 mmol, 5 eq) in MeCN and 2 N aq. HCl (1 ml). The reaction was stirred for 1 h maintaining the temperature below 10 °C. Water and Et_2O were added and the organic phase was separated, washed with brine, dried over Na_2SO_4 and the

solvent removed under reduced pressure. The crude product was purified by column chromatography (PE/EtOAc 9:1). A clear oil was obtained (0.35 g, 65 %). R_f = 0.21 (PE/EtOAc 9:1). ^{1}H NMR (300 MHz, $CDCl_3$) δ 7.46 – 7.29 (m, 5H), 5.14 (s, 2H), 3.72 – 3.60 (m, 2H), 2.45 (t, *J* = 7.2 Hz, 2H), 2.17 – 1.98 (m, 2H), 1.94 – 1.73 (m, 2H). ^{13}C NMR (75 MHz, $CDCl_3$) δ 172.34, 135.73, 128.69, 128.45, 128.36, 66.58, 64.90, 33.32, 23.82, 22.82. HRMS (APCI-MS): m/z $[M+H]^+$ calculated for $C_{12}H_{16}ClO_4S^+$: 291.0452, found 291.0451; $C_{12}H_{15}ClO_4S$ (290.76).

Ethyl 5-(chlorosulfonyl)pentanoate (17b)[187,258]

Ethyl 5-bromovalerate (3.00 g, 14.35 mmol, 1 eq) and thiourea (1.08 g, 14.35 mmol) were dissolved in EtOH and heated to reflux overnight. The solvent was removed under reduced pressure and the obtained solid was added at 5 °C to a suspension of *N*-chlorosuccinimide (9.58 g, 71.75 mmol, 5 eq) in acetonitrile and 2 N aq. HCl (5 ml). The reaction was stirred for 20 min below 10 °C and poured onto water. The aqueous phase was extracted with diethyl ether. The combined organic phases were washed with brine, dried over Na_2SO_4 and the solvent was removed under reduced pressure. The crude product was purified by column chromatography (PE/EtOAc 8:2). A clear oil was obtained (2.86 g, 87 %). R_f = 0.45 (PE/EtOAc 8:2). ^{1}H NMR (300 MHz, $CDCl_3$) δ 4.14 (q, *J* = 7.1 Hz, 2H), 3.77 – 3.61 (m, 2H), 2.39 (t, *J* = 7.1 Hz, 2H), 2.16 – 1.98 (m, 2H), 1.91 – 1.74 (m, 2H), 1.30 – 1.21 (m, 3H). ^{13}C NMR (75 MHz, $CDCl_3$) δ 172.52, 64.96, 60.72, 33.32, 23.83, 22.84, 14.23. HRMS (ESI-MS): m/z $[M+H]^+$ calculated for $C_7H_{14}ClO_4S^+$: 229.0296, found 229.0295; $C_7H_{13}ClO_4S$ (228.69).

***N*^{1}-(4-(7-Chloro-8-hydroxy-3-methyl-2,3,4,5-tetrahydro-1*H*-benzo[*d*]azepin-1-yl)phenyl)-*N*^{4}-(prop-2-yn-1-yl)succinimide (18)**

Succinic anhydride (0.16 g, 1.60 mmol, 1 eq) and propargylamine (0.10 ml, 1.60 mmol, 1 eq) were dissolved in DMF and stirred for 3 h at room temperature. HATU (0.67 g, 1.76 mmol, 1.1 eq), DIPEA (0.83 ml, 4.80 mmol, 3 eq), and **11a** (0.48 g, 1.60 mmol, 1 eq) were added and the reaction was stirred at rt overnight. The solvent was removed under reduced pressure and the crude product was purified by column chromatography (DCM/MeOH 95:5). A yellow sticky solid was obtained (0.34 g, 48 %). R_f = 0.13 (DCM/MeOH 95:5). ^{1}H NMR (400 MHz, CD_3OD) δ 7.76 – 7.53 (m, 2H), 7.33 – 7.05 (m, 3H), 6.43 (d*, *J* = 220.5 Hz, 1H), 4.66 – 4.48 (m, 1H), 3.96 (d, *J* = 2.5 Hz, 2H), 3.92 – 3.42 (m, 3H), 3.40 – 3.31 (m, 1H), 3.12 – 2.86 (m, 5H), 2.74 – 2.63 (m, 2H), 2.63 – 2.52 (m, 3H). ^{13}C NMR (101 MHz, CD_3OD) δ 172.80, 171.64, 151.98, 142.09, 138.14, 130.52, 129.43, 128.52, 120.45, 118.40, 116.27, 79.19, 70.76, 60.62, 56.13, 44.56, 31.23, 30.42, 30.04, 28.09. HRMS (ESI-MS): m/z $[M+H]^+$ calculated for $C_{24}H_{27}ClN_3O_3^+$: 440.1735, found 440.1741; $C_{24}H_{26}ClN_3O_3$ (439.94).

Ethyl 5-(*N*-(4-(7-chloro-3-methyl-8-((triisopropylsilyl)oxy)-2,3,4,5-tetrahydro-1*H*-benzo[*d*]azepin-1-yl)phenyl)sulfamoyl)pentanoate (19)

13 (0.50 g, 1.01 mmol, 1 eq) and pyridine (245 µl, 3.03 mmol, 3 eq) were dissolved in $CHCl_3$. **17b** (0.46 g, 2.02 mmol, 2 eq) was added and the reaction was stirred at 50 °C overnight. DCM was added to the reaction and the organic phase was washed with water and brine, dried over Na_2SO_4 and the solvent was removed under reduced pressure. The crude product was purified by flash chromatography (SiO_2, 0 min to 5 min to 25 min, 98:2 to 98:2 to 9:1, DCM/MeOH). A pale-yellow solid was obtained (0.37 g, 56 %). R_f = 0.20 (DCM/MeOH 95:5). ^{1}H NMR (400 MHz, $CDCl_3$) δ 7.33 – 7.27 (m, 2H), 7.11 – 7.02 (m, 3H), 6.11 (s, 1H), 4.76 – 4.53 (m, 1H), 4.07 (d, *J* = 7.1 Hz, 2H), 3.63 – 3.30 (m, 3H), 3.16 – 2.95 (m, 3H), 2.86 – 2.73 (m, 1H), 2.73 – 2.52 (m, 4H), 2.34 – 2.23 (m, 2H), 1.91 – 1.62 (m, 4H), 1.20 (t, *J* = 7.1 Hz, 3H), 0.95 – 0.86 (m, 21H). ^{13}C NMR (101 MHz, $CDCl_3$) δ 172.99, 150.47, 142.51, 137.16, 136.69, 132.18, 130.91, 129.31, 122.63, 120.87, 120.13, 61.86, 60.50, 56.73, 51.24, 46.36, 45.59, 33.62, 23.46, 22.99, 17.76, 14.20, 12.56. HRMS (ESI-MS): m/z $[M+H]^+$ calculated for $C_{33}H_{52}ClN_2O_5SSi^+$: 651.3049, found 651.3060; $C_{33}H_{51}ClN_2O_5SSi$ (651.38).

5-(*N*-(4-(7-Chloro-8-hydroxy-3-methyl-2,3,4,5-tetrahydro-1*H*-benzo[*d*]azepin-1-yl)phenyl)sulfamoyl)-*N*-(prop-2-yn-1-yl)pentanamide (20)

19 (0.34 g, 0.52 mmol, 1 eq) was dissolved in THF and LiOH (37 mg, 1.56 mmol, 3 eq) dissolved in water was added and the reaction was stirred at room temperature overnight. 0.1 N HCl (32 ml, 3.12 mmol, 6 eq) was added slowly at 0 °C. The solvent was removed by lyophilization and the residue was dissolved in DMF. HATU (236 mg, 0.62 mmol, 1.2 eq), DIPEA (269 µl, 1.56 mmol, 6 eq) and propargylamine (50 µl, 0.78 mmol, 1.5 eq) were added and the reaction was stirred at room temperature overnight. The solvent was removed under reduced pressure and the crude product was purified by flash chromatography (SiO_2, 0 min to 5 min to 6 min to 25 min, 100:0 to 100:0 to 95:5 to 8:2, DCM/MeOH). A yellow solid was obtained (0.24 g, 92 %). R_f = 0.18 (DCM/MeOH 9:1). ^{1}H NMR (400 MHz, CD_3OD) δ 7.30 – 7.23 (m, 2H), 7.19 – 7.10 (m, 3H), 6.23 (s, 1H), 4.51 (d, *J* = 9.6 Hz, 1H), 3.87 (d, *J* = 2.5 Hz, 2H), 3.63 – 3.36 (m, 3H), 3.25 – 3.16 (m, 1H), 3.14 – 3.05 (m, 2H), 2.97 – 2.85 (m, 2H), 2.82 – 2.74 (m, 3H), 2.53 (t, *J* = 2.6 Hz, 1H), 2.24 – 2.13 (m, 2H), 1.83 – 1.71 (m, 2H), 1.71 – 1.57 (m, 2H). ^{13}C NMR (101 MHz, CD_3OD) δ 173.62, 151.81, 141.96, 137.39, 130.66, 130.42, 129.14, 120.47, 118.31, 116.68, 79.22, 70.86, 60.74, 56.28, 50.55, 45.41, 44.97, 34.63, 31.15, 28.04, 23.84, 22.80. HRMS (ESI-MS): m/z $[M+H]^+$ calculated for $C_{25}H_{31}ClN_3O_4S^+$: 504.1718, found 504.1722; $C_{25}H_{30}ClN_3O_4S$ (504.04).

Benzyl 5-(*N*-(4-(7,8-bis((*tert*-butyldimethylsilyl)oxy)-3-methyl-2,3,4,5-tetrahydro-1*H*-benzo[*d*]azepin-1-yl)phenyl)sulfamoyl)pentanoate (21)

15 (0.48 g, 0.94 mmol, 1 eq) and pyridine (228 µl, 1.88 mmol, 3 eq) were dissolved in $CHCl_3$. **17a** (0.54 g, 1.88 mmol, 2 eq) was added and the reaction was stirred at 50 °C overnight. DCM was added to the reaction and the organic phase was washed with water and brine, dried over Na_2SO_4 and the solvent was removed under reduced pressure. The crude product was purified by flash chromatography (SiO_2, 0 min to 5 min to 25 min, 98:2 to 98:2 to 9:1, DCM/MeOH). A pale-yellow solid was obtained (0.42 g, 59 %). R_f = 0.70 (DCM/MeOH 95:5). ^{1}H NMR (400 MHz, $CDCl_3$) δ 7.38 – 7.31 (m, 5H), 7.28 – 7.23 (m, 2H), 7.08 (t, *J* = 10.1 Hz, 2H), 6.61 (s, 1H), 5.98 (s, 1H), 5.11 (s, *J* = 6.4 Hz, 2H), 4.88 (bs, 1H), 3.88 – 3.43 (m, 3H), 3.20 – 3.00 (m, 3H), 2.94 – 2.64 (m, 5H), 2.44 – 2.31 (m, 2H), 1.95 – 1.69 (m, 5H), 0.96 (s, *J* = 2.9 Hz, 9H), 0.79 (s, 9H), 0.15 (s, *J* = 8.0 Hz, 6H), -0.07 (s, 6H). ^{13}C NMR (101 MHz, $CDCl_3$) δ 172.72, 135.86, 129.36, 128.61, 128.30, 128.27, 122.53, 120.99, 66.38, 51.05, 33.61, 25.83, 23.39, 23.04, 18.40, 18.34, -4.17, -4.21. HRMS (ESI-MS): m/z $[M+H]^+$ calculated for $C_{41}H_{63}N_2O_6SSi_2^+$: 767.3940, found 767.3962; $C_{41}H_{62}N_2O_6SSi_2$ (767.19).

5-(*N*-(4-(7,8-Bis((*tert*-butyldimethylsilyl)oxy)-3-methyl-2,3,4,5-tetrahydro-1*H*-benzo[*d*]azepin-1-yl)phenyl)sulfamoyl)-*N*-(prop-2-yn-1-yl)pentanamide (22)

Pd/C (10 %; 0.04g, 10wt %) was added to a solution of **21** (0.40 g, 0.52 mmol, 1 eq) in MeOH and the reaction was heated to 60 °C under H_2-atmosphere. After 3 h the reaction was filtered over celite and the solvent was removed under reduced pressure. The residue was dissolved in DMF and HATU (0.24 g, 0.62 mmol, 1.2 eq), DIPEA (269 µl, 1.56 mmol, 3 eq) and propargyl amine (50 µl, 0.78 mmol, 1.5 eq) were added and the reaction was stirred at room temperature overnight. DCM was added and the organic phase was washed with water and brine, dried over Na_2SO_4 and the solvent removed under reduced pressure. The crude product was purified by flash chromatography (SiO_2, 0 min to 20 min, 100:0 to 9:1 DCM/MeOH). A pale-yellow solid was obtained (0.23 g, 62 %). R_f = 0.48 (DCM/MeOH 9:1). ^{1}H NMR (400 MHz, $CDCl_3$) δ 7.29 – 7.23 (m, 2H), 7.22 – 7.12 (m, 2H), 6.62 (s, 1H), 6.10 (s, 1H), 6.00 – 5.89 (m, 1H), 4.23 (d, *J* = 8.5 Hz, 1H), 4.10 – 4.04 (m, 2H), 3.22 – 3.00 (m, 4H), 2.98 – 2.79 (m, 2H), 2.75 – 2.64 (m, 1H), 2.48 – 2.33 (m, 4H), 2.31 – 2.23 (m, 3H), 1.96 – 1.80 (m, 4H), 1.01 (s, *J* = 2.9 Hz, 9H), 0.88 (s, *J* = 2.7 Hz, 9H), 0.20 (s, 6H), 0.08 – -0.03 (m, 6H). ^{13}C NMR (101 MHz, $CDCl_3$) δ 171.77, 158.70, 144.40, 144.23, 140.77, 136.94, 134.96, 133.84, 129.56, 122.48, 121.24, 121.15, 79.51, 71.70, 63.03, 57.53, 50.89, 50.84, 48.38, 47.70, 35.54, 35.34, 29.22, 25.91, 25.89, 23.64, 23.16, 18.41, 18.35, -4.15, -4.21. HRMS (ESI-MS): m/z $[M+H]^+$ calculated for $C_{37}H_{60}N_3O_5SSi_2^+$: 714.3787, found 714.3799; $C_{37}H_{59}N_3O_5SSi_2$ (714.13).

4-(3-Chloropropoxy)benzaldehyde (23)[178]

A suspension of 4-hydroxybenzaldehyde (5.00 g, 40.94 mmol, 1 eq), 1-bromo-3-chloropropane (8.06 ml, 81.88 mmol, 2 eq) and K_2CO_3 (16.85 g, 121.92 mmol, 3 eq) in MeCN was heated to reflux for 18 h. After cooling to room temperature, the solid was filtered off and the filtrate was dried in vacuo. The resulting residue was dissolved in EtOAc and washed with water and brine, dried over Na_2SO_4 and the solvent was removed under reduced pressure. The crude product was purified by column chromatography (PE/EtOAc 9:1). **23** (7.26 g, 89 %) was obtained as a yellow oil. R_f = 0.40 (PE/EtOAc 8:1). ^{1}H NMR (300 MHz, $CDCl_3$) δ 9.89 (s, 1H), 7.95 – 7.75 (m, 2H), 7.09 – 6.91 (m, 2H), 4.21 (t, *J* = 5.9 Hz, 2H), 3.76 (t, *J* = 6.2 Hz, 2H), 2.36 – 2.18 (m, 2H). ^{13}C NMR (75 MHz, $CDCl_3$) δ 190.8, 163.7, 132.0, 130.1, 114.8, 64.6, 41.2, 32.0. HRMS (ESI-MS): m/z [M+H$^+$] calculated for $C_{10}H_{12}ClO_2^+$: 199.0520, found 199.0516; $C_{10}H_{11}ClO_2$ (198.65).

4-(3-(Piperidin-1-yl)propoxy)benzaldehyde (24)[178]

23 (7.22 g, 36.34 mmol, 1 eq), piperidine (5.38 ml, 54.51 mmol, 1.5 eq), Na_2CO_3 (5.78 g, 54,51 mmol, 1.5 eq) and KI (0.30 g, 1.82 mmol, 5 mol %) were heated to reflux in MeCN for 20 h. The solvent was removed under reduced pressure and the residue was dissolved in DCM. The organic phase was washed with water and brine, dried over Na_2SO_4 and the solvent was removed under reduced pressure. Column chromatography (DCM/MeOH 9/1 + 0.1 % NEt_3) afforded **24** (6.79 g, 76 %) as a yellow oil. R_f = 0.48 (DCM/MeOH/7N NH_3 in MeOH 95:4:1). ^{1}H NMR (400 MHz, $CDCl_3$) δ 9.87 (s, 1H), 7.88 – 7.74 (m, 2H), 7.06 – 6.92 (m, 2H), 4.09 (t, *J* = 6.4 Hz, 2H), 2.51 – 2.31 (m, 6H), 2.06 – 1.94 (m, 2H), 1.63 – 1.54 (m, 4H), 1.50 – 1.38 (m, 2H). ^{13}C NMR (101 MHz, $CDCl_3$) δ 190.8, 164.2, 132.0, 129.8, 114.8, 66.9, 55.7, 54.7, 26.7, 26.0, 24.4. HRMS (ESI-MS): m/z [M+H$^+$] calculated for $C_{15}H_{22}NO_2^+$: 248.1645, found 248.1673; $C_{15}H_{21}NO_2$ (247.34).

Ethyl 1-(4-(3-(piperidin-1-yl)propoxy)benzyl)piperidine-4-carboxylate (25)[188]

Sodium triacetoxyborohydride (5.35 g, 25.23 mmol, 1.3 eq) was added to a solution of **24** (4.80 g, 19.41 mmol, 1 eq) and ethyl isonipecotate (3.29 ml, 21.35 mmol, 1.1 eq) in $CHCl_3$ at room temperature and the reaction was stirred for 20 h. A saturated solution of sodium bicarbonate was added and the organic phase was separated. The aqueous phase was extracted with DCM, the combined organic phases were washed with brine, dried over Na_2SO_4 and the solvent was removed under reduced pressure. Column chromatography (DCM/MeOH 95/5 + 0.1 % NH_3) afforded **25** (7.18 g, 95 %) as a yellow oil. R_f = 0.28 (DCM/MeOH/7N NH_3 in MeOH 95:4:1). ^{1}H NMR (300 MHz, $CDCl_3$) δ 7.22-7.16 (m, 2H), 6.87 – 6.78 (m, 2H), 4.12 (q, *J* = 7.1 Hz, 2H), 3.99 (t, *J* = 6.4 Hz, 2H), 3.41 (s, 2H), 2.83 (d, *J* = 11.6 Hz, 2H), 2.53 – 2.36 (m, 6H), 2.32 – 2.18 (m, 1H), 2.05 – 1.90 (m, 4H), 1.91 – 1.68 (m, 4H), 1.65-1.54 (m, 4H), 1.50 – 1.39 (m, 2H), 1.24 (t, *J* = 7.1 Hz, 3H). ^{13}C NMR (75 MHz, $CDCl_3$) δ 175.3, 158.1, 130.3,

114.2, 66.5, 62.7, 60.3, 56.1, 54.6, 52.8, 41.3, 28.3, 26.8, 25.9, 24.4, 14.2. HRMS (ESI-MS): m/z [M+H$^+$] calculated for $C_{23}H_{37}N_2O_3^+$: 389.2799, found 389.2800; $C_{23}H_{36}N_2O_3$ (388.55).

1-(4-(3-(Piperidin-1-yl)propoxy)benzyl)piperidine-4-carboxylic acid dihydrochloride (26)[188]

2 N aqueous HCl was added to a solution of **25** (2.06 g, 5.30 mmol, 1 eq) in THF and stirred at room temperature overnight. The solvent was evaporated, and the product was dried in vacuo. A sticky brown oil was obtained (**26**, 2.10 g, 92 %). ^{1}H NMR (300 MHz, CD_3OD) δ 7.55-7.47 (m, 2H), 7.07-6.98 (m, 2H), 4.27 (s, 2H), 4.14 (t, *J* = 5.8 Hz, 2H), 3.64-3.44 (m, 4H), 3.14 – 2.92 (m, 4H), 2.72 – 2.57 (m, 1H), 2.34 – 1.77 (m, 12H). ^{13}C NMR (101 MHz, CD_3OD) δ 173.6, 159.9, 132.8, 121.2, 114.8, 64.9, 59.7, 54.4, 53.1, 51.0, 38.2, 25.3, 23.8, 22.9, 21.3. HRMS (ESI-MS): m/z [M+H$^+$] calculated for $C_{21}H_{33}N_2O_3^+$: 361.2486, found 361.2490; $C_{21}H_{32}N_2O_3$*2 HCl (433.42).

1-(4-(3-(Piperidin-1-yl)propoxy)benzyl)-N-(prop-2-yn-1-yl)piperidine-4-carboxamide (27)[188]

26 (0.57 g, 1.44 mmol, 1 eq), HOBt (0.21 g, 1.58 mmol, 1.1 eq), EDC*HCl (0.30 g, 1.58 mmol, 1.1 eq) and DIPEA (0.98 ml, 5.76 mmol, 4 eq) were dissolved in a mixture of DCM and DMF (1:1) and stirred at room temperature for 30 min. Propargylamine (92 µl, 1.44 mmol, 1 eq) was added and the reaction was heated to 100 °C for 30 min in a microwave. Water was added to the reaction and the organic phase was separated. The aqueous phase was extracted with DCM, the combined organic phases were washed with brine, dried over Na_2SO_4 and the solvent removed under reduced pressure. Column chromatography (DCM/MeOH 9:1 + 0.1 % NH_3) afforded **27** as a yellow solid (0.57 g, 72 %). R_f = 0.42 (DCM/MeOH 9:1). ^{1}H NMR (300 MHz, $CDCl_3$) δ 7.22 – 7.16 (m, 2H), 6.87 – 6.80 (m, 2H), 5.64 (bt, *J* = 4.9 Hz, 1H), 4.04 (dd, *J* = 5.1, 2.6 Hz, 2H), 3.98 (t, *J* = 6.4 Hz, 2H), 3.42 (s, 2H), 2.96 – 2.86 (m, 2H), 2.52 – 2.32 (m, 6H), 2.22 (t, *J* = 2.6 Hz, 1H), 2.16 – 2.04 (m, 1H), 2.02 – 1.89 (m, 4H), 1.85 – 1.77 (m, 4H), 1.64 – 1.54 (m, 4H), 1.48 – 1.38 (m, 2H). ^{13}C NMR (75 MHz, $CDCl_3$) δ 174.76, 158.16, 130.24, 130.12, 114.19, 79.69, 71.63, 66.52, 62.57, 56.07, 54.66, 52.91, 43.20, 29.14, 28.80, 26.87, 25.98, 24.45. HRMS (ESI-MS): m/z [M+H$^+$] calculated for $C_{24}H_{36}N_3O_2^+$: 398.2802, found 398.2810; $C_{24}H_{35}N_3O_2$ (397.56).

***tert*-Butyl 4-((1*H*-imidazol-4-yl)methyl)piperidine-1-carboxylate (28)[259]**

N-Boc-4-piperidineacetaldehyde (0.50 g, 2.20 mmol, 1 eq) and *p*-toluenesulfonyl methyl isocyanide (0.47 g, 2.42 mmol, 1.1 eq) were dissolved in EtOH and sodium cyanide (10 mg, 0.22 mmol, 0.1 eq) was added and the reaction was stirred for 2 h at room temperature. The solvent was removed under reduced pressure and the residue was suspended in $CHCl_3$. The solid was filtered off and the filtrate was concentrated under reduced pressure. The residue was dissolved in sat. NH_3 in EtOH and the reaction was heated in a microwave for 2 h at 120 °C (7-10 bar). The solvent was removed under reduced pressure and the product was purified by column chromatography (DCM/MeOH 9:1). A brown

solid was obtained (0.35 g, 60 %). R_f = 0.44 (DCM/MeOH 9:1). ^{1}H NMR (300 MHz, $CDCl_3$) δ 7.65 – 7.53 (m, 1H), 6.77 (s, 1H), 4.17 – 4.01 (m, 2H), 2.73 – 2.58 (m, 2H), 2.53 (d, *J* = 6.9 Hz, 2H), 1.84 – 1.55 (m, 3H), 1.43 (s, 9H), 1.20 – 1.02 (m, 2H). ^{13}C NMR (75 MHz, $CDCl_3$) δ 154.97, 135.22, 134.31, 117.37, 79.44, 50.65, 36.46, 33.63, 31.93, 28.48. HRMS (ESI-MS): m/z $[M+H]^+$ calculated for $C_{14}H_{24}N_3O_2^+$: 266.1863, found 266.1865; $C_{14}H_{23}N_3O_2$ (265.36).

4-((1*H*-Imidazol-4-yl)methyl)piperidine (Immepip; 29)[259]

28 (0.30 g, 1.13 mmol, 1 eq) was stirred overnight at room temperature in a mixture of DCM and TFA (4:1, 15 ml). The solvent was removed under reduced pressure and the product was dried *in vacuo*. A brown solid was obtained. The product was used without further purification.

4-((1*H*-Imidazol-4-yl)methyl)-1-(prop-2-yn-1-yl)piperidine (30)

29 (0.44 g, 1.13 mmol, 1 eq) was dissolved in EtOH and Na_2CO_3 (0.60 g, 5.65 mmol, 5 eq) was added and the reaction was stirred at room temperature. After 30 min propargyl bromide (80 % in toluene; 189 µl, 1.70 mmol, 1.5 eq) was added and the reaction was stirred at room temperature overnight. The white solid was filtered off and the filtrate was concentrated under reduced pressure. The crude product was purified by column chromatography (DCM/MeOH 9:1). A pale brown solid was obtained (80 mg, 35 %). R_f = 0.45 (DCM/MeOH + 1 % NH_3 9:1). ^{1}H NMR (400 MHz, CD_3OD) δ 8.66 – 8.59 (m, 2H), 7.39 (s, 1H), 3.99 (d, *J* = 2.5 Hz, 2H), 3.63 – 3.53 (m, 2H), 3.30 (t, *J* = 2.5 Hz, 1H), 3.06 – 2.93 (m, 2H), 2.87 (d, *J* = 6.6 Hz, 2H), 2.12 – 1.99 (m, 3H), 1.77 – 1.60 (m, 2H). ^{13}C NMR (101 MHz, CD_3OD) δ 167.61, 133.82, 132.56, 116.58, 77.71, 73.80, 51.48, 45.31, 33.75, 30.58, 29.22. HRMS (ESI-MS): m/z $[M+H]^+$ calculated for $C_{12}H_{18}N_3^+$: 204.1490, found 204.1493; $C_{12}H_{17}N_3$ (203.29).

6-Bromohex-1-yne (31)[191]

Triphenylphosphine (2.23 g, 8.49 mmol, 1 eq) was added to a solution of 5-Hexyn-1-ol (1.10 ml, 10.19 mmol, 1.2 eq) in DCM and the reaction was stirred for 5 min at room temperature. Carbon tetrabromide (2.82 g, 8.49 mmol, 1 eq) was added and the reaction was stirred for 2 h. The solvent was removed under reduced pressure and the crude product was purified by column chromatography (PE/EtOAc 98:2). A clear oil was obtained (1.21 g, 88 %). ^{1}H NMR (300 MHz, $CDCl_3$) δ 3.44 (t, *J* = 6.6 Hz, 2H), 2.24 (td, *J* = 6.9, 2.6 Hz, 2H), 2.06 – 1.93 (m, 3H), 1.74 – 1.63 (m, 2H). ^{13}C NMR (75 MHz, $CDCl_3$) δ 83.65, 68.92, 33.17, 31.53, 26.82, 17.61. HRMS (EI-MS): m/z $[M\text{-}C_2H_4]^{\bullet+}$ calculated for $C_4H_5Br^{\bullet+}$: 131.9569, found 131.9577; C_6H_9Br (161.04).

4-((1*H*-Imidazol-4-yl)methyl)-1-(hex-5-yn-1-yl)piperidine (32)

29 (0.10 g, 0.25 mmol, 1 eq) was dissolved in EtOH and K_2CO_3 (0.17 g, 1.25 mmol, 5 eq) was added and the reaction was stirred at room temperature. After 30 min **31** (45 mg, 0.28 mmol, 1.1 eq) was added and the reaction was stirred overnight at room temperature. The white solid was filtered, and the filtrate was concentrated under reduced pressure. The crude product was purified by column chromatography (DCM/MeOH 9:1). A pale brown solid was obtained (50 mg, 80 %). R_f = 0.23 (DCM/MeOH 8:2). ^{1}H NMR (400 MHz, CD_3OD) δ 8.81 (s, 1H), 7.37 (s, 1H), 3.70 – 3.49 (m, 2H), 3.14 – 3.05 (m, 2H), 3.00 – 2.83 (m, 2H), 2.74 (d, *J* = 6.6 Hz, 2H), 2.31 – 2.22 (m, 3H), 2.00 – 1.81 (m, 5H), 1.64 – 1.46 (m, 4H). ^{13}C NMR (101 MHz, CD_3OD) δ 133.59, 131.23, 116.49, 82.49, 69.11, 56.37, 52.30, 33.19, 29.70, 28.68, 25.12, 22.79, 17.10. HRMS (ESI-MS): m/z $[M+H]^+$ calculated for $C_{15}H_{24}N_3^+$: 246.1965, found 246.1967; $C_{15}H_{23}N_3$ (245.37).

General procedure A

Ethylene glycol derivative (1 eq) and NEt_3 (2.5 eq) were dissolved in DCM. Methanesulfonyl chloride (2 eq) was added at 0 °C and the reaction was stirred at room temperature overnight. The white solid was filtered off and the filtrate was washed with saturated bicarbonate solution and brine, dried over Na_2SO_4 and the solvent was removed under reduced pressure. The crude product was purified by column chromatography (DCM/MeOH 98:2).

(Ethane-1,2-diylbis(oxy))bis(ethane-2,1-diyl) dimethanesulfonate (33a)[260]

The product was synthesized following general procedure A from triethylene glycol (7.00 g, 46.61 mmol, 1 eq), methanesulfonyl chloride (7.21 ml, 93.22 mmol, 2 eq) and NEt_3 (16.24 ml, 116.53 mmol, 2.5 eq). A yellow oil was obtained (13.48 g, 94 %). R_f = 0.80 (DCM/MeOH 98:2). ^{1}H NMR (300 MHz, $CDCl_3$) δ 4.38 – 4.28 (m, 4H), 3.75 – 3.69 (m, 4H), 3.63 (s, 4H), 3.03 (s, 6H). ^{13}C NMR (75 MHz, $CDCl_3$) δ 70.51, 69.25, 68.99, 37.62. HRMS (ESI-MS): m/z $[M+H]^+$ calculated for $C_8H_{19}O_8S_2^+$: 307.0516, found 307.0516; $C_8H_{18}O_8S_2$ (306.34).

((Oxybis(ethane-2,1-diyl))bis(oxy))bis(ethane-2,1-diyl) dimethanesulfonate (33b)[261]

The product was synthesized following general procedure A from tetraethylene glycol (10.00 g, 51.49 mmol, 1 eq), methanesulfonyl chloride (8.05 ml, 103.98 mmol, 2 eq) and NEt_3 (128.73 ml, 116.53 mmol, 2.5 eq). A yellow oil was obtained (14.03 g, 78 %). R_f = 0.70 (DCM/MeOH 98:2). ^{1}H NMR (300 MHz, $CDCl_3$) δ 4.42 – 4.29 (m, 4H), 3.80 – 3.70 (m, 4H), 3.68 – 3.58 (m, 8H), 3.06 (s, 6H). ^{13}C NMR (75 MHz, $CDCl_3$) δ 70.64, 70.51, 69.28, 69.02, 37.67. HRMS (ESI-MS): m/z $[M+H]^+$ calculated for $C_{10}H_{23}O_9S_2^+$: 351.0778, found 351.0783; $C_{10}H_{22}O_9S_2$ (350.40).

3,6,9,12-Tetraoxatetradecane-1,14-diyl dimethanesulfonate (33c)[262]

The product was synthesized following general procedure A from pentaethylene glycol (3.00 g, 12.59 mmol, 1 eq), methanesulfonyl chloride (1.95 ml, 25.18 mmol, 2 eq) and NEt_3 (4.38 ml, 31.47 mmol, 2.5 eq). A yellow oil was obtained (4.68 g, 94 %). R_f = 0.65 (DCM/MeOH 98:2). ^{1}H NMR (300 MHz, $CDCl_3$) δ 4.41 – 4.32 (m, 4H), 3.79 – 3.71 (m, 4H), 3.67 – 3.61 (m, 12H), 3.07 (s, 6H). ^{13}C NMR (75 MHz, $CDCl_3$) δ 70.64, 70.59, 70.52, 69.36, 69.03, 37.73. HRMS (ESI-MS): m/z $[M+H]^+$ calculated for $C_{12}H_{27}O_{10}S_2^+$: 395.1040, found 395.1045; $C_{12}H_{26}O_{10}S_2$ (394.45).

3,6,9,12,15-Pentaoxaheptadecane-1,17-diyl dimethanesulfonate (33d)[262]

The product was synthesized following general procedure A from hexaethylene glycol (3.00 g, 10.63 mmol, 1 eq), methanesulfonyl chloride (1.65 ml, 21.26 mmol, 2 eq) and NEt_3 (3.71 ml, 26.58 mmol, 2.5 eq). A yellow oil was obtained (4.51 g, 97 %). R_f = 0.68 (DCM/MeOH 98:2). ^{1}H NMR (300 MHz, $CDCl_3$) δ 4.38 – 4.31 (m, 4H), 3.77 – 3.70 (m, 4H), 3.65 – 3.57 (m, 16H), 3.06 (s, 6H). ^{13}C NMR (75 MHz, $CDCl_3$) δ 70.60, 70.56, 70.49, 69.43, 68.99, 37.72. HRMS (ESI-MS): m/z $[M+H]^+$ calculated for $C_{14}H_{31}O_{11}S_2^+$: 439.1302, found 439.1305; $C_{14}H_{30}O_{11}S_2$ (438.50).

General procedure B

The di-mesylate product or dibromide (1 eq) and sodium azide (4 eq) were dissolved in a mixture of EtOH and DMF (4:1) and the reaction was heated to reflux overnight. The solvents were removed under reduced pressure and the crude product was dissolved in diethyl ether. The organic phase was washed with saturated ammonium chloride solution and brine, dried over Na_2SO_4 and the solvent removed under reduced pressure. The product was dried *in vacuo*.

1,2-Bis(2-azidoethoxy)ethane (34a)[263]

The product was synthesized following general procedure B from **33a** (6.00 g, 19.59 mmol, 1 eq) and sodium azide (5.09 g, 78.36 mmol, 4 eq). A yellow oil was obtained (3.97 g, 99 %). R_f = 0.26 (DCM/MeOH 98:2). ^{1}H NMR (300 MHz, $CDCl_3$) δ 3.72 – 3.65 (m, 8H), 3.43 – 3.34 (m, 4H). ^{13}C NMR (75 MHz, $CDCl_3$) δ 70.76, 70.17, 50.71. HRMS (APCI-MS): m/z $[M+H]^+$ calculated for $C_6H_{13}N_6O_2^+$: 201.1095, found 201.1096; $C_6H_{12}N_6O_2$ (200.20).

1-Azido-2-(2-(2-(2-azidoethoxy)ethoxy)ethoxy)ethane (34b)[195]

The product was synthesized following general procedure B from **33b** (5.75 g, 16.41 mmol, 1 eq) and sodium azide (4.27 g, 65.64 mmol, 4 eq). A clear oil was obtained (3.70 g, 92 %). R_f = 0.23 (DCM/MeOH 98:2). ^{1}H NMR (300 MHz, $CDCl_3$) δ 3.71 – 3.62 (m, 12H), 3.43 – 3.33 (m, 4H). ^{13}C NMR (75

MHz, $CDCl_3$) δ 70.74, 70.07, 50.70. HRMS (ESI-MS): m/z $[M+H]^+$ calculated for $C_8H_{17}N_6O_3^+$: 245.1357, found 245.1359; $C_8H_{16}N_6O_3$ (244.26).

1,14-Diazido-3,6,9,12-tetraoxatetradecane (34c)[264]

The product was synthesized following general procedure B from **33c** (4.68 g, 11.86 mmol, 1 eq) and sodium azide (3.08 g, 47.44 mmol, 4 eq). A clear oil was obtained (3.23 g, 93 %). R_f = 0.20 (DCM/MeOH 98:2). ^{1}H NMR (300 MHz, $CDCl_3$) δ 3.70 – 3.62 (m, 16H), 3.41 – 3.33 (m, 4H). ^{13}C NMR (75 MHz, $CDCl_3$) δ 70.71, 70.69, 70.64, 70.04, 50.69. HRMS (ESI-MS): m/z $[M+Na]^+$ calculated for $C_{10}H_{20}N_6O_4Na^+$: 311.1438, found 311.1437; $C_{10}H_{20}N_6O_4$ (288.31).

1,17-Diazido-3,6,9,12,15-pentaoxaheptadecane (34d)[260]

The product was synthesized following general procedure B from **33d** (4.48 g, 10.22 mmol, 1 eq) and sodium azide (2.66 g, 40.88 mmol, 4 eq). A clear oil was obtained (3.31 g, 97 %). R_f = 0.19 (DCM/MeOH 98:2). ^{1}H NMR (300 MHz, $CDCl_3$) δ 3.59 – 3.43 (m, 20H), 3.28 – 3.16 (m, 4H). ^{13}C NMR (75 MHz, $CDCl_3$) δ 70.57, 70.52, 70.48, 69.94, 50.57. HRMS (ESI-MS): m/z $[M+H]^+$ calculated for $C_{12}H_{25}N_6O_5^+$: 333.1881, found 333.1882; $C_{12}H_{24}N_6O_5$ (332.36).

General procedure C

The diazide product (1 eq) was dissolved in a mixture of EtOAc/THF/1 N aq. HCl (5:1:5). Triphenylphosphine (1 eq) dissolved in diethyl ether was added slowly and the reaction was stirred at room temperature overnight. The white solid was filtered off. 4 N aq. HCl was added to the filtrate and the aqueous phase was washed with diethyl ether, basified with NaOH and subsequently extracted with DCM. The organic phase was dried over Na_2SO_4, and the solvent was removed under reduced pressure. The crude product was purified by column chromatography (DCM/MeOH + 1 % NH_3 95:5).

2-(2-(2-Azidoethoxy)ethoxy)ethan-1-amine (35a)[195]

The product was synthesized following general procedure C from **34a** (1.93 g, 9.64 mmol, 1 eq) and triphenylphosphine (2.53 g, 9.64 mmol, 1 eq). A clear oil was obtained (1.16 g, 69 %). R_f = 0.32 (DCM/MeOH + 1 % NH_3 95:5). ^{1}H NMR (300 MHz, $CDCl_3$) δ 3.70 – 3.57 (m, 6H), 3.53 – 3.46 (m, 2H), 3.41 – 3.33 (m, 2H), 2.91 – 2.78 (m, 2H), 1.55 (s, 2H). ^{13}C NMR (75 MHz, $CDCl_3$) δ 73.51, 70.68, 70.32, 70.08, 50.68, 41.77. HRMS (ESI-MS): m/z $[M+H]^+$ calculated for $C_6H_{15}N_4O_2^+$: 175.1190, found 175.1188; $C_6H_{14}N_4O_2$ (174.20).

2-(2-(2-(2-Azidoethoxy)ethoxy)ethoxy)ethan-1-amine (35b)[195]

The product was synthesized following general procedure C from **34b** (2.00 g, 8.19mmol, 1 eq) and triphenylphosphine (2.14 g, 8.19 mmol, 1 eq). A clear oil was obtained (1.37 g, 77 %). R_f = 0.30 (DCM/MeOH + 1 % NH_3 95:5). ^{1}H NMR (300 MHz, $CDCl_3$) δ 3.70 – 3.59 (m, 12H), 3.40 (dd, *J* = 6.8, 3.3 Hz, 2H), 3.04 (t, *J* = 5.0 Hz, 2H). ^{13}C NMR (75 MHz, $CDCl_3$) δ 70.49, 70.42, 70.09, 69.93, 69.37, 50.68, 40.41. HRMS (ESI-MS): m/z $[M+H]^+$ calculated for $C_8H_{19}N_4O_3^+$: 219.1452, found 219.1452; $C_8H_{18}N_4O_3$ (218.26).

14-Azido-3,6,9,12-tetraoxatetradecan-1-amine (35c) [195]

The product was synthesized following general procedure C from **34c** (3.53 g, 11.27 mmol, 1 eq) and triphenylphosphine (2.96 g, 11.27 mmol, 1 eq). A clear oil was obtained (1.38 g, 47 %). R_f = 0.22 (DCM/MeOH + 1 % NH_3 95:5). ^{1}H NMR (400 MHz, $CDCl_3$) δ 3.64 – 3.56 (m, 14H), 3.46 (t, *J* = 5.2 Hz, 2H), 3.34 (t, *J* = 5.1 Hz, 2H), 2.81 (t, *J* = 5.2 Hz, 2H), 1.45 (s, 2H). ^{13}C NMR (75 MHz, $CDCl_3$) δ 73.35, 70.68, 70.65, 70.60, 70.58, 70.54, 70.26, 70.01, 50.65, 41.76. HRMS (ESI-MS): m/z $[M+H]^+$ calculated for $C_{10}H_{23}N_4O_4^+$: 263.1714, found 263.1717; $C_{10}H_{22}N_4O_4$ (262.31).

17-Azido-3,6,9,12,15-pentaoxaheptadecan-1-amine (35d)[195]

The product was synthesized following general procedure C from **34d** (1.50 g, 4.51 mmol, 1 eq) and triphenylphosphine (1.18 g, 4.51 mmol, 1 eq). A clear oil was obtained (0.94 g, 68 %). R_f = 0.16 (DCM/MeOH + 1 % NH_3 95:5). ^{1}H NMR (300 MHz, $CDCl_3$) δ 3.70 – 3.60 (m, 18H), 3.55 – 3.48 (m, 2H), 3.43 – 3.33 (m, 2H), 2.91 – 2.81 (m, 2H), 2.00 (s, 2H). ^{13}C NMR (75 MHz, $CDCl_3$) δ 73.08, 70.67, 70.60, 70.55, 70.28, 70.03, 50.69, 41.71. HRMS (ESI-MS): m/z $[M+H]^+$ calculated for $C_{12}H_{27}N_4O_5^+$: 307.1976, found 307.1981; $C_{12}H_{26}N_4O_5$ (306.36).

General procedure D

Glutaryl chloride (1 eq) was added at 0 °C to a solution of the amine (2 eq) and NEt_3 (5 eq) in DCM and the reaction was stirred at room temperature overnight. The solvent was removed under reduced pressure and the crude product was purified by column chromatography (DCM/MeOH + 1 % NH_3 95:5).

***N*^{1},*N*^{5}-Bis(2-(2-(2-azidoethoxy)ethoxy)ethyl)glutaramide (36a)**

The product was synthesized following general procedure D from **35a** (1.50 g, 8.61 mmol, 2.2 eq), glutaryl chloride (501 µl, 3.91 mmol, 1 eq) and NEt_3 (2.74 ml, 19.55 mmol, 5 eq). A clear oil was obtained (1.59 g, 92 %). R_f = 0.46 (DCM/MeOH + 1 % NH_3 95:5). ^{1}H NMR (300 MHz, $CDCl_3$) δ 6.44 (bs, 2H), 3.70 – 3.61 (m, 12H), 3.60 – 3.54 (m, 4H), 3.48 – 3.33 (m, 8H), 2.21 (t, *J* = 6.9 Hz, 4H), 2.02 – 1.89

(m, 2H). ^{13}C NMR (75 MHz, $CDCl_3$) δ 172.72, 70.50, 70.23, 70.08, 69.80, 50.62, 39.17, 35.19, 21.97. HRMS (ESI-MS): m/z $[M+H]^+$ calculated for $C_{17}H_{33}N_8O_6^+$: 445.2518, found 445.2525; $C_{17}H_{32}N_8O_6$ (444.49).

N^1,N^5-Bis(2-(2-(2-(2-azidoethoxy)ethoxy)ethoxy)ethyl)glutaramide (36b)

The product was synthesized following general procedure D from **35b** (1.5 g, 6.87 mmol, 2.2 eq), glutaryl chloride (399 µl, 3.12 mmol, 1 eq) and NEt_3 (2.19 ml, 15.60 mmol, 5 eq). A clear oil was obtained (1.49 g, 90 %). R_f = 0.40 (DCM/MeOH + 1 % NH_3 95:5). ^{1}H NMR (300 MHz, $CDCl_3$) δ 6.54 (bs, 2H), 3.71 – 3.61 (m, 20H), 3.61 – 3.55 (m, 4H), 3.47 – 3.33 (m, 8H), 2.25 – 2.15 (m, 4H), 2.02 – 1.91 (m, 2H). ^{13}C NMR (101 MHz, $CDCl_3$) δ 172.65, 70.68, 70.56, 70.26, 70.07, 69.65, 50.67, 39.18, 35.08, 21.96. HRMS (ESI-MS): m/z $[M+H]^+$ calculated for $C_{21}H_{41}N_8O_8^+$: 533.3042, found 533.3053; $C_{21}H_{40}N_8O_8$ (532.60).

N^1,N^5-Bis(14-azido-3,6,9,12-tetraoxatetradecyl)glutaramide (36c)

The product was synthesized following general procedure D from **35c** (1.5 g, 5.72 mmol, 2.2 eq), glutaryl chloride (332 µl, 2.60 mmol, 1 eq) and NEt_3 (1.83 ml, 13.00 mmol, 5 eq). A clear oil was obtained (0.66 g, 41 %). R_f = 0.36 (DCM/MeOH + 1 % NH_3 95:5). ^{1}H NMR (300 MHz, $CDCl_3$) δ 6.67 – 6.44 (m, 2H), 3.67 – 3.52 (m, 32H), 3.44-3.32 (m, 8H), 2.24 – 2.13 (m, 4H), 1.95 (p, *J* = 6.4 Hz, 2H). ^{13}C NMR (75 MHz, $CDCl_3$) δ 172.71, 70.69, 70.63, 70.60, 70.53, 70.44, 70.23, 70.04, 69.61, 50.66, 39.19, 35.02, 21.97. HRMS (ESI-MS): m/z $[M+H]^+$ calculated for $C_{25}H_{49}N_8O_{10}^+$: 621.3566, found 621.3579; $C_{25}H_{48}N_8O_{10}$ (620.71).

N^1,N^5-Bis(17-azido-3,6,9,12,15-pentaoxaheptadecyl)glutaramide (36d)

The product was synthesized following general procedure D from **35d** (0.94 g, 3.07 mmol, 2.2 eq), glutaryl chloride (179 µl, 1.40 mmol, 1 eq) and pyridine (1.13 ml, 14.00 mmol, 10 eq) instead of NEt_3. A clear oil was obtained (0.34 g, 34 %). R_f = 0.30 (DCM/MeOH + 1 % NH_3 95:5). ^{1}H NMR (300 MHz, $CDCl_3$) δ 6.85 – 6.62 (m, 2H), 3.82 – 3.51 (m, 40H), 3.47 – 3.34 (m, 8H), 2.42 – 2.15 (m, 4H), 2.01 – 1.91 (m, 2H). ^{13}C NMR (75 MHz, $CDCl_3$) δ 172.88, 70.68, 70.66, 70.59, 70.52, 70.46, 70.19, 70.04, 69.74, 50.68, 39.19, 35.13. HRMS (ESI-MS): m/z $[M+H]^+$ calculated for $C_{29}H_{57}N_8O_{12}^+$: 709.4090, found 709.4109; $C_{29}H_{56}N_8O_{12}$ (708.81).

1,10-Diazidodecane (37a)[265]

The product was synthesized following general procedure B from 1,10-dibromodecane (5.00 g, 16.60 mmol, 1 eq) and sodium azide (3.10 g, 49.98 mmol, 3 eq). A clear oil was obtained (3.61 g, 97 %). ^{1}H NMR (300 MHz, $CDCl_3$) δ 3.26 (t, *J* = 6.9 Hz, 4H), 1.65 – 1.54 (m, 4H), 1.42 – 1.26 (m, 12H). ^{13}C

NMR (75 MHz, $CDCl_3$) δ 51.49, 29.37, 29.12, 28.85, 26.71. HRMS (APCI-MS): m/z $[M+H]^+$ calculated for $C_{10}H_{21}N_6^+$: 225.1822, found 225.1825; $C_{10}H_{20}N_6$ (224.31).

1,12-Diazidododecane (37b)[265]

The product was synthesized following general procedure B from 1,12-dibromododecane (5.00 g, 15.24 mmol, 1 eq) and sodium azide (2.97 g, 45.72 mmol, 3 eq). A clear oil was obtained (3.57 g, 93 %). ^{1}H NMR (300 MHz, $CDCl_3$) δ 3.25 (t, *J* = 6.9 Hz, 4H), 1.65 – 1.54 (m, 4H), 1.41 – 1.24 (m, 16H). ^{13}C NMR (75 MHz, $CDCl_3$) δ 51.50, 29.50, 29.47, 29.16, 28.86, 26.73. HRMS (APCI-MS): m/z $[M+H]^+$ calculated for $C_{12}H_{25}N_6^+$: 253.2135, found 253.2141; $C_{12}H_{24}N_6$ (252.37).

10-Azidodecan-1-amine (38a)[266]

Triphenylphosphine (1.40 g, 5.35 mmol, 1 eq) dissolved in THF was added dropwise to a solution of **37a** (3.60 g, 16.05 mmol, 3 eq) in THF. The reaction was stirred overnight. 1 N aq. HCl was added and the reaction was stirred for 2 h at room temperature. The organic solvent was removed under reduced pressure and the aqueous phase basified and extracted with DCM (3 x). The combined organic phases were washed with water and brine, dried over Na_2SO_4 and the solvent removed under reduced pressure. The crude product was purified by flash chromatography (0 min to 20 min, 98:2 DCM/MeOH to 9:1 DCM/MeOH). A clear oil was obtained (0.40 g, 38 %). R_f = 0.65 (DCM/MeOH + 1 % NH_3 95:5). ^{1}H NMR (400 MHz, $CDCl_3$) δ 3.18 (t, *J* = 7.0 Hz, 2H), 2.62 (t, *J* = 7.0 Hz, 2H), 1.58 – 1.47 (m, 2H), 1.40 – 1.20 (m, 16H). ^{13}C NMR (101 MHz, $CDCl_3$) δ 51.48, 42.15, 33.60, 29.49, 29.43, 29.41, 29.13, 28.83, 26.86, 26.70. HRMS (ESI-MS): m/z $[M+H]^+$ calculated for $C_{10}H_{23}N_4^+$: 199.1917, found 199.1920; $C_{10}H_{22}N_4$ (198.31).

12-Azidododecan-1-amine (38b)[267]

Triphenylphosphine (1.24 g, 4.71 mmol, 1 eq) dissolved in THF was added dropwise to a solution of **37b** (3.57 g, 14.14 mmol, 3 eq) in THF. The reaction was stirred overnight. 1 N aq. HCl was added and the reaction was stirred for 2 h at room temperature. The organic solvent was removed under reduced pressure and the aqueous phase basified and extracted with DCM (3 x). The combined organic phases were washed with water and brine, dried over Na_2SO_4 and the solvent removed under reduced pressure. The crude product was purified by flash chromatography (0 min to 20 min, 98:2 DCM/MeOH to 9:1 DCM/MeOH). A clear oil was obtained (0.35 g, 33 %). R_f = 0.65 (DCM/MeOH + 1 % NH_3 95:5). ^{1}H NMR (400 MHz, $CDCl_3$) δ 3.23 (t, *J* = 7.0 Hz, 2H), 2.65 (t, *J* = 7.0 Hz, 2H), 1.62 – 1.51 (m, 2H), 1.25 (s, 18H). ^{13}C NMR (101 MHz, $CDCl_3$) δ 51.49, 42.27, 33.86, 29.61, 29.56, 29.52, 29.50, 29.47, 29.15, 28.84, 26.90, 26.71. HRMS (ESI-MS): m/z $[M+H]^+$ calculated for $C_{12}H_{27}N_4^+$: 227.2230, found 227.2233; $C_{12}H_{26}N_4$ (226.37).

N^1,N^5-Bis(10-azidodecyl)glutaramide (39a)

The product was synthesized following general procedure D from **38a** (0.38 g, 1.91 mmol, 2.2 eq), glutaryl chloride (111 µl, 0.87 mmol, 1 eq) and NEt_3 (0.61 ml, 4.35 mmol, 5 eq). A white solid was obtained (0.23 g, 54 %). R_f = 0.43 (DCM/MeOH 98:2). ^{1}H NMR (400 MHz, $CDCl_3$) δ 5.96 (t, *J* = 5.7 Hz, 2H), 3.29 – 3.14 (m, 8H), 2.22 (t, *J* = 7.1 Hz, 4H), 1.91 (p, *J* = 7.1 Hz, 2H), 1.64 – 1.53 (m, 4H), 1.50 – 1.42 (m, 4H), 1.36 – 1.22 (m, 24H). ^{13}C NMR (101 MHz, $CDCl_3$) δ 172.52, 51.46, 39.53, 35.42, 29.61, 29.39, 29.37, 29.23, 29.09, 28.81, 26.91, 26.68, 22.19. HRMS (ESI-MS): m/z $[M+H]^+$ calculated for $C_{25}H_{49}N_8O_2^+$: 493.3973, found 493.3982; $C_{25}H_{48}N_8O_2$ (492.71).

N^1,N^5-Bis(10-azidodecyl)glutaramide (39b)

The product was synthesized following general procedure D from **38a** (0.34 g, 1.50 mmol, 2.2 eq), glutaryl chloride (86.7 µl, 0.68 mmol, 1 eq) and NEt_3 (0.48 ml, 3.41 mmol, 5 eq). A white solid was obtained (0.30 g, 81 %). R_f = 0.45 (DCM/MeOH 98:2). ^{1}H NMR (400 MHz, $CDCl_3$) δ 5.94 (t, *J* = 5.7 Hz, 2H), 3.30 – 3.14 (m, 8H), 2.22 (t, *J* = 7.1 Hz, 4H), 1.92 (p, *J* = 7.1 Hz, 2H), 1.66 – 1.53 (m, 4H), 1.52 – 1.40 (m, 4H), 1.40 – 1.19 (m, 32H). ^{13}C NMR (101 MHz, $CDCl_3$) δ 172.52, 51.48, 39.55, 35.42, 29.62, 29.51, 29.48, 29.45, 29.28, 29.13, 28.82, 26.94, 26.70, 22.19. HRMS (ESI-MS): m/z $[M+H]^+$ calculated for $C_{29}H_{57}N_8O_2^+$: 549.4599, found 459.4612; $C_{29}H_{56}N_8O_2$ (548.82).

General Procedure E

Both pharmacophores (1.1 eq Each) and the spacer (1 eq) were dissolved in DCM/MeOH (1:1). Ascorbic acid (0.3 eq) and $CuSO_4$*5 H_2O were added and the reaction was stirred for 72 hours at room temperature. The solvent was removed under reduced pressure and the crude product was purified by preparative HPLC.

N^1-(2-(2-(2-(4-((4-((4-(7-Chloro-8-hydroxy-3-methyl-2,3,4,5-tetrahydro-1*H*-benzo[*d*]azepin-1-yl)phenyl)amino)-4-oxobutanamido)methyl)-1*H*-1,2,3-triazol-1-yl)ethoxy)ethoxy)ethyl)-N^5-(2-(2-(2-(4-((1-(4-(3-(piperidin-1-yl)propoxy)benzyl)piperidine-4-carboxamido)methyl)-1*H*-1,2,3-triazol-1-yl)ethoxy)ethoxy)ethyl)glutaramide pentahydrotrifluoroacetate (40)

The product was synthesized following general procedure E from **27** (87 mg, 0.22 mmol, 1.1 eq), **18** (97 mg, 0.22 mmol, 1.1 eq), **36a** (89 mg, 0.20 mmol, 1 eq), ascorbic acid (11 mg, 0.06 mmol, 0.3 eq) and Cu_2SO_4*5 H_2O (5 mg, 0.02 mmol, 0.1 eq). A white solid was obtained (93 mg, 25 %). RP-HPLC: > 97 %, (t_R = 7.80 min, k = 1.84). ^{1}H NMR (400 MHz, CD_3OD) δ 7.94 – 7.83 (m, 2H), 7.72 – 7.50 (m, 2H), 7.47 – 7.36 (m, 2H), 7.32 – 7.06 (m, 3H), 7.07 – 6.97 (m, 2H), 6.69-6.15 (d*, *J* = 365.9 Hz, 1H), 4.62 – 4.47 (m, 4H), 4.46 – 4.37 (m, 4H), 4.31 – 4.21 (m, 2H), 4.12 (t, *J* = 5.8 Hz, 2H), 3.92 – 3.71 (m, 5H), 3.65 – 3.41 (m, 17H), 3.38 – 3.24 (m, 9H), 3.14 – 2.87 (m, 9H), 2.78 – 2.43 (m, 5H), 2.33 – 2.13 (m, 6H), 2.10

– 1.69 (m, 11H), 1.63 – 1.43 (m, 1H). ^{13}C NMR (101 MHz, CD_3OD) δ 174.05, 173.21, 171.64, 159.93, 144.99, 144.47, 138.22, 135.44, 132.61, 128.56, 123.54, 121.13, 120.33, 116.33, 114.76, 70.05, 70.02, 69.81, 69.12, 68.93, 64.76, 59.90, 54.36, 53.06, 51.13, 49.97, 44.50, 39.67, 38.95, 34.76, 34.40, 34.22, 31.34, 30.19, 25.92, 23.77, 22.91, 21.86, 21.29. HRMS (ESI-MS): m/z $[M+2H]^{2+}$ calculated for $C_{65}H_{95}ClN_{14}O_{11}^{2+}$: 641.3491, found 641.3502; $C_{65}H_{93}ClN_{14}O_{11}$*5 TFA (1852.11).

N^1-(2-(2-(2-(2-(4-((4-((4-(7-Chloro-8-hydroxy-3-methyl-2,3,4,5-tetrahydro-1*H*-benzo[*d*]azepin-1-yl)phenyl)amino)-4-oxobutanamido)methyl)-1*H*-1,2,3-triazol-1-yl)ethoxy)ethoxy)ethoxy)ethyl)-N^5-(2-(2-(2-(2-(4-((1-(4-(3-(piperidin-1-yl)propoxy)benzyl)piperidine-4-carboxamido)methyl)-1*H*-1,2,3-triazol-1-yl)ethoxy)ethoxy)ethoxy)ethyl)glutaramide pentahydrotrifluoroacetate (41)

The product was synthesized following general procedure E from **27** (87 mg, 0.22 mmol, 1.1 eq), **18** (97 mg, 0.22 mmol, 1.1 eq), **36b** (107 mg, 0.20 mmol, 1 eq), ascorbic acid (11 mg, 0.06 mmol, 0.3 eq) and Cu_2SO_4*5 H_2O (5 mg, 0.02 mmol, 0.1 eq). A white solid was obtained (97 mg, 25 %). RP-HPLC: > 99 %, (t_R = 8.39 min, k = 1.61). ^{1}H NMR (400 MHz, CD_3OD) δ 7.96 – 7.85 (m, 2H), 7.69 – 7.53 (m, 2H), 7.47 – 7.37 (m, 2H), 7.29 – 7.07 (m, 3H), 7.05 – 6.99 (m, 2H), 6.70-6.15 (d*, *J* = 221.5 Hz, 1H), 4.55 – 4.50 (m, 4H), 4.46 – 4.38 (m, 4H), 4.29 – 4.22 (m, 2H), 4.12 (t, *J* = 5.8 Hz, 2H), 3.87 – 3.73 (m, 5H), 3.64 – 3.46 (m, 25H), 3.34 – 3.25 (m, 9H), 3.11 – 2.89 (m, 9H), 2.76 – 2.65 (m, 2H), 2.65 – 2.44 (m, 3H), 2.28 – 2.14 (m, 6H), 2.09 – 1.69 (m, 11H), 1.60 – 1.43 (m, 1H). ^{13}C NMR (101 MHz, CD_3OD) δ 174.02, 173.19, 171.64, 159.93, 144.87, 138.23, 132.61, 130.56, 128.57, 123.60, 121.12, 120.35, 114.76, 70.11, 70.04, 69.99, 69.86, 69.09, 68.93, 64.77, 60.60, 59.89, 54.37, 53.06, 51.13, 50.01, 44.61, 39.68, 38.94, 34.73, 34.38, 34.20, 31.35, 30.21, 25.92, 23.76, 22.91, 21.82, 21.29. HRMS (ESI-MS): m/z $[M+H]^+$ calculated for $C_{69}H_{102}ClN_{14}O_{13}^+$: 1369.7434, found 1369.7426; $C_{69}H_{101}ClN_{14}O_{13}$*5 TFA (1940.22).

N^1-(14-(4-((4-((4-(7-Chloro-8-hydroxy-3-methyl-2,3,4,5-tetrahydro-1*H*-benzo[*d*]azepin-1-yl)phenyl)amino)-4-oxobutanamido)methyl)-1*H*-1,2,3-triazol-1-yl)-3,6,9,12-tetraoxatetradecyl)-N^5-(14-(4-((1-(4-(3-(piperidin-1-yl)propoxy)benzyl)piperidine-4-carboxamido)methyl)-1*H*-1,2,3-triazol-1-yl)-3,6,9,12-tetraoxatetradecyl)glutaramide pentahydrotrifluoroacetate (42)

The product was synthesized following general procedure E from **27** (44 mg, 0.11 mmol, 1.1 eq), **18** (50 mg, 0.11 mmol, 1.1 eq), **36c** (62 mg, 0.10 mmol, 1 eq), ascorbic acid (5.3 mg, 0.03 mmol, 0.3 eq) and Cu_2SO_4*5 H_2O (2.5 mg, 0.01 mmol, 0.1 eq). A white solid was obtained (35 mg, 17 %). RP-HPLC: > 99 %, (t_R = 8.60 min, k = 2.13). ^{1}H NMR (400 MHz, D_2O) δ 7.89 – 7.74 (m, 2H), 7.41 – 7.26 (m, 4H), 7.25 – 7.17 (m, 1H), 7.14 – 7.08 (m, 1H), 7.03 – 6.93 (m, 3H), 6.72 – 6.09 (d*, *J* = 252.5 Hz, 1H), 4.55 – 4.33 (m, 8H), 4.19 – 4.12 (m, 2H), 4.08 (t, *J* = 5.7 Hz, 2H), 3.89 – 3.69 (m, 5H), 3.56 – 3.46 (m, 33H), 3.28 – 3.15 (m, 7H), 3.11 – 2.79 (m, 10H), 2.71 – 2.44 (m, 5H), 2.20 – 2.09 (m, 6H), 2.04 – 1.93 (m, 2H), 1.90 – 1.83 (m, 2H), 1.81 – 1.56 (m, 7H), 1.48 – 1.32 (m, 1H). ^{13}C NMR (101 MHz, D_2O) δ 175.75,

174.54, 173.19, 173.10, 163.06, 162.70, 162.35, 159.24, 150.88, 150.46, 144.77, 144.36, 141.74, 138.82, 136.66, 136.25, 132.87, 131.91, 130.96, 130.38, 128.88, 128.23, 124.20, 121.97, 121.71, 121.18, 120.73, 119.21, 118.76, 118.40, 117.83, 116.57, 115.14, 114.93, 112.03, 69.61, 69.56, 69.46, 69.40, 68.80, 68.74, 68.67, 65.32, 60.15, 59.94, 56.13, 54.43, 53.37, 51.11, 49.97, 48.61, 45.37, 45.15, 44.55, 39.70, 38.90, 34.85, 34.39, 31.77, 30.84, 30.21, 25.74, 23.45, 22.85, 21.76, 21.12. HRMS (ESI-MS): m/z $[M+2H]^{2+}$ calculated for $C_{73}H_{111}ClN_{14}O_{15}^{2+}$: 729.4015, found 729.4023; $C_{73}H_{109}ClN_{14}O_{15}$*5 TFA (2028.32).

N^1-(17-(4-((4-((4-(7-Chloro-8-hydroxy-3-methyl-2,3,4,5-tetrahydro-1*H*-benzo[*d*]azepin-1-yl)phenyl)amino)-4-oxobutanamido)methyl)-1*H*-1,2,3-triazol-1-yl)-3,6,9,12,15-pentaoxaheptadecyl)-N^5-(17-(4-((1-(4-(3-(piperidin-1-yl)propoxy)benzyl)piperidine-4-carboxamido)methyl)-1*H*-1,2,3-triazol-1-yl)-3,6,9,12,15-pentaoxaheptadecyl)glutaramide pentahydrotrifluoroacetate (43)

The product was synthesized following general procedure E from **27** (87 mg, 0.22 mmol, 1.1 eq), **18** (97 mg, 0.22 mmol, 1.1 eq), **36d** (142 mg, 0.20 mmol, 1 eq), ascorbic acid (11 mg, 0.06 mmol, 0.3 eq) and Cu_2SO_4*5 H_2O (5 mg, 0.02 mmol, 0.1 eq). A white solid was obtained (18 mg, 4 %). RP-HPLC: > 98 %, (t_R = 8.80 min, k = 1.74). ^{1}H NMR (400 MHz, D_2O) δ 7.89 – 7.74 (m, 2H), 7.43 – 7.26 (m, 4H), 7.25 – 7.15 (m, 1H), 7.14 – 7.08 (m, 1H), 7.06 – 6.90 (m, 3H), 6.72 – 6.09 (d*i, *J* = 252.5 Hz, 1H), 4.53 – 4.34 (m, 8H), 4.21 – 4.13 (m, 2H), 4.08 (t, *J* = 5.7 Hz, 2H), 3.89 – 3.72 (m, 5H), 3.56 – 3.44 (m, 41H), 3.29 – 3.17 (m, 7H), 3.08 – 2.79 (m, 10H), 2.70 – 2.44 (m, 6H), 2.18 – 2.10 (m, 6H), 2.03 – 1.94 (m, 2H), 1.91 – 1.83 (m, 2H), 1.79 – 1.55 (m, 7H), 1.49 – 1.30 (m, 1H). ^{13}C NMR (101 MHz, D_2O) δ 175.75, 174.54, 173.19, 173.10, 163.06, 162.70, 162.35, 159.24, 150.88, 150.46, 144.77, 144.36, 141.74, 138.82, 136.66, 136.25, 132.87, 131.91, 130.96, 130.38, 128.88, 128.23, 124.20, 121.97, 121.71, 121.18, 120.73, 119.21, 118.76, 118.40, 117.83, 116.57, 115.14, 114.93, 112.03, 69.61, 69.56, 69.46, 69.40, 68.80, 68.74, 68.67, 65.32, 60.15, 59.94, 56.13, 54.43, 53.37, 51.11, 49.97, 48.61, 45.37, 45.15, 44.55, 39.70, 38.90, 34.85, 34.39, 31.77, 30.84, 30.21, 25.74, 23.45, 22.85, 21.76, 21.12. HRMS (ESI-MS): m/z $[M+2H]^{2+}$ calculated for $C_{77}H_{119}ClN_{14}O_{17}^{2+}$: 773.4278, found 773.4280; $C_{77}H_{117}ClN_{14}O_{17}$*5 TFA (2116.43).

N^1-(2-(2-(2-(4-((5-(N-(4-(7-Chloro-8-hydroxy-3-methyl-2,3,4,5-tetrahydro-1*H*-benzo[*d*]azepin-1-yl)phenyl)sulfamoyl)pentanamido)methyl)-1*H*-1,2,3-triazol-1-yl)ethoxy)ethoxy)ethyl)-N^5-(2-(2-(2-(4-((1-(4-(3-(piperidin-1-yl)propoxy)benzyl)piperidine-4-carboxamido)methyl)-1*H*-1,2,3-triazol-1-yl)ethoxy)ethoxy)ethyl)glutaramide pentahydrotrifluoroacetate (44)

The product was synthesized following general procedure E from **27** (47 mg, 118 µmol, 1.1 eq), **20** (59 mg, 118 µmol, 1.1 eq), **36a** (48 mg, 107 µmol, 1 eq), ascorbic acid (6 mg, 36 µmol, 0.3 eq) and Cu_2SO_4*5 H_2O (3 mg, 12 µmol, 0.1 eq). A white solid was obtained (19 mg, 9 %). RP-HPLC: > 97 %, (t_R =

8.07 min, k = 1.51). ^{1}H NMR (400 MHz, D_2O) δ 7.85 – 7.73 (m, 2H), 7.35 – 7.28 (m, 2H), 7.24 – 7.15 (m, 2H), 7.15 – 7.08 (m, 2H), 7.05 – 6.98 (m, 1H), 6.98 – 6.92 (m, 2H), 6.68 – 6.04 (d*, *J* = 253.7 Hz, 1H), 4.49 – 4.42 (m, 4H), 4.36 – 4.30 (m, 2H), 4.30 – 4.24 (m, 2H), 4.20 – 4.10 (m, 2H), 4.07 (t, *J* = 5.7 Hz, 2H), 3.85 – 3.64 (m, 5H), 3.57 – 3.35 (m, 18H), 3.29 – 3.04 (m, 10H), 3.03 – 2.80 (m, 9H), 2.56 – 2.44 (m, 1H), 2.21 – 2.07 (m, 8H), 2.01 – 1.92 (m, 2H), 1.91 – 1.82 (m, 2H), 1.81 – 1.51 (m, 11H), 1.47 – 1.31 (m, 1H). HRMS (ESI-MS): m/z $[M+2H]^{2+}$ calculated for $C_{66}H_{99}ClN_{14}O_{12}S^{2+}$: 673.3483, found 673.3492; $C_{66}H_{97}ClN_{14}O_{12}S$*5 TFA (1916.21).

N^1-(2-(2-(2-(2-(4-((5-(N-(4-(7-Chloro-8-hydroxy-3-methyl-2,3,4,5-tetrahydro-1*H*-benzo[*d*]azepin-1-yl)phenyl)sulfamoyl)pentanamido)methyl)-1*H*-1,2,3-triazol-1-yl)ethoxy)ethoxy)ethoxy)ethyl)-N^5-(2-(2-(2-(2-(4-((1-(4-(3-(piperidin-1-yl)propoxy)benzyl)piperidine-4-carboxamido)methyl)-1*H*-1,2,3-triazol-1-yl)ethoxy)ethoxy)ethoxy)ethyl)glutaramide pentahydrotrifluoroacetate (45)

The product was synthesized following general procedure E from **27** (19 mg, 48 µmol, 1.1 eq), **20** (24 mg, 48 µmol, 1.1 eq), **36b** (23 mg, 44 µmol, 1 eq), ascorbic acid (2.6 mg, 15 µmol, 0.3 eq) and Cu_2SO_4*5 H_2O (1.3 mg, 5 µmol, 0.1 eq). A white solid was obtained (19 mg, 20 %). RP-HPLC: > 98 %, (t_R = 8.63 min, k = 1.69). ^{1}H NMR (400 MHz, D_2O) δ 7.91 – 7.68 (m, 2H), 7.43 – 7.28 (m, 2H), 7.26 – 6.85 (m, 7H), 6.69 – 6.05 (d*, *J* = 254.5 Hz, 1H), 4.50 – 4.41 (m, 6H), 4.35 – 4.25 (m, 4H), 4.16 – 4.05 (m, 4H), 3.87 – 3.77 (m, 4H), 3.61 – 3.35 (m, 26H), 3.27 – 3.07 (m, 10H), 3.03 – 2.72 (m, 9H), 2.56 – 2.44 (m, 1H), 2.26 – 2.02 (m, 8H), 2.01 – 1.93 (m, 2H), 1.91 – 1.83 (m, 2H), 1.78 – 1.54 (m, 10H), 1.48 – 1.32 (m, 1H). ^{13}C NMR (101 MHz, D_2O) δ 175.74, 162.75, 159.23, 150.41, 144.35, 136.65, 136.17, 132.87, 130.93, 129.55, 128.90, 124.18, 124.07, 121.77, 121.62, 121.17, 117.82, 115.13, 69.56, 69.45, 69.39, 68.76, 68.71, 65.32, 60.15, 54.44, 53.37, 51.10, 50.47, 50.00, 45.17, 44.40, 39.70, 38.90, 34.84, 34.72, 34.39, 30.25, 25.74, 23.52, 23.45, 22.85, 22.20, 21.76, 21.11. HRMS (ESI-MS): m/z $[M+2H]^{2+}$ calculated for $C_{70}H_{107}ClN_{14}O_{14}S^{2+}$: 717.3745, found 717.3752; $C_{70}H_{105}ClN_{14}O_{14}S$*5 TFA (2004.32).

N^1-(10-(4-((4-((4-(7-Chloro-8-hydroxy-3-methyl-2,3,4,5-tetrahydro-1*H*-benzo[*d*]azepin-1-yl)phenyl)amino)-4-oxobutanamido)methyl)-1*H*-1,2,3-triazol-1-yl)decyl)-N^5-(10-(4-((1-(4-(3-(piperidin-1-yl)propoxy)benzyl)piperidine-4-carboxamido)methyl)-1*H*-1,2,3-triazol-1-yl)decyl)glutaramide pentahydrotrifluoroacetate (46)

The product was synthesized following general procedure E from **27** (52 mg, 0.13 mmol, 1.1 eq), **18** (57 mg, 0.13 mmol, 1.1 eq), **39a** (60 mg, 0.11 mmol, 1 eq), ascorbic acid (7.0 mg, 0.03 mmol, 0.3 eq) and Cu_2SO_4*5 H_2O (2.5 mg, 0.01 mmol, 0.1 eq). A white solid was obtained (12 mg, 5 %). RP-HPLC: > 97 %, (t_R = 11.34 min, k = 2.53). ^{1}H NMR (400 MHz, CD_3OD) δ 7.90 – 7.79 (m, 2H), 7.70 – 7.54 (m, 2H), 7.47 – 7.38 (m, 2H), 7.29 – 7.08 (m, 3H), 7.06 – 6.99 (m, 2H), 6.70 – 6.15 (d*, *J* = 220.5 Hz 1H), 4.64 – 4.48 (m, 1H), 4.47 – 4.39 (m, 2H), 4.37 – 4.22 (m, 6H), 4.12 (t, *J* = 5.8 Hz, 2H), 3.91 – 3.43 (m, 7H),

3.40 – 3.26 (m, 12H), 3.16 – 2.89 (m, 13H), 2.76 – 2.65 (m, 1H), 2.64 – 2.46 (m, 3H), 2.28 – 2.15 (m, 6H), 2.10 – 1.70 (m, 16H), 1.58 – 1.42 (m, 5H), 1.33 – 1.22 (m, 24H). ^{13}C NMR (101 MHz, CD_3OD) δ 175.26, 174.67, 173.07, 161.35, 153.43, 143.47, 139.63, 136.79, 133.98, 131.94, 130.86, 129.92, 129.20, 124.10, 122.51, 121.76, 119.84, 117.73, 116.17, 66.16, 61.99, 61.31, 57.54, 55.76, 54.48, 52.53, 51.35, 45.99, 41.08, 40.39, 36.34, 35.78, 35.58, 32.72, 31.83, 31.60, 31.26, 31.22, 30.45, 30.37, 30.29, 29.98, 27.94, 27.41, 27.28, 25.18, 24.32, 23.48, 22.68. HRMS (ESI-MS): m/z $[M+2H]^{2+}$ calculated for $C_{73}H_{111}ClN_{14}O_7^{2+}$: 665.4219, found 665.4227; $C_{73}H_{109}ClN_{14}O_7$*5 TFA (1900.33).

N^1-(12-(4-((4-((4-(7-Chloro-8-hydroxy-3-methyl-2,3,4,5-tetrahydro-1*H*-benzo[*d*]azepin-1-yl)phenyl)amino)-4-oxobutanamido)methyl)-1*H*-1,2,3-triazol-1-yl)dodecyl)-N^5-(12-(4-((1-(4-(3-(piperidin-1-yl)propoxy)benzyl)piperidine-4-carboxamido)methyl)-1*H*-1,2,3-triazol-1-yl)dodecyl)glutaramide pentahydrotrifluoroacetate (47)

The product was synthesized following general procedure E from **27** (44 mg, 0.11 mmol, 1.1 eq), **18** (50 mg, 0.11 mmol, 1.1 eq), **39b** (55 mg, 0.10 mmol, 1 eq), ascorbic acid (5.3 mg, 0.03 mmol, 0.3 eq) and Cu_2SO_4*5 H_2O (2.5 mg, 0.01 mmol, 0.1 eq). A white solid was obtained (27 mg, 14 %). RP-HPLC: > 97 %, (t_R = 12.93 min, k = 3.68). ^{1}H NMR (400 MHz, CD_3OD) δ 7.90 – 7.79 (m, 2H), 7.69 – 7.53 (m, 2H), 7.46 – 7.37 (m, 2H), 7.29 – 7.06 (m, 3H), 7.05 – 6.99 (m, 2H), 6.70 – 6.15 (d*, *J* = 218.2 Hz, 1H), 4.64 – 4.50 (m, 1H), 4.46 – 4.39 (m, 4H), 4.37 – 4.22 (m, 6H), 4.12 (t, *J* = 5.7 Hz, 2H), 3.88 – 3.48 (m, 7H), 3.33 – 3.26 (m, 7H), 3.13 (t, *J* = 7.1 Hz, 4H), 3.08 – 2.92 (m, 9H), 2.75 – 2.67 (m, 2H), 2.64 – 2.45 (m, 3H), 2.28 – 2.16 (m, 6H), 2.06 – 1.72 (m, 15H), 1.59 – 1.44 (m, 5H), 1.32 – 1.23 (m, 32H). ^{13}C NMR (101 MHz, CD_3OD) δ 180.15, 180.05, 179.46, 177.85, 167.26, 166.12, 158.20, 150.69, 148.30, 144.41, 141.61, 138.77, 136.74, 135.68, 134.72, 128.90, 127.30, 126.55, 124.61, 122.53, 120.96, 70.96, 66.80, 66.09, 62.34, 60.55, 59.25, 57.31, 56.15, 50.76, 45.87, 45.20, 41.12, 40.58, 40.40, 37.53, 36.61, 36.41, 36.07, 36.03, 35.41, 35.37, 35.35, 35.30, 35.28, 35.17, 34.82, 32.78, 32.23, 32.07, 29.95, 29.10, 28.26, 27.48. HRMS (ESI-MS): m/z $[M+2H]^{2+}$ calculated for $C_{77}H_{119}ClN_{14}O_7^{2+}$: 693.4532, found 693.4544; $C_{77}H_{117}ClN_{14}O_7$*5 TFA (1956.44).

General procedure F

A pharmacophore (1 eq), a spacer (5 eq), ascorbic acid (0.3 eq), $CuSO_4$*5 H_2O (0.1 eq) and Tris[(1-benzyl-1*H*-1,2,3-triazol-4-yl)methyl]amine (TBTA; 0.2 eq) were dissolved in a mixture of *tert*-BuOH and water (1:1) and the reaction was stirred at room temperature for 24 h. The solvent was removed under reduced pressure and the crude product was purified by preparative HPLC or flash chromatography.

N^1-(2-(2-(2-Azidoethoxy)ethoxy)ethyl)-N^5-(2-(2-(2-(4-((1-(4-(3-(piperidin-1-yl)propoxy)benzyl)piperidine-4-carboxamido)methyl)-1*H*-1,2,3-triazol-1-yl)ethoxy)ethoxy)ethyl)glutaramide (48a)

The product was synthesized following general procedure F from **27** (100 mg, 0.25 mmol, 1 eq), **36a** (0.56 g, 1.25 mmol, 5 eq), $CuSO_4$*5 H_2O (7.5 mg, 0.03 mmol, 0.1 eq), ascorbic acid (14 mg, 0.08 mmol, 0.3 eq) and TBTA (27 mg, 0.05 mmol, 0.2 eq). The crude product was purified by flash chromatography (DCM/MeOH 9:1). A sticky oil was obtained (70 mg, 32 %). R_f= 0.18 (DCM/MeOH + 1 % NH_3 9:1). ^{1}H NMR (300 MHz, CD_3OD) δ 7.87 (s, 1H), 7.29 – 7.15 (m, 2H), 6.93 – 6.77 (m, 2H), 4.58 – 4.49 (m, 2H), 4.41 (s, 2H), 4.01 (t, *J* = 6.1 Hz, 2H), 3.91 – 3.81 (m, 2H), 3.69 – 3.42 (m, 16H), 3.39 – 3.27 (m, 6H), 2.92 (d, *J* = 11.6 Hz, 2H), 2.72 – 2.46 (m, 6H), 2.21 (t, *J* = 7.4 Hz, 5H), 2.09 – 1.95 (m, 4H), 1.94 – 1.82 (m, 2H), 1.81 – 1.58 (m, 8H), 1.56 – 1.43 (m, 2H). ^{13}C NMR (75 MHz, CD_3OD) δ 176.25, 174.00, 173.98, 158.36, 144.89, 130.68, 128.81, 123.50, 113.89, 70.12, 70.04, 69.95, 69.84, 69.73, 69.21, 69.16, 69.00, 65.74, 62.04, 55.62, 53.97, 52.40, 50.33, 49.96, 42.39, 38.95, 34.78, 34.75, 34.21, 28.07, 25.72, 24.78, 23.43, 21.89. HRMS (ESI-MS): m/z $[M+H]^+$ calculated for $C_{41}H_{68}N_{11}O_8^+$: 842.5247, found 842.5250; $C_{41}H_{67}N_{11}O_8$ (842.06).

N^1-(2-(2-(2-(2-Azidoethoxy)ethoxy)ethoxy)ethyl)-N^5-(2-(2-(2-(2-(4-((1-(4-(3-(piperidin-1-yl)propoxy)benzyl)piperidine-4-carboxamido)methyl)-1*H*-1,2,3-triazol-1-yl)ethoxy)ethoxy)ethoxy)ethyl)glutaramide (48b)

The product was synthesized following general procedure F from **27** (100 mg, 0.25 mmol, 1 eq), **36b** (0.67 g, 1.25 mmol, 5 eq), $CuSO_4$*5 H_2O (7.5 mg, 0.03 mmol, 0.1 eq), ascorbic acid (14 mg, 0.08 mmol, 0.3 eq) and TBTA (27 mg, 0.05 mmol, 0.2 eq). The crude product was purified by flash chromatography (DCM/MeOH 9:1). A sticky oil was obtained (70 mg, 30 %). R_f= 0.17 (DCM/MeOH+1 % NH_3 9:1). ^{1}H NMR (300 MHz, CD_3OD) δ 7.91 (s, 1H), 7.51 – 7.36 (m, 2H), 7.06 – 6.90 (m, 2H), 4.55 (t, *J* = 5.0 Hz, 2H), 4.42 (s, 2H), 4.18 – 4.08 (m, 4H), 3.87 (t, *J* = 5.0 Hz, 2H), 3.68 – 3.49 (m, 24H), 3.46 – 3.19 (m, 11H), 2.98 – 2.84 (m, 2H), 2.58 – 2.43 (m, 1H), 2.29 – 2.18 (m, 6H), 2.08 – 1.78 (m, 11H), 1.75 – 1.55 (m, 2H). ^{13}C NMR (75 MHz, CD_3OD) δ 174.36, 174.00, 168.44, 159.63, 132.43, 123.59, 122.29, 114.60, 70.22, 70.20, 70.12, 70.09, 70.05, 70.00, 69.87, 69.71, 69.12, 68.96, 64.89, 59.67, 54.31, 52.90, 50.74, 50.36, 49.99, 38.96, 38.93, 34.73, 34.21, 25.81, 23.74, 22.88, 21.85, 21.45. HRMS (ESI-MS): m/z $[M+H]^+$ calculated for $C_{45}H_{76}N_{11}O_{10}^+$: 930.5771, found 930.5769; $C_{45}H_{75}N_{11}O_{10}$ (930.16).

General Procedure G

The first pharmacophore which is coupled to the linker (1 eq), the second pharmacophore (1.2 eq), ascorbic acid (0.3 eq), $CuSO_4$*5 H_2O (0.1 eq) and Tris[(1-benzyl-1*H*-1,2,3-triazol-4-yl)methyl]amine (TBTA; 0.2 eq) were dissolved in a mixture of *tert*-BuOH and water (1:1) and the reaction was stirred

at room temperature for 24 h. The solvent was removed under reduced pressure and the crude product was purified by preparative HPLC.

N^1-(2-(2-(2-(4-((5-(*N*-(4-(7,8-Dihydroxy-3-methyl-2,3,4,5-tetrahydro-1*H*-benzo[*d*]azepin-1-yl)phenyl)sulfamoyl)pentanamido)methyl)-1*H*-1,2,3-triazol-1-yl)ethoxy)ethoxy)ethyl)-N^5-(2-(2-(2-(4-((1-(4-(3-(piperidin-1-yl)propoxy)benzyl)piperidine-4-carboxamido)methyl)-1*H*-1,2,3-triazol-1-yl)ethoxy)ethoxy)ethyl)glutaramide pentahydrotrifluoroacetate (49)

The product was synthesized following general procedure G from **48a** (25 mg, 30 µmol, 1 eq), **22** (25 mg, 36 µmol, 1.2 eq), $CuSO_4$*5 H_2O (1.0 mg, 3 µmol, 0.1 eq), ascorbic acid (2 mg, 9 µmol, 0.3 eq) and TBTA (3 mg, 6 µmol, 0.2 eq). The crude product was stirred for 2 h in 10 % aq. TFA, before purification by preparative HPLC. A yellow oil was obtained (39 mg, 69 %). RP-HPLC: > 96 %, (t_R = 7.52 min, k = 1.34). ^{1}H NMR (400 MHz, CD_3OD) δ 7.87 (s, 2H), 7.44 – 7.39 (m, 2H), 7.33 – 7.22 (m, 2H), 7.21 – 7.10 (m, 2H), 7.06 – 6.99 (m, 2H), 6.74 – 6.66 (m, 1H), 6.56 – 6.00 (d*, *J* = 220.9 Hz, 1H), 4.55 – 4.37 (m, 10H), 4.24 (s, 2H), 4.12 (t, *J* = 5.7 Hz, 2H), 3.88 – 3.69 (m, 6H), 3.65 – 3.40 (m, 19H), 3.15 – 2.87 (m, 12H), 2.61 – 2.44 (m, 1H), 2.28 – 2.17 (m, 9H), 2.08 – 1.64 (m, 17H), 1.60 – 1.46 (m, 1H). ^{13}C NMR (101 MHz, CD_3OD) δ 174.06, 159.93, 144.75, 144.45, 143.75, 137.41, 132.61, 129.22, 128.61, 123.53, 120.37, 116.75, 115.45, 114.76, 70.02, 69.81, 69.11, 68.93, 64.76, 59.90, 54.37, 53.07, 51.14, 50.56, 49.97, 44.56, 44.35, 39.68, 38.94, 34.77, 34.68, 34.26, 25.92, 23.83, 23.77, 22.92, 22.77, 21.88, 21.29. HRMS (ESI-MS): m/z $[M+H]^+$ calculated for $C_{66}H_{99}ClN_{14}O_{13}S^+$: 1327.7231, found 1327.7226; $C_{66}H_{98}ClN_{14}O_{13}S$*5 TFA (1897.77).

N^1-(2-(2-(2-(2-(4-((5-(*N*-(4-(7,8-Dihydroxy-3-methyl-2,3,4,5-tetrahydro-1*H*-benzo[*d*]azepin-1-yl)phenyl)sulfamoyl)pentanamido)methyl)-1*H*-1,2,3-triazol-1-yl)ethoxy)ethoxy)ethoxy)ethyl)-N^5-(2-(2-(2-(2-(4-((1-(4-(3-(piperidin-1-yl)propoxy)benzyl)piperidine-4-carboxamido)methyl)-1*H*-1,2,3-triazol-1-yl)ethoxy)ethoxy)ethoxy)ethyl)glutaramide pentahydrotrifluoroacetate (50)

The product was synthesized following general procedure G from **48b** (28 mg, 30 µmol, 1 eq), **22** (25 mg, 36 µmol, 1.2 eq), $CuSO_4$*5 H_2O (1.0 mg, 3 µmol, 0.1 eq), ascorbic acid (2 mg, 9 µmol, 0.3 eq) and TBTA (3 mg, 6 µmol, 0.2 eq). The crude product was stirred for 2 h in 10 % aq. TFA, before purification by preparative HPLC. A yellow oil was obtained (7 mg, 12 %). RP-HPLC: > 96 %, (t_R = 7.69 min, k = 1.40). ^{1}H NMR (600 MHz, CD_3OD) δ 7.93 – 7.86 (m, 2H), 7.44 – 7.40 (m, 2H), 7.33 – 7.22 (m, 2H), 7.21 – 7.10 (m, 2H), 7.04 – 7.01 (m, 2H), 6.73 – 6.67 (m, 1H), 6.56 – 6.01 (d*, *J* = 331.0 Hz, 1H), 4.57 – 4.37 (m, 10H), 4.24 (s, 2H), 4.12 (t, *J* = 5.8 Hz, 2H), 3.90 – 3.70 (m, 6H), 3.60 – 3.49 (m, 28H), 3.16 – 2.85 (m, 12H), 2.54 – 2.48 (m, 1H), 2.27 – 2.16 (m, 9H), 2.07 – 1.67 (m, 16H), 1.58 – 1.47 (m, 1H). ^{13}C NMR (151 MHz, CD_3OD) δ 175.42, 175.29, 175.20, 161.34, 146.04, 145.69, 145.17, 138.85, 138.14, 134.01, 130.60, 129.92, 124.99, 124.97, 122.53, 121.91, 121.75, 116.16, 71.52, 71.51, 71.44, 71.40,

71.38, 71.25, 70.49, 70.33, 66.16, 62.28, 61.29, 55.77, 54.52, 54.47, 40.33, 36.14, 35.64, 27.31, 25.22, 25.18, 24.33, 24.17, 23.23, 22.68. HRMS (ESI-MS): m/z $[M+H]^+$ calculated for $C_{70}H_{107}ClN_{14}O_{15}S^+$: 1415.7756, found 1415.7754; $C_{70}H_{106}ClN_{14}O_{15}S$*5 TFA (1985.88).

N^1-(2-(2-(2-(4-((4-((1*H*-Imidazol-5-yl)methyl)piperidin-1-yl)methyl)-1*H*-1,2,3-triazol-1-yl)ethoxy)ethoxy)ethyl)-N^5-(2-(2-(2-azidoethoxy)ethoxy)ethyl)glutaramide trihydrotrifluoroacetate (51)

The product was synthesized following general procedure F from **30** (30 mg, 0.15 mmol, 1 eq), **36a** (0.33 g, 0.75 mmol, 5 eq), $CuSO_4$*5 H_2O (5.0 mg, 0.02 mmol, 0.1 eq), ascorbic acid (9 mg, 0.05 mmol, 0.3 eq) and TBTA (15 mg, 0.03 mmol, 0.2 eq). The crude product was purified by preparative HPLC. A yellow oil was obtained (75 mg, 53 %). ^{1}H NMR (400 MHz, CD_3OD) δ 8.84 (s, 1H), 8.25 (s, 1H), 7.40 (s, 1H), 4.68 – 4.62 (m, 2H), 4.49 (s, 2H), 3.97 – 3.89 (m, 2H), 3.73 – 3.55 (m, 16H), 3.52 (t, *J* = 5.6 Hz, 2H), 3.45 – 3.29 (m, 4H), 3.20 – 2.97 (m, 2H), 2.86 – 2.69 (m, 2H), 2.25 (t, *J* = 7.5 Hz, 4H), 2.04 – 1.86 (m, 5H), 1.71 – 1.48 (m, 2H). ^{13}C NMR (101 MHz, CD_3OD) δ 174.13, 174.07, 133.60, 131.25, 127.26, 116.53, 70.09, 69.97, 69.93, 69.82, 69.69, 69.17, 69.12, 68.75, 52.01, 50.34, 50.14, 38.96, 38.90, 34.82, 34.73, 33.01, 28.55, 21.89. HRMS (ESI-MS): m/z $[M+H]^+$ calculated for $C_{29}H_{50}N_{11}O_6^+$: 648.3940, found 648.3948; $C_{29}H_{49}N_{11}O_6$*3 TFA (989.85).

N^1-(2-(2-(2-Azidoethoxy)ethoxy)ethyl)-N^5-(2-(2-(2-(4-((5-(*N*-(4-(7-chloro-8-hydroxy-3-methyl-2,3,4,5-tetrahydro-1*H*-benzo[*d*]azepin-1-yl)phenyl)sulfamoyl)pentanamido)methyl)-1*H*-1,2,3-triazol-1-yl)ethoxy)ethoxy)ethyl)glutaramide (52a)

The product was synthesized following general procedure F from **20** (50 mg, 99 µmol, 1 eq), **36a** (0.22 g, 0.50 mmol, 5 eq), $CuSO_4$*5 H_2O (2.5 mg, 10 µmol, 0.1 eq), ascorbic acid (5.3 mg, 30 µmol, 0.3 eq) and TBTA (10.6 mg, 20 µmol, 0.2 eq). The crude product was purified by flash chromatography (DCM/MeOH 9:1). A sticky oil was obtained (30 mg, 32 %). R_f= 0.4 (DCM/MeOH 8:2). ^{1}H NMR (400 MHz, CD_3OD) δ 7.89 (s, 1H), 7.46 – 7.27 (m, 2H), 7.26 – 7.13 (m, 3H), 6.39 – 6.16 (m, 1H), 4.62 – 4.47 (m, 4H), 4.42 (s, 2H), 3.98 – 3.81 (m, 3H), 3.70 – 3.45 (m, 18H), 3.39 – 3.31 (m, 6H), 3.17 – 3.01 (m, 3H), 2.28 – 2.15 (m, 6H), 1.92 – 1.61 (m, 6H). ^{13}C NMR (101 MHz, CD_3OD) δ 174.06, 173.87, 151.95, 144.74, 137.54, 130.74, 130.11, 129.13, 123.56, 120.44, 70.10, 70.03, 69.94, 69.87, 69.83, 69.71, 69.19, 69.14, 68.96, 50.57, 50.34, 49.99, 44.79, 38.95, 34.78, 34.75, 34.26, 30.81, 23.85, 22.77. HRMS (ESI-MS): m/z $[M+H]^+$ calculated for $C_{42}H_{63}ClN_{11}O_{10}S^+$: 948.4163, found 948.4163; $C_{42}H_{62}ClN_{11}O_{10}S$ (948.54).

N^1-(2-(2-(2-(2-Azidoethoxy)ethoxy)ethoxy)ethyl)-N^5-(2-(2-(2-(2-(4-((5-(*N*-(4-(7-chloro-8-hydroxy-3-methyl-2,3,4,5-tetrahydro-1*H*-benzo[*d*]azepin-1-yl)phenyl)sulfamoyl)pentanamido)methyl)-1*H*-1,2,3-triazol-1-yl)ethoxy)ethoxy)ethoxy)ethyl)glutaramide (52b)

The product was synthesized following general procedure F from **20** (50 mg, 99 µmol, 1 eq), **36b** (0.26 g, 0.50 mmol, 5 eq), $CuSO_4$*5 H_2O (2.5 mg, 10 µmol, 0.1 eq), ascorbic acid (5.3 mg, 30 µmol, 0.3 eq) and TBTA (10.6 mg, 20 µmol, 0.2 eq). The crude product was purified by flash chromatography (DCM/MeOH 9:1). A sticky oil was obtained (28 mg, 27 %). R_f= 0.4 (DCM/MeOH 8:2). ^{1}H NMR (400 MHz, CD_3OD) δ 7.88 (s, 1H), 7.38 – 7.22 (m, 2H), 7.20 – 7.13 (m, 2H), 7.10 (s, 1H), 6.21 (s, 1H), 4.54 (t, *J* = 5.1 Hz, 2H), 4.41 (s, 2H), 4.31 (d, *J* = 8.6 Hz, 1H), 3.86 (t, *J* = 5.0 Hz, 2H), 3.68 – 3.49 (m, 22H), 3.39 – 3.31 (m, 6H), 3.24 – 2.74 (m, 7H), 2.50 – 2.40 (m, 3H), 2.28 – 2.11 (m, 6H), 2.00 – 1.53 (m, 7H). ^{13}C NMR (101 MHz, CD_3OD) δ 174.04, 173.85, 151.19, 144.64, 138.09, 136.82, 132.30, 130.27, 129.11, 123.57, 120.43, 117.54, 116.41, 70.22, 70.19, 70.13, 70.10, 70.06, 70.02, 69.87, 69.70, 69.16, 69.13, 68.96, 62.22, 56.87, 50.43, 50.37, 50.01, 45.95, 38.96, 34.73, 34.25, 33.22, 23.86, 22.79, 21.82. HRMS (ESI-MS): m/z $[M+H]^+$ calculated for $C_{46}H_{71}ClN_{11}O_{12}S^+$: 1036.4687, found 1036.4683; $C_{46}H_{70}ClN_{11}O_{12}S$ (1036.64).

N^1-(2-(2-(2-(4-((4-((1*H*-Imidazol-5-yl)methyl)piperidin-1-yl)methyl)-1*H*-1,2,3-triazol-1-yl)ethoxy)ethoxy)ethyl)-N^5-(2-(2-(2-(4-((5-(*N*-(4-(7-chloro-8-hydroxy-3-methyl-2,3,4,5-tetrahydro-1*H*-benzo[*d*]azepin-1-yl)phenyl)sulfamoyl)pentanamido)methyl)-1*H*-1,2,3-triazol-1-yl)ethoxy)ethoxy)ethyl)glutaramide pentahydrotrifluoroacetate (53)

The product was synthesized following general procedure G from **51** (30 mg, 30 µmol, 1 eq), **20** (15 mg, 30 µmol, 1 eq), $CuSO_4$*5 H_2O (1.0 mg, 3 µmol, 0.1 eq), ascorbic acid (2 mg, 9 µmol, 0.3 eq) and TBTA (3 mg, 6 µmol, 0.2 eq). A yellow oil was obtained (6 mg, 12 %). RP-HPLC: > 98 %, (t_R = 7.80 min, k = 1.43). ^{1}H NMR (600 MHz, CD_3OD) δ 8.82 (d, *J* = 1.2 Hz, 1H), 8.20 (s, 1H), 7.88 (s, 1H), 7.37 (s, 1H), 7.34 – 7.28 (m, 2H), 7.26 – 7.18 (m, 3H), 6.70 – 6.17 (d*, *J* = 304.2 Hz, 1H), 4.62 – 4.60 (m, 2H), 4.56 – 4.52 (m, 3H), 4.45 (s, 2H), 4.40 (s, 2H), 3.91 – 3.84 (m, 5H), 3.63 – 3.53 (m, 12H), 3.49 – 3.45 (m, 5H), 3.33 – 3.31 (m, 3H), 3.16 – 3.01 (m, 6H), 2.97 (s, 3H), 2.80 – 2.68 (m, 2H), 2.26 – 2.18 (m, 7H), 1.99 – 1.93 (m, 3H), 1.88 – 1.83 (m, 2H), 1.82 – 1.76 (m, 2H), 1.74 – 1.68 (m, 2H), 1.63 – 1.43 (m, 2H). ^{13}C NMR (151 MHz, CD_3OD) δ 175.50, 175.44, 175.25, 163.00, 162.78, 146.13, 139.13, 137.58, 135.05, 132.65, 130.93, 128.58, 124.91, 121.79, 117.92, 71.42, 71.35, 71.21, 70.52, 70.33, 70.13, 40.34, 40.29, 36.22, 36.13, 36.08, 35.64, 25.23, 24.16, 23.30. HRMS (ESI-MS): m/z $[M+H]^+$ calculated for $C_{54}H_{80}ClN_{14}O_{10}S^+$: 1151.5586, found 1151.5591; $C_{54}H_{79}ClN_{14}O_{10}S$*5 TFA (1721.94).

N^1-(2-(2-(2-(2-(4-((4-((1*H*-Imidazol-5-yl)methyl)piperidin-1-yl)methyl)-1*H*-1,2,3-triazol-1-yl)ethoxy)ethoxy)ethoxy)ethyl)-N^5-(2-(2-(2-(2-(4-((5-(*N*-(4-(7-chloro-8-hydroxy-3-methyl-2,3,4,5-tetrahydro-1*H*-benzo[*d*]azepin-1-yl)phenyl)sulfamoyl)pentanamido)methyl)-1*H*-1,2,3-triazol-1-yl)ethoxy)ethoxy)ethoxy)ethyl)glutaramide pentahydrotrifluoroacetate (54)

The product was synthesized following general procedure E from **30** (24 mg, 118 µmol, 1.1 eq), **20** (59 mg, 118 µmol, 1.1 eq), **36b** (57 mg, 107 µmol, 1 eq), ascorbic acid (6 mg, 36 µmol, 0.3 eq) and Cu_2SO_4*5 H_2O (3 mg, 12 µmol, 0.1 eq). A white solid was obtained (6 mg, 3 %). RP-HPLC: > 98 %, (t_R = 8.42 min, k = 1.62). ^{1}H NMR (600 MHz, D_2O) δ 8.48 (s, 1H), 8.14 (s, 1H), 7.74 (s, 1H), 7.26 – 6.99 (m, 6H), 6.69 - 6.05 (d*, *J* = 384.9 Hz, 1H), 4.56 – 4.53 (m, 2H), 4.45 – 4.41 (m, 4H), 4.33 (s, 2H), 4.25 (s, 2H), 3.88 – 3.84 (m, 2H), 3.83 – 3.76 (m, 4H), 3.70 – 3.35 (m, 28H), 3.31 – 2.95 (m, 9H), 2.96 – 2.87 (m, 4H), 2.87 – 2.81 (m, 4H), 2.67 – 2.54 (m, 3H), 2.18 – 2.09 (m, 7H), 1.91 – 1.31 (m, 11H). HRMS (ESI-MS): m/z $[M+2H]^{2+}$ calculated for $C_{58}H_{89}ClN_{14}O_{12}S^{2+}$: 620.3091, found 620.3100; $C_{58}H_{87}ClN_{14}O_{12}S$*5 TFA (1810.05).

N^1-(2-(2-(2-(4-(4-(4-((1*H*-Imidazol-5-yl)methyl)piperidin-1-yl)butyl)-1*H*-1,2,3-triazol-1-yl)ethoxy)ethoxy)ethyl)-N^5-(2-(2-(2-(4-((5-(*N*-(4-(7-chloro-8-hydroxy-3-methyl-2,3,4,5-tetrahydro-1*H*-benzo[*d*]azepin-1-yl)phenyl)sulfamoyl)pentanamido)methyl)-1*H*-1,2,3-triazol-1-yl)ethoxy)ethoxy)ethyl)glutaramide pentahydrotrifluoroacetate (55)

The product was synthesized following general procedure G from **52a** (30 mg, 31.60 µmol, 1 eq), **32** (9.30 mg, 37.90 µmol, 1.2 eq), ascorbic acid (1.69 mg, 9.60 µmol, 0.3 eq) Cu_2SO_4*5 H_2O (0.80 mg, 3.20 µmol, 0.1 eq), and TBTA (3 mg, 6 µmol, 0.2 eq). A white solid was obtained (9 mg, 16 %). RP-HPLC: > 99 %, (t_R = 7.81 min, k = 1.43). ^{1}H NMR (600 MHz, CD_3OD) δ 7.87 (s, 1H), 7.76 (s, 1H), 7.55 – 7.53 (m, 1H), 7.28 – 7.22 (m, 2H), 7.17 – 7.13 (m, 2H), 7.07 (s, 1H), 6.76 (s, 1H), 6.19 (s, 1H), 4.54 – 4.50 (m, 4H), 4.40 (s, 2H), 4.24 (d, *J* = 8.8 Hz, 1H), 3.86 (t, *J* = 5.3 Hz, 4H), 3.59 – 3.56 (m, 4H), 3.55 – 3.53 (m, 4H), 3.49 – 3.45 (m, 4H), 3.34 – 3.31 (m, 2H), 3.12 – 2.88 (m, 7H), 2.84 – 2.68 (m, 4H), 2.50 (d, *J* = 6.8 Hz, 2H), 2.46 – 2.40 (m, 2H), 2.36 (s, 3H), 2.34 – 2.15 (m, 8H), 2.10 – 2.01 (m, 2H), 1.90 – 1.84 (m, 2H), 1.83 – 1.77 (m, 2H), 1.75 – 1.53 (m, 10H), 1.32 – 1.25 (m, 2H). ^{13}C NMR (151 MHz, CD_3OD) δ 175.44, 175.27, 152.56, 148.69, 146.14, 145.47, 140.20, 138.07, 135.76, 134.20, 131.52, 130.49, 124.93, 123.98, 121.82, 118.74, 117.79, 71.44, 71.24, 71.23, 70.55, 70.54, 70.45, 70.35, 64.14, 59.48, 58.49, 54.71, 51.76, 51.36, 51.27, 47.68, 40.35, 40.34, 37.17, 36.17, 36.10, 35.66, 35.32, 32.40, 28.55, 26.77, 26.08, 25.27, 24.19, 23.29. HRMS (ESI-MS): m/z $[M+2H]^{2+}$ calculated for $C_{57}H_{87}ClN_{14}O_{10}S^{2+}$: 597.3064, found 597.3071; $C_{57}H_{85}ClN_{14}O_{10}S$*5 TFA (1764.02).

N^1-(2-(2-(2-(2-(4-(4-(4-((1*H*-Imidazol-5-yl)methyl)piperidin-1-yl)butyl)-1*H*-1,2,3-triazol-1-yl)ethoxy)ethoxy)ethoxy)ethyl)-N^5-(2-(2-(2-(2-(4-((5-(*N*-(4-(7-chloro-8-hydroxy-3-methyl-2,3,4,5-tetrahydro-1*H*-benzo[*d*]azepin-1-yl)phenyl)sulfamoyl)pentanamido)methyl)-1*H*-1,2,3-triazol-1-yl)ethoxy)ethoxy)ethoxy)ethyl)glutaramide pentahydrotrifluoroacetate (56)

The product was synthesized following general procedure G from **52b** (28 mg, 27.00 µmol, 1 eq), **32** (7.90 mg, 32.40 µmol, 1.2 eq), ascorbic acid (1.69 mg, 8.1 µmol, 0.3 eq) Cu_2SO_4*5 H_2O (0.67 mg, 2.70 µmol, 0.1 eq), and TBTA (2.87 mg, 5.40 µmol, 0.2 eq). A white solid was obtained (6 mg, 12 %). RP-HPLC: > 99 %, (t_R = 8.05 min, k = 1.51). ^{1}H NMR (600 MHz, CD_3OD) δ 7.89 (s, 1H), 7.78 (s, 1H), 7.56 – 7.54 (m, 1H), 7.28 – 7.24 (m, 2H), 7.18 – 7.14 (m, 2H), 7.08 (s, 1H), 6.76 (s, 1H), 6.20 (s, 1H), 4.56 – 4.50 (m, 4H), 4.41 (s, 2H), 4.25 (d, *J* = 8.8 Hz, 1H), 3.87 (t, *J* = 5.1 Hz, 4H), 3.62 – 3.55 (m, 16H), 3.52 (t, *J* = 5.6 Hz, 4H), 3.35 – 3.32 (m, 4H), 3.17 – 2.86 (m, 7H), 2.85 – 2.67 (m, 4H), 2.55 – 2.48 (m, 2H), 2.46 – 2.39 (m, 2H), 2.39 – 2.35 (m, 3H), 2.25 – 2.18 (m, 6H), 2.10 – 2.00 (m, 2H), 1.90 – 1.78 (m, 4H), 1.75 – 1.54 (m, 9H), 1.34 – 1.26 (m, 3H). ^{13}C NMR (151 MHz, CD_3OD) δ 175.41, 175.25, 152.56, 148.67, 146.04, 145.48, 140.20, 138.08, 135.76, 134.20, 131.52, 130.50, 124.97, 124.00, 121.82, 118.73, 117.79, 71.55, 71.49, 71.48, 71.43, 71.28, 71.27, 70.54, 70.52, 70.44, 70.36, 64.15, 59.54, 58.49, 54.73, 51.76, 51.41, 51.31, 40.35, 37.23, 36.14, 36.10, 35.65, 35.33, 32.46, 28.58, 26.84, 26.11, 25.27, 24.20, 23.24. HRMS (ESI-MS): m/z $[M+H]^+$ calculated for $C_{61}H_{94}ClN_{14}O_{12}S^+$: 1281.6579, found 1281.6573; $C_{61}H_{93}ClN_{14}O_{12}S$*5 TFA (1850.62).

***N*-(Prop-2-yn-1-yl)acetamide (57)**

Acetyl chloride (1.80 g, 23.40 mmol, 1.3 eq) was dissolved in DCM and added to a solution of propargylamine (1.00 g, 18.00 mmol, 1 eq) and Et_3N (2.70 g, 27.00 mmol, 1.5 eq) in DCM. The reaction was stirred at room temperature overnight. After the solvent was evaporated the crude product was purified by column chromatography (DCM/MeOH 95:5). A white solid was obtained (1.4 g, 80 %). R_f = 0.82 (DCM/MeOH 9:1). ^{1}H NMR (300 MHz, $CDCl_3$) δ 5.87 (s, 1H), 4.04 (dd, *J* = 5.3, 2.6 Hz, 2H), 2.23 (t, *J* = 2.6 Hz, 1H), 2.00 (s, 3H). ^{13}C NMR (75 MHz, $CDCl_3$) δ 169.78, 79.53, 71.58, 29.28, 23.03. HRMS (EI-MS): m/z $[M+H^{\cdot+}]$ calculated for $C_5H_7NO^{\cdot+}$: 97.05222, found 97.05218; C_5H_7NO (97.12).

N^1-(2-(2-(2-(4-(Acetamidomethyl)-1*H*-1,2,3-triazol-1-yl)ethoxy)ethoxy)ethyl)-N^5-(2-(2-(2-azidoethoxy)ethoxy)ethyl)glutaramide (58)

The product was synthesized following general procedure F from **57** (100 mg, 1.03 mmol, 1 eq), **36a** (2.29 g, 5.15 mmol, 5 eq), $CuSO_4$*5 H_2O (7.5 mg, 0.03 mmol, 0.1 eq), ascorbic acid (14 mg, 0.08 mmol, 0.3 eq) and TBTA (27 mg, 0.05 mmol, 0.2 eq). The crude product was purified by flash chromatography (DCM/MeOH 9:1). A pale red solid was obtained (0.46 g, 83 %). R_f = 0.40 (DCM/MeOH 9:1). ^{1}H NMR (300 MHz, $CDCl_3$) δ 7.67 (s, 1H), 7.14 (t, *J* = 5.9 Hz, 1H), 6.77 (t, *J* = 5.6 Hz, 1H), 6.52 (t, *J* =

5.5 Hz, 1H), 4.51 – 4.37 (m, 4H), 3.86 – 3.76 (m, 2H), 3.62 – 3.49 (m, 12H), 3.47 – 3.42 (m, 2H), 3.40 – 3.30 (m, 6H), 2.23 – 2.09 (m, 4H), 1.97 – 1.81 (m, 5H). ^{13}C NMR (75 MHz, $CDCl_3$) δ 172.97, 172.86, 170.52, 144.94, 123.43, 70.49, 70.45, 70.18, 70.07, 70.04, 69.78, 69.72, 69.21, 50.59, 50.16, 39.24, 39.17, 35.22, 34.92, 23.02, 22.00. HRMS (ESI-MS): m/z $[M+H]^+$ calculated for $C_{22}H_{40}N_9O_7^+$: 542.3045, found 542.3048; $C_{22}H_{39}N_9O_7$ (541.61).

N^1-(2-(2-(2-(4-(Acetamidomethyl)-1*H*-1,2,3-triazol-1-yl)ethoxy)ethoxy)ethyl)-N^5-(2-(2-(2-(4-((1-(4-(3-(piperidin-1-yl)propoxy)benzyl)piperidine-4-carboxamido)methyl)-1*H*-1,2,3-triazol-1-yl)ethoxy)ethoxy)ethyl)glutaramide tetrahydrotrifluoroacetate (59)

The product was synthesized following general procedure G from **58** (27 mg, 50.40 µmol, 1 eq), **27** (20 mg, 50.40 µmol, 1 eq), ascorbic acid (2.70 mg, 15.12 µmol, 0.3 eq) Cu_2SO_4*5 H_2O (1.30 mg, 5.04 µmol, 0.1 eq), and TBTA (5.30 mg, 10.08 µmol, 0.2 eq). A white solid was obtained (21 mg, 30 %). RP-HPLC: > 99 %, (t_R = 6.62 min, k = 1.06). ^{1}H NMR (400 MHz, CD_3OD) δ 7.98 (s, 2H), 7.48 – 7.38 (m, 2H), 7.07 – 6.98 (m, 2H), 4.71 – 4.32 (m, 8H), 4.30 – 4.21 (m, 2H), 4.12 (t, *J* = 5.7 Hz, 2H), 3.92 – 3.82 (m, 4H), 3.61 – 3.44 (m, 16H), 3.37 – 3.31 (m, 4H), 3.05 – 2.89 (m, 4H), 2.36 – 2.11 (m, 7H), 2.10 – 1.67 (m, 15H), 1.61 – 1.45 (m, 1H). ^{13}C NMR (101 MHz, CD_3OD) δ 174.07, 159.92, 132.60, 121.13, 114.75, 70.02, 69.82, 69.81, 69.13, 68.92, 64.76, 59.89, 54.36, 53.06, 51.13, 50.10, 38.93, 34.76, 25.92, 23.77, 22.92, 21.88, 21.29. HRMS (ESI-MS): m/z $[M+H]^+$ calculated for $C_{46}H_{75}N_{12}O_9^+$: 939.5774, found 939.5780; $C_{46}H_{74}N_{12}O_9$*4 TFA (1395.27).

N^1-(2-(2-(2-(4-(4-(4-((1*H*-Imidazol-5-yl)methyl)piperidin-1-yl)butyl)-1*H*-1,2,3-triazol-1-yl)ethoxy)ethoxy)ethyl)-N^5-(2-(2-(2-(4-(acetamidomethyl)-1*H*-1,2,3-triazol-1-yl)ethoxy)ethoxy)ethyl)glutaramide tetrahydrotrifluoroacetate (60)

The product was synthesized following general procedure G from **58** (10.80 mg, 20.00 µmol, 1 eq), **30** (5 mg, 20.00 µmol, 1 eq), ascorbic acid (1.06 mg, 6.00 µmol, 0.3 eq) Cu_2SO_4*5 H_2O (0.50 mg, 2.00 µmol, 0.1 eq), and TBTA (2.12 mg, 4.00 µmol, 0.2 eq). A white solid was obtained (6 mg, 24 %). RP-HPLC: > 99 %, (t_R = 5.95 min, k = 0.85). ^{1}H NMR (600 MHz, CD_3OD) δ 8.85 – 8.82 (m, 1H), 7.89 (s, 1H), 7.80 (s, 1H), 7.41 – 7.36 (m, 1H), 4.55 – 4.52 (m, 4H), 4.41 (s, 2H), 3.88 – 3.85 (m, 4H), 3.61 – 3.54 (m, 11H), 3.49 – 3.46 (m, 4H), 3.33 – 3.31 (m, 2H), 3.16 – 3.09 (m, 2H), 2.99 – 2.88 (m, 2H), 2.77 – 2.73 (m, 4H), 2.22 – 2.18 (m, 4H), 2.01 – 1.68 (m, 14H), 1.59 – 1.47 (m, 2H). ^{13}C NMR (151 MHz, CD_3OD) δ 175.46, 175.43, 173.17, 147.97, 146.13, 135.07, 132.63, 124.94, 124.19, 117.93, 71.44, 71.43, 71.24, 71.21, 70.54, 70.47, 70.37, 57.93, 53.75, 51.37, 51.31, 40.35, 40.34, 36.17, 36.14, 35.69, 34.65, 31.14, 30.18, 27.44, 25.49, 24.60, 23.29, 22.51. HRMS (ESI-MS): m/z $[M+H]^+$ calculated for $C_{37}H_{63}N_{12}O_7^+$: 787.4937, found 787.4947; $C_{37}H_{62}N_{12}O_7$*4 TFA (1243.07).

N^1-(2-(2-(2-(4-(Acetamidomethyl)-1*H*-1,2,3-triazol-1-yl)ethoxy)ethoxy)ethyl)-N^5-(2-(2-(2-(4-((5-(*N*-(4-(7-chloro-8-hydroxy-3-methyl-2,3,4,5-tetrahydro-1*H*-benzo[*d*]azepin-1-yl)phenyl)sulfamoyl)pentanamido)methyl)-1*H*-1,2,3-triazol-1-yl)ethoxy)ethoxy)ethyl)glutaramide trihydrotrifluoroacetate (61)

The product was synthesized following general procedure G from **58** (27 mg, 50.40 µmol, 1 eq), **20** (25 mg, 50.40 µmol, 1 eq), ascorbic acid (2.70 mg, 15.12 µmol, 0.3 eq) Cu_2SO_4*5 H_2O (1.30 mg, 5.04 µmol, 0.1 eq), and TBTA (5.30 mg, 10.08 µmol, 0.2 eq). A white solid was obtained (15 mg, 21 %). RP-HPLC: > 99 %, (t_R = 9.14 min, k = 1.85). ^{1}H NMR (400 MHz, CD_3OD) δ 7.91 – 7.82 (m, 2H), 7.36 – 7.16 (m, 5H), 6.70 – 6.16 (d*, *J* = 214.9 Hz 1H), 4.66 – 4.44 (m, 6H), 4.43 – 4.39 (m, 4H), 3.93 – 3.69 (m, 6H), 3.64 – 3.50 (m, 10H), 3.49 – 3.45 (m, 4H), 3.34 – 3.31 (m, 2H), 3.18 – 3.01 (m, 4H), 2.98 (s, 3H), 2.25 – 2.17 (m, 6H), 1.98 – 1.63 (m, 10H). ^{13}C NMR (101 MHz, CD_3OD) δ 174.05, 173.82, 171.75, 161.79, 144.70, 137.71, 129.53, 129.25, 123.54, 120.38, 116.17, 70.02, 69.82, 69.13, 68.96, 68.93, 56.10, 50.61, 49.97, 38.93, 34.76, 34.67, 34.30, 34.25, 23.82, 22.77, 21.87, 21.12. HRMS (ESI-MS): m/z $[M+H]^+$ calculated for $C_{47}H_{70}ClN_{12}O_{11}S^+$: 1045.4691, found 1045.4707; $C_{47}H_{69}ClN_{12}O_{11}S$*3 TFA (1387.72).

N^1-(2-(2-(2-(4-(Acetamidomethyl)-1*H*-1,2,3-triazol-1-yl)ethoxy)ethoxy)ethyl)-N^5-(2-(2-(2-(4-((5-(*N*-(4-(7,8-dihydroxy-3-methyl-2,3,4,5-tetrahydro-1*H*-benzo[*d*]azepin-1-yl)phenyl)sulfamoyl)pentanamido)methyl)-1*H*-1,2,3-triazol-1-yl)ethoxy)ethoxy)ethyl)glutaramide trihydrotrifluoroacetate (62)

The product was synthesized following general procedure G from **58** (16.10 mg, 29.70 µmol, 1 eq), **22** (25.40 mg, 35.60 µmol, 1.2 eq), ascorbic acid (2 mg, 8.90 µmol, 0.3 eq) Cu_2SO_4*5 H_2O (1 mg, 3.00 µmol, 0.1 eq), and TBTA (3.18 mg, 6.00 µmol, 0.2 eq). A white solid was obtained (8 mg, 20 %). RP-HPLC: > 99 %, (t_R = 7.94 min, k = 1.47). ^{1}H NMR (600 MHz, CD_3OD) δ 7.91 – 7.85 (m, 2H), 7.34 – 7.22 (m, 2H), 7.22 – 7.10 (m, 2H), 6.73 – 6.66 (d*, J = 331.6 Hz, 1H), 6.01 (s, 1H), 4.55 – 4.52 (m, 4H), 4.51 – 4.42 (m, 1H), 4.41 – 4.37 (m, 4H), 3.88 – 3.82 (m, 5H), 3.76 – 3.70 (m, 1H), 3.61 – 3.50 (m, 10H), 3.48 – 3.40 (m, 5H), 3.32 – 3.31 (m, 2H), 3.17 – 2.86 (m, 8H), 2.25 – 2.18 (m, 6H), 1.95 (s, 3H), 1.88 – 1.83 (m, 2H), 1.82 – 1.75 (m, 2H), 1.74 – 1.66 (m, 2H). ^{13}C NMR (151 MHz, CD_3OD) δ 175.48, 175.22, 173.18, 146.10, 146.00, 145.27, 145.22, 138.91, 138.84, 138.09, 134.20, 130.58, 129.92, 129.83, 124.96, 121.92, 121.75, 119.02, 118.82, 118.13, 116.84, 71.43, 71.23, 71.21, 70.54, 70.37, 70.34, 62.29, 60.76, 57.84, 51.98, 51.38, 51.37, 45.96, 45.86, 40.34, 36.17, 36.15, 36.06, 35.70, 35.64, 32.33, 25.21, 24.18, 23.28, 22.51. HRMS (ESI-MS): m/z $[M+H]^+$ calculated for $C_{47}H_{71}N_{12}O_{12}S^+$: 1027.5030, found 1027.5038; $C_{47}H_{70}N_{12}O_{12}S$*3 TFA (1369.28).

_N_-(4-(7-Chloro-8-hydroxy-3-methyl-2,3,4,5-tetrahydro-1_H_-benzo[_d_]azepin-1-yl)phenyl)methanesulfonamide hydrotrifluoroacetate(63)[176]

Methanesulfonyl chloride (13.2 µl, 0.17 mmol, 1.2 eq) was added to a solution of **13** (64 mg, 0.14 mmol, 1 eq) and NEt_3 (39.5 µl, 0.28 mmol, 2 eq) in DCM and the reaction was stirred overnight. The organic phase was washed with saturated bicarbonate solution and brine, dried over Na_2SO_4 and the solvent was removed under reduced pressure. The crude product was dissolved in THF and TBAF (1 M in THF; 210 µl, 0.21 mmol, 1.5 eq) was added and the reaction was stirred at room temperature for 30 min. The solvent was removed under reduced pressure and the crude product was purified by preparative HPLC. A white solid was obtained (23 mg, 33 %). RP-HPLC: > 98 %, (t_R = 9.03 min, k = 1.81). ^{1}H NMR (400 MHz, CD_3OD) δ 7.45 – 7.07 (m, 5H), 6.43 (d*, *J* = 214.9 Hz, 1H), 4.67 – 4.49 (m, 1H), 3.93 – 3.31 (m, 4H), 3.24 – 2.94 (m, 8H). ^{13}C NMR (101 MHz, CD_3OD) δ 143.27, 139.18, 137.43, 132.00, 130.84, 130.60, 122.09, 119.90, 117.58, 61.95, 57.51, 45.93, 39.43, 31.80, 9.19. HRMS (ESI-MS): m/z $[M+H]^+$ calculated for $C_{18}H_{22}ClN_2O_3S^+$: 381.1034, found 381.1041; $C_{18}H_{21}ClN_2O_3S$*TFA (494.91).

_N_-(4-(7,8-Dihydroxy-3-methyl-2,3,4,5-tetrahydro-1_H_-benzo[_d_]azepin-1-yl)phenyl)methanesulfonamide hydrotrifluoroacetate(64)

Methanesulfonyl chloride (25.5 µl, 0.33 mmol, 1.1 eq) was added to a solution of **15** (154 mg, 0.30 mmol, 1 eq) and pyridine (72.6 µl, 0.90 mmol, 3 eq) in $CHCl_3$ and the reaction was stirred overnight. The organic phase was washed with saturated bicarbonate solution and brine, dried over Na_2SO_4 and the solvent was removed under reduced pressure. The crude product was dissolved in THF and TBAF (1 M in THF; 720 µl, 0.72 mmol, 2.4 eq) was added and the reaction was stirred at room temperature for 30 min. The solvent was removed under reduced pressure and the crude product was purified by preparative HPLC. A white solid was obtained (37 mg, 26 %). RP-HPLC: > 98 %, (t_R = 6.13 min, k = 0.91). ^{1}H NMR (400 MHz, D_2O) δ 7.27 – 7.21 (m, 1H), 7.19 – 7.12 (m, 2H), 7.09 – 7.03 (m, 1H), 6.73 (d, *J* = 8.3 Hz, 1H), 6.60 – 6.60 (d*, *J* = 241.0 Hz, 1H), 4.51 – 4.37 (m, 1H), 4.17 – 3.70 (m, 1H), 3.65 – 3.35 (m, 2H), 3.21 – 2.89 (m, 5H), 2.87 – 2.67 (m, 4H). HRMS (ESI-MS): m/z $[M+H]^+$ calculated for $C_{18}H_{23}N_2O_4S^+$: 363.1373, found 363.1374; $C_{18}H_{22}N_2O_4S$*TFA (476.47).

8-Chloro-3-methyl-5-(4-nitrophenyl)-2,3,4,5-tetrahydro-1_H_-benzo[_d_]azepin-7-yl acetate (65)

11a (0.13 g, 0.35 mmol, 1 eq) and NEt_3 (98.4 µl, 0.70 mmol, 2 eq) were dissolved in DCM and cooled to 0 °C. Acetylchloride (37.8 µl, 0.53 mmol, 1.5 eq) was added slowly and the reaction was stirred at room temperature overnight. The solvent was removed under reduced pressure and the product was purified by column chromatography (98:2 DCM/MeOH). An orange solid was obtained (0.10 g, 77 %). R_f = 0.48 (98:2 DCM/MeOH + 1 % NH_3). ^{1}H NMR (300 MHz, $CDCl_3$) δ 8.23 – 8.17 (m, 2H), 7.37 – 7.30 (m, 2H), 7.24 (s, 1H), 6.41 (s, 1H), 4.37 (d, *J* = 7.5 Hz, 1H), 3.09 – 2.91 (m, 3H), 2.81 – 2.73

(m, 2H), 2.54 – 2.45 (m, 1H), 2.40 (s, 3H), 2.27 (s, 3H). ^{13}C NMR (75 MHz, $CDCl_3$) δ 168.52, 149.57, 146.74, 145.15, 142.67, 140.44, 131.40, 129.21, 124.78, 123.98, 123.52, 61.67, 56.66, 49.53, 47.77, 35.57, 20.62. HRMS (ESI-MS): m/z $[M+H]^+$ calculated for $C_{19}H_{20}ClN_2O_4^+$: 375.1106, found 375.1113; $C_{19}H_{19}ClN_2O_4$ (374.82).

5-(4-Aminophenyl)-8-chloro-3-methyl-2,3,4,5-tetrahydro-1*H*-benzo[*d*]azepin-7-yl acetate (66)

65 (0.14 g, 0.37 mmol, 1 eq) and Pd/C (10 %) (0.01 g, 10 wt %) were dissolved in a mixture of THF and MeOH (1:1) and the reaction was stirred overnight under H_2-atmosphere. The reaction was filtered over celite and the solvent was removed under reduced pressure. The crude product was dried *in vacuo.* A yellow solid was obtained (0.12 g, 95 %). The product was used without further purification. HRMS (ESI-MS): m/z $[M+H]^+$ calculated for $C_{19}H_{22}ClN_2O_2^+$: 345.1364, found 345.1370; $C_{19}H_{21}ClN_2O_2$ (344.84).

3-(1,3-Dioxoisoindolin-2-yl)propane-1-sulfonyl chloride (67)[187]

Thiourea (0.38 g, 5.00 mmol, 1 eq) and 3-bromopropylphthalimide (1.34 g, 5.00 mmol, 1 eq) were dissolved in EtOH and heated to reflux for 1 h. The solvent was removed under reduced pressure and the resulting white solid was added to a suspension of *N*-chlorosuccinimide in MeCN and 2 N aq. HCl (1.62 ml, 3.24 mmol, 0.65 eq) at 10 °C. The reaction was stirred at 10 °C for 30 min and the reaction was quenched with water. The aqueous phase was extracted with diethyl ether. The organic phase was washed with brine, dried over Na_2SO_4 and the solvent was removed under reduced pressure. The crude product was purified by column chromatography (3:1 PE/EtOAc). A white solid was obtained (1.29 g, 89 %). R_f = 0.80 (1:1 PE/EtOAc). ^{1}H NMR (300 MHz, $CDCl_3$) δ 7.90 – 7.82 (m, 2H), 7.79 – 7.72 (m, 2H), 3.89 (t, *J* = 6.5 Hz, 2H), 3.80 – 3.70 (m, 2H), 2.51 – 2.35 (m, 2H). ^{13}C NMR (75 MHz, $CDCl_3$) δ 168.20, 134.43, 131.74, 123.61, 62.86, 35.55, 24.13. HRMS (ESI-MS): m/z $[M+H]^+$ calculated for $C_{11}H_{11}ClNO_4S^+$: 288.0092, found 288.0092; $C_{11}H_{10}ClNO_4S$ (287.71).

8-Chloro-5-(4-((3-(1,3-dioxoisoindolin-2-yl)propyl)sulfonamido)phenyl)-3-methyl-2,3,4,5-tetrahydro-1*H*-benzo[*d*]azepin-7-yl acetate (68)

66 (0.10 g, 0.29 mmol, 1 eq) and pyridine (70 µl, 0.87 mmol, 3 eq) were dissolved in chloroform. **67** (0.13 g, 0.44 mmol, 1.5 eq) was added and the reaction was stirred at 50 °C overnight. The solvent was removed under reduced pressure and the crude product was purified by column chromatography (95:5 DCM/MeOH + 1 % NH_3). A yellow oil was obtained (0.11 g, 62 %). R_f = 0.30 (95:5 DCM/MeOH + 1 % NH_3). ^{1}H NMR (400 MHz, $CDCl_3$) δ 7.81 – 7.76 (m, 2H), 7.70 – 7.66 (m, 2H), 7.21 – 7.13 (m, 3H), 7.07 – 7.00 (m, 2H), 6.38 (s, 1H), 4.23 (d, *J* = 8.0 Hz, 1H), 3.84 – 3.72 (m, 2H), 3.26 – 2.68 (m, 7H), 2.48 – 2.33 (m, 4H), 2.29 – 2.13 (m, 5H). ^{13}C NMR (101 MHz, $CDCl_3$) δ 168.68, 168.26, 145.04, 144.16, 140.21,

135.37, 134.21, 131.83, 130.89, 129.52, 124.15, 123.43, 123.19, 121.27, 62.38, 56.50, 53.48, 49.17, 48.48, 47.46, 36.19, 23.24, 20.65. HRMS (ESI-MS): m/z $[M+H]^+$ calculated for $C_{30}H_{31}ClN_3O_6S^+$: 596.1617, found 596.1623; $C_{30}H_{30}ClN_3O_6S$ (596.10).

3-Amino-*N*-(4-(7-chloro-8-hydroxy-3-methyl-2,3,4,5-tetrahydro-1*H*-benzo[*d*]azepin-1-yl)phenyl)propane-1-sulfonamide dihydrotrifluoroacetate (69)

Hydrazine hydrate (83 µl, 1.70 mmol, 10 eq) was added to a solution of **68** (0.1 g, 0.17 mmol, 1 eq) in EtOH and the reaction was heated to reflux overnight. The reaction was cooled to 0 °C and the white solid was filtered off. The solvent of the filtrate was evaporated under reduced pressure and the crude product was purified by preparative HPLC. A sticky solid was obtained (25 mg, 23 %). ^{1}H NMR (400 MHz, CD_3OD) δ 7.46 – 7.09 (m, 5H), 6.82 – 5.80 (m, 1H), 4.57 (d, *J* = 9.7 Hz, 1H), 3.93 – 3.30 (m, 4H), 3.28 – 3.18 (m, 2H), 3.14 – 2.87 (m, 7H), 2.26 – 2.06 (m, 2H). HRMS (ESI-MS): m/z $[M+H]^+$ calculated for $C_{20}H_{27}ClN_3O_3S^+$: 424.1456, found 424.1459; $C_{20}H_{26}ClN_3O_3S$*2 TFA (652.00).

Oxybis(ethane-2,1-diyl) dimethanesulfonate (70)[268]

The product was synthesized following general procedure A from diethylene glycol (5.00 g, 47.12 mmol, 1 eq), methanesulfonyl chloride (7.29 ml, 94.24 mmol, 2 eq) and NEt_3 (16.42 ml, 117.80 mmol, 2.5 eq). A yellow oil was obtained (11.87 g, 96 %). R_f = 0.80 (DCM/MeOH 98:2). ^{1}H NMR (300 MHz, $CDCl_3$) δ 4.37 – 4.28 (m, 4H), 3.78 – 3.68 (m, 4H), 3.02 (s, 6H). ^{13}C NMR (75 MHz, $CDCl_3$) δ 69.05, 68.97, 37.57. HRMS (ESI-MS): m/z $[M+H]^+$ calculated for $C_6H_{15}O_7S_2^+$: 263.0254, found 263.0254; $C_6H_{14}O_7S_2$ (262.29).

1-Azido-2-(2-azidoethoxy)ethane (71)[269]

The product was synthesized following general procedure B from **70** (5.00 g, 19.06 mmol, 1 eq) and sodium azide (4.96 g, 76.24 mmol, 4 eq). A yellow oil was obtained (2.91 g, 98 %). R_f = 0.35 (DCM/MeOH 98:2). ^{1}H NMR (300 MHz, $CDCl_3$) δ 3.72 – 3.64 (m, 4H), 3.45 – 3.36 (m, 4H). ^{13}C NMR (75 MHz, $CDCl_3$) δ 70.10, 50.76. HRMS (APCI-MS): m/z $[M+H]^+$ calculated for $C_4H_9N_6O^+$: 157.0832, found 157.0835; $C_4H_8N_6O$ (156.15).

2-(2-Azidoethoxy)ethan-1-amine (72)[270]

The product was synthesized following general procedure C from **71** (3.36 g, 21.52 mmol, 1 eq) and triphenylphosphine (5.64 g, 21.52 mmol, 1 eq). A clear oil was obtained (1.68 g, 60 %). R_f = 0.38 (DCM/MeOH + 1 % NH_3 95:5). ^{1}H NMR (300 MHz, $CDCl_3$) δ 3.88 (s, 2H), 3.64 – 3.59 (m, 2H), 3.58 – 3.52 (m, 2H), 3.39 – 3.31 (m, 2H), 2.92 (t, *J* = 5.1 Hz, 2H). ^{13}C NMR (75 MHz, $CDCl_3$) δ 71.47, 69.90, 50.71,

41.06. HRMS (ESI-MS): m/z $[M+H]^+$ calculated for $C_4H_{11}N_4O^+$: 131.0927, found 131.0927; $C_4H_{10}N_4O$ (130.15).

General procedure H

20 (1 eq) and the linker (1.5 eq) were dissolved in DCM/MeOH (4:1). $CuSO_4$*5 H_2O (0.1 eq) and ascorbic acid (0.3 eq) were added and the reaction was stirred at room temperature for 72 h. The solvents were removed under reduced pressure and the crude product was purified by HPLC.

5-(*N*-(4-(7-Chloro-8-hydroxy-3-methyl-2,3,4,5-tetrahydro-1*H*-benzo[*d*]azepin-1-yl)phenyl)sulfamoyl)-*N*-((1-(2-(2-hydroxyethoxy)ethyl)-1*H*-1,2,3-triazol-4-yl)methyl)pentanamide trihydrotrifluoroacetate (73a)

The product was synthesized following general procedure H from **20** (25 mg, 49.60 µmol, 1 eq), **72** (9.7 mg, 74.40 µmol, 1.5 eq), $CuSO_4$*5 H_2O (1.2 mg, 4.96 µmol, 0.1 eq) and ascorbic acid (2.62 mg, 14.88 µmol, 0.3 eq). A white solid was obtained (7 mg, 14 %). RP-HPLC: > 97 %, (t_R = 7.34 min, k = 1.29). ^{1}H NMR (400 MHz, CD_3OD) δ 7.89 (s, 1H), 7.41 – 7.09 (m, 5H), 6.16 (s, 1H), 4.65 – 4.48 (m, 3H), 4.39 (s, 2H), 3.95 – 3.32 (m, 8H), 3.18 – 2.99 (m, 6H), 2.96 (s, 3H), 2.24 (t, *J* = 6.9 Hz, 2H), 1.87 – 1.61 (m, 4H). HRMS (ESI-MS): m/z $[M+H]^+$ calculated for $C_{29}H_{41}ClN_7O_5S^+$: 634.2573, found 634.2578; $C_{29}H_{40}ClN_7O_5S$*3 TFA (976.26).

***N*-((1-(2-(2-(2-Aminoethoxy)ethoxy)ethyl)-1*H*-1,2,3-triazol-4-yl)methyl)-5-(*N*-(4-(7-chloro-8-hydroxy-3-methyl-2,3,4,5-tetrahydro-1*H*-benzo[*d*]azepin-1-yl)phenyl)sulfamoyl)pentanamide trihydrotrifluoroacetate(73b)**

The product was synthesized following general procedure H from **20** (25 mg, 49.60 µmol, 1 eq), **36a** (13 mg, 74.40 µmol, 1.5 eq), $CuSO_4$*5 H_2O (1.2 mg, 4.96 µmol, 0.1 eq) and ascorbic acid (2.62 mg, 14.88 µmol, 0.3 eq). A white solid was obtained (4 mg, 8 %). RP-HPLC: > 97 %, (t_R = 7.50 min, k = 1.34). ^{1}H NMR (400 MHz, CD_3OD) δ 7.87 (s, 1H), 7.42 – 7.08 (m, 5H), 6.16 (s, 1H), 4.63 – 4.46 (m, 3H), 4.40 (s, 2H), 3.95 – 3.44 (m, 12H), 3.19 – 2.98 (m, 6H), 2.96 (s, 3H), 2.24 (t, *J* = 6.9 Hz, 2H), 1.85 – 1.66 (m, 4H). HRMS (ESI-MS): m/z $[M+H]^+$ calculated for $C_{31}H_{45}ClN_7O_6S^+$: 678.2835, found 678.2841; $C_{31}H_{44}ClN_6O_7S$*3 TFA (1020.32).

General procedure I

The primary amine (1.5 eq) was dissolved in DMF (30 µL). NEt_3 (10 eq) and the fluorescent dye NHS-ester (1 eq) in DMF (60 µL) were added and the reaction was shaken for 2.5 h in the dark at room temperature. The reaction was quenched with 10 % aqueous TFA (20 µL), and the crude product was purified by preparative HPLC.

5-((3-(*N*-(4-(7-Chloro-8-hydroxy-3-methyl-2,3,4,5-tetrahydro-1*H*-benzo[*d*]azepin-1-yl)phenyl)sulfamoyl)propyl)carbamoyl)-2-(6-(dimethylamino)-3-(dimethyliminio)-3*H*-xanthen-9-yl)benzoate hydrotrifluoroacetate (74)

The product was synthesized following general procedure I from **69** (1.86 mg, 2.85 µmol, 1.5 eq), NEt_3 (2.53 µl, 19 µmol, 10 eq) and 5- carboxytetramethylrhodamine succinimidyl ester (5-TAMRA NHS ester) (1.00 mg, 1.90 µmol, 1 eq). A pink solid was obtained (1.6 mg, 89 %). RP-HPLC: > 97 %, (t_R = 11.27 min, k = 2.51). HRMS (ESI-MS): m/z $[M+H]^+$ calculated for $C_{45}H_{47}ClN_5O_7S^+$: 836.2879, found 836.2884; $C_{45}H_{46}ClN_5O_7S$*TFA (950.28).

Triammonium 2-((*E*)-3-((*E*)-1-(6-((3-(*N*-(4-(7-chloro-8-hydroxy-3-methyl-2,3,4,5-tetrahydro-1*H*-benzo[*d*]azepin-1-yl)phenyl)sulfamoyl)propyl)amino)-6-oxohexyl)-3-methyl-5-sulfonato-3-(3-sulfonatopropyl)indolin-2-ylidene)prop-1-en-1-yl)-1-(2-methoxyethyl)-3-methyl-3-(3-sulfonatopropyl)-3*H*-indol-1-ium-5-sulfonate (75)

The product was synthesized following general procedure I from **69** (0.25 mg, 0.38 µmol, 2 eq) NEt_3 (0.25 µl, 1.90 µmol, 10 eq) and DY-549P1-NHS-ester (0.2 mg, 0.19 µmol, 1 eq). A pink solid was obtained (0.1 mg, 39 %). RP-HPLC: > 97 %, (t_R 3.59 min, k = 0.21). HRMS (ESI-MS): m/z $[M-2H]^{2-}$ calculated for $C_{56}H_{70}ClN_5O_{17}S^{2-}$: 639.6535, found 639.6545; $C_{56}H_{72}ClN_5O_{17}S$*3 NH_3 (1335.06).

2-(3,6-Bis(dimethylamino)xanthylium-9-yl)-5-((2-(2-(4-((5-(*N*-(4-(7-chloro-8-hydroxy-3-methyl-2,3,4,5-tetrahydro-1*H*-benzo[*d*]azepin-1-yl)phenyl)sulfamoyl)pentanamido)methyl)-1*H*-1,2,3-triazol-1-yl)ethoxy)ethyl)carbamoyl)benzoate dihydrotrifluoroacetate(76)

The product was synthesized following general procedure I from **73a** (3.16 mg, 3.24 µmol, 1.5 eq), NEt_3 (3.04 µl, 21.60 µmol, 10 eq) and 5- carboxytetramethylrhodamine succinimidyl ester (5-TAMRA NHS ester) (1.14 mg, 2.16 µmol, 1 eq). A pink solid was obtained (1.4 mg, 51 %). RP-HPLC: > 98 %, (t_R = 10.69 min, k = 2.33). HRMS (ESI-MS): m/z $[M+H]^+$ calculated for $C_{54}H_{61}ClN_9O_9S^+$: 1046.3996, found 1046.3995; $C_{54}H_{60}ClN_9O_9S$*2 TFA (1274.68).

Triammonium 2-((*E*)-3-((*E*)-1-(6-((2-(2-(4-((5-(*N*-(4-(7-chloro-8-hydroxy-3-methyl-2,3,4,5-tetrahydro-1*H*-benzo[*d*]azepin-1-yl)phenyl)sulfamoyl)pentanamido)methyl)-1H-1,2,3-triazol-1-yl)ethoxy)ethyl)amino)-6-oxohexyl)-3-methyl-5-sulfonato-3-(3-sulfonatopropyl)indolin-2-ylidene)prop-1-en-1-yl)-1-(2-methoxyethyl)-3-methyl-3-(3-sulfonatopropyl)-3*H*-indol-1-ium-5-sulfonate (77)

The product was synthesized following general procedure I from **73a** (0.28 mg, 0.29 µmol, 1.5 eq), NEt_3 (0.27 µl, 1.90 µmol, 10 eq) and DY-549P1-NHS-ester (0.2 mg, 0.19 µmol, 1 eq). A pink solid was obtained (0.14 mg, 47 %). RP-HPLC: > 96 %, (t_R = 3.60 min, k = 0.12). HRMS (ESI-MS): m/z $[M-2H]^{2-}$ calculated for $C_{65}H_{84}ClN_9O_{19}S_5^{2-}$: 744.7093, found 744.7106; $C_{65}H_{86}ClN_9O_{19}S_5$*3 NH_3 (1544.29).

2-(3,6-Bis(dimethylamino)xanthylium-9-yl)-5-((2-(2-(2-(4-((5-(*N*-(4-(7-chloro-8-hydroxy-3-methyl-2,3,4,5-tetrahydro-1*H*-benzo[*d*]azepin-1-yl)phenyl)sulfamoyl)pentanamido)methyl)-1*H*-1,2,3-triazol-1-yl)ethoxy)ethoxy)ethyl)carbamoyl)benzoate dihydrotrifluoroacetate (78)

The product was synthesized following general procedure I from **73b** (2.64 mg, 2.59 µmol, 1.5 eq), NEt_3 (2.43 µl, 17.30 µmol, 10 eq) and 5- carboxytetramethylrhodamine succinimidyl ester (5-TAMRA NHS ester) (0.91 mg, 1.73 µmol, 1 eq). A pink solid was obtained (1.71 mg, 75 %). RP-HPLC: > 95 %, (t_R = 10.75 min, k = 2.35). HRMS (ESI-MS): m/z $[M+H]^+$ calculated for $C_{56}H_{65}ClN_9O_{10}S^+$: 1090.4258, found 1090.4258; $C_{56}H_{64}ClN_9O_{10}S$*2 TFA (1318.74).

Triammonium 2-((*E*)-3-((*E*)-1-(6-((2-(2-(2-(4-((5-(*N*-(4-(7-Chloro-8-hydroxy-3-methyl-2,3,4,5-tetrahydro-1*H*-benzo[*d*]azepin-1-yl)phenyl)sulfamoyl)pentanamido)methyl)-1*H*-1,2,3-triazol-1-yl)ethoxy)ethoxy)ethyl)amino)-6-oxohexyl)-3-methyl-5-sulfonato-3-(3-sulfonatopropyl)indolin-2-ylidene)prop-1-en-1-yl)-1-(2-methoxyethyl)-3-methyl-3-(3-sulfonatopropyl)-3*H*-indol-1-ium-5-sulfonate (79)

The product was synthesized following general procedure I from **73b** (0.30 mg, 0.29 µmol, 1.5 eq), NEt_3 (0.27 µl, 1.90 µmol, 10 eq) and DY-549P1-NHS-ester (0.2 mg, 0.19 µmol, 1 eq). A pink solid was obtained (0.14 mg, 47 %). RP-HPLC: > 95 %, (t_R = 3.78 min, k = 0.18). HRMS (ESI-MS): m/z $[M+2H]^{2+}$ calculated for $C_{67}H_{92}ClN_9O_{20}S_5^{2+}$: 768.7370, found 768.7386; $C_{67}H_{90}ClN_9O_{20}S_5$*3 NH_3 (1588.34).

***N*-(2-(2-Azidoethoxy)ethyl)-1-(4-(3-(piperidin-1-yl)propoxy)benzyl)piperidine-4-carboxamide (80)**

26 (100 mg, 0.23 mmol, 1 eq), 1-ethyl-3-(3-dimethylaminopropyl)carbodiimide (48 mg, 0.25 mmol, 1.1 eq), 1-hydroxybenzotriazole (34 mg, 0.25 mmol, 1.1 eq), and DIPEA (119 mg, 0.92 mmol, 4 eq) were dissolved in DMF/DCM (1/1) in a microwave vial and stirred at room temperature for 30 min. **35b** (50 mg, 0.23 mmol, 1 eq) was added and the reaction was stirred for 30 min at 100 °C in a microwave reactor (sealed vial). The solvent was removed under reduced pressure and the crude

product was purified by column chromatography (DCM/MeOH 95/5 + 0.1 % NH_3). A brown oil was obtained (85 mg, 65 %). R_f = 0.36 (DCM/MeOH/7N NH_3 in MeOH 90:9:1). ^{1}H NMR (300 MHz, $CDCl_3$) δ 7.20 – 7.12 (m, 2H), 6.84 – 6.75 (m, 2H), 6.08 (t, *J* = 5.2 Hz, 1H), 3.95 (t, *J* = 6.4 Hz, 2H), 3.66 – 3.55 (m, 10H), 3.53 – 3.46 (m, 2H), 3.37 (m, 6H), 2.87 (m, 2H), 2.50 – 2.30 (m, 6H), 2.13 – 1.84 (m, 5H), 1.73 (m, 4H), 1.56 (m, 4H), 1.47 – 1.33 (m, 2H). ^{13}C NMR (101 MHz, $CDCl_3$) δ 175.1, 158.1, 130.2, 130.2, 114.1, 70.7, 70.6, 70.6, 70.2, 70.1, 69.9, 66.5, 62.6, 56.0, 54.6, 53.0, 50.7, 43.4, 39.0, 28.9, 26.8, 25.9, 24.4. HRMS (ESI-MS): m/z [M+H$^+$] calculated for $C_{29}H_{49}N_6O_5^+$: 561.3759, found 561.3767; $C_{29}H_{48}N_6O_5$ (560.74).

_N_-(2-(2-Aminoethoxy)ethyl)-1-(4-(3-(piperidin-1-yl)propoxy)benzyl)piperidine-4-carboxamide trihydrotrifluoroacetate (81)

Triphenylphosphine (60 mg, 0.23 mmol, 1.5 eq) was added to a solution of **80** (85 mg, 0.15 mmol, 1 eq) in THF and the reaction was stirred for 4 h at 45 °C. Water was added and the reaction was stirred for another 2 h at the same temperature. THF was removed under reduced pressure and trifluoroacetic acid (200 µl) was added to the aqueous solution. The crude product was purified by preparative HPLC. A colorless oil was obtained for **81** (79 mg, 60 %). R_f = 0.22 (DCM/MeOH/7N NH_3 in MeOH 90:9:1). ^{1}H NMR (400 MHz, DMSO-d_6) δ 10.05-9.65 (m, 2H), 8.04 (t, *J* = 5.4 Hz, 1H), 7.90 (br s, 3H), 7.45-7.37 m, 2H), 7.06-6.93 (m, 2H), 4.27-4.26 (m, 2H), 4.06 (t, *J* = 5.9 Hz, 2H), 3.66 – 3.43 (m, 12H), 3.42 – 3.28 (m, 4H), 3.26 – 3.13 (m, 4H), 3.02 – 2.75 (m, 6H), 2.42 – 2.29 (m, 1H), 2.20 – 2.05 (m, 2H), 1.92 – 1.54 (m, 9H), 1.46-1.28 (m, 1H). ^{13}C NMR (101 MHz, DMSO-d_6) δ 173.3, 159.5, 159.0, 158.7, 133.3, 122.2, 118.5, 115.6, 115.1, 70.2, 70.1, 70.1, 70.0, 69.4, 67.1, 65.5, 59.0, 53.8, 52.6, 51.0, 39.0, 38.9, 26.2, 23.9, 23.0, 21.7. HRMS (ESI-MS): m/z [M+H$^+$] calculated for $C_{29}H_{51}N_4O_5^+$: 535.3854, found 535.3855; $C_{29}H_{50}N_4O_5$*3 TFA (876.81).

2-(6-(Dimethylamino)-3-(dimethyliminio)-3H-xanthen-9-yl)-5-((1-oxo-1-(1-(4-(3-(piperidin-1-yl)propoxy)benzyl)piperidin-4-yl)-5,8,11-trioxa-2-azatridecan-13-yl)carbamoyl)benzoate dihydrotrifluoroacetate (82)

81 (7.89 mg, 9 µmol, 1.5 eq) was dissolved in DMF (30µl). NEt_3 (6.68 mg, 66 µmol, 11 eq) and 5-Carboxytetramethylrhodamine succinimidyl ester (5-TAMRA NHS ester) (3.17 mg, 6 µmol, 1 eq) in DMF (60 µl) were added and the reaction was shaken for 2.5 h in the dark at room temperature. The reaction was quenched with 10 % aqueous TFA (20 µl) and the crude product was purified by preparative HPLC. A pink solid was obtained for **82** (5.7 mg, 4.9 µmol, 82 %). RP-HPLC: 99 %, (t_R = 9.84 min, *k* = 2.07). ^{1}H NMR (600 MHz, DMSO-d_6) δ 9.84 – 9.57 (m, 1H), 9.48 (br s, 1H), 8.95 (t, *J* = 5.5 Hz, 1H), 8.65 (br s, 1H), 8.28 (d, *J* = 7.9 Hz, 1H), 8.01 (t, *J* = 5.7 Hz, 1H), 7.54 (br s, 1H), 7.45-7.38 (m, 2H), 7.10-6.97 (m, 4H), 6.94 (br s, 2H), 6.56 (br s, 2H), 4.20 (s, 2H), 4.05 (t, *J* = 6.0 Hz, 2H), 3.64 – 3.43 (m,

18H), 3.29 – 3.04 (m, 16H), 2.94 – 2.82 (m, 4H), 2.39-2.32 (m, 1H), 2.18 – 2.08 (m, 2H), 2.04 – 1.60 (m, 9H), 1.45 – 1.31 (m, 1H). HRMS (ESI-MS): m/z [M+H$^+$] calculated for $C_{54}H_{71}N_6O_9^+$: 947.5277, found 947.5293; $C_{54}H_{70}N_6O_9$*2 TFA (1175.23).

6.2 Pharmacological experimental procedures

In the following chapter the cell biological methods and the procedures for the different assay systems are described.

6.2.1 Materials

Dulbecco's Modified Eagle's Medium (DMEM), L-glutamine, fetal calf serum (FCS), trypsin, and HEPES were purchased from Sigma-Aldrich (Munich, Germany). Leibovitz' L-15 medium (L-15), bovine serum albumin (BSA), and geneticin (G418) were purchased from Fisher Scientific (Nidderau, Germany). Stable transfected cell lines were used as previously published. Radioligands [^{3}H]UR-PI-294[203] and [^{3}H]UR-DE-257[206] were synthesized and characterized at the University of Regensburg. [^{3}H]SCH-23390, [^{3}H]*N*-methylspiperone and [^{3}H]mepyramine were purchased from Novandi Chemistry AB (Södertälje, Sweden). Furimazine (Nano-Glo© Live Cell Substrate) was purchased from Promega. All data were analyzed using GraphPad Prism 9 software (San Diego, CA, USA). Phosphate-buffered saline solution (PBS) was made with Millipore water containing 137 mM NaCl, 2.7 mM KCl, 10 mM Na_2HPO_4, and 1.8 mM KH_2PO_4 adjusted to a pH of 7.4. Binding buffer (BB) was prepared with Millipore water containing 50 mM Tris·HCl, 1mM EDTA, 5 mM $MgCl_2$, and 100 µg/ml bacitracin adjusted to a pH of 7.4.

6.2.2 Radioligand competition binding experiments at the dopamine receptors

Cell homogenates containing the $D_{2long}R$, D_3R, and $D_{4.4}R$ were kindly provided by Dr. Lisa Forster, University of Regensburg. Homogenates containing the D_1R and D_5R were kindly provided by Denise Mönnich, University of Regensburg. Radioligand binding experiments with cell homogenates were performed as previously described with minor modifications.[201,205] For radioligand competition binding assays homogenates were incubated in BB at a final concentration of 0.3 µg (D_1R), 0.3 µg ($D_{2long}R$), 0.7 µg (D_3R), 0.5-1.0 µg ($D_{4.4}R$), or 0.4 µg (D_5R) protein/well. [^{3}H]SCH-23390 (D_1R (K_d = 0.23 nM) and D_5R (K_d = 0.20 nM)) was added in final concentrations of 0.2, 0.4, 1.0 nM (D_1R) and 1.0 nM (D_5R). [^{3}H]*N*-methylspiperone ($D_{2long}R$ (K_d = 0.0149 nM), D_3R (K_d = 0.0258 nM), $D_{4.4}R$ (K_d = 0.078 nM)) was added in final concentrations of 0.05 nM ($D_{2long}R$, D_3R) or 0.1 nM ($D_{4.4}R$). Non labelled compounds were added in increasing concentrations for the displacement of the radioligands. After incubation of 60 min ($D_{2long}R$, D_3R, and $D_{4.4}R$) or 120 min (D_1R and D_5R) at room temperature, bound radioligand was separated from free radioligand through PEI-coated GF/C filters using a Brandel harvester (Brandel Inc., Unterföhring, Germany), Filters were transferred to (flexible) 1450-401 96-well sample plates (PerkinElmer, Rodgau, Germany) and after incubation with scintillation cocktail (Rotiszint eco plus, Carl

Roth, Karlsruhe, Germany) for at least 3 h, radioactivity was measured using a MicroBeta2 plate counter (PerkinElmer, Waltham, MA, USA). Competition binding curves were fitted using a four-parameter fit ("log(agonist) vs. response-variable slope"). Calculations of pK_i values with SEM and graphical presentations were conducted with GraphPad Prism 9 software (San Diego, CA, USA).

6.2.3 Radioligand competition binding experiments at the histamine receptors

Radioligand competition binding experiments were performed as previously described by Pockes et al. with minor modifications.[157,241] All experiments were carried out on whole HEK cells instead of Sf9 membranes. Generation of the stable HEK293-SP-FLAG-hH_1R and HEK293-SP-FLAG-hH_2R cell lines was conducted as described for the HEK293-SP-FLAG-hH_3R and HEK293-SP-FLAG-hH_4R.[202] Ligand dilutions of unlabeled compounds were prepared 10-fold concentrated in L-15 with 1 % BSA and 10 µL/well were transferred to a flat-bottom polypropylene 96-well microtiter plate (Greiner Bio-One, Frickenhausen, Germany), as well as 10 µL/well of the respective radioligand ([^{3}H]mepyramine (H_1R, K_d 4.5 nM); [^{3}H]UR-DE-257 (H_2R, K_d 66.9 nM); [^{3}H]UR-PI-294 (H_3R, K_d 5.0 nM; H_4R, K_d 5.1 nM)). The cells were adjusted to a density of 1.25 x 10^6 cells/mL and 80 µL of the cell suspension were added to each well (total volume of 100 µL). After incubation of 60 min at room temperature, bound radioligand was separated from free radioligand through PEI-coated GF/C filters using a Brandel harvester (Brandel Inc., Unterföhring, Germany), Filters were transferred to (flexible) 1450-401 96-well sample plates (PerkinElmer, Rodgau, Germany) and after incubation with scintillation cocktail (Rotiszint eco plus, Carl Roth, Karlsruhe, Germany) for at least 3 h, radioactivity was measured using a MicroBeta2 plate counter (PerkinElmer, Waltham, MA, USA). All data were analyzed using GraphPad Prism9 software (San Diego, CA, USA). The normalized competition binding curves were then fitted with a four-parameter logistic fit yielding pIC_{50}-values. These were transformed into pK_i-values using the Cheng-Prusoff equation.[271]

6.2.4 NanoBRET Binding Experiments at the H_3R

All NanoBRET experiments that are presented in chapter 4 were performed by Dr. Lukas Grätz, currently Karolinska Institutet, Stockholm, former University of Regensburg as previously published.[157] BRET-based Saturation/Real-Time Kinetic/Competition Binding at the NLuc-H_3R were performed as previously described by Bartole & Grätz et al. with minor modifications.[202] For the determination of nonspecific binding, clobenpropit (500-fold excess) was used instead of thioperamide. Dissociation was initiated by the addition of 250 nM clobenpropit (500-fold excess) instead of thioperamide. For competition binding experiments **82** was used in a concentration of 500 pM. Histamine

dihydrochloride (his) was from TCI Chemicals (Tokyo, Japan). Imetit dihydrobromide (imet), (R)-(-)-α-methylhistamine dihydrobromide (RAMH), (S)-(+)-α-methylhistamine dihydrobromide (SAMH), clobenpropit dihydrobromide (clob) and thioperamide maleate (thio) were from Tocris Bioscience (Ellisville, MO, USA). Z27743747 (Z-cmpd) was from Enamine Ltd. (Kyiv, Ukraine). Pitolisant hydrochloride (pito) was kindly provided by Prof. Dr. Katarzyna Kiec-Kononowicz (Jagiellonian University, Krakow). Significant differences between pK_d values were assessed using a two-tailed t-test ($p < 0.05$).

Competition binding experiments of novel bivalent ligands were performed in a similar way with minor modifications. Cells for the NanoBRET assays were detached from the cell culture flask 3 h prior to the assay by trypsinization and centrifuged (700 RPM, 5 min). The cell pellet was resuspended in L-15 medium supplemented with 5 % FCS and 10 mM HEPES. Cell density was adjusted to 1.25 million cells/ml and 70 µl of the cell solution was seeded in each well of a 96 well plate (Brand, Wertheim, Germany). The plates were incubated 3 h at 37 °C in a water-saturated atmosphere containing 5 % CO_2. Ligand dilutions of unlabeled compounds were prepared 10-fold concentrated in L-15 with 1 % BSA and 10 mM HEPES. Subsequently 10 µl of ligand solution, 10 µl fluorescent tracer solution (c (**82**) = 5 nM), and 10 µl of furimazine (dilution 1:1000) were added to each well. BRET signal was measured for at least 60 min. pK_i values were determined at 60 min after addition of the ligands. All data were analyzed using GraphPad Prism9 software (San Diego, CA, USA). The normalized competition binding curves were then fitted with a four-parameter logistic fit yielding pIC_{50}-values. These were transformed into pK_i-values using the Cheng-Prusoff equation.[271]

6.2.5 cAMP determination

cAMP determination experiments were performed as previously described with minor midfications.[272] HEK293T cells were grown in DMEM medium supplemented with 2 mM L-glutamine, 100 U/ml penicillin/streptomycin, MEM nonessential amino acids solution (1/100) and 5 % (v/v) heat inactivated fetal bovine serum (FBS) (all supplements from Invitrogen, Paisley, Scotland, UK). The transfection vectors for the hD_1R and hH_3R were used as previously described.[61] Cells were transiently transfected as previously described.[131,273] Cells growing in 35-mm diameter six-well plates were transiently transfected with cDNA by the ramified polyehtylenimine (PEI; Sigma-Aldrich) method. Cells were incubated 4 h with cDNAs (2 µg/ well), ramified PEI (5 ml/mg cDNA of 10 mM PEI) and 150 mM of NaCl in 1 ml serum-free medium. After 4 h the medium was changed to fresh supplemented DMEM as described above. 48 h after transfection the medium was changed to serum-free DMEM and the cells were incubated for 2 h at 37 °C in a humid atmosphere containing 5 % CO_2. Then, cells were detached, suspended in growing medium containing 50 µM zardaverine (phosphodiesterase inhibitor, TOCRIS)

and plated in 384-well microplates with a density of 2500 cells/well. Cells were pretreated 15 min with the antagonists (or vehicle) before adding the agonist. 15 min later 0.5 µM of forskolin or vehicle was added and another 15 min later the components of Lance Ultra cAMP kit (PerkinElmer, Waltham, MA, USA) as indicated by the manufacturer. After 1 h fluorescence at 665 nm was analyzed on a PHERAstar Flagship microplate reader equipped with an HTRF optical module (BMG Lab technologies, Offenburg, Germany). cAMP concentrations were determined using a calibration curve and converted into normalized dose-response curves, which were then fitted with a four-parameter logistic fit yielding pIC_{50}- or pEC_{50} values with GraphPad Prism9 software (San Diego, CA, USA).

6.2.6 *In vitro* neuroprotection experiments

Primary cortex cells of mouse embryonal fetuses were kindly prepared by Jaume Lillo and Iu Raich as previously published.[274]

Human amyloid β_{1-42} (Aβ) was dissolved in 2 µl DMSO by sonication. Ham's F-10 Nutrient Mix (Gibco) was added and the Aβ was stored in the fridge overnight.

10 days after seeding Aβ (final concentration = 500 nM) and the ligands (solutions in Neurobasal-A medium, Gibco) were added to the cells. The cells were incubated for additional seven days at 37 °C in a humid atmosphere containing 5 % CO_2. Determination of percentage of live cells was assessed after seven days by trypan blue staining using a countless II FL automated cell counter (Thermo Fisher Scientific, Waltham, MA, USA). Data was analyzed using Prism GraphPad 9.

6.2.7 Flow cytometry

Flow cytometric saturation binding experiments at the H_3 receptor were performed with a FACSCanto II flow cytometer (Becton Dickinson, Heidelberg, Germany) equipped with an argon laser (488 nm) and a red diode laser (640 and 635 nm) as described previously.[157] Fluorescence signals were recorded using the following instrument settings: excitation: 488 nm, emission: 585 ± 21 nm (PE channel). All samples were prepared and incubated in 1.5 ml cups (Eppendorf, Hamburg, Germany). Cells were seeded 5 to 6 days prior to the experiment in cell culture flasks. On the day of the experiment the cells were treated with trypsin/EDTA (0.05 %/0.02 %) (Sigma-Aldrich, Munich, Germany), detached and suspended in cell culture medium followed by centrifugation. The cells were resuspended in Leibovitz' L-15 medium (Fisher Scientific, Nidderau, Germany)) with 1 % BSA (in the following referred to as L-15 medium). The cell density was adjusted to 100 000 cells/ml. For the total binding experiments 2.5 µl of a solution of the fluorescent ligand (100-fold concentrated to final concentration) in L-15 medium and 2.5 µl of L-15 medium were added to 245 µl of the cell suspension. For the nonspecific binding

experiments 2.5 µl of solution of the fluorescent ligand (100-fold concentrated to final concentration) and 2.5 µl of a 1 mM solution of clobenpropit in L-15 medium were added to 245 µl of the cell suspension. UR-NR266 (**82**) was used at final concentrations of 0.02-10 nm. All samples were incubated at 22 °C in the dark under shaking for 1 h. All experiments were performed in duplicate.

6.2.8 Design of the BRET-based G_{i2} activity sensor and BRET measurements of ligand-induced G_{i2} activation

These experiments were performed by Dr. Hannes Schihada, currently University of Marburg, former Karolinska Institutet, Stockholm as described previously.[157] The G_{i2} BRET sensor was generated by fusing cpVenus N-terminally to $G_{\gamma 2}$ and inserting Nluc between C112 / E115 in $G_{\alpha i2}$, according to the design of a previous FRET-based G_{i2} sensor.[226] These subunits were then cloned into one polycistronic vector along with native $G_{\beta 1}$, separated by a T2A self-cleaving peptide sequence and an internal ribosome entry site (IRES) ($G_{\beta 1}$-T2A-cpVenus-$G_{\gamma 2}$-IRES-$G_{\alpha i2}$-Nluc). All constructs were cloned using established DNA restriction enzymes and ligases and verified by sequencing (Eurofins genomics).

For the BRET measurements, HEK293A cells were transiently transfected in suspension with wildtype H_3R and G_{i2} BRET sensor (1:1 plasmid ratio) using Lipofectamine 2000 (Thermofisher Scientific, Nidderau, Germany) (2 µl transfection reagent / µg total plasmid) and seeded onto poly-D-lysine-precoated, white 96-well plates (Greiner Bio-One, Frickenhausen, Germany) (30,000 cells / well). 48 hours after transfection, cells were washed with HBSS (Gibco/Life technologies, Carlsbad, USA) and incubated with a 1/1,000 stock solution of furimazine (Promega, Mannheim, Germany). Five minutes later, baseline BRET was recorded in three consecutive reads (4 minutes), 10-fold serial ligand dilutions or vehicle control were added, and the ligand-induced BRET ratio was recorded in 17 consecutive reads (36 minutes). For competition experiments, cells grown in 96-well plates were washed 48 hours after transfection as described above and incubated with the 1/1,000 stock solution of furimazine along with the indicated concentrations of compound **82** or ultrapure water (solvent control). After recording the basal BRET ratio, all wells pre-incubated with **82** were stimulated with 1 nM imetit. Wells pre-incubated with ultrapure water were treated with HBSS (vehicle control for imetit treatment). All experiments were conducted using a CLARIOstar plate reader (BMG Labtech, Ortenberg, Germany) recording Nluc and cpVenus emission intensities with 450/80 nm (Gain 3600) and 530/30 nm (Gain 4000) monochromator settings, respectively, and an integration time of 0.3 seconds. Raw BRET ratios were defined as acceptor emission / donor emission. The three BRET ratios prior ligand / vehicle addition were averaged and defined as $BRET_{basal}$. To quantify ligand-induced BRET changes, ΔBRET was calculated for each well and time point as a percent over basal ($[(BRET_{stim} - BRET_{basal})/BRET_{basal}] \times 100$). Subsequently, the average ΔBRET of vehicle-treated control wells was subtracted. Ligand

concentration response curves were generated based on vehicle-corrected ΔBRET measured as a mean of three subsequent reads, 23 minutes after ligand addition.

6.2.9 Off-target screening using the NanoBRET binding assay

These experiments were performed by Dr. Lukas Grätz, Karolinska Institutet, Stockholm (former University of Regensburg) and Dr. Laura J. Humphrys, University of Regensburg as described previously.[157] The Nluc construct of the mouse smoothened receptor[246] was kindly provided by Prof. Dr. Gunnar Schulte (Karolinska Institutet), the adenosine A_3 receptor[220] by Prof. Dr. Stephen J. Hill (University of Nottingham), the β_1 adrenoceptor by Dr. Ulrike Zabel (University of Würzburg), the muscarinic acetylcholine M_2 receptor[245] by Dr. Lukas Grätz (University of Regensburg) and the dopamine D_1 receptor by Denise Mönnich (University of Regensburg). All other constructs were made for these purposes by Dr. Lukas Grätz and Dr. Hannes Schihada. For the BRET-based off-target screening, HEK293T cells were transiently transfected in suspension with 1 µg of cDNA per mL of cell suspension (300,000 cells/mL). The receptors were the histamine H_3, β_1 adrenoceptor, cannabinoid receptor type 1 and 2, adenosine A_3, mouse smoothened, dopamine $D_{1/2long/3}$, muscarinic acetylcholine $M_{1/2/3/4/5}$ and angiotensin II type 1 receptor and were prepared by replacing the receptor sequence of the NLuc-A_3 construct. After 5 min incubation, the mixtures were combined and incubated at room temperature for a further 10min. HEK293T cells were suspended at 300,000 cells/mL in DMEM (10 % FCS) and 1 mL of cell suspension was added to each receptor/PEI mix. Seeding consisted of 100 µL cDNA/cell/PEI mixture per well on a poly-$_D$-lysine (mol wt 70,000-150,000, Sigma-Aldrich, Taufkirchen, Germany) coated white 96 well plate (cellGrade, Brand, Wertheim, Germany), with 4 wells per receptor construct. Cells were used 36 hours after transfection. Media was aspirated and washed with HBSS/0.5 % BSA, before being replaced with 90 µL HBSS/0.5 % BSA plus furimazine (1:1000 dilution) and incubated for 5 min at 37 °C. Bioluminescence and fluorescence were read on the Tecan GENics Pro, using the same parameters as the other BRET experiments at 37 °C. The baseline was read for 5 cycles, and the response post ligand addition for another 10 min. Buffer control and 200 nM **12** were used in duplicate for each receptor.

6.3 Fluorescence Properties and Microscopy

In the following chapter the methods and procedures for the recording of excitation and emission spectra and the fluorescence microscopy experiments are described.

6.3.1 Excitation and emission spectra and quantum yield

Excitation and emission spectra of the fluorescent ligands were recorded in PBS and PBS supplemented with 1 % BSA using a Cary Eclipse spectrofluorometer (Varian Inc., Mulgrave, Victoria, Australia) at 22 °C, using acryl cuvettes (10 x 10 mm, Sarstedt, Nümbrecht, Germany) as described previously.[157] The slit adjustments (excitation/emission) were 5/10 nm for excitation spectra and 10/5 nm for emission spectra. Net spectra were calculated by subtracting the respective vehicle reference spectrum and corrected emission spectra were calculated by multiplying the net emission spectra with the respective lamp correction spectrum. The quantum yield was determined according to previously described procedures[202,225] with minor modifications using a Cary Eclipse spectrofluorometer (Varian Inc., Mulgrave, Victoria, Australia) at 22 °C, using acryl cuvettes (10 x 10 mm, Sarstedt, Nümbrecht, Germany) and cresyl violet perchlorate (Biomol GmbH – Life Science Shop, Hamburg, Germany) as a red fluorescent standard. Absorption spectra were recorded with UV/Vis spectroscopy (350-850 nm, scan rate: 300 nm/min, slits: fixed 2 nm) at concentration of 2 µM for cresyl violet (in EtOH, $\lambda_{abs,max}$ = 575 nm) and the fluorescent ligands (in PBS buffer and PBS + 1 % BSA). The quantum yields were calculated for three different slit adjustments (exc./em.): 5/5 nm, 10/5 nm, 10/10 nm.

6.3.2 Live cell confocal microscopy at the D_1R

Cell culture and transfection was kindly done by Dr. Irene Reyes-Resina, Universidad de Barcelona. Confocal images were recorded by Dr. Steffen Pockes, University of Regensburg with kind assistance from Manel Bosch, Universidad de Barcelona. HEK293T cells were transfected with the D_1R as described in chapter 6.2.5 . with minor modifications. Cells were seeded in 35 mm wells containing 1.5 cover slips. 48 h after transfection medium was changed to OptiMem media (Gibco) supplemented with 10 mM HEPES. Imaging was performed using a Zeiss LSM880 Laser Scanning Confocal Microscope equipped with a "Plan-Apochromat" 40x/1,3 Oil DIC M27 objective and a photomultiplier tube (PTM) detector. For excitation an DPSS laser with a wavelength of 561 nm was used. Fluorescence was detected within an emission window of 569-669 nm. Image size was set to 512 x 512 pixels. After adjusting the focus, time-lapse images were recorded in intervals between 0.32 and 1 s. **76** was added

in a final concentration of 50 nM. Dissociation was induced by the addition of SCH-23390 (1000-fold excess).

Time-lapse confocal images were processed using the ImageJ software. Contrast was adjusted for each file to facilitate the visualization of the fluorescence signal. Total fluorescence was plotted as a function of time using GraphPad Prism9 software (GraphPad, San Diego, USA). The time of addition of **76** was set as 0 min. Data was fitted using the "Association – one conc. of hot ligand" or "association then dissociation" functions from Prism9. K_{on}, K_{off} and kintetic K_d values were calculated by Prism9.

6.3.3 Live cell confocal microscopy at the H_3R

These experiments were performed by Dr. Ali Isbilir, Max Delbrück Center, Berlin as described previously.[157] HEK293 cells stably transfected with a vector plasmid for H_3R expression were maintained in Dulbecco's Modified Eagle's Medium (DMEM) (PAN Biotech, Aidenbach, Germany) supplemented with 10 % Fetal Bovine Serum (FBS) (PAN, Aidenbach, Germany Biotech), 1 % L-Glutamine (PAN Biotech, Aidenbach, Germany), penicillin (100 U/mL), and streptomycin (100 µg/mL) at 37 °C and 5 % CO_2. Cells were passaged every 2-3 days.

For imaging, 300,000 HEK293-H_3R cells were seeded on Poly-D-Lysine coated coverslips in 6-well plates. 24 hours later, coverslips were transferred to an Attofluor cell chamber (Thermo Fisher Scientific, Nidderau, Germany) and supplemented with Fluorobrite DMEM medium (ThermoFisher, Nidderau, Germany), and then the chamber was placed on the microscope stage.

Imaging was performed using a Leica SP8 laser scanning confocal microscope equipped with a 40X/1.25 NA oil immersion objective, a white light laser (WLL) and photon counting hybrid (HyD) detectors. For excitation, the WLL was set to 552 nm at 10 % power. Fluorescence was detected within an emission window of 557-764 nm. Image size was set to 512 x 512 pixels, and the scanning speed was 700 Hz. After adjusting the focus, time-lapse cell imaging was performed with 1 second interval between each image. After imaging 10 seconds of baseline, fluorescence ligand was added by using a micropipette at a final concentration of 5 nM. After imaging 4-5 minutes, clobenpropit was added at a final concentration of 2.5 µM maintaining the 5 nM fluorescent ligand concentration and imaging was completed after 20 minutes.

Time-lapse confocal images were processed using the ImageJ software. Contrast was adjusted for each file to faciliate the visualization of fluorescence signal. Total fluorescence (in arbitrary units) was plotted as a function of time using the Origin 2018 software. Association and dissociation kinetics were calculated using the "ExpDec" function in the software. Each kinetic data was pooled and plotted as a scatter dot-plot using the GraphPad 7 software.

Experiments to demonstrate the photobleaching properties were performed according to the method described above. The fluorescent ligand was immobilized in 0.5 % agarose film in 1 µM final concentration of the fluorescent ligand UR-NR266 (**82**) and imaged over a period of 20 minutes.

6.3.4 TIRF-Imaging at the H_3R

These experiments were conducted by Dr. Jan Möller, Max Delbrück Center, Berlin as described previuosly.[157] For single-molecule experiments CHO-cells (ATTC/ LGC Standards,Wesel, Germany, were seeded 24 hours before transfection. Transfection was done 4-6 hours before TIRF-imaging using Lipofectamine 2000 (Thermofisher Scientific, Nidderau, Germany). For each single well of a 6-well cell culture plate (Brand, Wertheim, Germany) 2µg of the desired DNA were diluted in 500µL Opti-MEM (Thermofisher Scientific, Nidderau, Germany) and mixed with another dilution containing 6µL Lipofectamine 2000 transfection reagent in 500µL Opti-MEM. After incubation at 25 °C for 20 minutes this mixture (total = 1 mL) was added to a single well of cell culture plate, containing 1mL of DMEM-F12 medium (Thermofisher Scientific, Nidderau, Germany). After 4-6 hours expression levels were sufficient for single-molecule experiments and the medium got exchanged with new DMEM-F12 medium.

All TIRF-imaging experiments were performed with transiently transfected CHO cells as described above. To measure image based the labeling efficiency of UR-NR-266 (**82**) a C-terminally mNeonGreen tagged H_3R was expressed (H3-mNG). Cells were labeled with 10 nM of **82** for 15 minutes. After labeling cells were washed once with PBS and taken for imaging to an Attofluor™ Cell Chamber (Invitrogen, Carlsbad, USA) in sterile filtered PBS (Sigma-Aldrich, Munich, Germany) containing 3 nM of **82**. For single-molecule imaging, a TIRF illuminated Nikon Eclipse Ti2 microscope (Nikon, Tokyo, Japan) equipped with a 100X 1.49NA automated correction collar objective and 405, 488, 561, 647 nm laser diodes coupled via an automated N-Storm module and four iXon Ultra 897 EMCCD cameras (Andor, Tokyo, Japan) was used. Objective and sample were kept at 20 °C during imaging. The automated objective collar was on, exposure times were set to 40 ms and the perfect focus system (Nikon, Tokyo, Japan) was activated. Emission of TAMRA was recorded using a Cy3 Filter (Chroma, Vermont, USA) and mNeonGreen was recorded using a GFP Filter (Chroma, Vermont, USA).

Image analysis of the obtained TIRF-movies was done by first cropping the image to the desired size, region and frame-number using Fiji.[275] Afterwards movies were loaded in the Matlab environment (Mathworks) using u-Track[276] and requested parameters were adjusted according to above mentioned imaging conditions. Spot-Detection, Tracking and Motion-Analysis modules were then applied and analyzed as previously described, as well as the assignment of diffusion classes.[243]

7. References

1. Fredriksson, R.; Lagerström, M. C.; Lundin, L.-G.; Schiöth, H. B. The G-protein-coupled receptors in the human genome form five main families. Phylogenetic analysis, paralogon groups, and fingerprints. *Molecular pharmacology* **2003**, *636*, 1256–1272. DOI: 10.1124/mol.63.6.1256.

2. Lagerström, M. C.; Schiöth, H. B. Structural diversity of G protein-coupled receptors and significance for drug discovery. *Nat Rev Drug Discov* **2008**, *74*, 339–357. DOI: 10.1038/nrd2518.

3. Katritch, V.; Cherezov, V.; Stevens, R. C. Diversity and modularity of G protein-coupled receptor structures. *Trends in pharmacological sciences* **2012**, *331*, 17–27. DOI: 10.1016/j.tips.2011.09.003.

4. Kobilka, B. K. G protein coupled receptor structure and activation. *Biochimica et biophysica acta* **2007**, *17684*, 794–807. DOI: 10.1016/j.bbamem.2006.10.021.

5. Wacker, D.; Stevens, R. C.; Roth, B. L. How Ligands Illuminate GPCR Molecular Pharmacology. *Cell* **2017**, *1703*, 414–427. DOI: 10.1016/j.cell.2017.07.009.

6. Hauser, A. S.; Attwood, M. M.; Rask-Andersen, M.; Schiöth, H. B.; Gloriam, D. E. Trends in GPCR drug discovery: new agents, targets and indications. *Nat Rev Drug Discov* **2017**, *1612*, 829–842. DOI: 10.1038/nrd.2017.178.

7. Sriram, K.; Insel, P. A. G Protein-Coupled Receptors as Targets for Approved Drugs: How Many Targets and How Many Drugs? *Molecular pharmacology* **2018**, *934*, 251–258. DOI: 10.1124/mol.117.111062.

8. Alexander, S. P. H.; Christopoulos, A.; Davenport, A. P.; Kelly, E.; Mathie, A.; Peters, J. A.; Veale, E. L.; Armstrong, J. F.; Faccenda, E.; Harding, S. D.; Pawson, A. J.; Sharman, J. L.; Southan, C.; Davies, J. A. THE CONCISE GUIDE TO PHARMACOLOGY 2019/20: G protein-coupled receptors. *British Journal of Pharmacology* **2019**, *176 Suppl 1*, S21-S141. DOI: 10.1111/bph.14748.

9. Laschet, C.; Dupuis, N.; Hanson, J. The G protein-coupled receptors deorphanization landscape. *Biochemical pharmacology* **2018**, *153*, 62–74. DOI: 10.1016/j.bcp.2018.02.016.

10. Hauser, A. S.; Gloriam, D. E.; Bräuner-Osborne, H.; Foster, S. R. Novel approaches leading towards peptide GPCR de-orphanisation. *British Journal of Pharmacology* **2020**, *1775*, 961–968. DOI: 10.1111/bph.14950.

11. Bockaert, J.; Pin, J. P. Molecular tinkering of G protein-coupled receptors: an evolutionary success. *The EMBO journal* **1999**, *187*, 1723–1729. DOI: 10.1093/emboj/18.7.1723.

12. Wootten, D.; Christopoulos, A.; Marti-Solano, M.; Babu, M. M.; Sexton, P. M. Mechanisms of signalling and biased agonism in G protein-coupled receptors. *Nat Rev Mol Cell Biol* **2018**, *1910*, 638–653. DOI: 10.1038/s41580-018-0049-3.

13. Lefkowitz, R. J. A brief history of G-protein coupled receptors (Nobel Lecture). *Angewandte Chemie (International ed. in English)* **2013**, *5225*, 6366–6378. DOI: 10.1002/anie.201301924.

14. Barwich, A.-S.; Bschir, K. The manipulability of what? The history of G-protein coupled receptors. *Biol Philos* **2017**, *326*, 1317–1339. DOI: 10.1007/s10539-017-9608-9.

15. Gurevich, V. V.; Gurevich, E. V. GPCR Signaling Regulation: The Role of GRKs and Arrestins. *Front. Pharmacol.* **2019**, *10*, 125. DOI: 10.3389/fphar.2019.00125.

16. Hilger, D.; Masureel, M.; Kobilka, B. K. Structure and dynamics of GPCR signaling complexes. *Nature structural & molecular biology* **2018**, *251*, 4–12. DOI: 10.1038/s41594-017-0011-7.

17. Latorraca, N. R.; Venkatakrishnan, A. J.; Dror, R. O. GPCR Dynamics: Structures in Motion. *Chemical reviews* **2017**, *1171*, 139–155. DOI: 10.1021/acs.chemrev.6b00177.

18. Kenakin, T. Theoretical Aspects of GPCR-Ligand Complex Pharmacology. *Chemical reviews* **2017**, *1171*, 4–20. DOI: 10.1021/acs.chemrev.5b00561.

19. Dunn, H. A.; Ferguson, S. S. G. PDZ Protein Regulation of G Protein-Coupled Receptor Trafficking and Signaling Pathways. *Mol Pharmacol* **2015**, *884*, 624–639. DOI: 10.1124/mol.115.098509.

20. Ellisdon, A. M.; Halls, M. L. Compartmentalization of GPCR signalling controls unique cellular responses. *Biochem Soc Trans* **2016**, *442*, 562–567. DOI: 10.1042/BST20150236.

21. Komolov, K. E.; Benovic, J. L. G protein-coupled receptor kinases: Past, present and future. *Cellular Signalling* **2018**, *41*, 17–24. DOI: 10.1016/j.cellsig.2017.07.004.

22. Peterson, Y. K.; Luttrell, L. M. The Diverse Roles of Arrestin Scaffolds in G Protein-Coupled Receptor Signaling. *Pharmacol Rev* **2017**, *693*, 256–297. DOI: 10.1124/pr.116.013367.

23. Downes, G. B.; Gautam, N. The G protein subunit gene families. *Genomics* **1999**, *623*, 544–552. DOI: 10.1006/geno.1999.5992.

24. Farrens, D. L.; Altenbach, C.; Yang, K.; Hubbell, W. L.; Khorana, H. G. Requirement of rigid-body motion of transmembrane helices for light activation of rhodopsin. *Science* **1996**, *2745288*, 768–770. DOI: 10.1126/science.274.5288.768.

25. Oldham, W. M.; Hamm, H. E. Heterotrimeric G protein activation by G-protein-coupled receptors. *Nat Rev Mol Cell Biol* **2008**, *91*, 60–71. DOI: 10.1038/nrm2299.

26. Marinissen, M. J.; Gutkind, J. G-protein-coupled receptors and signaling networks: emerging paradigms. *Trends in Pharmacological Sciences* **2001**, *227*, 368–376. DOI: 10.1016/s0165-6147(00)01678-3.

27. Kristiansen, K. Molecular mechanisms of ligand binding, signaling, and regulation within the superfamily of G-protein-coupled receptors: molecular modeling and mutagenesis approaches to receptor structure and function. *Pharmacology & Therapeutics* **2004**, *1031*, 21–80. DOI: 10.1016/j.pharmthera.2004.05.002.

28. Cabrera-Vera, T. M.; Vanhauwe, J.; Thomas, T. O.; Medkova, M.; Preininger, A.; Mazzoni, M. R.; Hamm, H. E. Insights into G protein structure, function, and regulation. *Endocr Rev* **2003**, *246*, 765–781. DOI: 10.1210/er.2000-0026.

29. Knall, C.; Johnson, G. L. G-protein regulatory pathways: Rocketing into the twenty-first century. *Journal of Cellular Biochemistry* **1998**, *72S30-31*, 137–146. DOI: 10.1002/(SICI)1097-4644(1998)72:30/31.

30. Kamato, D.; Mitra, P.; Davis, F.; Osman, N.; Chaplin, R.; Cabot, P. J.; Afroz, R.; Thomas, W.; Zheng, W.; Kaur, H.; Brimble, M.; Little, P. J. Gaq proteins: molecular pharmacology and therapeutic potential. *Cell. Mol. Life Sci.* **2017**, *748*, 1379–1390. DOI: 10.1007/s00018-016-2405-9.

31. Smrcka, A. V.; Fisher, I. G-protein βγ subunits as multi-functional scaffolds and transducers in G-protein-coupled receptor signaling. *Cell. Mol. Life Sci.* **2019**, *7622*, 4447–4459. DOI: 10.1007/s00018-019-03275-2.

32. Krapivinsky, G.; Kennedy, M. E.; Nemec, J.; Medina, I.; Krapivinsky, L.; Clapham, D. E. Gbeta binding to GIRK4 subunit is critical for G protein-gated K+ channel activation. *The Journal of biological chemistry* **1998**, *27327*, 16946–16952. DOI: 10.1074/jbc.273.27.16946.

33. Logothetis, D. E.; Kurachi, Y.; Galper, J.; Neer, E. J.; Clapham, D. E. The beta gamma subunits of GTP-binding proteins activate the muscarinic K+ channel in heart. *Nature* **1987**, *3256102*, 321–326. DOI: 10.1038/325321a0.

34. Pitcher, J. A.; Inglese, J.; Higgins, J. B.; Arriza, J. L.; Casey, P. J.; Kim, C.; Benovic, J. L.; Kwatra, M. M.; Caron, M. G.; Lefkowitz, R. J. Role of beta gamma subunits of G proteins in targeting the beta-adrenergic receptor kinase to membrane-bound receptors. *Science* **1992**, *2575074*, 1264–1267. DOI: 10.1126/science.1325672.

35. Tang, W. J.; Gilman, A. G. Type-specific regulation of adenylyl cyclase by G protein beta gamma subunits. *Science* **1991**, *2545037*, 1500–1503. DOI: 10.1126/science.1962211.

36. Smrcka, A. V. G protein βγ subunits: central mediators of G protein-coupled receptor signaling. *Cellular and molecular life sciences : CMLS* **2008**, *6514*, 2191–2214. DOI: 10.1007/s00018-008-8006-5.

37. Weis, W. I.; Kobilka, B. K. The Molecular Basis of G Protein-Coupled Receptor Activation. *Annual review of biochemistry* **2018**, *87*, 897–919. DOI: 10.1146/annurev-biochem-060614-033910.

38. Magalhaes, A. C.; Dunn, H.; Ferguson, S. S. Regulation of GPCR activity, trafficking and localization by GPCR-interacting proteins. *British Journal of Pharmacology* **2012**, *1656*, 1717–1736. DOI: 10.1111/j.1476-5381.2011.01552.x.

39. Tobin, A. B. G-protein-coupled receptor phosphorylation: where, when and by whom. *British Journal of Pharmacology* **2008**, *153 Suppl 1S1*, S167-76. DOI: 10.1038/sj.bjp.0707662.

40. Cahill, T. J.; Thomsen, A. R. B.; Tarrasch, J. T.; Plouffe, B.; Nguyen, A. H.; Yang, F.; Huang, L.-Y.; Kahsai, A. W.; Bassoni, D. L.; Gavino, B. J.; Lamerdin, J. E.; Triest, S.; Shukla, A. K.; Berger, B.; Little, J.; Antar, A.; Blanc, A.; Qu, C.-X.; Chen, X.; Kawakami, K.; Inoue, A.; Aoki, J.; Steyaert, J.; Sun, J.-P.; Bouvier, M.; Skiniotis, G.; Lefkowitz, R. J. Distinct conformations of GPCR-β-arrestin complexes mediate desensitization, signaling, and endocytosis. *Proceedings of the National Academy of Sciences of the United States of America* **2017**, *11410*, 2562–2567. DOI: 10.1073/pnas.1701529114.

41. Stephen S. G. Ferguson. Evolving Concepts in G Protein-Coupled Receptor Endocytosis: The Role in Receptor Desensitization and Signaling. *Pharmacol Rev* **2001**, *531*, 1–24.

42. Peterson, Y. K.; Luttrell, L. M. The Diverse Roles of Arrestin Scaffolds in G Protein-Coupled Receptor Signaling. *Pharmacol Rev* **2017**, *693*, 256–297. DOI: 10.1124/pr.116.013367.

43. Luttrell, L. M.; Ferguson, S. S.; Daaka, Y.; Miller, W. E.; Maudsley, S.; Della Rocca, G. J.; Lin, F.; Kawakatsu, H.; Owada, K.; Luttrell, D. K.; Caron, M. G.; Lefkowitz, R. J. Beta-arrestin-dependent formation of beta2 adrenergic receptor-Src protein kinase complexes. *Science* **1999**, *2835402*, 655–661. DOI: 10.1126/science.283.5402.655.

44. Kolch, W. Coordinating ERK/MAPK signalling through scaffolds and inhibitors. *Nat Rev Mol Cell Biol* **2005**, *611*, 827–837. DOI: 10.1038/nrm1743.

45. Roberts, P. J.; Der, C. J. Targeting the Raf-MEK-ERK mitogen-activated protein kinase cascade for the treatment of cancer. *Oncogene* **2007**, *2622*, 3291–3310. DOI: 10.1038/sj.onc.1210422.

46. Sturm, O. E.; Orton, R.; Grindlay, J.; Birtwistle, M.; Vyshemirsky, V.; Gilbert, D.; Calder, M.; Pitt, A.; Kholodenko, B.; Kolch, W. The mammalian MAPK/ERK pathway exhibits properties of a negative feedback amplifier. *Science signaling* **2010**, *3153*, ra90. DOI: 10.1126/scisignal.2001212.

47. Smith, J. S.; Lefkowitz, R. J.; Rajagopal, S. Biased signalling: from simple switches to allosteric microprocessors. *Nat Rev Drug Discov* **2018**, *174*, 243–260. DOI: 10.1038/nrd.2017.229.

48. Brunton, L. L. Goodman and Gilman's manual of pharmacology and therapeutics. 2nd ed.; *McGraw-Hill Education Medical*, New York, **2014**.

49. Seifert, R.; Wenzel-Seifert, K. Constitutive activity of G-protein-coupled receptors: cause of disease and common property of wild-type receptors. *Naunyn-Schmiedeberg's Arch Pharmacol* **2002**, *3665*, 381–416. DOI: 10.1007/s00210-002-0588-0.

50. Kenakin, T.; Christopoulos, A. Signalling bias in new drug discovery: detection, quantification and therapeutic impact. *Nat Rev Drug Discov* **2013**, *123*, 205–216. DOI: 10.1038/nrd3954.

51. Klein Herenbrink, C.; Sykes, D. A.; Donthamsetti, P.; Canals, M.; Coudrat, T.; Shonberg, J.; Scammells, P. J.; Capuano, B.; Sexton, P. M.; Charlton, S. J.; Javitch, J. A.; Christopoulos, A.; Lane, J. R. The role of kinetic context in apparent biased agonism at GPCRs. *Nat Commun* **2016**, *71*, 10842. DOI: 10.1038/ncomms10842.

52. Urban, J. D.; Clarke, W. P.; Zastrow, M. von; Nichols, D. E.; Kobilka, B.; Weinstein, H.; Javitch, J. A.; Roth, B. L.; Christopoulos, A.; Sexton, P. M.; Miller, K. J.; Spedding, M.; Mailman, R. B. Functional selectivity and classical concepts of quantitative pharmacology. *J Pharmacol Exp Ther* **2007**, *3201*, 1–13. DOI: 10.1124/jpet.106.104463.

53. Urban, J. D.; Clarke, W. P.; Zastrow, M. von; Nichols, D. E.; Kobilka, B.; Weinstein, H.; Javitch, J. A.; Roth, B. L.; Christopoulos, A.; Sexton, P. M.; Miller, K. J.; Spedding, M.; Mailman, R. B. Functional selectivity and classical concepts of quantitative pharmacology. *J Pharmacol Exp Ther* **2007**, *3201*, 1–13. DOI: 10.1124/jpet.106.104463.

54. Eiger, D. S.; Pham, U.; Gardner, J.; Hicks, C.; Rajagopal, S. GPCR systems pharmacology: a different perspective on the development of biased therapeutics. *American journal of physiology. Cell physiology* **2022**, *3225*, C887-C895. DOI: 10.1152/ajpcell.00449.2021.

55. Michel, M. C.; Charlton, S. J. Biased Agonism in Drug Discovery-Is It Too Soon to Choose a Path? *Mol Pharmacol* **2018**, *934*, 259–265. DOI: 10.1124/mol.117.110890.

56. Rajagopal, S.; Kim, J.; Ahn, S.; Craig, S.; Lam, C. M.; Gerard, N. P.; Gerard, C.; Lefkowitz, R. J. Beta-arrestin- but not G protein-mediated signaling by the "decoy" receptor CXCR7. *Proceedings of the National Academy of Sciences of the United States of America* **2010**, *1072*, 628–632. DOI: 10.1073/pnas.0912852107.

57. Onfroy, L.; Galandrin, S.; Pontier, S. M.; Seguelas, M.-H.; Du N'Guyen; Sénard, J.-M.; Galés, C. G protein stoichiometry dictates biased agonism through distinct receptor-G protein partitioning. *Scientific reports* **2017**, *71*, 7885. DOI: 10.1038/s41598-017-07392-5.

58. Thomsen, A. R. B.; Plouffe, B.; Cahill, T. J.; Shukla, A. K.; Tarrasch, J. T.; Dosey, A. M.; Kahsai, A. W.; Strachan, R. T.; Pani, B.; Mahoney, J. P.; Huang, L.; Breton, B.; Heydenreich, F. M.; Sunahara, R. K.; Skiniotis, G.; Bouvier, M.; Lefkowitz, R. J. GPCR-G Protein-β-Arrestin Super-Complex Mediates Sustained G Protein Signaling. *Cell* **2016**, *1664*, 907–919. DOI: 10.1016/j.cell.2016.07.004.

59. Ahn, S.; Wei, H.; Garrison, T. R.; Lefkowitz, R. J. Reciprocal regulation of angiotensin receptor-activated extracellular signal-regulated kinases by beta-arrestins 1 and 2. *The Journal of biological chemistry* **2004**, *2799*, 7807–7811. DOI: 10.1074/jbc.C300443200.

60. Mohammad Nezhady, M. A.; Rivera, J. C.; Chemtob, S. Location Bias as Emerging Paradigm in GPCR Biology and Drug Discovery. *iScience* **2020**, *2310*, 101643. DOI: 10.1016/j.isci.2020.101643.

61. Ferrada, C.; Moreno, E.; Casadó, V.; Bongers, G.; Cortés, A.; Mallol, J.; Canela, E. I.; Leurs, R.; Ferré, S.; Lluís, C.; Franco, R. Marked changes in signal transduction upon heteromerization of dopamine D1 and histamine H3 receptors. *British Journal of Pharmacology* **2009**, *1571*, 64–75. DOI: 10.1111/j.1476-5381.2009.00152.x.

62. Bourque, K.; Jones-Tabah, J.; Devost, D.; Clarke, P. B. S.; Hébert, T. E. Exploring functional consequences of GPCR oligomerization requires a different lens. *Progress in molecular biology and translational science* **2020**, *169*, 181–211. DOI: 10.1016/bs.pmbts.2019.11.001.

63. Gurevich, V. V.; Gurevich, E. V. GPCRs and Signal Transducers: Interaction Stoichiometry. *Trends in pharmacological sciences* **2018**, *397*, 672–684. DOI: 10.1016/j.tips.2018.04.002.

64. Gomes, I.; Ayoub, M. A.; Fujita, W.; Jaeger, W. C.; Pfleger, K. D. G.; Devi, L. A. G Protein-Coupled Receptor Heteromers. *Annual review of pharmacology and toxicology* **2016**, *56*, 403–425. DOI: 10.1146/annurev-pharmtox-011613-135952.

65. Calebiro, D.; Rieken, F.; Wagner, J.; Sungkaworn, T.; Zabel, U.; Borzi, A.; Cocucci, E.; Zürn, A.; Lohse, M. J. Single-molecule analysis of fluorescently labeled G-protein-coupled receptors reveals complexes with distinct dynamics and organization. *Proceedings of the National Academy of Sciences of the United States of America* **2013**, *1102*, 743–748. DOI: 10.1073/pnas.1205798110.

66. George, S. R.; Fan, T.; Xie, Z.; Tse, R.; Tam, V.; Varghese, G.; O'Dowd, B. F. Oligomerization of mu- and delta-opioid receptors. Generation of novel functional properties. *The Journal of biological chemistry* **2000**, *27534*, 26128–26135. DOI: 10.1074/jbc.M000345200.

67. Smith, N. J.; Milligan, G. Allostery at G protein-coupled receptor homo- and heteromers: uncharted pharmacological landscapes. *Pharmacol Rev* **2010**, *624*, 701–725. DOI: 10.1124/pr.110.002667.

68. Gallo, M.; Defaus, S.; Andreu, D. Disrupting GPCR Complexes with Smart Drug-like Peptides. *Pharmaceutics* **2022**, *141*, 161. DOI: 10.3390/pharmaceutics14010161.

69. Young, B. M.; Nguyen, E.; Chedrawe, M. A. J.; Rainey, J. K.; Dupré, D. J. Differential Contribution of Transmembrane Domains IV, V, VI, and VII to Human Angiotensin II Type 1 Receptor Homomer Formation. *Journal of Biological Chemistry* **2017**, *2928*, 3341–3350. DOI: 10.1074/jbc.M116.750380.

70. Lee, L. T. O.; Ng, S. Y. L.; Chu, J. Y. S.; Sekar, R.; Harikumar, K. G.; Miller, L. J.; Chow, B. K. C. Transmembrane peptides as unique tools to demonstrate the in vivo action of a cross-class GPCR heterocomplex. *The FASEB Journal* **2014**, *286*, 2632–2644. DOI: 10.1096/fj.13-246868.

71. Calebiro, D.; Sungkaworn, T. Single-Molecule Imaging of GPCR Interactions. *Trends in pharmacological sciences* **2018**, *392*, 109–122. DOI: 10.1016/j.tips.2017.10.010.

72. Hern, J. A.; Baig, A. H.; Mashanov, G. I.; Birdsall, B.; Corrie, J. E. T.; Lazareno, S.; Molloy, J. E.; Birdsall, N. J. M. Formation and dissociation of M1 muscarinic receptor dimers seen by total internal reflection fluorescence imaging of single molecules. *Proceedings of the National Academy of Sciences of the United States of America* **2010**, *1076*, 2693–2698. DOI: 10.1073/pnas.0907915107.

73. Kasai, R. S.; Suzuki, K. G. N.; Prossnitz, E. R.; Koyama-Honda, I.; Nakada, C.; Fujiwara, T. K.; Kusumi, A. Full characterization of GPCR monomer-dimer dynamic equilibrium by single molecule imaging. *J Cell Biol* **2011**, *1923*, 463–480. DOI: 10.1083/jcb.201009128.

74. Franco, R.; Reyes-Resina, I.; Navarro, G. Dopamine in Health and Disease: Much More Than a Neurotransmitter. *Biomedicines* **2021**, *92*, 109. DOI: 10.3390/biomedicines9020109.

75. Klein, M. O.; Battagello, D. S.; Cardoso, A. R.; Hauser, D. N.; Bittencourt, J. C.; Correa, R. G. Dopamine: Functions, Signaling, and Association with Neurological Diseases. *Cell Mol Neurobiol* **2019**, *391*, 31–59. DOI: 10.1007/s10571-018-0632-3.

76. Christenson, J. G.; Dairman, W.; Udenfriend, S. Preparation and properties of a homogeneous aromatic l-amino acid decarboxylase from hog kidney. *Archives of Biochemistry and Biophysics* **1970**, *1411*, 356–367. DOI: 10.1016/0003-9861(70)90144-x.

77. Kebabian, J. W.; Calne, D. B. Multiple receptors for dopamine. *Nature* **1979**, *2775692*, 93–96. DOI: 10.1038/277093a0.

78. Hornykiewicz, O. Parkinson's disease: from brain homogenate to treatment. *Federation proceedings* **1973**, *322*, 183–190.

79. Davis, K. L.; Kahn, R. S.; Ko, G.; Davidson, M. Dopamine in schizophrenia: a review and reconceptualization. *AJP* **1991**, *14811*, 1474–1486. DOI: 10.1176/ajp.148.11.1474.

80. Robertson, M. M.; Eapen, V.; Singer, H. S.; Martino, D.; Scharf, J. M.; Paschou, P.; Roessner, V.; Woods, D. W.; Hariz, M.; Mathews, C. A.; Črnčec, R.; Leckman, J. F. Gilles de la Tourette syndrome. *Nat Rev Dis Primers* **2017**, *31*, 16097. DOI: 10.1038/nrdp.2016.97.

81. Castellanos, F. X.; Tannock, R. Neuroscience of attention-deficit/hyperactivity disorder: the search for endophenotypes. *Nat Rev Neurosci* **2002**, *38*, 617–628. DOI: 10.1038/nrn896.

82. Jakel, R. J.; Maragos, W. F. Neuronal cell death in Huntington's disease: a potential role for dopamine. *Trends in Neurosciences* **2000**, *236*, 239–245. DOI: 10.1016/s0166-2236(00)01568-x.

83. Wise, R. A.; Robble, M. A. Dopamine and Addiction. *Annual review of psychology* **2020**, *71*, 79–106. DOI: 10.1146/annurev-psych-010418-103337.

84. Lee, S. P.; So, C. H.; Rashid, A. J.; Varghese, G.; Cheng, R.; Lança, A. J.; O'Dowd, B. F.; George, S. R. Dopamine D1 and D2 receptor Co-activation generates a novel phospholipase C-mediated calcium signal. *The Journal of biological chemistry* **2004**, *27934*, 35671–35678. DOI: 10.1074/jbc.m401923200.

85. Mishra, A.; Singh, S.; Shukla, S. Physiological and Functional Basis of Dopamine Receptors and Their Role in Neurogenesis: Possible Implication for Parkinson's disease. *Journal of Experimental Neuroscience* **2018**, *12*, 1179069518779829. DOI: 10.1177/1179069518779829.

86. Beaulieu, J.-M.; Gainetdinov, R. R. The physiology, signaling, and pharmacology of dopamine receptors. *Pharmacol Rev* **2011**, *631*, 182–217. DOI: 10.1124/pr.110.002642.

87. Hall, A.; Provins, L.; Valade, A. Novel Strategies To Activate the Dopamine D1 Receptor: Recent Advances in Orthosteric Agonism and Positive Allosteric Modulation. *Journal of Medicinal Chemistry* **2019**, *621*, 128–140. DOI: 10.1021/acs.jmedchem.8b01767.

88. Missale, C.; Nash, S. R.; Robinson, S. W.; Jaber, M.; Caron, M. G. Dopamine receptors: from structure to function. *Physiological Reviews* **1998**, *781*, 189–225. DOI: 10.1152/physrev.1998.78.1.189.

89. Beaulieu, J.-M.; Espinoza, S.; Gainetdinov, R. R. Dopamine receptors - IUPHAR Review 13. *British Journal of Pharmacology* **2015**, *1721*, 1–23. DOI: 10.1111/bph.12906.

90. Ha, C. M.; Park, D.; Han, J.-K.; Jang, J.; Park, J.-Y.; Hwang, E. M.; Seok, H.; Chang, S. Calcyon forms a novel ternary complex with dopamine D1 receptor through PSD-95 protein and plays a role in dopamine receptor internalization. *Journal of Biological Chemistry* **2012**, *28738*, 31813–31822. DOI: 10.1074/jbc.M112.370601.

91. Valjent, E.; Corvol, J.-C.; Pagès, C.; Besson, M.-J.; Maldonado, R.; Caboche, J. Involvement of the Extracellular Signal-Regulated Kinase Cascade for Cocaine-Rewarding Properties. *J. Neurosci.* **2000**, *2023*, 8701–8709. DOI: 10.1523/JNEUROSCI.20-23-08701.2000.

92. Valjent, E.; Pascoli, V.; Svenningsson, P.; Paul, S.; Enslen, H.; Corvol, J.-C.; Stipanovich, A.; Caboche, J.; Lombroso, P. J.; Nairn, A. C.; Greengard, P.; Hervé, D.; Girault, J.-A. Regulation of a protein phosphatase cascade allows convergent dopamine and glutamate signals to activate ERK in the striatum. *Proc. Natl. Acad. Sci. U.S.A.* **2005**, *1022*, 491–496. DOI: 10.1073/pnas.0408305102.

93. Pascoli, V.; Besnard, A.; Hervé, D.; Pagès, C.; Heck, N.; Girault, J.-A.; Caboche, J.; Vanhoutte, P. Cyclic adenosine monophosphate-independent tyrosine phosphorylation of NR2B mediates cocaine-induced extracellular signal-regulated kinase activation. *Biological psychiatry* **2011**, *693*, 218–227. DOI: 10.1016/j.biopsych.2010.08.031.

94. Grenader, A.; Healy, D. P. Fenoldopam is a partial agonist at dopamine-1 (DA1) receptors in LLC-PK1 cells. *J Pharmacol Exp Ther* **1991**, *2581*, 193–198.

95. Brogden, R. N.; Markham, A. Fenoldopam: a review of its pharmacodynamic and pharmacokinetic properties and intravenous clinical potential in the management of hypertensive urgencies and emergencies. *Drugs* **1997**, *544*, 634–650. DOI: 10.2165/00003495-199754040-00008.

96. Braun, A.; Fabbrini, G.; Mouradian, M. M.; Serrati, C.; Barone, P.; Chase, T. N. Selective D-1 dopamine receptor agonist treatment of Parkinson's disease. *J. Neural Transmission* **1987**, *681-2*, 41–50. DOI: 10.1007/BF01244638.

97. Lorio, L. C.; Barnett, A.; Leitz, F. H.; Houser, V. P. SCH23390, a Potential Benzazepine Antipsychotic with Unique Interactions on Dopaminergic Systems. *J. Pharmacol.* **1983***226*, 462–468.

98. Billard, W.; Ruperto, V.; Crosby, G.; Iorio, L. C.; Barnett, A. Characterization of the binding of 3H-SCH 23390, a selective D-1 receptor antagonist ligand, in rat striatum. *Life Sciences* **1984**, *3518*, 1885–1893. DOI: 10.1016/0024-3205(84)90540-x.

99. Lovenberg, T. W.; Brewster, W. K.; Mottola, D. M.; Lee, R. C.; Riggs, R. M.; Nichols, D. E.; Lewis, M. H.; Mailman, R. B. Dihydrexidine, a novel selective high potency full dopamine D-1 receptor agonist. *European Journal of Pharmacology* **1989**, *1661*, 111–113. DOI: 10.1016/0014-2999(89)90690-0.

100. Blanchet, P. J.; Fang, J.; Gillespie, M.; Sabounjian, L.; Locke, K. Effects of the Full Dopamine D1 Receptor Agonist Dihydrexidine in Parkinson's Disease. *Clin. Neuropharmacol.* **1998***21*, 339–343.

101. Lewis, M. A.; Hunihan, L.; Watson, J.; Gentles, R. G.; Hu, S.; Huang, Y.; Bronson, J.; Macor, J. E.; Beno, B. R.; Ferrante, M.; Hendricson, A.; Knox, R. J.; Molski, T. F.; Kong, Y.; Cvijic, M. E.; Rockwell, K. L.; Weed, M. R.; Cacace, A. M.; Westphal, R. S.; Alt, A.; Brown, J. M. Discovery of D1 Dopamine Receptor Positive Allosteric Modulators: Characterization of Pharmacology and Identification of Residues that Regulate Species Selectivity. *J Pharmacol Exp Ther* **2015**, *3543*, 340–349. DOI: 10.1124/jpet.115.224071.

102. Wang, X.; Heinz, B. A.; Qian, Y.-W.; Carter, J. H.; Gadski, R. A.; Beavers, L. S.; Little, S. P.; Yang, C. R.; Beck, J. P.; Hao, J.; Schaus, J. M.; Svensson, K. A.; Bruns, R. F. Intracellular Binding Site for a Positive Allosteric Modulator of the Dopamine D1 Receptor. *Mol Pharmacol* **2018**, *944*, 1232–1245. DOI: 10.1124/mol.118.112649.

103. Best CH, Dale HH, Dudley HW, Thorpe WV. The nature of the vaso-dilator constituents of certain tissue extracts. *The Journal of Physiology.* **1927**, 397–417.

104. Dale, H. H.; Laidlaw, P. P. The physiological action of β-iminazolylethylamine. *The Journal of Physiology.* **1910**, 318–344. DOI: 10.1113/jphysiol.1910.sp001406.

105. Panula, P.; Chazot, P. L.; Cowart, M.; Gutzmer, R.; Leurs, R.; Liu, W. L. S.; Stark, H.; Thurmond, R. L.; Haas, H. L. International Union of Basic and Clinical Pharmacology. XCVIII. Histamine Receptors. *Pharmacol Rev* **2015**, *673*, 601–655. DOI: 10.1124/pr.114.010249.

106. Aures, D.; Håkanson, R.; Schauer, A. Histidine decarboxylase and dopa decarboxylase in the rat stomach. Properties and cellular localization. *European Journal of Pharmacology* **1968**, *33*, 217–234. DOI: 10.1016/0014-2999(68)90135-0.

107. Hough, L. B. Genomics Meets Histamine Receptors: New Subtypes, New Receptors. *Mol Pharmacol* **2001**, *593*, 415–419. DOI: 10.1124/mol.59.3.415.

108. Bovet, D.; A. M. Staub. Protective action of some phenolic ethers in histamine intoxication. *CR Seances Soc. Biol. Fil* **1937***124*, 547–549.

109. Sjöqvist, F.; Lasagna, L. The hypnotic efficacy of doxylamine. *Clinical pharmacology and therapeutics* **1967**, *81*, 48–54. DOI: 10.1002/cpt196781part148.

110. BLACK, J. W.; Duncan, W. A.; DURANT, C. J.; Ganellin, C. R.; PARSONS, E. M. Definition and antagonism of histamine H 2 -receptors. *Nature* **1972**, *2365347*, 385–390. DOI: 10.1038/236385a0.

111. Hill, S. J.; Ganellin, C. R.; Timmerman, H.; Schwartz, J. C.; Shankley, N. P.; Young, J. M.; Schunack, W.; Levi, R.; Haas, H. L. International Union of Pharmacology. XIII. Classification of histamine receptors. *Pharmacol Rev* **1997**, *493*, 253–278.

112. Arrang, J. M.; Garbarg, M.; Schwartz, J. C. Auto-inhibition of brain histamine release mediated by a novel class (H3) of histamine receptor. *Nature* **1983**, *3025911*, 832–837. DOI: 10.1038/302832a0.

113. Nakamura, T.; Itadani, H.; Hidaka, Y.; Ohta, M.; Tanaka, K. Molecular cloning and characterization of a new human histamine receptor, HH4R. *Biochemical and Biophysical Research Communications* **2000**, *2792*, 615–620. DOI: 10.1006/bbrc.2000.4008.

114. Arrang, J. M.; Garbarg, M.; Lancelot, J. C.; Lecomte, J. M.; Pollard, H.; Robba, M.; Schunack, W.; Schwartz, J. C. Highly potent and selective ligands for histamine H3-receptors. *Nature* **1987**, *3276118*, 117–123. DOI: 10.1038/327117a0.

115. Lovenberg, T. W.; Roland, B. L.; Wilson, S. J.; Jiang, X.; Pyati, J.; Huvar, A.; Jackson, M. R.; Erlander, M. G. Cloning and Functional Expression of the Human Histamine H 3 Receptor. *Mol Pharmacol* **1999**, *556*, 1101–1107. DOI: 10.1124/mol.55.6.1101.

116. COGÉ, F.; GUÉNIN, S.-P.; AUDINOT, V.; RENOUARD-TRY, A.; BEAUVERGER, P.; MACIA, C.; OUVRY, C.; NAGEL, N.; RIQUE, H.; BOUTIN, J. A.; GALIZZI, J.-P. Genomic organization and characterization of splice variants of the human histamine H3 receptor. *Biochem J* **2001**, *3552*, 279–288. DOI: 10.1042/bj3550279.

117. Riddy, D. M.; Cook, A. E.; Diepenhorst, N. A.; Bosnyak, S.; Brady, R.; La Mannoury Cour, C.; Mocaer, E.; Summers, R. J.; Charman, W. N.; Sexton, P. M.; Christopoulos, A.; Langmead, C. J. Isoform-Specific Biased Agonism of Histamine H3 Receptor Agonists. *Mol Pharmacol* **2017**, *912*, 87–99. DOI: 10.1124/mol.116.106153.

118. Nieto-Alamilla, G.; Márquez-Gómez, R.; García-Gálvez, A.-M.; Morales-Figueroa, G.-E.; Arias-Montaño, J.-A. The Histamine H3 Receptor: Structure, Pharmacology, and Function. *Mol Pharmacol* **2016**, *905*, 649–673. DOI: 10.1124/mol.116.104752.

119. Łażewska, D.; Bajda, M.; Kaleta, M.; Zaręba, P.; Doroz-Płonka, A.; Siwek, A.; Alachkar, A.; Mogilski, S.; Saad, A.; Kuder, K.; Olejarz-Maciej, A.; Godyń, J.; Stary, D.; Sudoł, S.; Więcek, M.; Latacz, G.; Walczak, M.; Handzlik, J.; Sadek, B.; Malawska, B.; Kieć-Kononowicz, K. Rational design of new multitarget histamine H3 receptor ligands as potential candidates for treatment of Alzheimer's disease. *European Journal of Medicinal Chemistry* **2020**, *207*, 112743. DOI: 10.1016/j.ejmech.2020.112743.

120. Ellenbroek, B. A.; Ghiabi, B. The other side of the histamine H3 receptor. *Trends in Neurosciences* **2014**, *374*, 191–199. DOI: 10.1016/j.tins.2014.02.007.

121. Passani, M. B.; Lin, J.-S.; Hancock, A.; Crochet, S.; Blandina, P. The histamine H3 receptor as a novel therapeutic target for cognitive and sleep disorders. *Trends in Pharmacological Sciences* **2004**, *2512*, 618–625. DOI: 10.1016/j.tips.2004.10.003.

122. Rapanelli, M.; Frick, L.; Pogorelov, V.; Ohtsu, H.; Bito, H.; Pittenger, C. Histamine H3R receptor activation in the dorsal striatum triggers stereotypies in a mouse model of tic disorders. *Transl Psychiatry* **2017**, *71*, e1013. DOI: 10.1038/tp.2016.290.

123. Esbenshade, T. A.; Browman, K. E.; Bitner, R. S.; Strakhova, M.; Cowart, M. D.; Brioni, J. D. The histamine H3 receptor: an attractive target for the treatment of cognitive disorders. *British Journal of Pharmacology* **2008**, *1546*, 1166–1181. DOI: 10.1038/bjp.2008.147.

124. Łażewska, D.; Kieć-Kononowicz, K. Progress in the development of histamine H3 receptor antagonists/inverse agonists: a patent review (2013-2017). *Expert Opinion on Therapeutic Patents* **2018**, *283*, 175–196. DOI: 10.1080/13543776.2018.1424135.

125. Pullen, L. C.; Picone, M.; Tan, L.; Johnston, C.; Stark, H. Cognitive Improvements in Children with Prader-Willi Syndrome Following Pitolisant Treatment-Patient Reports. *The Journal of Pediatric Pharmacology and Therapeutics* **2019**, *242*, 166–171. DOI: 10.5863/1551-6776-24.2.166.

126. Giovannini, M. G.; Efoudebe, M.; Passani, M. B.; Baldi, E.; Bucherelli, C.; Giachi, F.; Corradetti, R.; Blandina, P. Improvement in Fear Memory by Histamine-Elicited ERK2 Activation in Hippocampal CA3 Cells. *J. Neurosci.* **2003**, *2327*, 9016–9023. DOI: 10.1523/JNEUROSCI.23-27-09016.2003.

127. Silver, R. B.; Mackins, C. J.; Smith, N. C.; Koritchneva, I. L.; Lefkowitz, K.; Lovenberg, T. W.; Levi, R. Coupling of histamine H3 receptors to neuronal Na+/H+ exchange: a novel protective mechanism in myocardial ischemia. *Proc. Natl. Acad. Sci. U.S.A.* **2001**, *985*, 2855–2859. DOI: 10.1073/pnas.051599198.

128. Drutel, G.; Peitsaro, N.; Karlstedt, K.; Wieland, K.; Smit, M. J.; Timmerman, H.; Panula, P.; Leurs, R. Identification of Rat H 3 Receptor Isoforms with Different Brain Expression and Signaling Properties. *Mol Pharmacol* **2001**, *591*, 1–8. DOI: 10.1124/mol.59.1.1.

129. Ferrada, C.; Moreno, E.; Casadó, V.; Bongers, G.; Cortés, A.; Mallol, J.; Canela, E. I.; Leurs, R.; Ferré, S.; Lluís, C.; Franco, R. Marked changes in signal transduction upon heteromerization of dopamine D1 and histamine H3 receptors. *British Journal of Pharmacology* **2009**, *1571*, 64–75. DOI: 10.1111/j.1476-5381.2009.00152.x.

130. Moreno, E.; Hoffmann, H.; Gonzalez-Sepúlveda, M.; Navarro, G.; Casadó, V.; Cortés, A.; Mallol, J.; Vignes, M.; McCormick, P. J.; Canela, E. I.; Lluís, C.; Moratalla, R.; Ferré, S.; Ortiz, J.; Franco, R. Dopamine D1-histamine H3 receptor heteromers provide a selective link to MAPK signaling in GABAergic neurons of the direct striatal pathway. *Journal of Biological Chemistry* **2011**, *2867*, 5846–5854. DOI: 10.1074/jbc.M110.161489.

131. Rodríguez-Ruiz, M.; Moreno, E.; Moreno-Delgado, D.; Navarro, G.; Mallol, J.; Cortés, A.; Lluís, C.; Canela, E. I.; Casadó, V.; McCormick, P. J.; Franco, R. Heteroreceptor Complexes Formed by Dopamine D1, Histamine H3, and N-Methyl-D-Aspartate Glutamate Receptors as Targets to Prevent Neuronal Death in Alzheimer's Disease. *Mol Neurobiol* **2017**, *546*, 4537–4550. DOI: 10.1007/s12035-016-9995-y.

132. Moreno, E.; Moreno-Delgado, D.; Navarro, G.; Hoffmann, H. M.; Fuentes, S.; Rosell-Vilar, S.; Gasperini, P.; Rodríguez-Ruiz, M.; Medrano, M.; Mallol, J.; Cortés, A.; Casadó, V.; Lluís, C.; Ferré, S.; Ortiz, J.; Canela, E.; McCormick, P. J. Cocaine disrupts histamine H3 receptor modulation of dopamine D1 receptor signaling: σ1-D1-H3 receptor complexes as key targets for reducing cocaine's effects. *J. Neurosci.* **2014**, *3410*, 3545–3558. DOI: 10.1523/JNEUROSCI.4147-13.2014.

133. Moreno-Delgado, D.; Puigdellívol, M.; Moreno, E.; Rodríguez-Ruiz, M.; Botta, J.; Gasperini, P.; Chiarlone, A.; Howell, L. A.; Scarselli, M.; Casadó, V.; Cortés, A.; Ferré, S.; Guzmán, M.; Lluís, C.; Alberch,

J.; Canela, E. I.; Ginés, S.; McCormick, P. J. Modulation of dopamine D1 receptors via histamine H3 receptors is a novel therapeutic target for Huntington's disease. *eLife* **2020**, *9.* DOI: 10.7554/eLife.51093.

134. Portoghese, P. S.; Ronsisvalle, G.; Larson, D. L.; Yim, C. B.; Sayre, L. M.; Takemori, A. E. Opioid agonist and antagonist bivalent ligands as receptor probes. *Life Sciences* **1982**, *3112-13*, 1283–1286. DOI: 10.1016/0024-3205(82)90362-9.

135. Erez, M.; Takemori, A. E.; Portoghese, P. S. Narcotic antagonistic potency of bivalent ligands which contain beta-naltrexamine. Evidence for bridging between proximal recognition sites. *Journal of Medicinal Chemistry* **1982**, *257*, 847–849. DOI: 10.1021/jm00349a016.

136. Portoghese, P. S. Bivalent ligands and the message-address concept in the design of selective opioid receptor antagonists. *Trends in Pharmacological Sciences* **1989**, *106*, 230–235. DOI: 10.1016/0165-6147(89)90267-8.

137. Vauquelin, G.; Bricca, G.; van Liefde, I. Avidity and positive allosteric modulation/cooperativity act hand in hand to increase the residence time of bivalent receptor ligands. *Fundamental & clinical pharmacology* **2014**, *285*, 530–543. DOI: 10.1111/fcp.12052.

138. Huang, B.; St Onge, C. M.; Ma, H.; Zhang, Y. Design of bivalent ligands targeting putative GPCR dimers. *Drug Discovery Today* **2021**, *261*, 189–199. DOI: 10.1016/j.drudis.2020.10.006.

139. Isabelle Berque-Bestel, Frank Lezoualc'h and Ralf Jockers. Bivalent Ligands as Specific Pharmacological Tools for G Protein-Coupled Receptor Dimers. *Current Drug Discovery Technologies* **2008***5*, 312–318. DOI: 10.2174/157016308786733591.

140. Shonberg, J.; Scammells, P. J.; Capuano, B. Design strategies for bivalent ligands targeting GPCRs. *ChemMedChem* **2011**, *66*, 963–974. DOI: 10.1002/cmdc.201100101.

141. Perez, M.; Pauwels, P. J.; Fourrier, C.; Chopin, P.; Valentin, J.-P.; John, G. W.; Marien, M.; Halazy, S. Dimerization of sumatriptan as an efficient way to design a potent, centrally and orally active 5-HT1B agonist. *Bioorganic & Medicinal Chemistry Letters* **1998**, *86*, 675–680. DOI: 10.1016/s0960-894x(98)00090-0.

142. Daniels, D. J.; Lenard, N. R.; Etienne, C. L.; Law, P.-Y.; Roerig, S. C.; Portoghese, P. S. Opioid-induced tolerance and dependence in mice is modulated by the distance between pharmacophores in a bivalent ligand series. *Proc. Natl. Acad. Sci. U.S.A.* **2005**, *10252*, 19208–19213. DOI: 10.1073/pnas.0506627102.

143. Ciruela, F.; Jacobson, K. A.; Fernández-Dueñas, V. Portraying G protein-coupled receptors with fluorescent ligands. *ACS chemical biology* **2014**, *99*, 1918–1928. DOI: 10.1021/cb5004042.

144. Soave, M.; Briddon, S. J.; Hill, S. J.; Stoddart, L. A. Fluorescent ligands: Bringing light to emerging GPCR paradigms. *British Journal of Pharmacology* **2020**, *1775*, 978–991. DOI: 10.1111/bph.14953.

145. Iliopoulos-Tsoutsouvas, C.; Kulkarni, R. N.; Makriyannis, A.; Nikas, S. P. Fluorescent probes for G-protein-coupled receptor drug discovery. *Expert opinion on drug discovery* **2018**, *1310*, 933–947. DOI: 10.1080/17460441.2018.1518975.

146. Vernall, A. J.; Hill, S. J.; Kellam, B. The evolving small-molecule fluorescent-conjugate toolbox for Class A GPCRs. *British Journal of Pharmacology* **2014**, *1715*, 1073–1084. DOI: 10.1111/bph.12265.

147. Stoddart, L. A.; Vernall, A. J.; Bouzo-Lorenzo, M.; Bosma, R.; Kooistra, A. J.; Graaf, C. de; Vischer, H. F.; Leurs, R.; Briddon, S. J.; Kellam, B.; Hill, S. J. Development of novel fluorescent histamine H1-receptor antagonists to study ligand-binding kinetics in living cells. *Sci Rep* **2018**, *81*, 1572. DOI: 10.1038/s41598-018-19714-2.

148. Baker, J. G.; Middleton, R.; Adams, L.; May, L. T.; Briddon, S. J.; Kellam, B.; Hill, S. J. Influence of fluorophore and linker composition on the pharmacology of fluorescent adenosine A1 receptor ligands. *British Journal of Pharmacology* **2010**, *1594*, 772–786. DOI: 10.1111/j.1476-5381.2009.00488.x.

149. Vernall, A. J.; Stoddart, L. A.; Briddon, S. J.; Ng, H. W.; Laughton, C. A.; Doughty, S. W.; Hill, S. J.; Kellam, B. Conversion of a non-selective adenosine receptor antagonist into A3-selective high affinity fluorescent probes using peptide-based linkers. *Organic & Biomolecular Chemistry* **2013**, *1134*, 5673–5682. DOI: 10.1039/C3OB41221K.

150. Borgarelli, C.; Klingl, Y. E.; Escamilla-Ayala, A.; Munck, S.; van den Bosch, L.; Borggraeve, W. M. de; Ismalaj, E. Lighting Up the Plasma Membrane: Development and Applications of Fluorescent Ligands for Transmembrane Proteins. *Chemistry – A European Journal* **2021**, *2734*, 8605–8641. DOI: 10.1002/chem.202100296.

151. Stoddart, L. A.; Kilpatrick, L. E.; Briddon, S. J.; Hill, S. J. Probing the pharmacology of G protein-coupled receptors with fluorescent ligands. *Neuropharmacology* **2015**, *98*, 48–57. DOI: 10.1016/j.neuropharm.2015.04.033.

152. Stoddart, L. A.; Kilpatrick, L. E.; Hill, S. J. NanoBRET Approaches to Study Ligand Binding to GPCRs and RTKs. *Trends in pharmacological sciences* **2018**, *392*, 136–147. DOI: 10.1016/j.tips.2017.10.006.

153. Machleidt, T.; Woodroofe, C. C.; Schwinn, M. K.; Méndez, J.; Robers, M. B.; Zimmerman, K.; Otto, P.; Daniels, D. L.; Kirkland, T. A.; Wood, K. V. NanoBRET--A Novel BRET Platform for the Analysis of Protein-Protein Interactions. *ACS chemical biology* **2015**, *108*, 1797–1804. DOI: 10.1021/acschembio.5b00143.

154. Hall, M. P.; Unch, J.; Binkowski, B. F.; Valley, M. P.; Butler, B. L.; Wood, M. G.; Otto, P.; Zimmerman, K.; Vidugiris, G.; Machleidt, T.; Robers, M. B.; Benink, H. A.; Eggers, C. T.; Slater, M. R.; Meisenheimer, P. L.; Klaubert, D. H.; Fan, F.; Encell, L. P.; Wood, K. V. Engineered luciferase reporter from a deep sea shrimp utilizing a novel imidazopyrazinone substrate. *ACS chemical biology* **2012**, *711*, 1848–1857. DOI: 10.1021/cb3002478.

155. Wang, L.; Frei, M. S.; Salim, A.; Johnsson, K. Small-Molecule Fluorescent Probes for Live-Cell Super-Resolution Microscopy. *Journal of the American Chemical Society* **2019**, *1417*, 2770–2781. DOI: 10.1021/jacs.8b11134.

156. Ma, Z.; Du, L.; Li, M. Toward fluorescent probes for G-protein-coupled receptors (GPCRs). *Journal of Medicinal Chemistry* **2014**, *5720*, 8187–8203. DOI: 10.1021/jm401823z.

157. Rosier, N.; Grätz, L.; Schihada, H.; Möller, J.; Işbilir, A.; Humphrys, L. J.; Nagl, M.; Seibel, U.; Lohse, M. J.; Pockes, S. A Versatile Sub-Nanomolar Fluorescent Ligand Enables NanoBRET Binding Studies and Single-Molecule Microscopy at the Histamine H3 Receptor. *Journal of Medicinal Chemistry* **2021**, *6415*, 11695–11708. DOI: 10.1021/acs.jmedchem.1c01089.

158. Gentzsch, C.; Seier, K.; Drakopoulos, A.; Jobin, M.-L.; Lanoiselée, Y.; Koszegi, Z.; Maurel, D.; Sounier, R.; Hübner, H.; Gmeiner, P.; Granier, S.; Calebiro, D.; Decker, M. Selective and Wash-Resistant Fluorescent Dihydrocodeinone Derivatives Allow Single-Molecule Imaging of μ-Opioid Receptor Dimerization. *Angew. Chem.* **2020**, *13215*, 6014–6020. DOI: 10.1002/ange.201912683.

159. Hippius, H.; Neundörfer, G. The discovery of Alzheimer's disease. *Dialogues in Clinical Neuroscience* **2003**, *51*, 101–108. DOI: 10.31887/DCNS.2003.5.1/hhippius.

160. World Health Organization. Dementia Fact Sheet. https://www.who.int/en/news-room/fact-sheets/detail/dementia (accessed 2022-06-30).

161. Vaz, M.; Silvestre, S. Alzheimer's disease: Recent treatment strategies. *European Journal of Pharmacology* **2020**, *887*, 173554. DOI: 10.1016/j.ejphar.2020.173554.

162. Bejanin, A.; Schonhaut, D. R.; La Joie, R.; Kramer, J. H.; Baker, S. L.; Sosa, N.; Ayakta, N.; Cantwell, A.; Janabi, M.; Lauriola, M.; O'Neil, J. P.; Gorno-Tempini, M. L.; Miller, Z. A.; Rosen, H. J.; Miller, B. L.;

Jagust, W. J.; Rabinovici, G. D. Tau pathology and neurodegeneration contribute to cognitive impairment in Alzheimer's disease. *Brain : a journal of neurology* **2017**, *14012*, 3286–3300. DOI: 10.1093/brain/awx243.

163. Breijyeh, Z.; Karaman, R. Comprehensive Review on Alzheimer's Disease: Causes and Treatment. *Molecules* **2020**, *2524*, 5789. DOI: 10.3390/molecules25245789.

164. Hardy, J. A.; Higgins, G. A. Alzheimer's disease: the amyloid cascade hypothesis. *Science* **1992**, *2565054*, 184–185. DOI: 10.1126/science.1566067.

165. Foroutan, N.; Hopkins, R. B.; Tarride, J.-E.; Florez, I. D.; Levine, M. Safety and efficacy of active and passive immunotherapy in mild-to-moderate Alzheimer's disease: A systematic review and network meta-analysis. *Clinical and investigative medicine. Medecine clinique et experimentale* **2019**, *421*, E53-E65. DOI: 10.25011/cim.v42i1.32393.

166. Dhillon, S. Aducanumab: First Approval. *Drugs* **2021**, *8112*, 1437–1443. DOI: 10.1007/s40265-021-01569-z.

167. Mahase, E. Aducanumab: European agency rejects Alzheimer's drug over efficacy and safety concerns. *BMJ (Clinical research ed.)* **2021**, *375*, n3127. DOI: 10.1136/bmj.n3127.

168. Blennow, K.; Zetterberg, H. Biomarkers for Alzheimer's disease: current status and prospects for the future. *Journal of internal medicine* **2018**, *2846*, 643–663. DOI: 10.1111/joim.12816.

169. Makin, S. The amyloid hypothesis on trial. *Nature* **2018**, *5597715*, S4-S7. DOI: 10.1038/d41586-018-05719-4.

170. Jack, C. R.; Bennett, D. A.; Blennow, K.; Carrillo, M. C.; Feldman, H. H.; Frisoni, G. B.; Hampel, H.; Jagust, W. J.; Johnson, K. A.; Knopman, D. S.; Petersen, R. C.; Scheltens, P.; Sperling, R. A.; Dubois, B. A/T/N: An unbiased descriptive classification scheme for Alzheimer disease biomarkers. *Neurology* **2016**, *875*, 539–547. DOI: 10.1212/WNL.0000000000002923.

171. Kvartsberg, H.; Duits, F. H.; Ingelsson, M.; Andreasen, N.; Öhrfelt, A.; Andersson, K.; Brinkmalm, G.; Lannfelt, L.; Minthon, L.; Hansson, O.; Andreasson, U.; Teunissen, C. E.; Scheltens, P.; van der Flier, W. M.; Zetterberg, H.; Portelius, E.; Blennow, K. Cerebrospinal fluid levels of the synaptic protein neurogranin correlates with cognitive decline in prodromal Alzheimer's disease. *Alzheimer's & dementia : the journal of the Alzheimer's Association* **2015**, *1110*, 1180–1190. DOI: 10.1016/j.jalz.2014.10.009.

172. Uleman, J. F.; Melis, R. J. F.; Quax, R.; van der Zee, E. A.; Thijssen, D.; Dresler, M.; van de Rest, O.; van der Velpen, I. F.; Adams, H. H. H.; Schmand, B.; Kok, I. M. C. M. de; Bresser, J. de; Richard, E.; Verbeek, M.; Hoekstra, A. G.; Rouwette, Etiënne A. J. A.; Olde Rikkert, Marcel G. M. Mapping the multicausality of Alzheimer's disease through group model building. *GeroScience* **2021**, *432*, 829–843. DOI: 10.1007/s11357-020-00228-7.

173. Hiller, C.; Kühhorn, J.; Gmeiner, P. Class A G-protein-coupled receptor (GPCR) dimers and bivalent ligands. *Journal of Medicinal Chemistry* **2013**, *5617*, 6542–6559. DOI: 10.1021/jm4004335.

174. Bourne, J. A. SCH 23390: the first selective dopamine D1-like receptor antagonist. *CNS Drug Reviews* **2001**, *74*, 399–414. DOI: 10.1111/j.1527-3458.2001.tb00207.x.

175. Zhang, J.; Xiong, B.; Zhen, X.; Zhang, A. Dopamine D1 receptor ligands: where are we now and where are we going. *Medicinal research reviews* **2009**, *292*, 272–294. DOI: 10.1002/med.20130.

176. Burnett, D. A.; Greenlee, W. J.; Mckirtrick, B.; Su, J.; Zhu, Z.; Sasikumar, T. K.; Mazzola, R.; Qiang, L.; Ye, Y.; Mckittrick, B. Selective D1/D5 receptor antagonists for the treatment of obesity and CNS disorders. *US2005075325 (A1)*, **2004.**

177. Andersen, P. H.; Jansen, J. A. Dopamine receptor agonists: selectivity and dopamine D1 receptor efficacy. *European Journal of Pharmacology* **1990**, *1886*, 335–347. DOI: 10.1016/0922-4106(90)90194-3.

178. Apodaca, R.; Dvorak, C. A.; Xiao, W.; Barbier, A. J.; Boggs, J. D.; Wilson, S. J.; Lovenberg, T. W.; Carruthers, N. I. A new class of diamine-based human histamine H3 receptor antagonists: 4-(aminoalkoxy)benzylamines. *Journal of Medicinal Chemistry* **2003**, *4618*, 3938–3944. DOI: 10.1021/jm030185v.

179. Wingen, K.; Schwed, J. S.; Isensee, K.; Weizel, L.; Zivković, A.; Odadzic, D.; Odazic, D.; Stark, H. Benzylpiperidine variations on histamine H3 receptor ligands for improved drug-likeness. *Bioorganic & medicinal chemistry letters* **2014**, *2410*, 2236–2239. DOI: 10.1016/j.bmcl.2014.03.098.

180. Zhang, Y.; Gilliam, A.; Maitra, R.; Damaj, M. I.; Tajuba, J. M.; Seltzman, H. H.; Thomas, B. F. Synthesis and biological evaluation of bivalent ligands for the cannabinoid 1 receptor. *Journal of Medicinal Chemistry* **2010**, *5319*, 7048–7060. DOI: 10.1021/jm1006676.

181. LaFrate, A. L.; Carlson, K. E.; Katzenellenbogen, J. A. Steroidal bivalent ligands for the estrogen receptor: design, synthesis, characterization and binding affinities. *Bioorganic & medicinal chemistry* **2009**, *1710*, 3528–3535. DOI: 10.1016/j.bmc.2009.04.016.

182. Karellas, P.; McNaughton, M.; Baker, S. P.; Scammells, P. J. Synthesis of bivalent beta2-adrenergic and adenosine A1 receptor ligands. *Journal of Medicinal Chemistry* **2008**, *5119*, 6128–6137. DOI: 10.1021/jm800613s.

183. Bonger, K. M.; van den Berg, R. J. B. H. N.; Knijnenburg, A. D.; Heitman, L. H.; van Koppen, C. J.; Timmers, C. M.; Overkleeft, H. S.; van der Marel, G. A. Discovery of selective luteinizing hormone receptor agonists using the bivalent ligand method. *ChemMedChem* **2009**, *47*, 1189–1195. DOI: 10.1002/cmdc.200900058.

184. Hein, C. D.; Liu, X.-M.; Wang, D. Click chemistry, a powerful tool for pharmaceutical sciences. *Pharmaceutical research* **2008**, *2510*, 2216–2230. DOI: 10.1007/s11095-008-9616-1.

185. Neumeyer, J. L.; Baindur, N.; Niznik, H. B.; Guan, H. C.; Seeman, P. (+/-)-3-Allyl-6-bromo-7,8-dihydroxy-1-phenyl-2,3,4,5-tetrahydro-1H-3- benzazepin, a new high-affinity D1 dopamine receptor ligand: synthesis and structure-activity relationship. *Journal of Medicinal Chemistry* **1991**, *3412*, 3366–3371. DOI: 10.1021/jm00116a004.

186. Shen, J.; Zhang, L.; Song, W.; Meng, T.; Wang, X.; Chen, L.; Feng, L.; Xu, Y.; Shen, J. Design, synthesis and biological evaluation of bivalent ligands against A(1)-D(1) receptor heteromers. *Acta pharmacologica Sinica* **2013**, *343*, 441–452. DOI: 10.1038/aps.2012.151.

187. Yang, Z.; Xu, J. Convenient and Environment-Friendly Synthesis of Sulfonyl Chlorides from S-Alkylisothiourea Salts via N-Chlorosuccinimide Chlorosulfonation. *Synthesis* **2013**, *4512*, 1675–1682. DOI: 10.1055/s-0033-1338743.

188. Wingen, K.; Stark, H. Scaffold variations in amine warhead of histamine H_3 receptor antagonists. *Drug Discovery Today: Technologies* **2013**, *104*, e483-9. DOI: 10.1016/j.ddtec.2013.07.001.

189. Kitbunnadaj, R.; Zuiderveld, O. P.; Esch, I. J. P. de; Vollinga, R. C.; Bakker, R.; Lutz, M.; Spek, A. L.; Cavoy, E.; Deltent, M.-F.; Menge, W. M. P. B.; Timmerman, H.; Leurs, R. Synthesis and structure-activity relationships of conformationally constrained histamine H(3) receptor agonists. *Journal of Medicinal Chemistry* **2003**, *4625*, 5445–5457. DOI: 10.1021/jm030905y.

190. Kitbunnadaj, R.; Zuiderveld, O. P.; Christophe, B.; Hulscher, S.; Menge, W. M. P. B.; Gelens, E.; Snip, E.; Bakker, R. A.; Celanire, S.; Gillard, M.; Talaga, P.; Timmerman, H.; Leurs, R. Identification of 4-(1H-imidazol-4(5)-ylmethyl)pyridine (immethridine) as a novel, potent, and highly selective histamine H(3) receptor agonist. *Journal of Medicinal Chemistry* **2004**, *4710*, 2414–2417. DOI: 10.1021/jm049932u.

191. Coombs, J. R.; Zhang, L.; Morken, J. P. Enantiomerically enriched tris(boronates): readily accessible conjunctive reagents for asymmetric synthesis. *J. Am. Chem. Soc.* **2014**, *13646*, 16140–16143. DOI: 10.1021/ja510081r.

192. Neuhaus, D. Nuclear Overhauser Effect. eMagRes; *John Wiley & Sons, Ltd*, Hoboken, New Jersey, **2011.** DOI: 10.1002/9780470034590.emrstm0350.pub2.

193. Friebolin, H. Ein- und zweidimensionale NMR-Spektroskopie - Eine Einführung. 5. Auflage; *Wiley-VCH*, Weinheim, **2013**.

194. Ansari, S. M.; Robien, W.; Schlederer, M.; Wolschann, P. 1H-NMR investigations of the conformation of aryl-(hydroxynaphthyl)-methylpiperidines. Intramolecular interactions, IV. *Monatsh Chem* **1989**, *12011*, 1003–1014. DOI: 10.1007/BF00808772.

195. Iyer, S. S.; Anderson, A. S.; Reed, S.; Swanson, B.; Schmidt, J. G. Synthesis of orthogonal end functionalized oligoethylene glycols of defined lengths. *Tetrahedron Letters* **2004**, *4522*, 4285–4288. DOI: 10.1016/j.tetlet.2004.04.004.

196. Cogé, F.; Guénin, S. P.; Audinot, V.; Renouard-Try, A.; Beauverger, P.; Macia, C.; Ouvry, C.; Nagel, N.; Rique, H.; Boutin, J. A.; Galizzi, J. P. Genomic organization and characterization of splice variants of the human histamine H3 receptor. *Biochem J* **2001**, *355Pt 2*, 279–288. DOI: 10.1042/0264-6021:3550279.

197. Liu, C.; Ma, X.; Jiang, X.; Wilson, S. J.; Hofstra, C. L.; Blevitt, J.; Pyati, J.; Li, X.; Chai, W.; Carruthers, N.; Lovenberg, T. W. Cloning and pharmacological characterization of a fourth histamine receptor (H(4)) expressed in bone marrow. *Molecular pharmacology* **2001**, *593*, 420–426. DOI: 10.1124/mol.59.3.420.

198. Sedaghat Doost, A.; Akbari, M.; Stevens, C. V.; Setiowati, A. D.; van der Meeren, P. A review on nuclear overhauser enhancement (NOE) and rotating-frame overhauser effect (ROE) NMR techniques in food science: Basic principles and applications. *Trends in Food Science & Technology* **2019**, *86*, 16–24. DOI: 10.1016/j.tifs.2019.02.001.

199. Sandström, C.; Kenne, L. Hydroxy Protons in Structural Studies of Carbohydrates by NMR Spectroscopy. In *ACS Symposium Series*; American Chemical Society, **2006**; pp 114–132. DOI: 10.1021/bk-2006-0930.ch006.

200. Čuperlović-Culf, M. NMR metabolomics in cancer research. Woodhead Publishing series in biomedicine, Vol. 63; *Woodhead Publ*, Oxford, **2013**.

201. Forster, L.; Grätz, L.; Mönnich, D.; Bernhardt, G.; Pockes, S. A Split Luciferase Complementation Assay for the Quantification of β-Arrestin2 Recruitment to Dopamine D2-Like Receptors. *International journal of molecular sciences* **2020**, *2117.* DOI: 10.3390/ijms21176103.

202. Bartole, E.; Grätz, L.; Littmann, T.; Wifling, D.; Seibel, U.; Buschauer, A.; Bernhardt, G. UR-DEBa242: A Py-5-Labeled Fluorescent Multipurpose Probe for Investigations on the Histamine H3 and H4 Receptors. *Journal of Medicinal Chemistry* **2020**, *6310*, 5297–5311. DOI: 10.1021/acs.jmedchem.0c00160.

203. Igel, P.; Schnell, D.; Bernhardt, G.; Seifert, R.; Buschauer, A. Tritium-labeled N(1)-3-(1H-imidazol-4-yl)propyl-N(2)-propionylguanidine ((3)HUR-PI294), a high-affinity histamine H(3) and H(4) receptor radioligand. *ChemMedChem* **2009**, *42*, 225–231. DOI: 10.1002/cmdc.200800349.

204. Sunahara, R. K.; Guan, H. C.; O'Dowd, B. F.; Seeman, P.; Laurier, L. G.; Ng, G.; George, S. R.; Torchia, J.; van Tol, H. H.; Niznik, H. B. Cloning of the gene for a human dopamine D5 receptor with higher affinity for dopamine than D1. *Nature* **1991**, *3506319*, 614–619. DOI: 10.1038/350614a0.

205. Tropmann, K.; Bresinsky, M.; Forster, L.; Mönnich, D.; Buschauer, A.; Wittmann, H.-J.; Hübner, H.; Gmeiner, P.; Pockes, S.; Strasser, A. Abolishing Dopamine D2long/D3 Receptor Affinity of Subtype-Selective Carbamoylguanidine-Type Histamine H2 Receptor Agonists. *Journal of Medicinal Chemistry* **2021**, *6412*, 8684–8709. DOI: 10.1021/acs.jmedchem.1c00692.

206. Baumeister, P.; Erdmann, D.; Biselli, S.; Kagermeier, N.; Elz, S.; Bernhardt, G.; Buschauer, A. (3) HUR-DE257: development of a tritium-labeled squaramide-type selective histamine H2 receptor antagonist. *ChemMedChem* **2015**, *101*, 83–93. DOI: 10.1002/cmdc.201402344.

207. Ishikawa, M.; Shinei, R.; Yokoyama, F.; Yamauchi, M.; Oyama, M.; Okuma, K.; Nagayama, T.; Kato, K.; Kakui, N.; Sato, Y. Role of hydrophobic substituents on the terminal nitrogen of histamine in receptor binding and agonist activity: development of an orally active histamine type 3 receptor agonist and evaluation of its antistress activity in mice. *Journal of Medicinal Chemistry* **2010**, *539*, 3840–3844. DOI: 10.1021/jm901890s.

208. Igel, P.; Dove, S.; Buschauer, A. Histamine H4 receptor agonists. *Bioorganic & medicinal chemistry letters* **2010**, *2024*, 7191–7199. DOI: 10.1016/j.bmcl.2010.10.041.

209. Garbarg, M.; Arrang, J. M.; Rouleau, A.; Ligneau, X.; Tuong, M. D.; Schwartz, J. C.; Ganellin, C. R. S-2-(4-imidazolyl)ethylisothiourea, a highly specific and potent histamine H3 receptor agonist. *The Journal of pharmacology and experimental therapeutics* **1992**, *2631*, 304–310.

210. Seamon, K. B.; Padgett, W.; Daly, J. W. Forskolin: unique diterpene activator of adenylate cyclase in membranes and in intact cells. *Proc. Natl. Acad. Sci. U.S.A.* **1981**, *786*, 3363–3367. DOI: 10.1073/pnas.78.6.3363.

211. Insel, P. A.; Ostrom, R. S. Forskolin as a tool for examining adenylyl cyclase expression, regulation, and G protein signaling. *Cellular and molecular neurobiology* **2003**, *233*, 305–314. DOI: 10.1023/a:1023684503883.

212. Baldwin, T. A.; Li, Y.; Brand, C. S.; Watts, V. J.; Dessauer, C. W. Insights into the Regulatory Properties of Human Adenylyl Cyclase Type 9. *Mol Pharmacol* **2019**, *954*, 349–360. DOI: 10.1124/mol.118.114595.

213. Ostrom, K. F.; LaVigne, J. E.; Brust, T. F.; Seifert, R.; Dessauer, C. W.; Watts, V. J.; Ostrom, R. S. Physiological roles of mammalian transmembrane adenylyl cyclase isoforms. *Physiological Reviews* **2022**, *1022*, 815–857. DOI: 10.1152/physrev.00013.2021.

214. Chen, J.; Iyengar, R. Inhibition of cloned adenylyl cyclases by mutant-activated Gi-alpha and specific suppression of type 2 adenylyl cyclase inhibition by phorbol ester treatment. *Journal of Biological Chemistry* **1993**, *26817*, 12253–12256. DOI: 10.1016/S0021-9258(18)31381-4.

215. Federman, A. D.; Conklin, B. R.; Schrader, K. A.; Reed, R. R.; Bourne, H. R. Hormonal stimulation of adenylyl cyclase through Gi-protein beta gamma subunits. *Nature* **1992**, *3566365*, 159–161. DOI: 10.1038/356159a0.

216. Drakopoulos, A.; Decker, M. Development and Biological Applications of Fluorescent Opioid Ligands. *ChemPlusChem* **2020**, *856*, 1354–1364. DOI: 10.1002/cplu.202000212.

217. Monsma, F. J.; Barton, A. C.; Kang, H. C.; Brassard, D. L.; Haugland, R. P.; Sibley, D. R. Characterization of novel fluorescent ligands with high affinity for D1 and D2 dopaminergic receptors. *Journal of Neurochemistry* **1989**, *525*, 1641–1644. DOI: 10.1111/j.1471-4159.1989.tb09220.x.

218. Kshirsagar, T.; Nakano, A. H.; Law, P.-Y.; Elde, R.; Portoghese, P. S. NTI4F: a non-peptide fluorescent probe selective for functional delta opioid receptors. *Neuroscience Letters* **1998**, *2492-3*, 83–86. DOI: 10.1016/S0304-3940(98)00379-6.

219. Grätz, L.; Tropmann, K.; Bresinsky, M.; Müller, C.; Bernhardt, G.; Pockes, S. NanoBRET binding assay for histamine H2 receptor ligands using live recombinant HEK293T cells. *Sci Rep* **2020**, *101*, 13288. DOI: 10.1038/s41598-020-70332-3.

220. Stoddart, L. A.; Johnstone, E. K. M.; Wheal, A. J.; Goulding, J.; Robers, M. B.; Machleidt, T.; Wood, K. V.; Hill, S. J.; Pfleger, K. D. G. Application of BRET to monitor ligand binding to GPCRs. *Nat Methods* **2015**, *127*, 661–663. DOI: 10.1038/nmeth.3398.

221. Laasfeld, T.; Ehrminger, R.; Tahk, M.-J.; Veiksina, S.; Kõlvart, K. R.; Min, M.; Kopanchuk, S.; Rinken, A. Budded baculoviruses as a receptor display system to quantify ligand binding with TIRF microscopy. *Nanoscale* **2021**, *134*, 2436–2447. DOI: 10.1039/d0nr06737g.

222. Rüttinger, S.; Lamarre, B.; Knight, A. E. Single molecule genotyping by TIRF microscopy. *Journal of fluorescence* **2008**, *185*, 1021–1026. DOI: 10.1007/s10895-008-0386-2.

223. Ticau, S.; Friedman, L. J.; Ivica, N. A.; Gelles, J.; Bell, S. P. Single-molecule studies of origin licensing reveal mechanisms ensuring bidirectional helicase loading. *Cell* **2015**, *1613*, 513–525. DOI: 10.1016/j.cell.2015.03.012.

224. Qiu, B.; Simon, M. C. BODIPY 493/503 Staining of Neutral Lipid Droplets for Microscopy and Quantification by Flow Cytometry. *Bio-protocol* **2016**, *617.* DOI: 10.21769/BioProtoc.1912.

225. Keller, M.; Erdmann, D.; Pop, N.; Pluym, N.; Teng, S.; Bernhardt, G.; Buschauer, A. Red-fluorescent argininamide-type NPY Y1 receptor antagonists as pharmacological tools. *Bioorganic & medicinal chemistry* **2011**, *199*, 2859–2878. DOI: 10.1016/j.bmc.2011.03.045.

226. Schihada, H.; Shekhani, R.; Schulte, G. Quantitative assessment of constitutive G protein-coupled receptor activity with BRET-based G protein biosensors. *Science signaling* **2021**, *14699*, eabf1653. DOI: 10.1126/scisignal.abf1653.

227. Lichtman, J. W.; Conchello, J.-A. Fluorescence microscopy. *Nat Methods* **2005**, *212*, 910–919. DOI: 10.1038/nmeth817.

228. Im, K.; Mareninov, S.; Diaz, M. F. P.; Yong, W. H. An Introduction to Performing Immunofluorescence Staining. In *Biobanking*; Humana Press, New York, NY, **2019**; pp 299–311. DOI: 10.1007/978-1-4939-8935-5_26.

229. Yuste, R. Fluorescence microscopy today. *Nat Methods* **2005**, *212*, 902–904. DOI: 10.1038/nmeth1205-902.

230. Sanderson, M. J.; Smith, I.; Parker, I.; Bootman, M. D. Fluorescence microscopy. *Cold Spring Harbor protocols* **2014**, *201410*, pdb.top071795. DOI: 10.1101/pdb.top071795.

231. Smith, C. L. Basic confocal microscopy. *Current protocols in neuroscience* **2011**, *56*, Chapter 2.2.1–2.2.18. DOI: 10.1002/0471142301.ns0202s56.

232. Windaus, A.; Vogt, W. Synthese des Imidazolyl-äthylamins. *Ber. Dtsch. Chem. Ges.* **1907**, *403*, 3691–3695. DOI: 10.1002/cber.190704003164.

233. Garbarg, M., Arrang, J. M., Rouleau, A., Ligneau, X., Tuong, M. D., Schwartz, J. C., & Ganellin, C. D. S-[2-(4-imidazolyl) ethyl] isothiourea, a highly specific and potent histamine H3 receptor agonist. *Journal of Pharmacology and Experimental Therapeutics* **1992**, *1263*, 304–310.

234. van der Goot, H.; Schepers, M. J.; Sterk, G. J.; Timmerman, H. Isothiourea analogues of histamine as potent agonists or antagonists of the histamine H3-receptor. *European Journal of Medicinal Chemistry* **1992**, *275*, 511–517. DOI: 10.1016/0223-5234(92)90185-4.

235. Schaller, D.; Hagenow, S.; Stark, H.; Wolber, G. Ligand-guided homology modeling drives identification of novel histamine H3 receptor ligands. *PLOS ONE* **2019**, *146*, e0218820. DOI: 10.1371/journal.pone.0218820.

236. Ligneau, X.; Perrin, D.; Landais, L.; Camelin, J.-C.; Calmels, T. P. G.; Berrebi-Bertrand, I.; Lecomte, J.-M.; Parmentier, R.; Anaclet, C.; Lin, J.-S.; Bertaina-Anglade, V.; La Rochelle, C. D.; d'Aniello, F.; Rouleau, A.; Gbahou, F.; Arrang, J.-M.; Ganellin, C. R.; Stark, H.; Schunack, W.; Schwartz, J.-C. BF2.649 1-{3-3-(4-Chlorophenyl)propoxypropyl}piperidine, hydrochloride, a nonimidazole inverse agonist/antagonist at the human histamine H3 receptor: Preclinical pharmacology. *The Journal of pharmacology and experimental therapeutics* **2007**, *3201*, 365–375. DOI: 10.1124/jpet.106.111039.

237. Schihada, H.; Ma, X.; Zabel, U.; Vischer, H. F.; Schulte, G.; Leurs, R.; Pockes, S.; Lohse, M. J. Development of a Conformational Histamine H3 Receptor Biosensor for the Synchronous Screening of Agonists and Inverse Agonists. *ACS Sensors* **2020**, *56*, 1734–1742. DOI: 10.1021/acssensors.0c00397.

238. Wulff, B. S.; Hastrup, S.; Rimvall, K. Characteristics of recombinantly expressed rat and human histamine H3 receptors. *European Journal of Pharmacology* **2002**, *4531*, 33–41. DOI: 10.1016/s0014-2999(02)02382-8.

239. Lim, H. D.; van Rijn, R. M.; Ling, P.; Bakker, R. A.; Thurmond, R. L.; Leurs, R. Evaluation of histamine H1-, H2-, and H3-receptor ligands at the human histamine H4 receptor: identification of 4-methylhistamine as the first potent and selective H4 receptor agonist. *The Journal of pharmacology and experimental therapeutics* **2005**, *3143*, 1310–1321. DOI: 10.1124/jpet.105.087965.

240. Mocking, T. A. M.; Verweij, E. W. E.; Vischer, H. F.; Leurs, R. Homogeneous, Real-Time NanoBRET Binding Assays for the Histamine H3 and H4 Receptors on Living Cells. *Mol Pharmacol* **2018**, *946*, 1371–1381. DOI: 10.1124/mol.118.113373.

241. Pockes, S.; Wifling, D.; Keller, M.; Buschauer, A.; Elz, S. Highly Potent, Stable, and Selective Dimeric Hetarylpropylguanidine-Type Histamine H2 Receptor Agonists. *ACS Omega* **2018**, *33*, 2865–2882. DOI: 10.1021/acsomega.8b00128.

242. Sungkaworn, T.; Jobin, M.-L.; Burnecki, K.; Weron, A.; Lohse, M. J.; Calebiro, D. Single-molecule imaging reveals receptor-G protein interactions at cell surface hot spots. *Nature* **2017**, *5507677*, 543–547. DOI: 10.1038/nature24264.

243. Möller, J.; Isbilir, A.; Sungkaworn, T.; Osberg, B.; Karathanasis, C.; Sunkara, V.; Grushevskyi, E. O.; Bock, A.; Annibale, P.; Heilemann, M.; Schütte, C.; Lohse, M. J. Single-molecule analysis reveals agonist-specific dimer formation of μ-opioid receptors. *Nature chemical biology* **2020**, *169*, 946–954. DOI: 10.1038/s41589-020-0566-1.

244. Allikalt, A.; Purkayastha, N.; Flad, K.; Schmidt, M. F.; Tabor, A.; Gmeiner, P.; Hübner, H.; Weikert, D. Fluorescent ligands for dopamine D2/D3 receptors. *Sci Rep* **2020**, *101*, 21842. DOI: 10.1038/s41598-020-78827-9.

245. Grätz, L.; Laasfeld, T.; Allikalt, A.; Gruber, C. G.; Pegoli, A.; Tahk, M.-J.; Tsernant, M.-L.; Keller, M.; Rinken, A. BRET- and fluorescence anisotropy-based assays for real-time monitoring of ligand binding to M2 muscarinic acetylcholine receptors. *Biochimica et biophysica acta. Molecular cell research* **2021**, *18683*, 118930. DOI: 10.1016/j.bbamcr.2020.118930.

246. Kozielewicz, P.; Bowin, C.-F.; Turku, A.; Schulte, G. A NanoBRET-Based Binding Assay for Smoothened Allows Real-time Analysis of Ligand Binding and Distinction of Two Binding Sites for BODIPY-cyclopamine. *Mol Pharmacol* **2020**, *971*, 23–34. DOI: 10.1124/mol.119.118158.

247. Soave, M.; Stoddart, L. A.; Brown, A.; Woolard, J.; Hill, S. J. Use of a new proximity assay (NanoBRET) to investigate the ligand-binding characteristics of three fluorescent ligands to the human β1-adrenoceptor expressed in HEK-293 cells. *Pharmacology research & perspectives* **2016**, *45*, e00250. DOI: 10.1002/prp2.250.

248. Staszewski, M.; Nelic, D.; Jończyk, J.; Dubiel, M.; Frank, A.; Stark, H.; Bajda, M.; Jakubik, J.; Walczyński, K. Guanidine Derivatives: How Simple Structural Modification of Histamine H3R

Antagonists Has Led to the Discovery of Potent Muscarinic M2R/M4R Antagonists. *ACS chemical neuroscience* **2021**, *1213*, 2503–2519. DOI: 10.1021/acschemneuro.1c00237.

249. Pándy-Szekeres, G.; Munk, C.; Tsonkov, T. M.; Mordalski, S.; Harpsøe, K.; Hauser, A. S.; Bojarski, A. J.; Gloriam, D. E. GPCRdb in 2018: adding GPCR structure models and ligands. *Nucleic acids research* **2018**, *46D1*, D440-D446. DOI: 10.1093/nar/gkx1109.

250. Borzęcka, W.; Lavandera, I.; Gotor, V. Synthesis of enantiopure fluorohydrins using alcohol dehydrogenases at high substrate concentrations. *The Journal of organic chemistry* **2013**, *7814*, 7312–7317. DOI: 10.1021/jo400962c.

251. Wierenga, W.; Harrison, A. W.; Evans, B. R.; Chidester, C. G. Antibacterial benzisoxazolones. An unusual rearrangement product from o-nitrostyrene oxide en route to the photolabile carbonyl protecting group, (o-nitrophenyl)ethylene glycol. *J. Org. Chem.* **1984**, *493*, 438–442. DOI: 10.1021/jo00177a010.

252. Guss, C. O.; Mautner, H. G. The reaction of p-nitrostyrene oxide with phenol. *J. Org. Chem.* **1951**, *166*, 887–891. DOI: 10.1021/jo01146a009.

253. Sterling, J.; Herzig, Y.; Goren, T.; Finkelstein, N.; Lerner, D.; Goldenberg, W.; Miskolczi, I.; Molnar, S.; Rantal, F.; Tamas, T.; Toth, G.; Zagyva, A.; Zekany, A.; Finberg, J.; Lavian, G.; Gross, A.; Friedman, R.; Razin, M.; Huang, W.; Krais, B.; Chorev, M.; Youdim, M. B.; Weinstock, M. Novel dual inhibitors of AChE and MAO derived from hydroxy aminoindan and phenethylamine as potential treatment for Alzheimer's disease. *Journal of Medicinal Chemistry* **2002**, *4524*, 5260–5279. DOI: 10.1021/jm020120c.

254. Moreno, L.; Párraga, J.; Galán, A.; Cabedo, N.; Primo, J.; Cortes, D. Synthesis of new antimicrobial pyrrolo2,1-aisoquinolin-3-ones. *Bioorganic & medicinal chemistry* **2012**, *2022*, 6589–6597. DOI: 10.1016/j.bmc.2012.09.033.

255. Bower, J. F.; Szeto, P.; Gallagher, T. Cyclic sulfamidates as lactam precursors. An efficient asymmetric synthesis of (-)-aphanorphine. *Chemical communications (Cambridge, England)* **2005***46*, 5793–5795. DOI: 10.1039/b510761j.

256. Toste, F. D.; Still, I. W. J. A New Route to the Synthesis of the Naturally Occurring Benzopentathiepin Varacin. *J. Am. Chem. Soc.* **1995**, *11727*, 7261–7262. DOI: 10.1021/ja00132a033.

257. Vergara, J.; Gimeno, N.; Cano, M.; Barberá, J.; Romero, P.; Serrano, J. L.; Ros, M. B. Mesomorphism from Bent-Core Based Ionic Dendritic Macromolecules. *Chem. Mater.* **2011**, *2322*, 4931–4940. DOI: 10.1021/cm201809r.

258. Watkins, C. J.; Romero, M. M. R.; Moore, K. G.; Ritchie, J.; Finn, P. W.; Kalvinsh, I.; Loza, E.; Dikovska, K.; Gailite, V.; Vorona, M.; Piskunova, I.; Starchenkov, I.; Adrianov, V.; Harris, C. J.; Duffy, J. E. S. Carbamic acid compounds compromising a sulfonamide linkage as HDAC inhibitors. *WO0230879 (A2)*, **2001.**

259. Kitbunnadaj, R.; Hashimoto, T.; Poli, E.; Zuiderveld, O. P.; Menozzi, A.; Hidaka, R.; Esch, I. J. P. de; Bakker, R. A.; Menge, W. M. P. B.; Yamatodani, A.; Coruzzi, G.; Timmerman, H.; Leurs, R. N-substituted piperidinyl alkyl imidazoles: discovery of methimepip as a potent and selective histamine H3 receptor agonist. *Journal of Medicinal Chemistry* **2005**, *486*, 2100–2107. DOI: 10.1021/jm049475h.

260. Andrus, M.; Turner, T.; Prince, J. Multiple drug resistance reversal agent. *WO0160387 (A1)*, **2001.**

261. Newman, M. S.; Barbee, T. G.; Blakesley, C. N.; Zia-ud-Din; Gromelski, S.; Khanna, V. K.; Lee, L.-F.; Radhakrishnan, J.; Robey, R. L. High-dilution cyclization of polyoxapentacosanodinitriles. *J. Org. Chem.* **1975**, *4020*, 2863–2870. DOI: 10.1021/jo00908a003.

262. Merz, A.; Karl, A.; Futterer, T.; Stacherdinger, N.; Schneider, O.; Lex, J.; Luboch, E.; Biernat, J. F. Syntheses and Reactions of Crown Ether-Bridged Stilbenes. *Liebigs Ann. Chem.* **1994**, *199412*, 1199–1209. DOI: 10.1002/jlac.199419941211.

263. Gansow, O. A.; Kausar, A. R.; Triplett, K. B. Synthesis and characterization of some bifunctional 2b:2:1 cryptands. *Journal of Heterocyclic Chemistry* **1981**, *182*, 297–302. DOI: 10.1002/jhet.5570180214.

264. Bonger, K. M.; van den Berg, R. J. B. H. N.; Heitman, L. H.; IJzerman, A. P.; Oosterom, J.; Timmers, C. M.; Overkleeft, H. S.; van der Marel, G. A. Synthesis and evaluation of homo-bivalent GnRHR ligands. *Bioorganic & Medicinal Chemistry* **2007**, *1514*, 4841–4856. DOI: 10.1016/j.bmc.2007.04.065.

265. Thomas, J. R.; Liu, X.; Hergenrother, P. J. Size-specific ligands for RNA hairpin loops. *J. Am. Chem. Soc.* **2005**, *12736*, 12434–12435. DOI: 10.1021/ja051685b.

266. Roe, S.; Gunaratnam, M.; Spiteri, C.; Sharma, P.; Alharthy, R. D.; Neidle, S.; Moses, J. E. Synthesis and biological evaluation of hybrid acridine-HSP90 ligand conjugates as telomerase inhibitors. *Organic & Biomolecular Chemistry* **2015**, *1331*, 8500–8504. DOI: 10.1039/c5ob01177a.

267. Romuald, C.; Cazals, G.; Enjalbal, C.; Coutrot, F. Straightforward synthesis of a double-lasso macrocycle from a nonsymmetrical c2daisy chain. *Organic letters* **2013**, *151*, 184–187. DOI: 10.1021/ol303186j.

268. Bai, S.; Li, S.; Xu, J.; Peng, X.; Sai, K.; Chu, W.; Tu, Z.; Zeng, C.; Mach, R. H. Synthesis and structure-activity relationship studies of conformationally flexible tetrahydroisoquinolinyl triazole carboxamide and triazole substituted benzamide analogues as σ2 receptor ligands. *Journal of Medicinal Chemistry* **2014**, *5710*, 4239–4251. DOI: 10.1021/jm5001453.

269. Lehn, J. M.; Skene, W. G. Dynamers: polymeric materials exhibiting reversible formation and component exchange. *WO2004003044 (A2)*, **2003.**

270. van Wandelen, L. T. M.; van Ameijde, J.; Mady, A. S. A.; Wammes, A. E. M.; Bode, A.; Poot, A. J.; Ruijtenbeek, R.; Liskamp, R. M. J. Directed modulation of protein kinase C isozyme selectivity with bisubstrate-based inhibitors. *ChemMedChem* **2012**, *712*, 2113–2121. DOI: 10.1002/cmdc.201200349.

271. Yung-Chi, C.; Prusoff, W. H. Relationship between the inhibition constant (KI) and the concentration of inhibitor which causes 50 per cent inhibition (I50) of an enzymatic reaction. *Biochemical pharmacology* **1973**, *2223*, 3099–3108. DOI: 10.1016/0006-2952(73)90196-2.

272. Franco, R.; Reyes-Resina, I.; Aguinaga, D.; Lillo, A.; Jiménez, J.; Raïch, I.; Borroto-Escuela, D. O.; Ferreiro-Vera, C.; Canela, E. I.; Sánchez de Medina, V.; Del Ser-Badia, A.; Fuxe, K.; Saura, C. A.; Navarro, G. Potentiation of cannabinoid signaling in microglia by adenosine A2A receptor antagonists. *Glia* **2019**, *6712*, 2410–2423. DOI: 10.1002/glia.23694.

273. Navarro, G.; Borroto-Escuela, D. O.; Fuxe, K.; Franco, R. Purinergic signaling in Parkinson's disease. Relevance for treatment. *Neuropharmacology* **2016**, *104*, 161–168. DOI: 10.1016/j.neuropharm.2015.07.024.

274. Lillo, J.; Lillo, A.; Zafra, D. A.; Miralpeix, C.; Rivas-Santisteban, R.; Casals, N.; Navarro, G.; Franco, R. Identification of the Ghrelin and Cannabinoid CB2 Receptor Heteromer Functionality and Marked Upregulation in Striatal Neurons from Offspring of Mice under a High-Fat Diet. *International journal of molecular sciences* **2021**, *2216.* DOI: 10.3390/ijms22168928.

275. Schindelin, J.; Arganda-Carreras, I.; Frise, E.; Kaynig, V.; Longair, M.; Pietzsch, T.; Preibisch, S.; Rueden, C.; Saalfeld, S.; Schmid, B.; Tinevez, J.-Y.; White, D. J.; Hartenstein, V.; Eliceiri, K.; Tomancak, P.; Cardona, A. Fiji: an open-source platform for biological-image analysis. *Nat Methods* **2012**, *97*, 676–682. DOI: 10.1038/nmeth.2019.

276. Jaqaman, K.; Loerke, D.; Mettlen, M.; Kuwata, H.; Grinstein, S.; Schmid, S. L.; Danuser, G. Robust single-particle tracking in live-cell time-lapse sequences. *Nat Methods* **2008**, *58*, 695–702. DOI: 10.1038/nmeth.1237.

8. Appendix

8.1 HPLC purity and stability analyses

The HPLC purity and stability runs are presented as follows. 0 min describes the purity control from a sample taken directly after purification by preparative HPLC. Stability controls were conducted with samples from the stock solutions that were prepared for pharmacological assays. Therefore, some of them display a DMSO peak after approximately 3 min and the peak intensity differs from the purity sample. Retention time t_R is given in minutes. Following abbreviations were used: h (hours), min (minutes), d (days), m (months). Differences in intensities are caused by the HPLC injector and don't indicate decomposition of the compounds, as no change in retention time or additional peaks were detected.

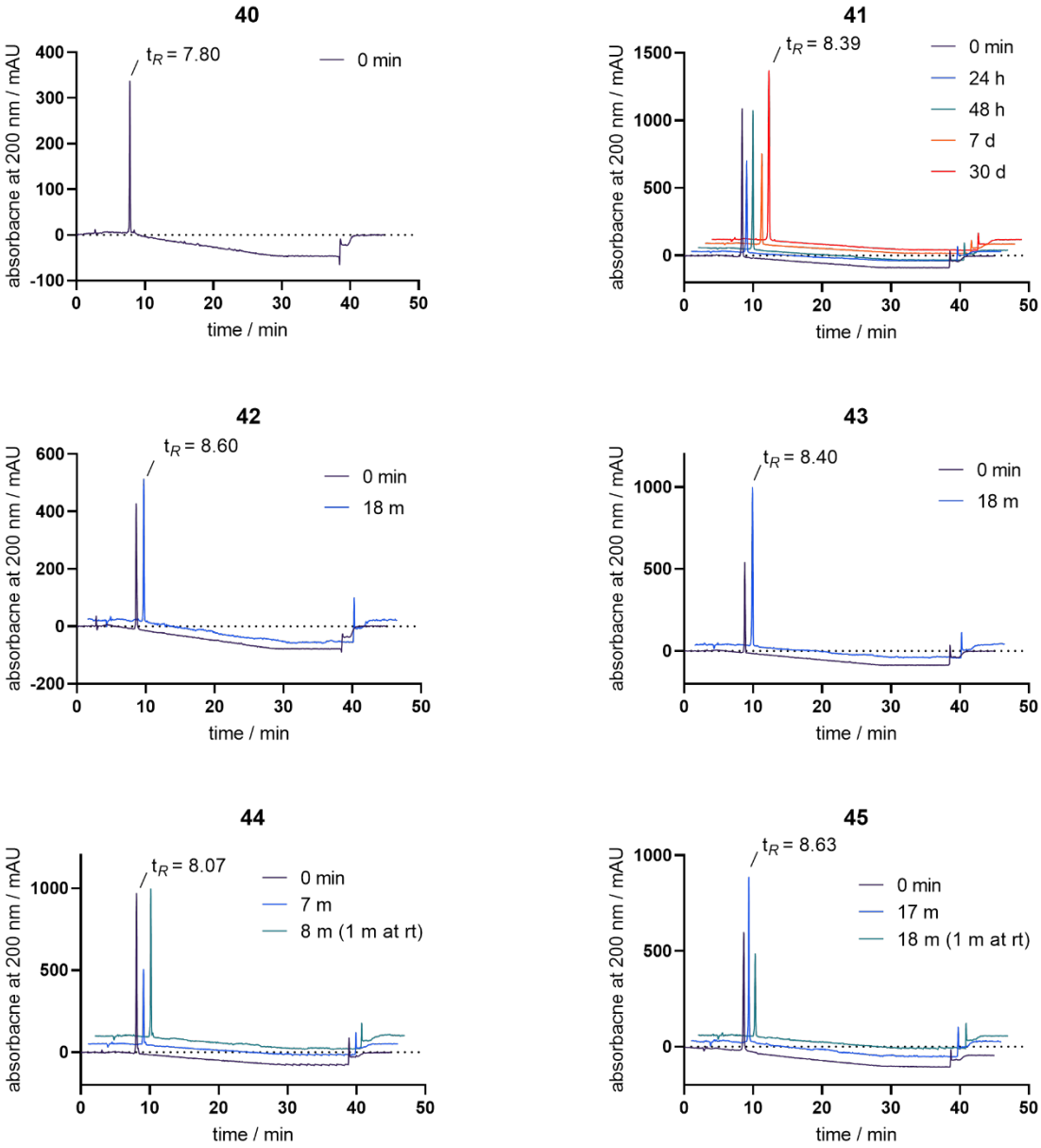

Figure 8.1: HPLC stability and purity controls of compounds **40-45**.

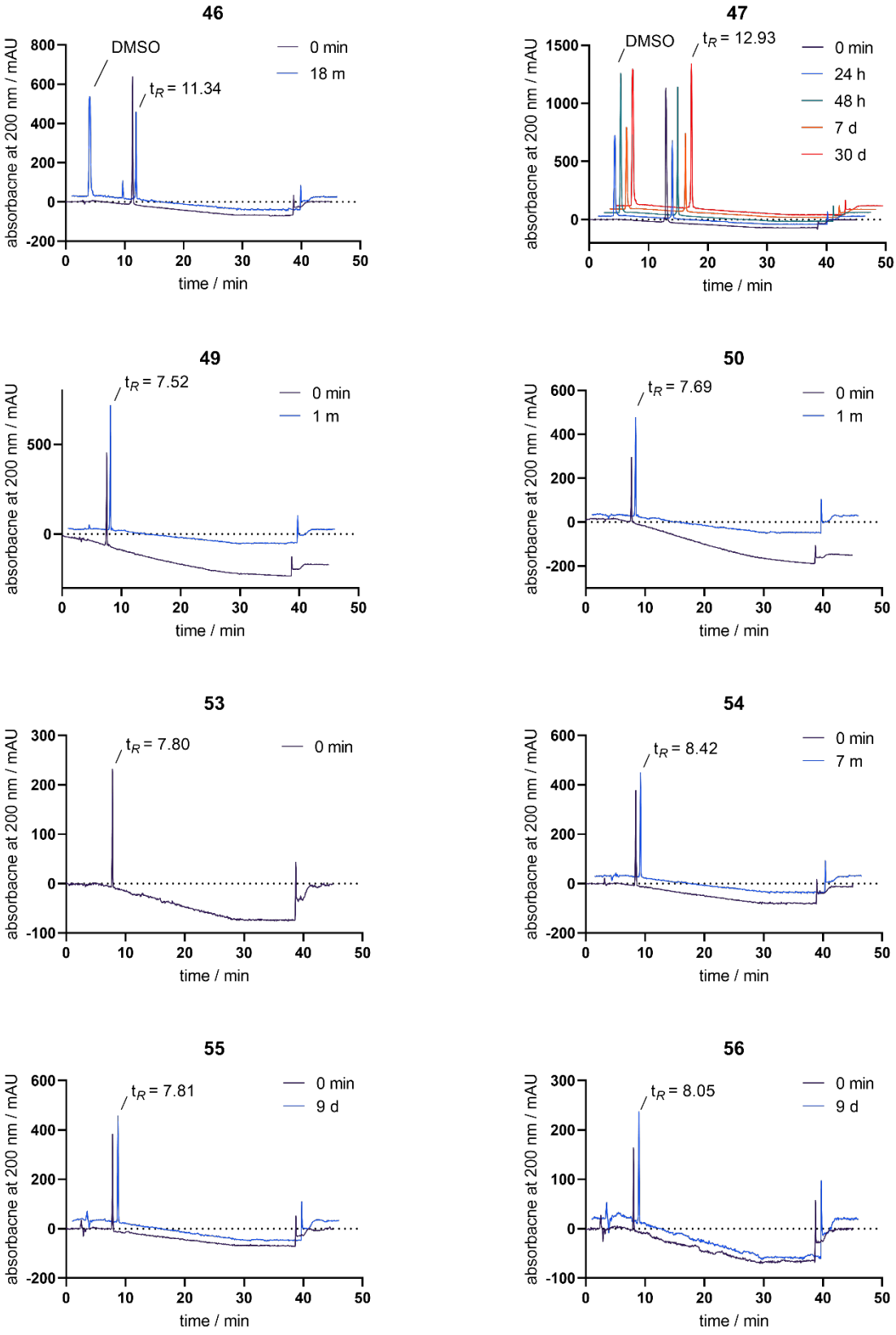

Figure 8.2: HPLC stability and purity controls of compounds **46**, **47**, **49**, **50** and **53-56**.

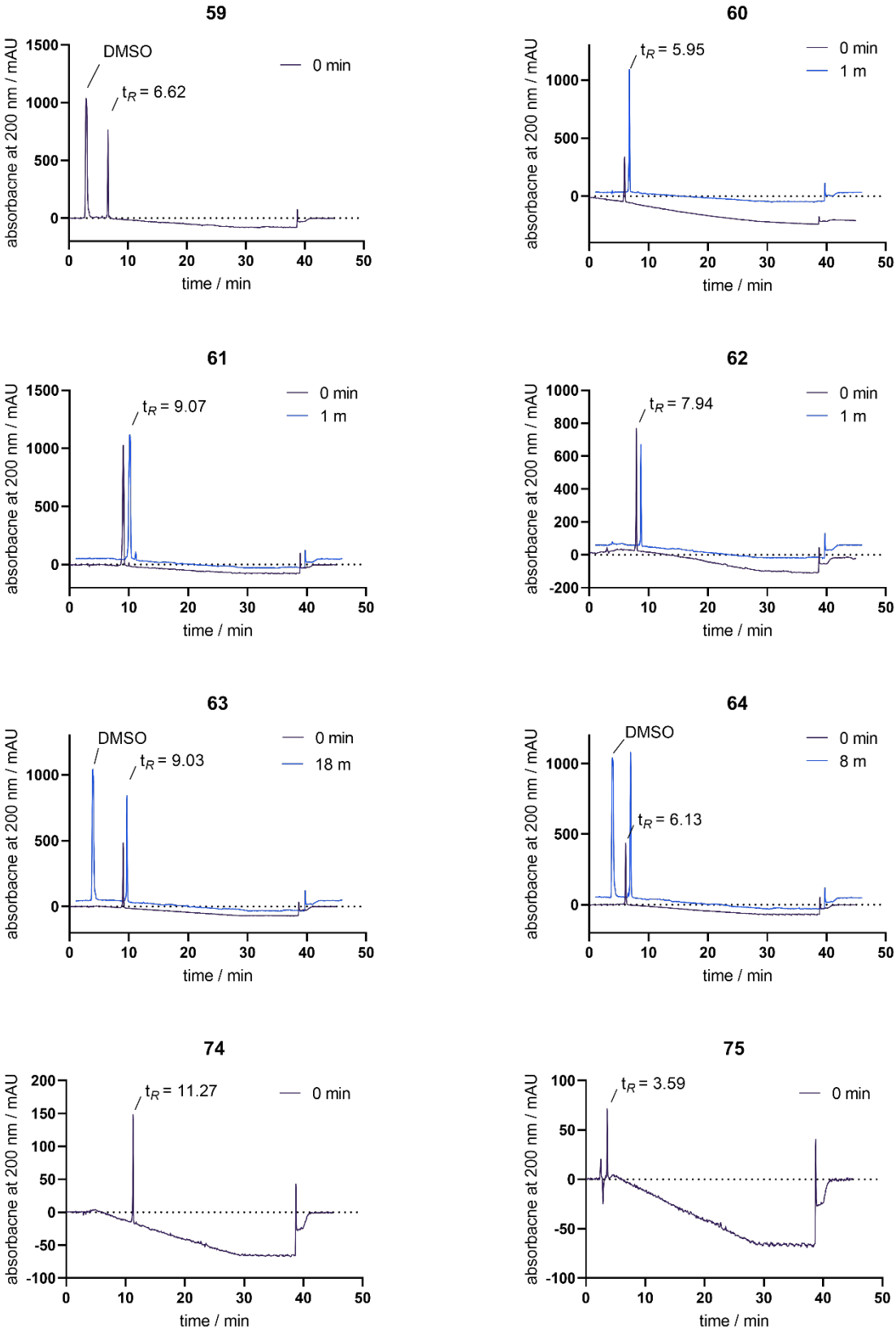

Figure 8.3: HPLC stability and purity controls of compounds **59-64**, **74**, and **75**.

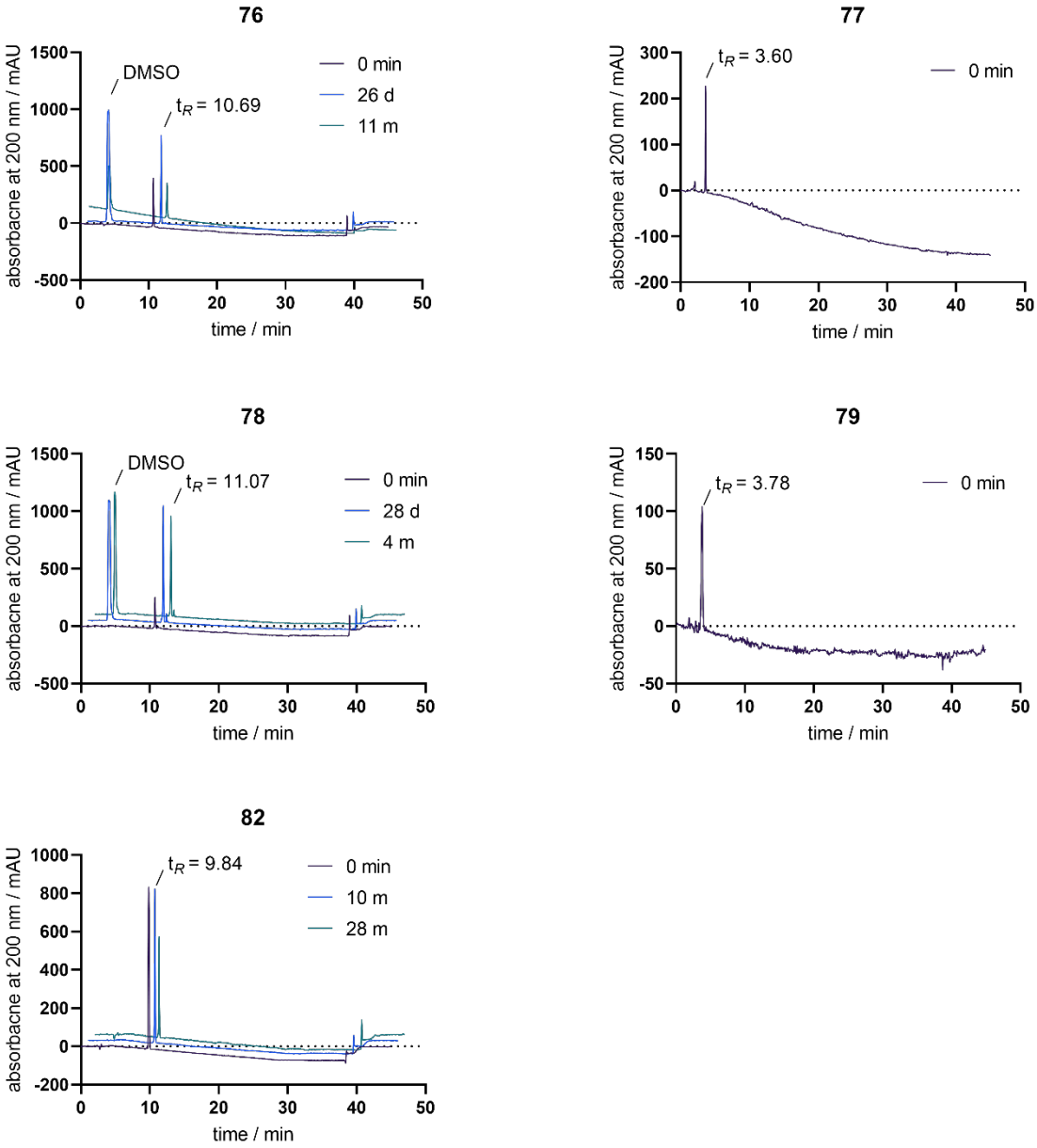

Figure 8.4: HPLC stability and purity controls of compounds **76-79** and **82**.

8.2 Chemical structures and ^{1}H NMR spectra of bivalent, endcapped and reference ligands

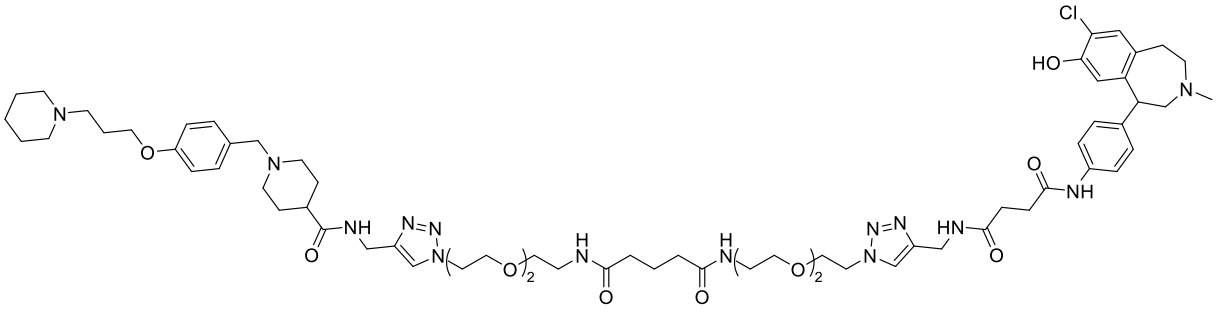

40

Chemical Formula: $C_{65}H_{93}ClN_{14}O_{11}$
Molecular Weight: 1281,9960

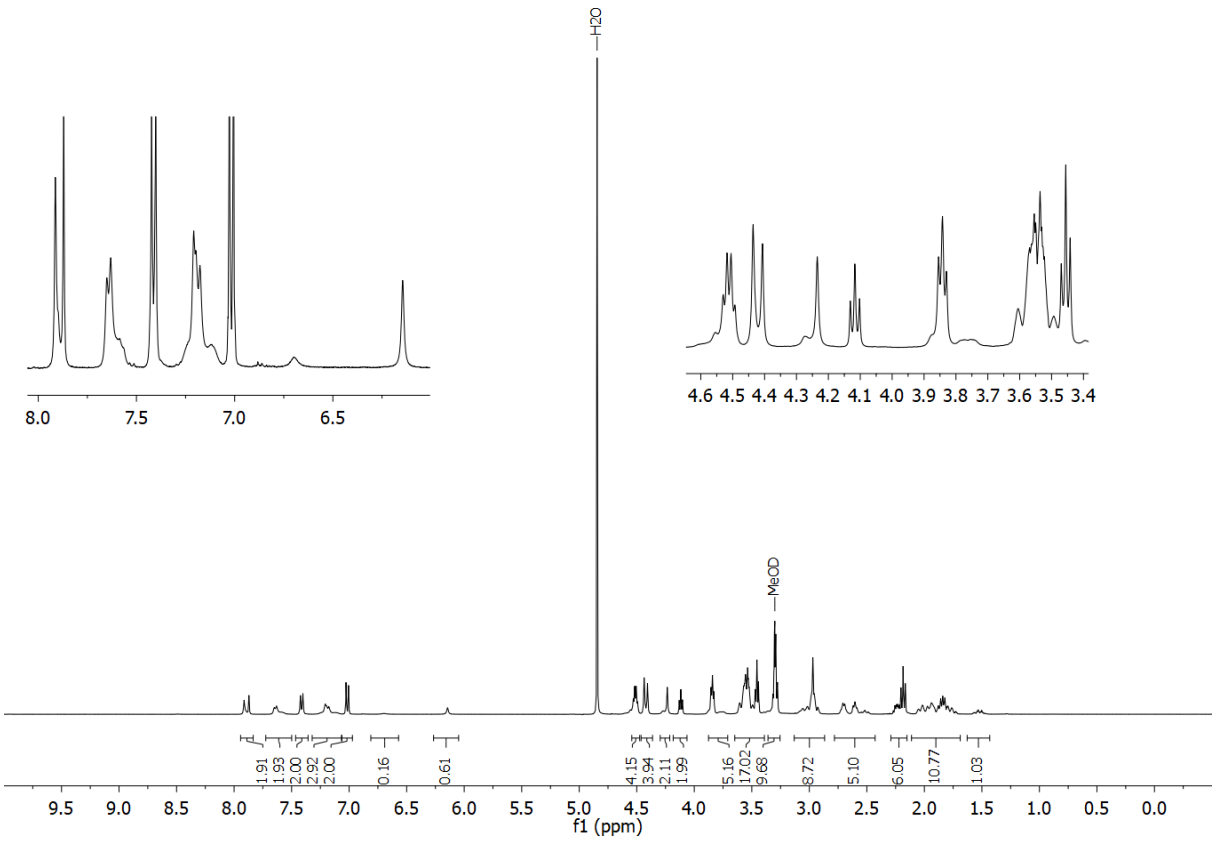

Figure 8.5: Chemical structure (upper section) and ^{1}H NMR spectrum (400 MHz, CD_3OD; lower section) of compound **40**.

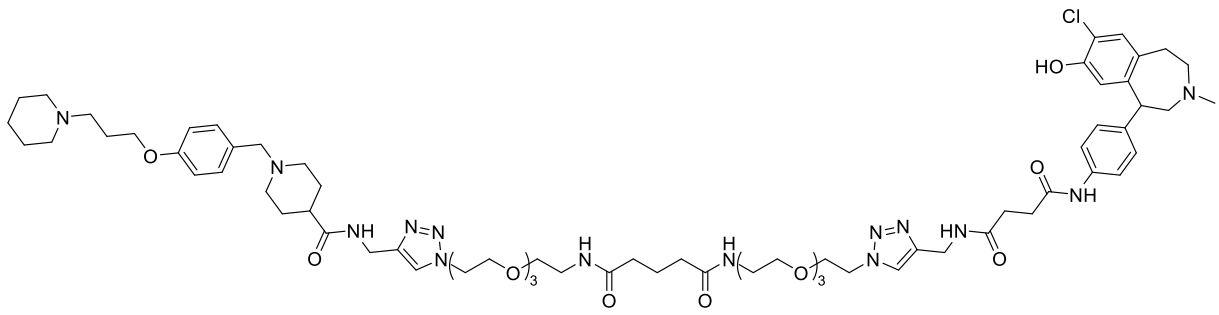

41

Chemical Formula: $C_{69}H_{101}ClN_{14}O_{13}$

Molecular Weight: 1370,1020

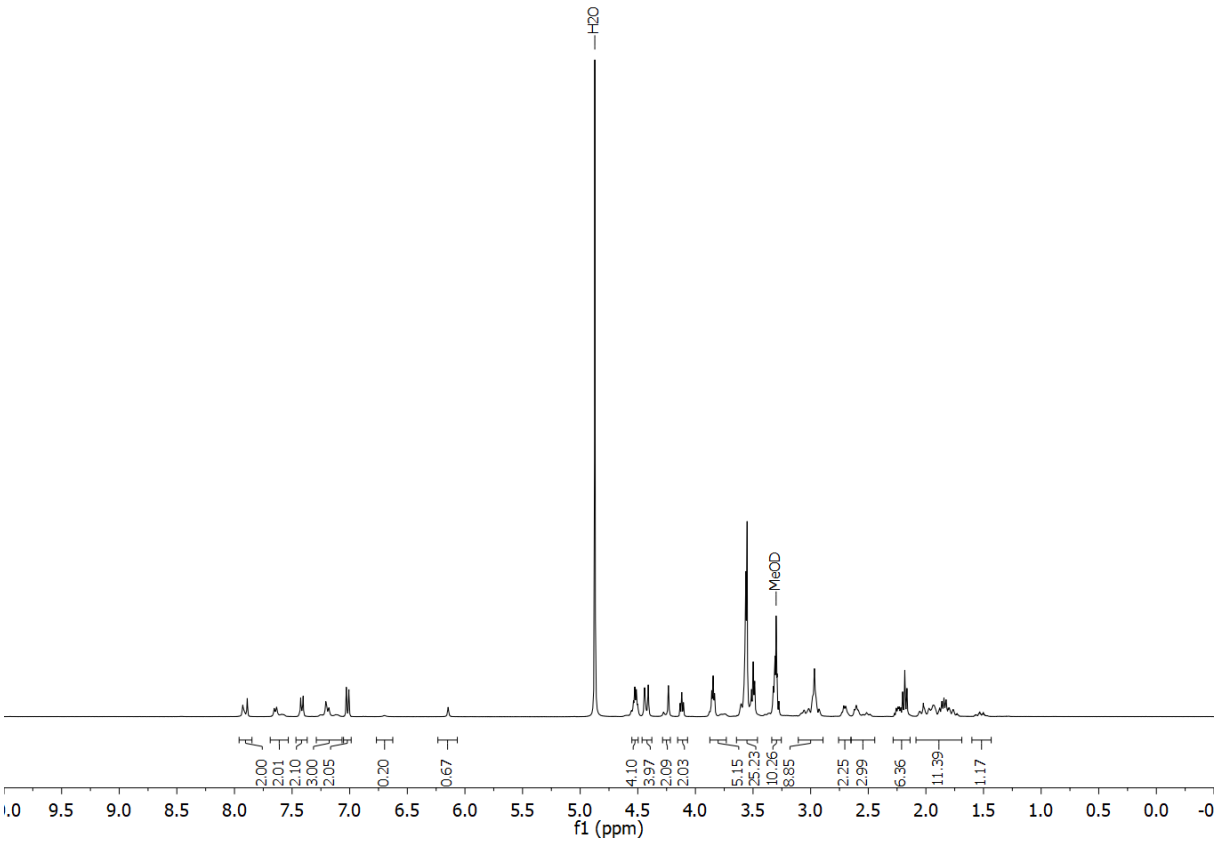

Figure 8.6: Chemical structure (upper section) and ^{1}H NMR spectrum (400 MHz, CD_3OD; lower section) of compound **41**.

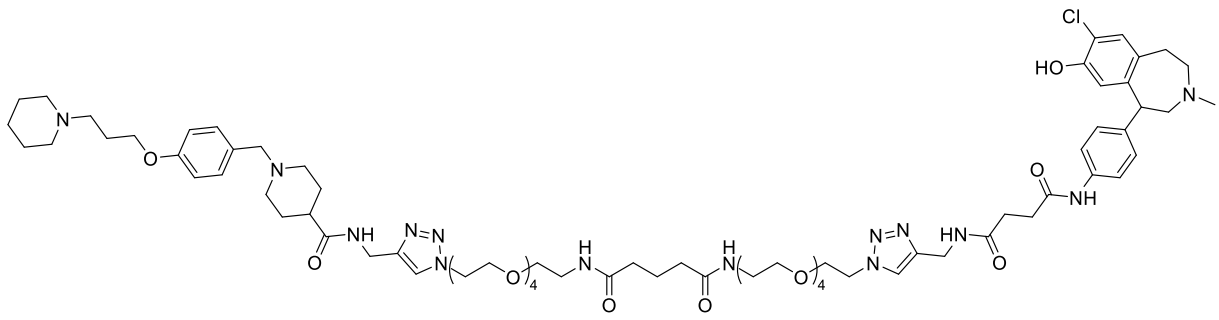

42
Chemical Formula: $C_{73}H_{109}ClN_{14}O_{15}$
Molecular Weight: 1458,2080

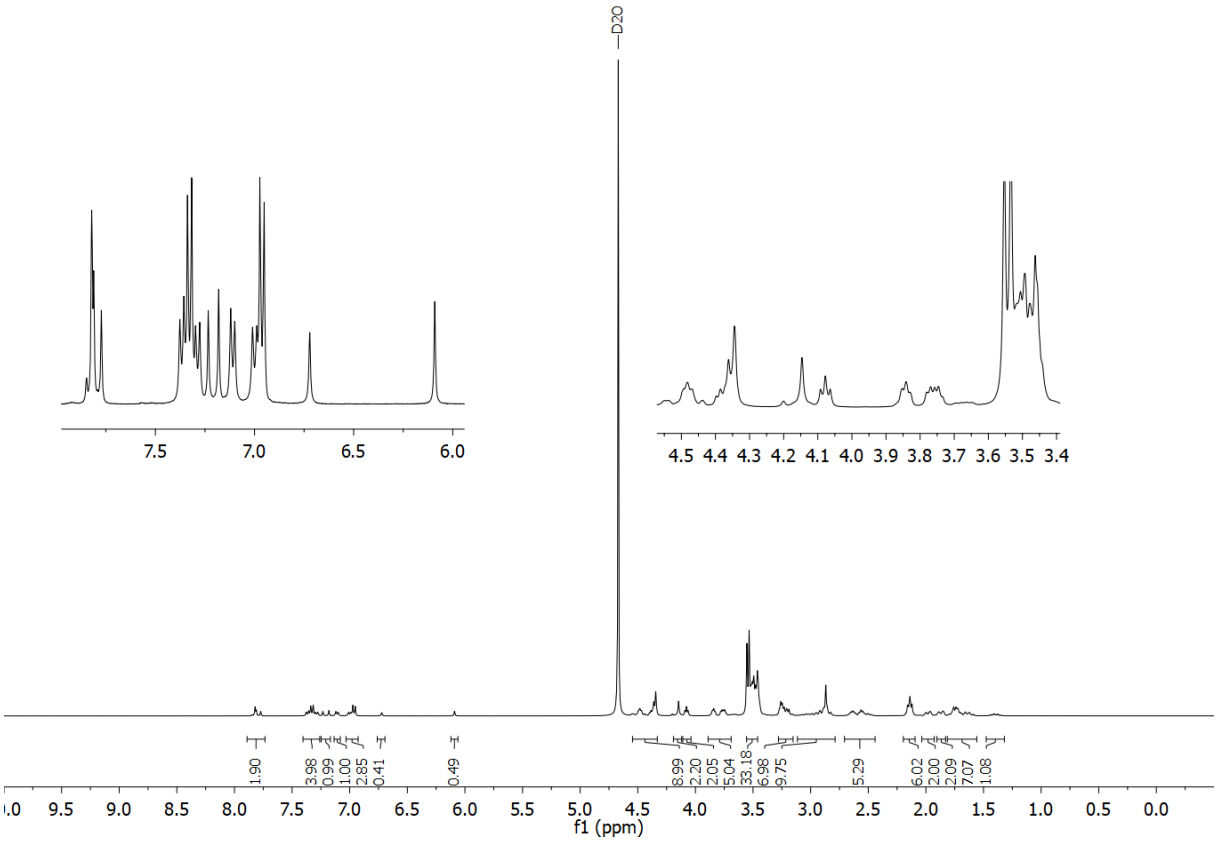

Figure 8.7: Chemical structure (upper section) and ^{1}H NMR spectrum (400 MHz, D_2O; lower section) of compound **42**.

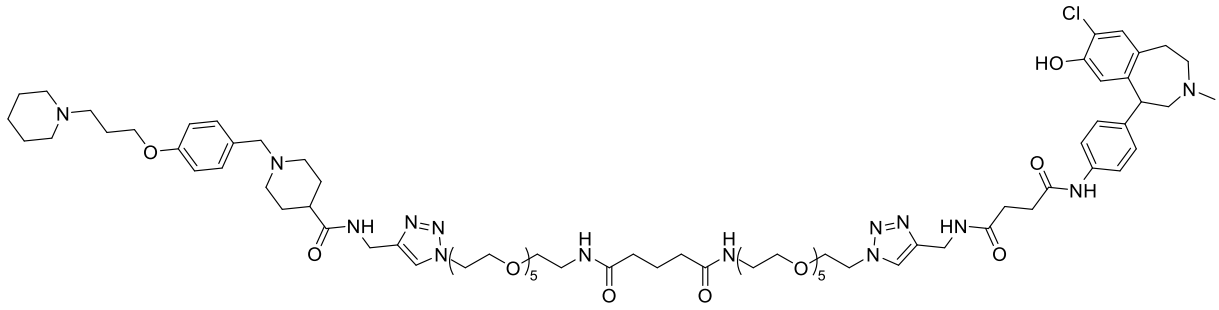

43

Chemical Formula: $C_{77}H_{117}ClN_{14}O_{17}$

Molecular Weight: 1546,3140

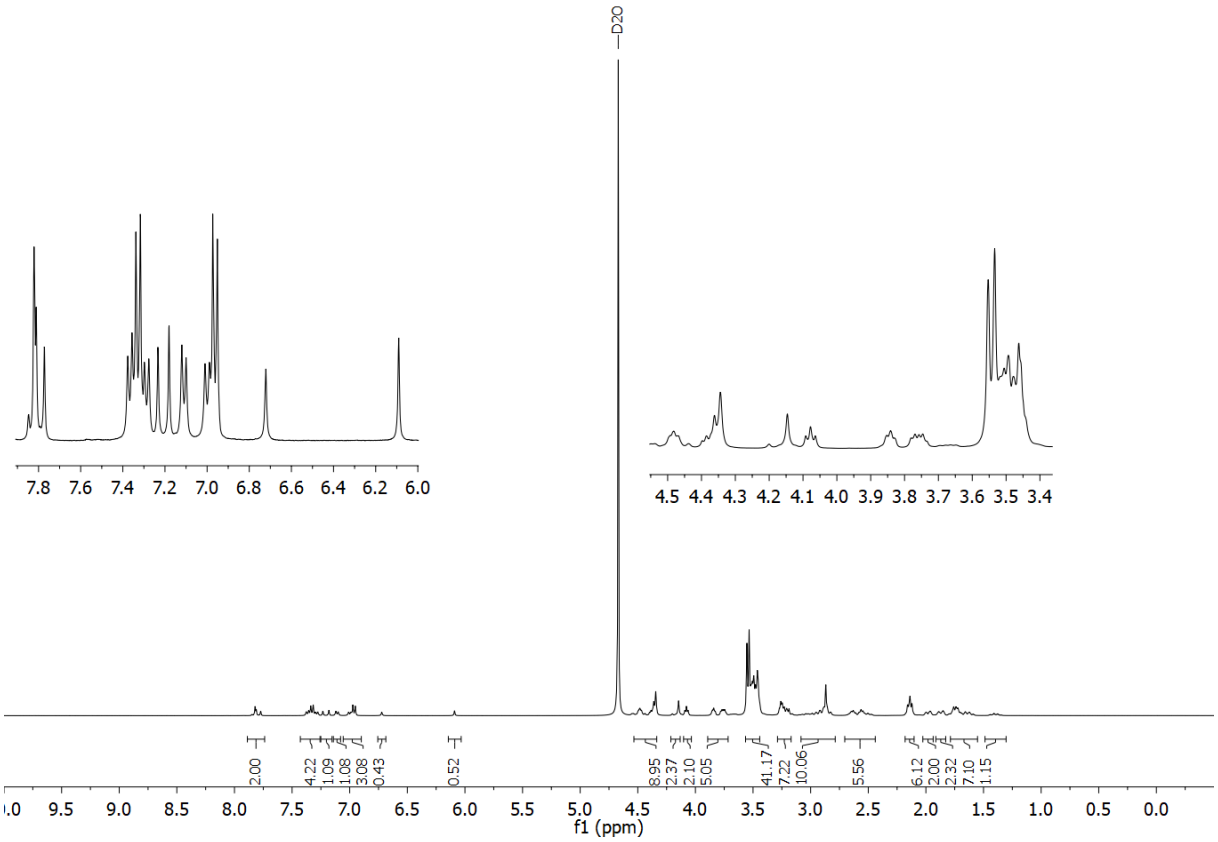

Figure 8.8: Chemical structure (upper section) and ^{1}H NMR spectrum (400 MHz, D_2O; lower section) of compound **43**.

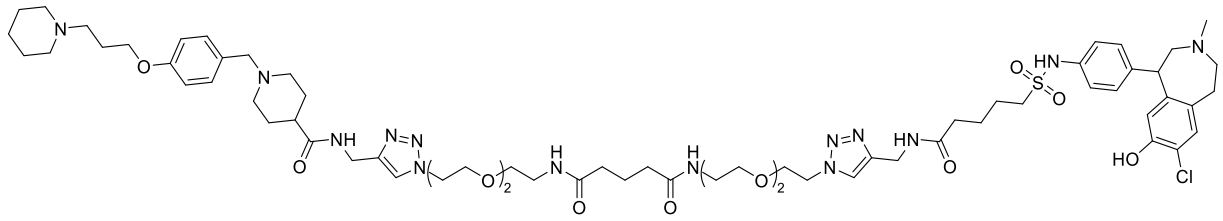

44

Chemical Formula: $C_{66}H_{97}ClN_{14}O_{12}S$

Molecular Weight: 1346,0980

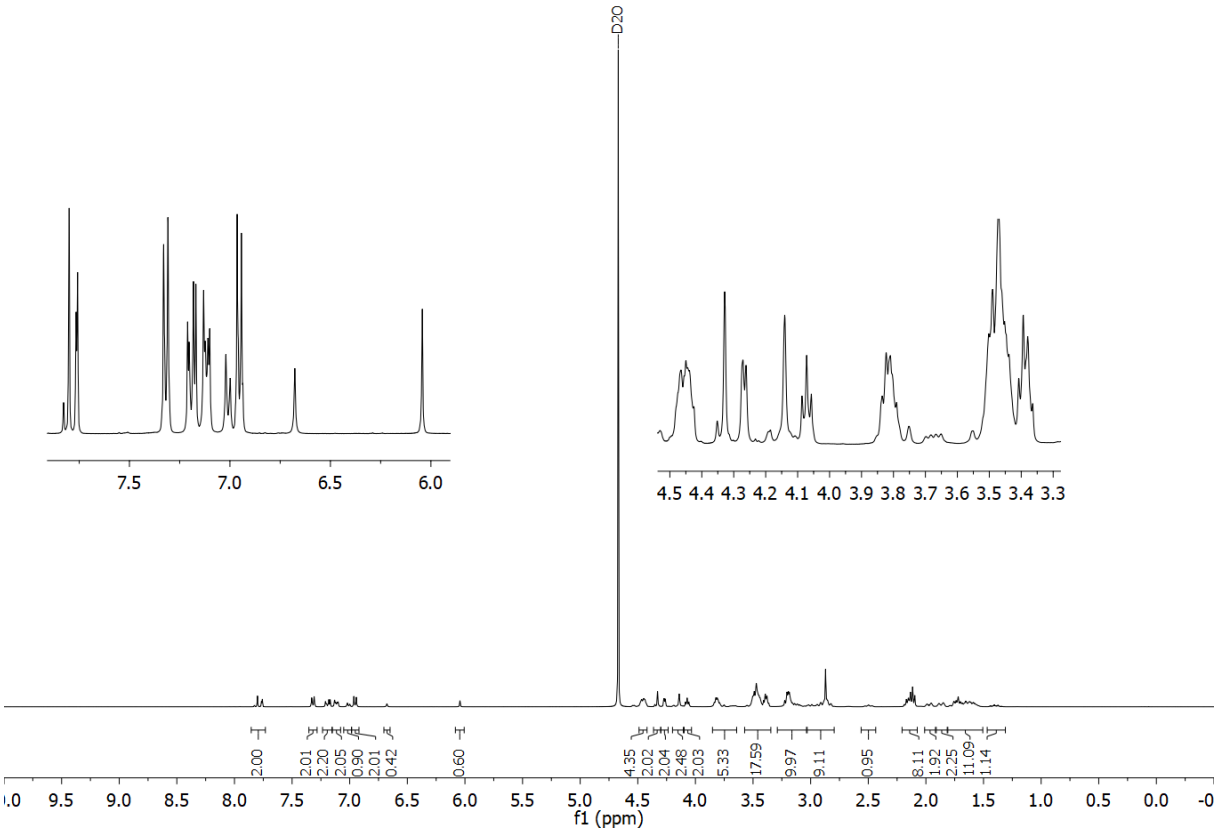

Figure 8.9: Chemical structure (upper section) and ^{1}H NMR spectrum (400 MHz, D_2O; lower section) of compound **44**.

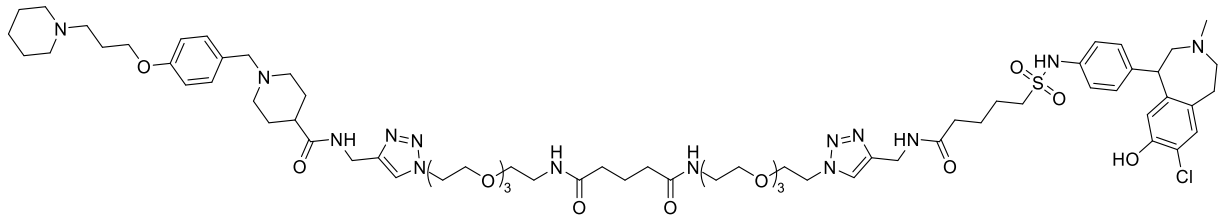

45

Chemical Formula: $C_{70}H_{105}ClN_{14}O_{14}S$

Molecular Weight: 1434,2040

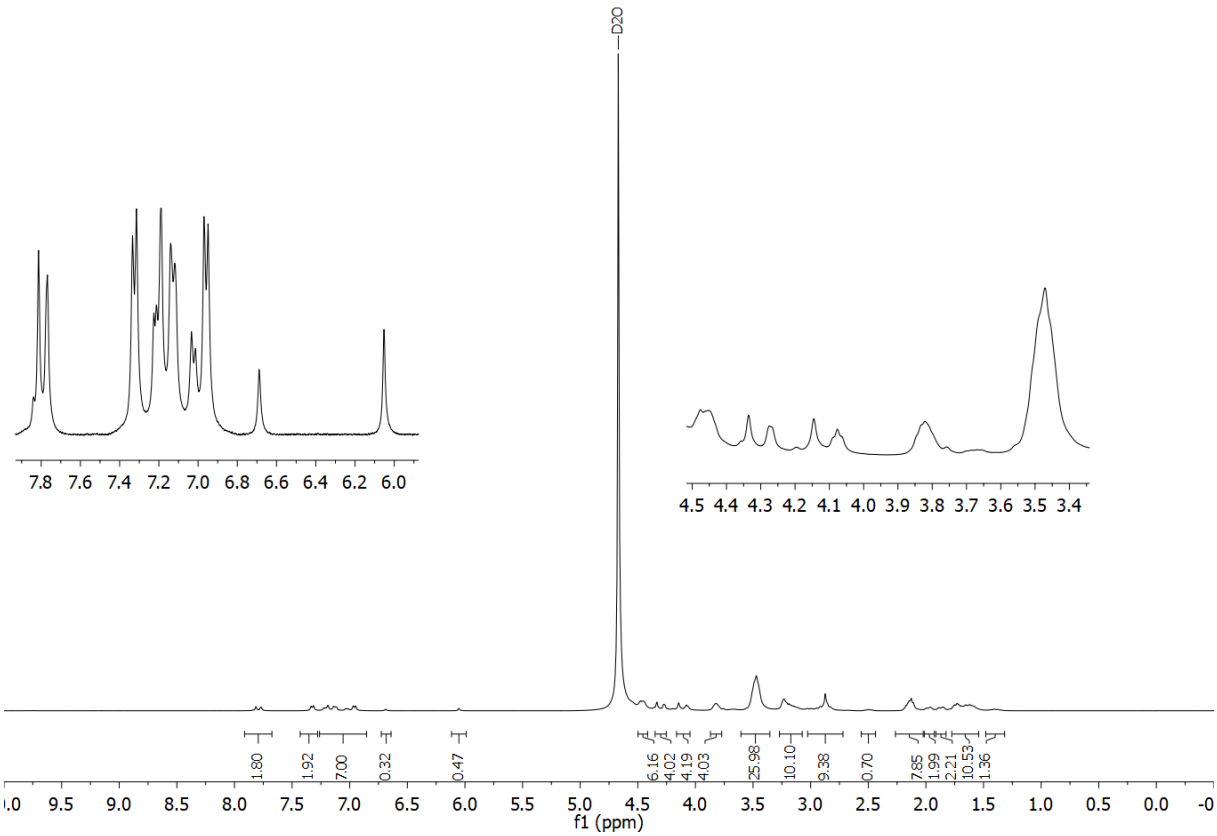

Figure 8.10: Chemical structure (upper section) and ^{1}H NMR spectrum (400 MHz, D_2O; lower section) of compound **45**.

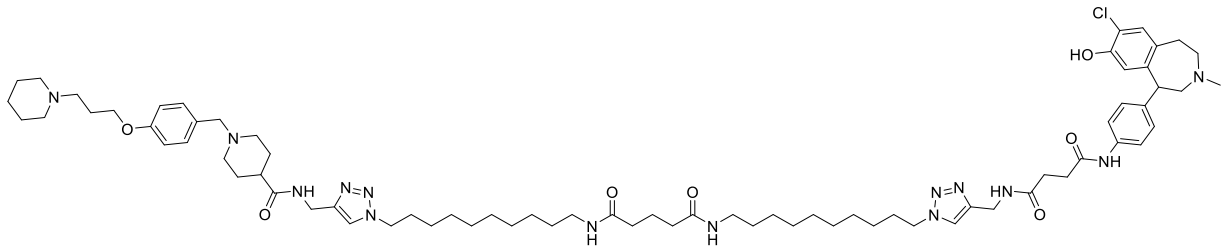

46

Chemical Formula: $C_{73}H_{109}ClN_{14}O_7$

Exact Mass: 1328,8292

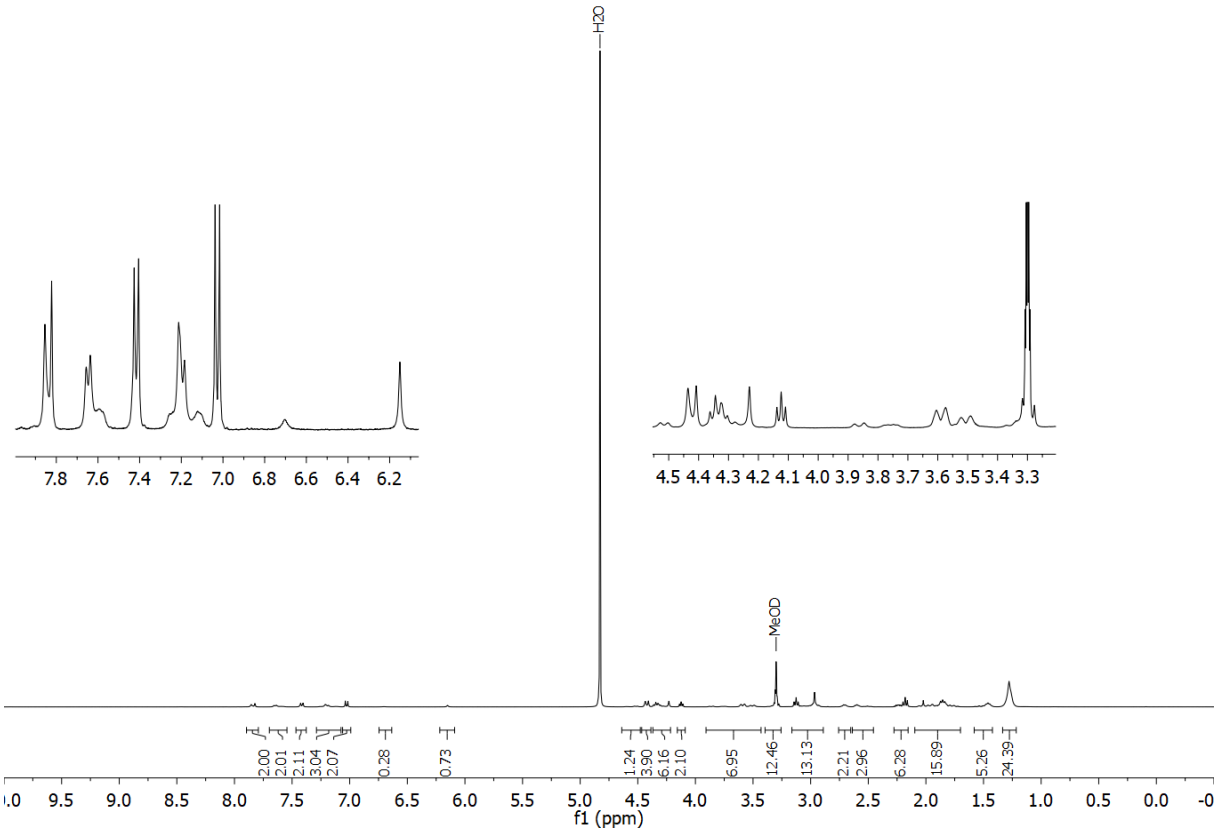

Figure 8.11: Chemical structure (upper section) and ^{1}H NMR spectrum (400 MHz, CD_3OD; lower section) of compound **46**.

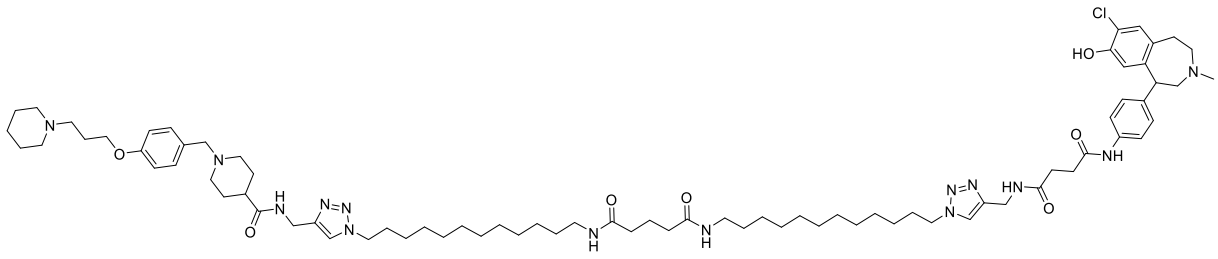

47
Chemical Formula: $C_{77}H_{117}ClN_{14}O_7$
Exact Mass: 1384,8918

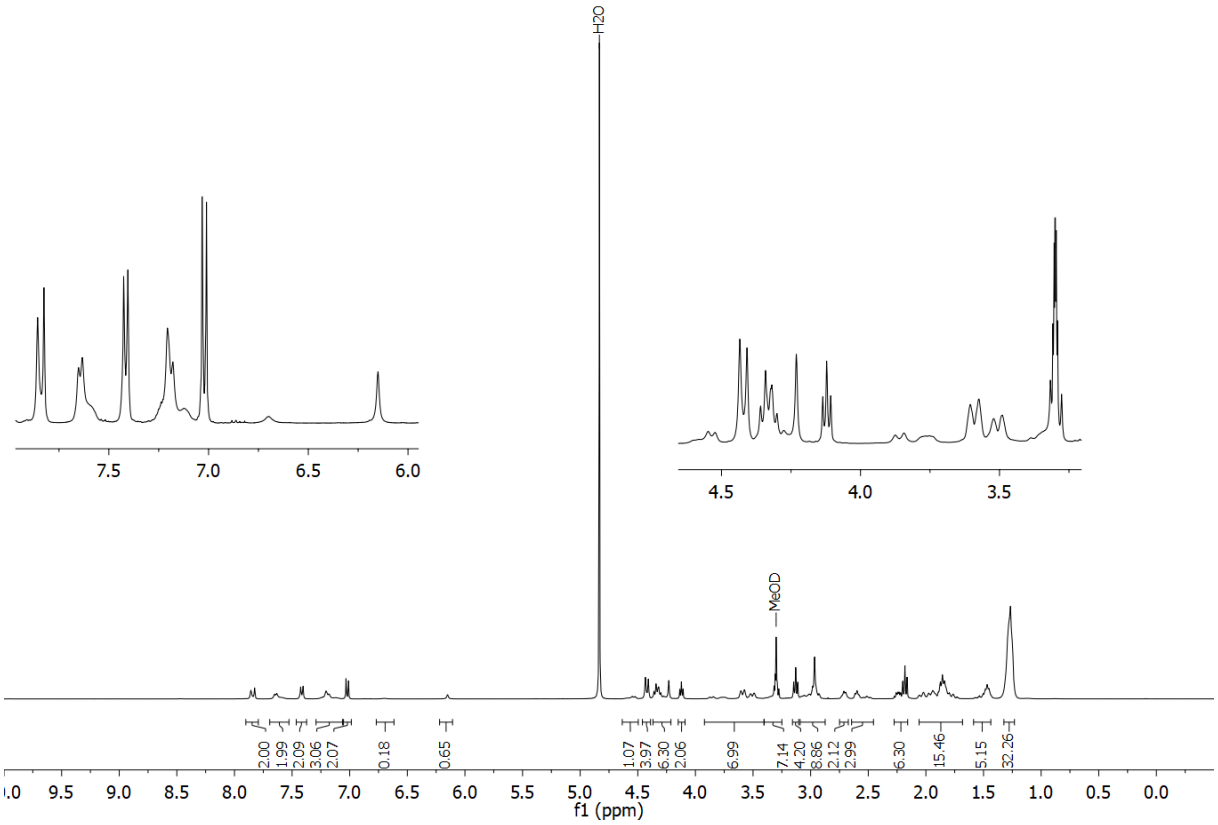

Figure 8.12: Chemical structure (upper section) and ^{1}H NMR spectrum (400 MHz, CD_3OD; lower section) of compound **47**.

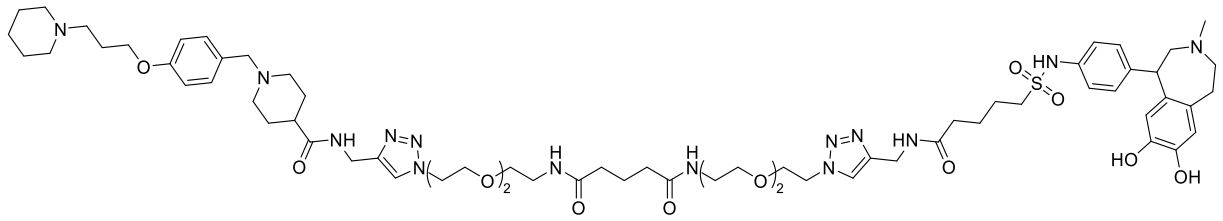

49

Chemical Formula: $C_{66}H_{98}N_{14}O_{13}S$

Exact Mass: 1326,7158

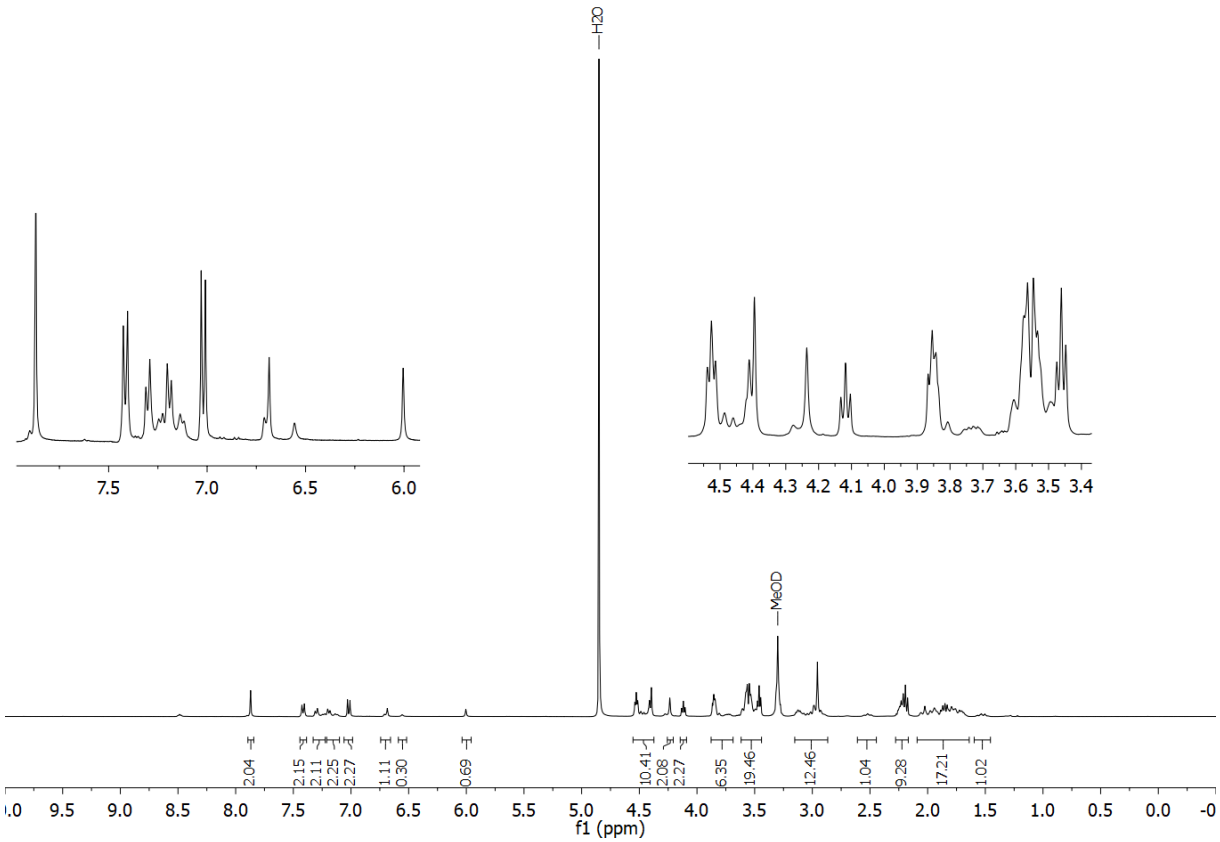

Figure 8.13: Chemical structure (upper section) and ^{1}H NMR spectrum (400 MHz, CD_3OD; lower section) of compound **49**.

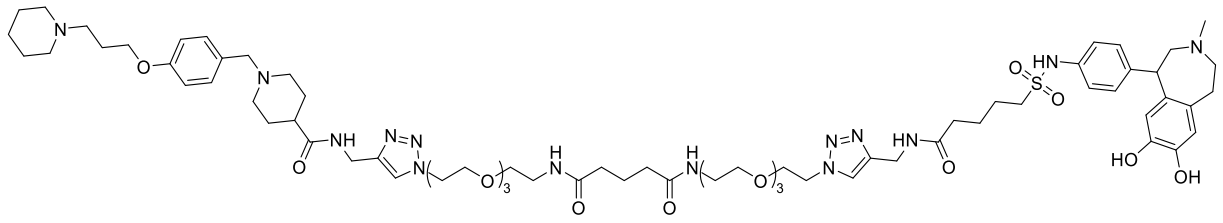

50

Chemical Formula: $C_{70}H_{106}N_{14}O_{15}S$

Molecular Weight: 1415,7610

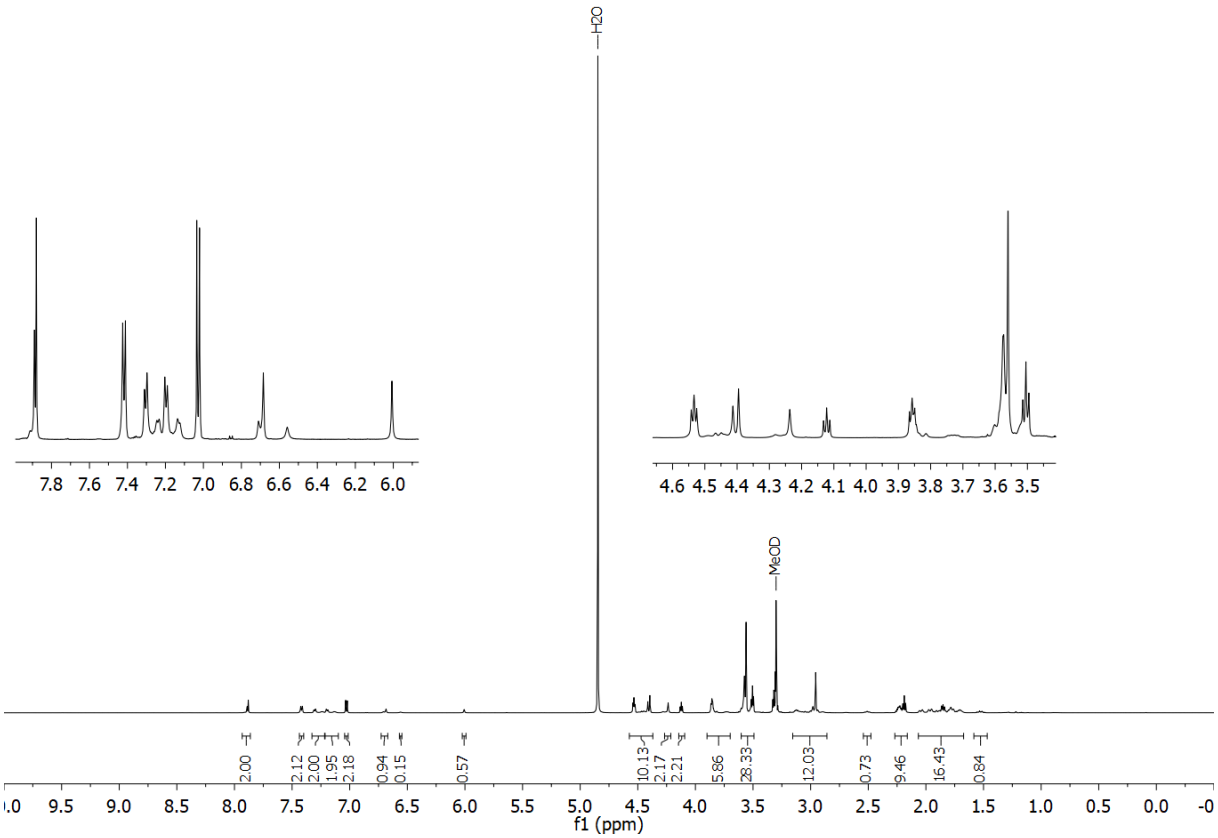

Figure 8.14: Chemical structure (upper section) and ^{1}H NMR spectrum (600 MHz, CD_3OD; lower section) of compound **50**.

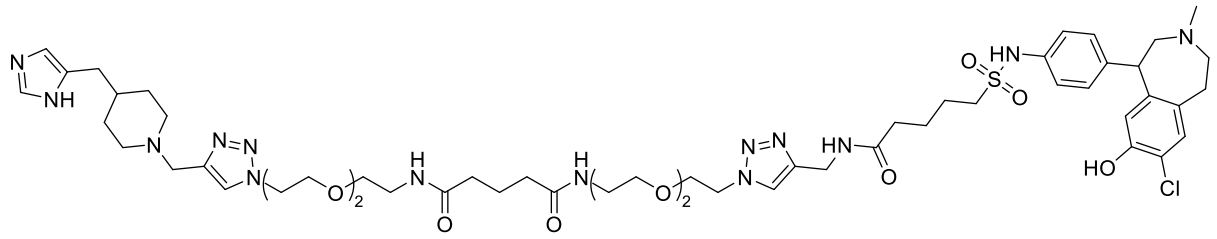

53

Chemical Formula: $C_{54}H_{79}ClN_{14}O_{10}S$

Molecular Weight: 1151,8240

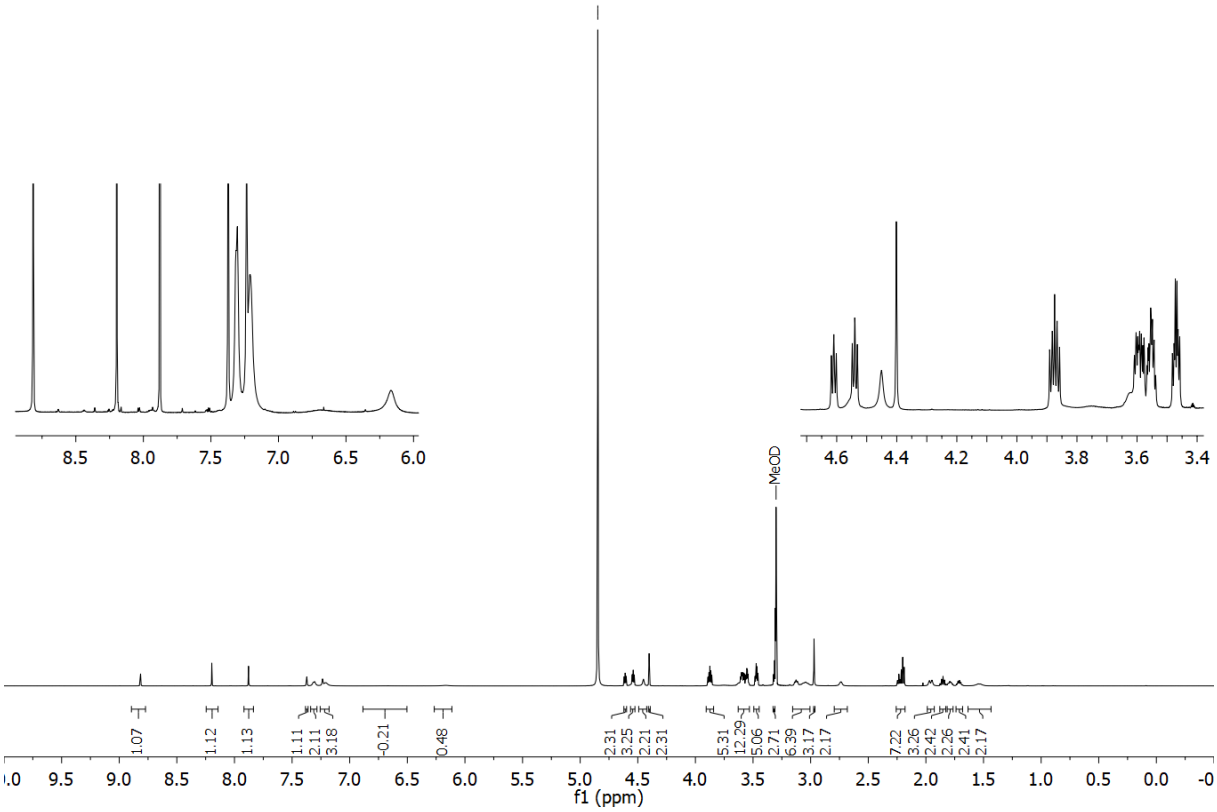

Figure 8.15: Chemical structure (upper section) and ^{1}H NMR spectrum (600 MHz, CD_3OD; lower section) of compound **53**.

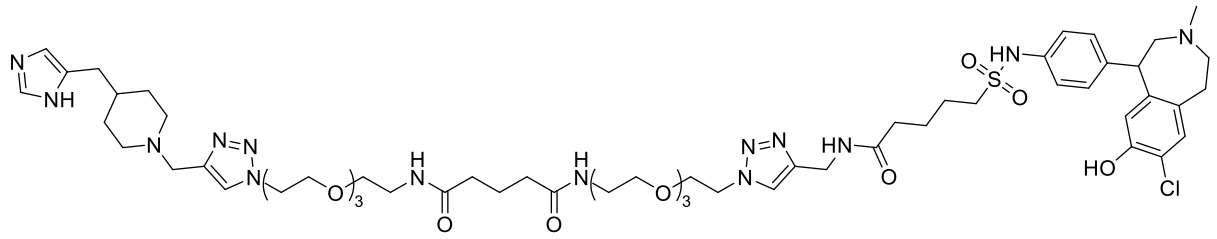

54

Chemical Formula: $C_{58}H_{87}ClN_{14}O_{12}S$

Molecular Weight: 1239,9300

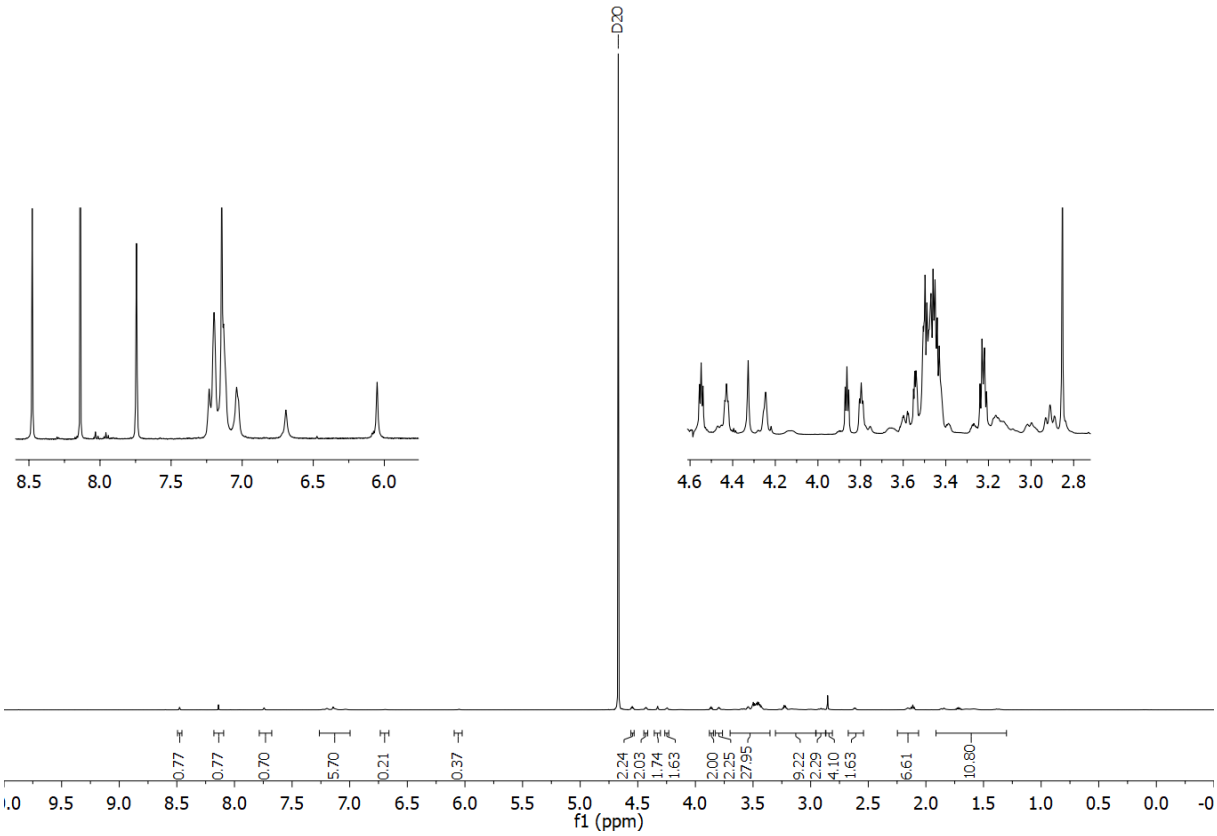

Figure 8.16: Chemical structure (upper section) and ^{1}H NMR spectrum (600 MHz, D_2O; lower section) of compound **54**.

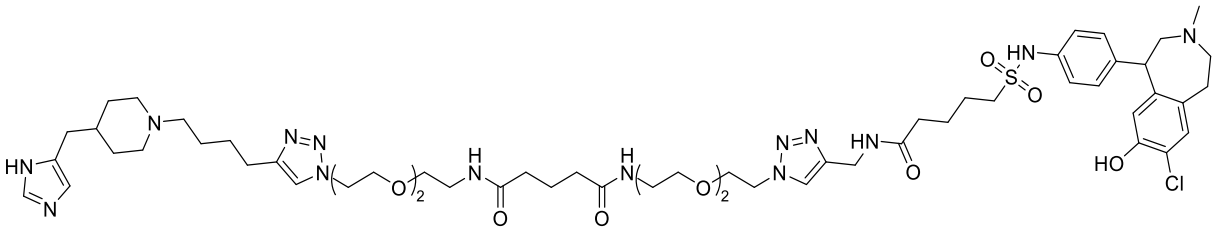

55

Chemical Formula: $C_{57}H_{85}ClN_{14}O_{10}S$

Exact Mass: 1192,5982

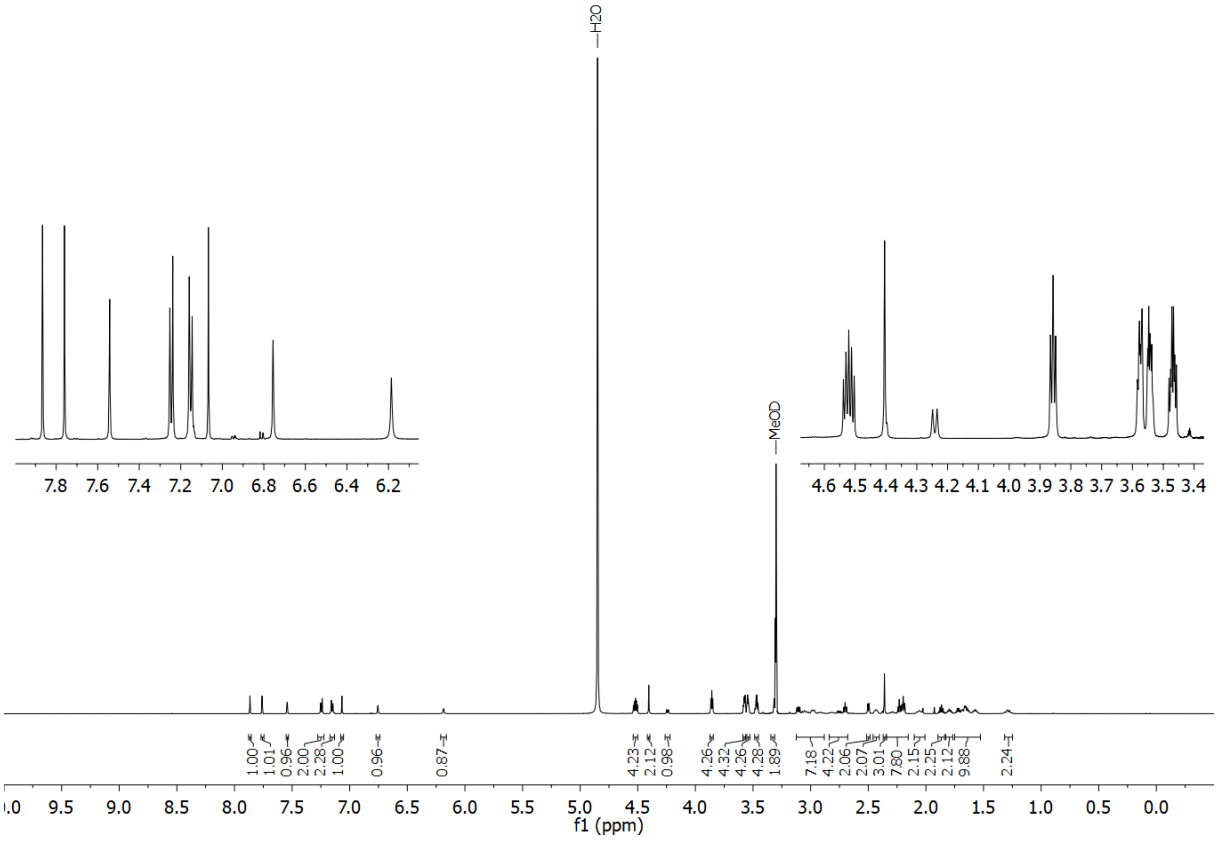

Figure 8.17: Chemical structure (upper section) and ^{1}H NMR spectrum (600 MHz, CD_3OD; lower section) of compound **55**.

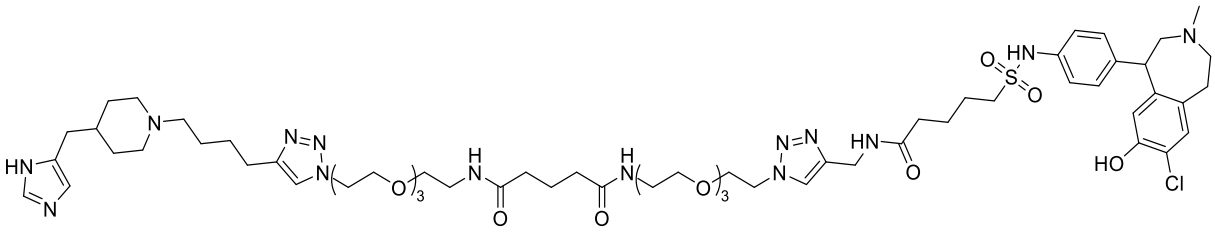

56

Chemical Formula: $C_{61}H_{93}ClN_{14}O_{12}S$

Molecular Weight: 1282,0110

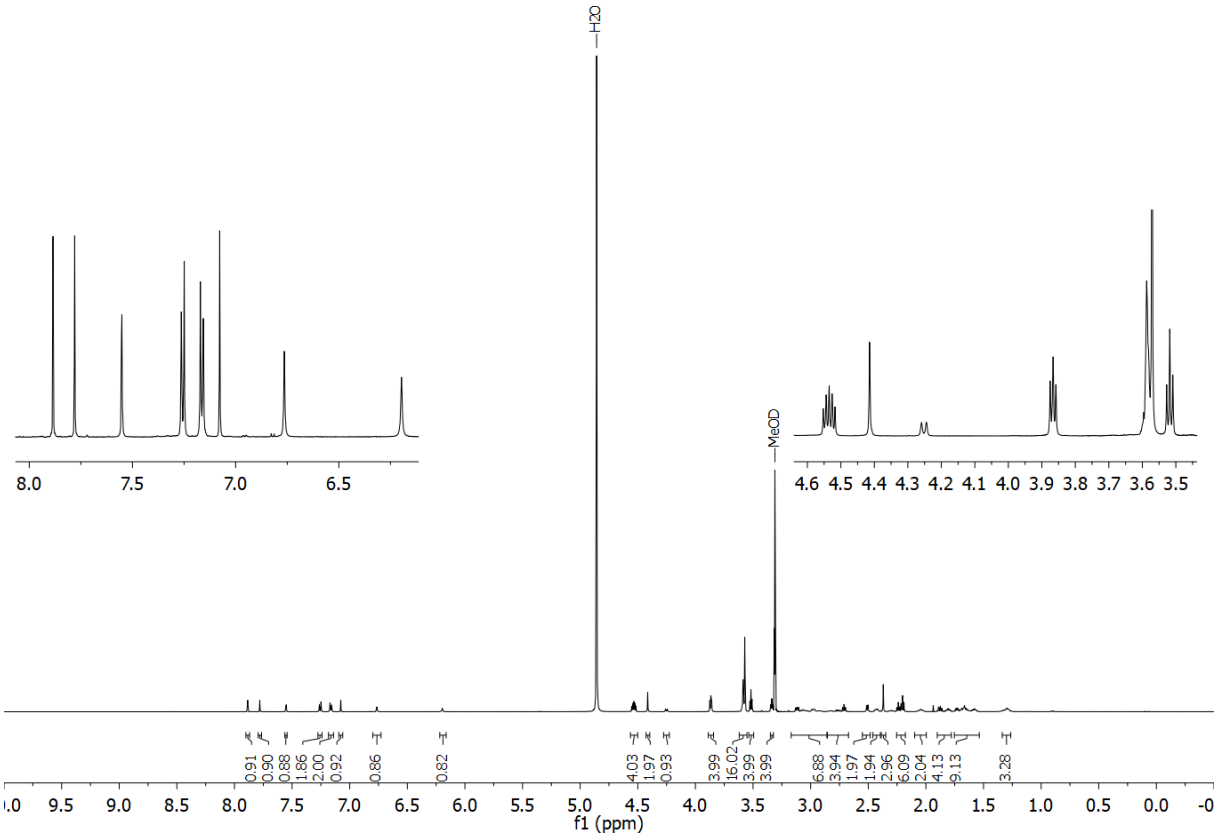

Figure 8.18: Chemical structure (upper section) and ^{1}H NMR spectrum (600 MHz, CD_3OD; lower section) of compound **56**.

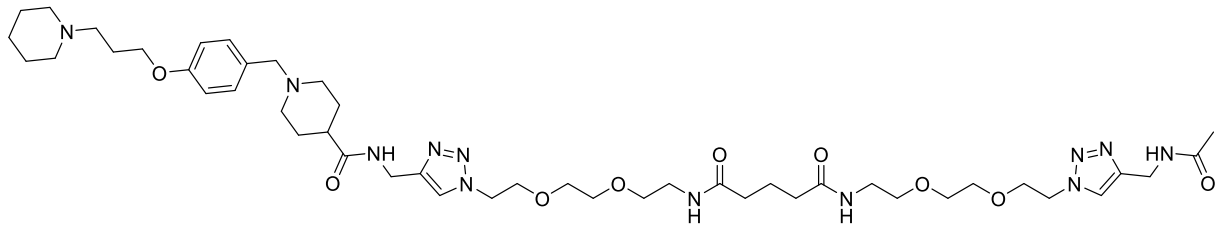

59

Chemical Formula: $C_{46}H_{74}N_{12}O_9$

Exact Mass: 938,5702

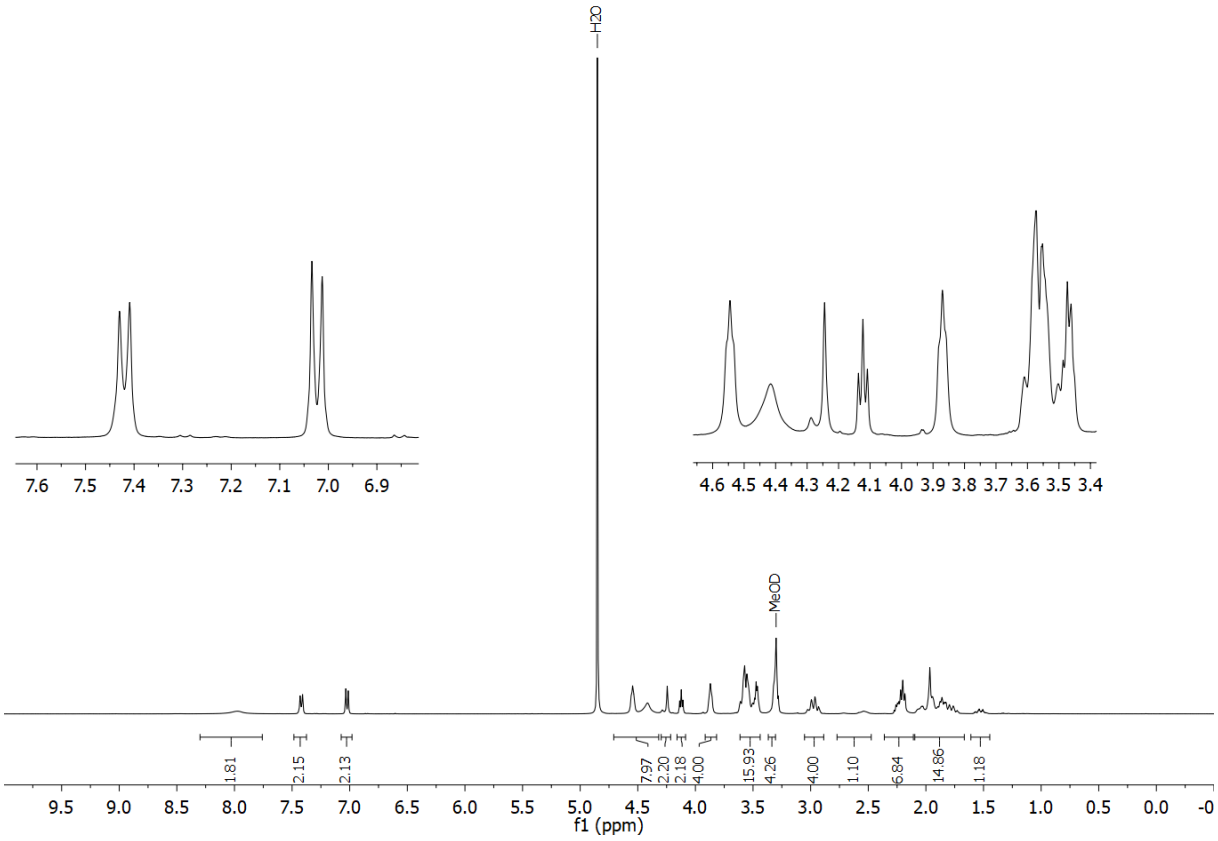

Figure 8.19: Chemical structure (upper section) and ^{1}H NMR spectrum (400 MHz, CD_3OD; lower section) of compound **59**.

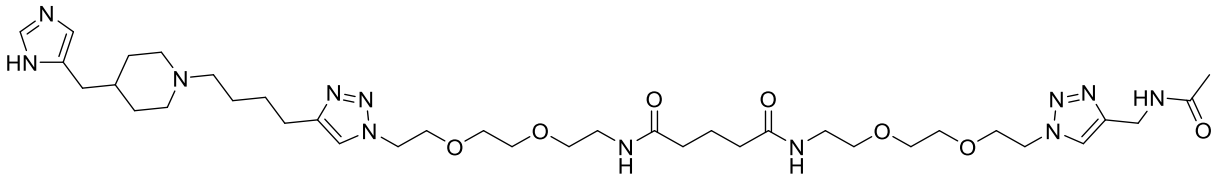

60

Chemical Formula: $C_{37}H_{62}N_{12}O_7$

Molecular Weight: 786,9800

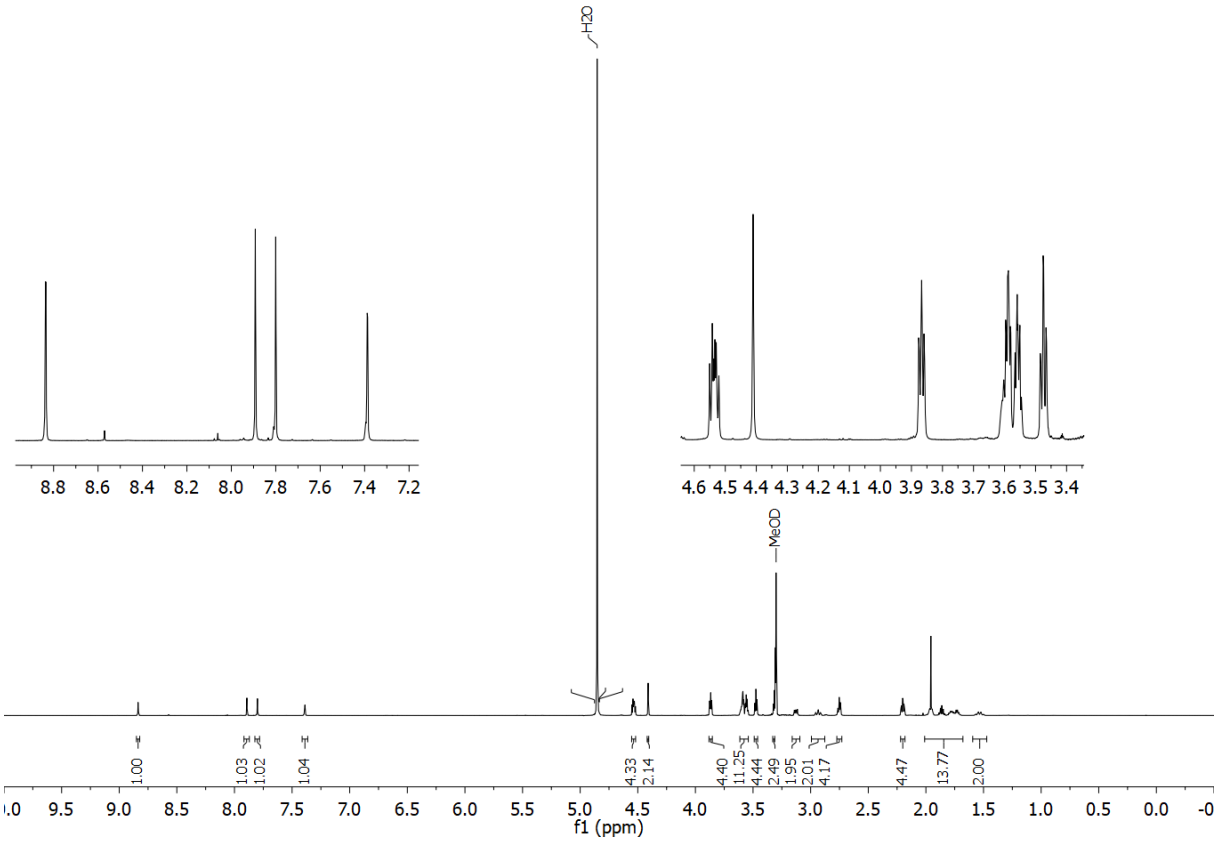

Figure 8.20: Chemical structure (upper section) and ^{1}H NMR spectrum (600 MHz, CD_3OD; lower section) of compound **60**.

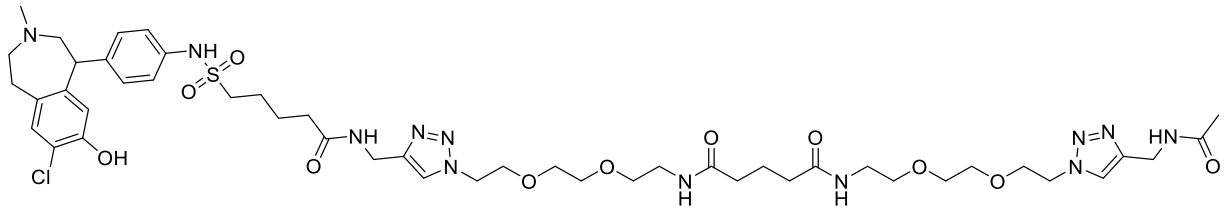

61

Chemical Formula: $C_{47}H_{69}ClN_{12}O_{11}S$

Exact Mass: 1044,4618

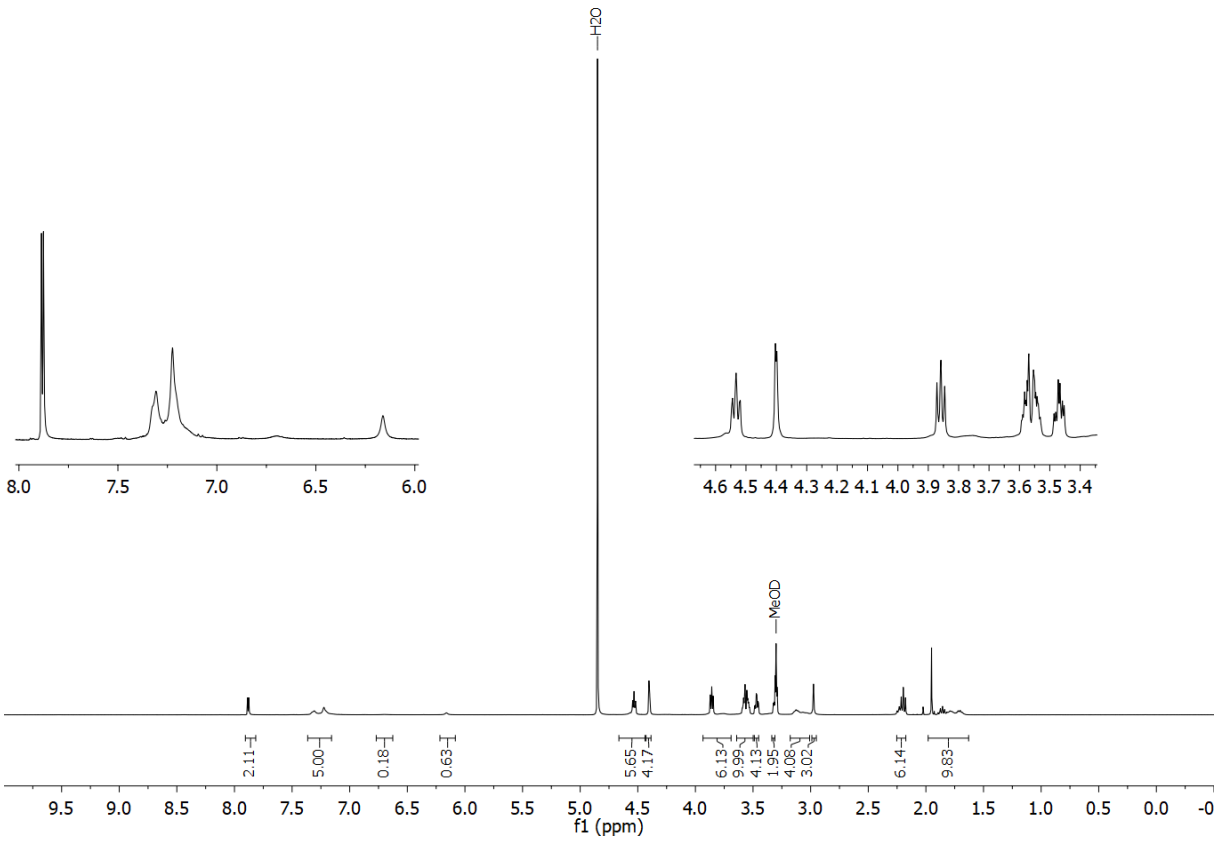

Figure 8.21: Chemical structure (upper section) and ^{1}H NMR spectrum (400 MHz, CD_3OD; lower section) of compound **61**.

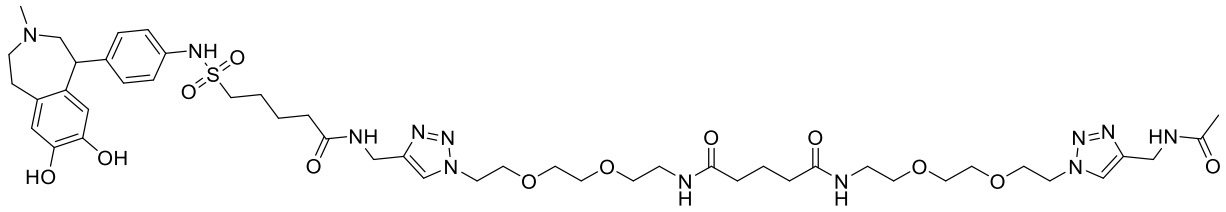

62

Chemical Formula: $C_{47}H_{70}N_{12}O_{12}S$

Exact Mass: 1026,4957

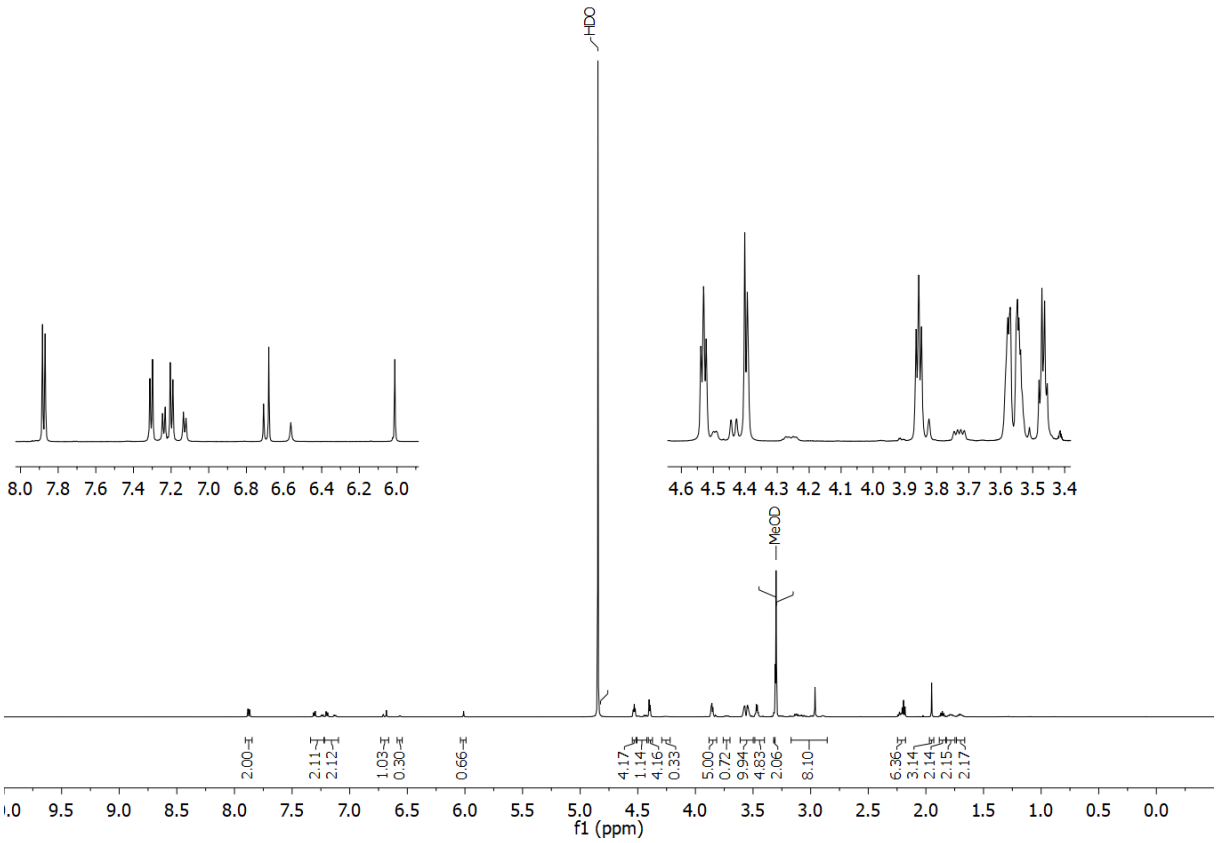

Figure 8.22: Chemical structure (upper section) and ^{1}H NMR spectrum (600 MHz, CD_3OD; lower section) of compound **62**.

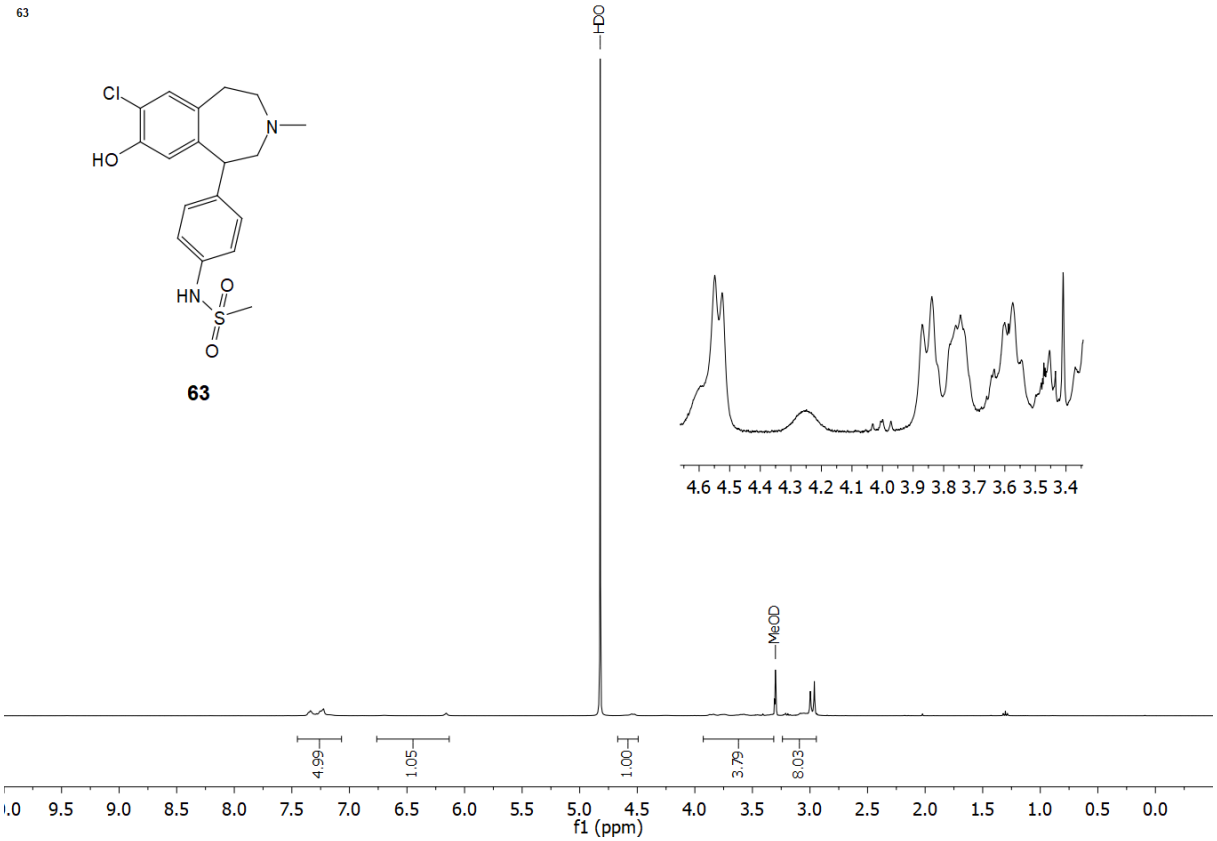

Figure 8.23: Chemical structure and ^{1}H NMR spectrum (400 MHz, CD_3OD) of compound **63**.

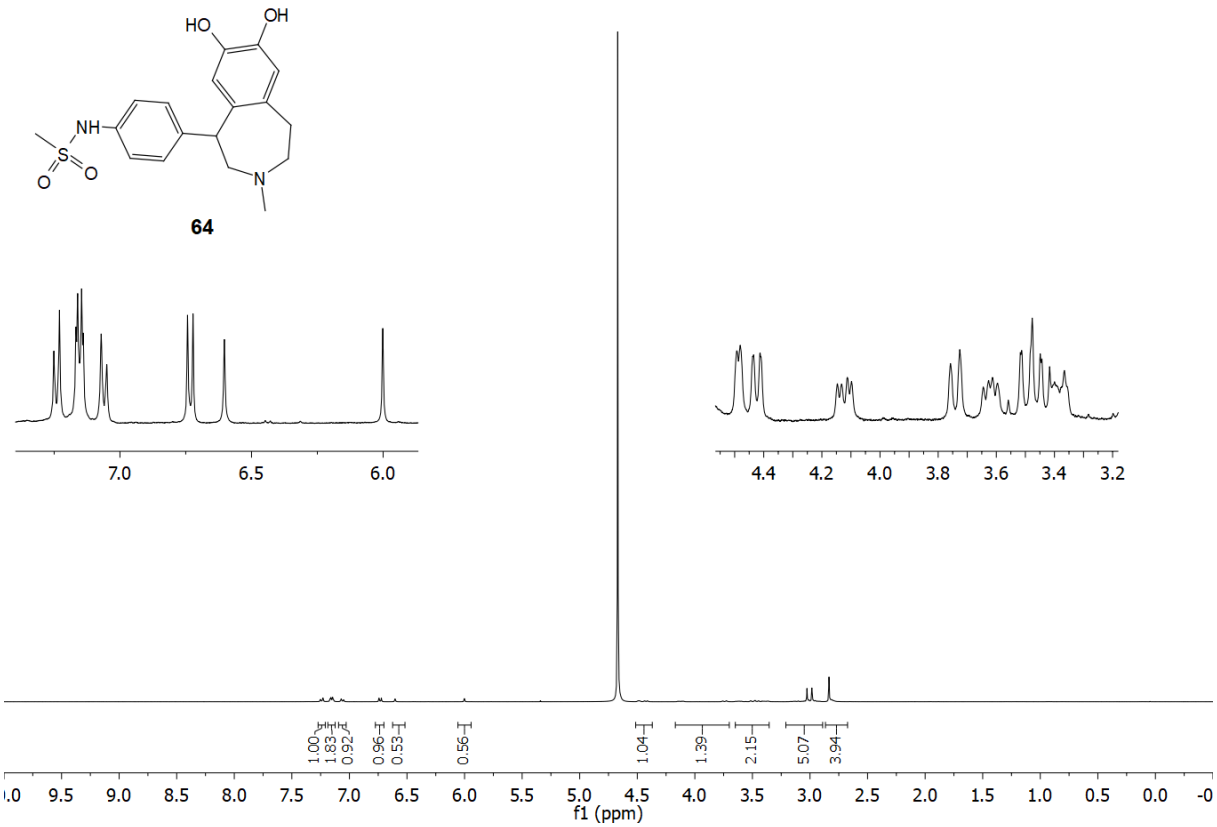

Figure 8.24: Chemical structure and ^{1}H NMR spectrum (400 MHz, D_2O) of compound **64**.

8.3 Chemical structures of fluorescent ligands and ^{1}H NMR spectrum of 82

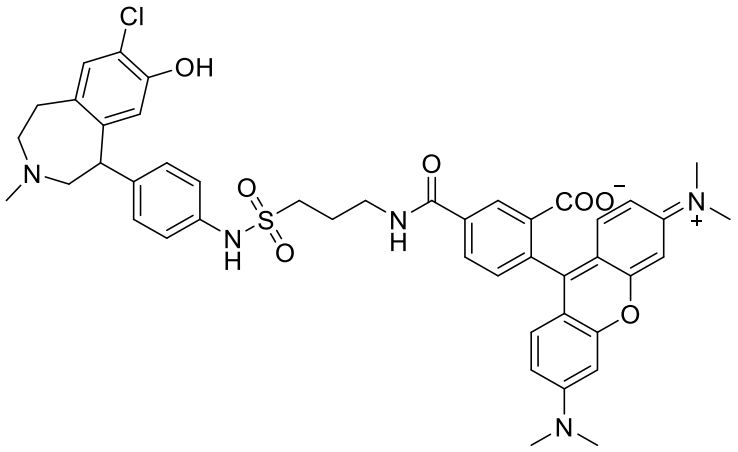

74
Chemical Formula: $C_{45}H_{46}ClN_5O_7S$
Exact Mass: 835,2806

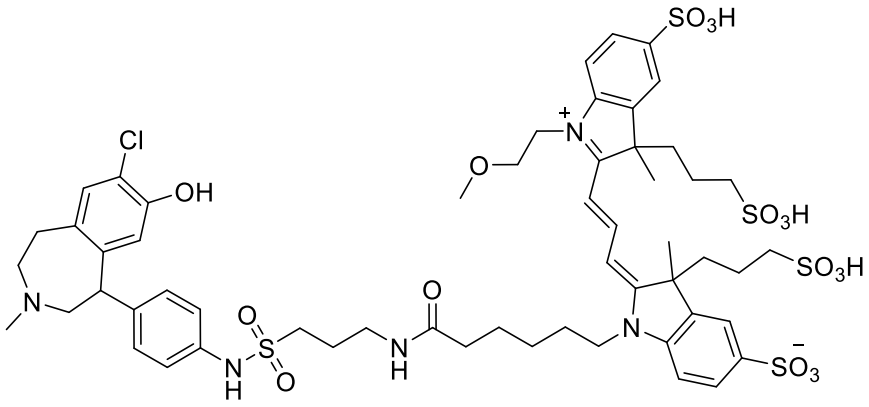

75
Chemical Formula: $C_{56}H_{72}ClN_5O_{17}S_5$
Exact Mass: 1281,3215

Figure 8.25: Chemical structures of fluorescent ligands **74** and **75**.

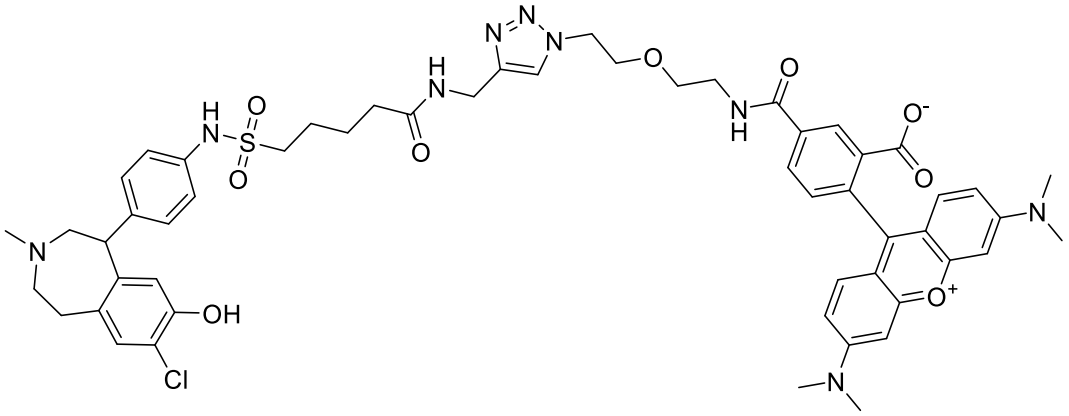

76
Chemical Formula: $C_{54}H_{60}ClN_9O_9S$
Exact Mass: 1045,3923

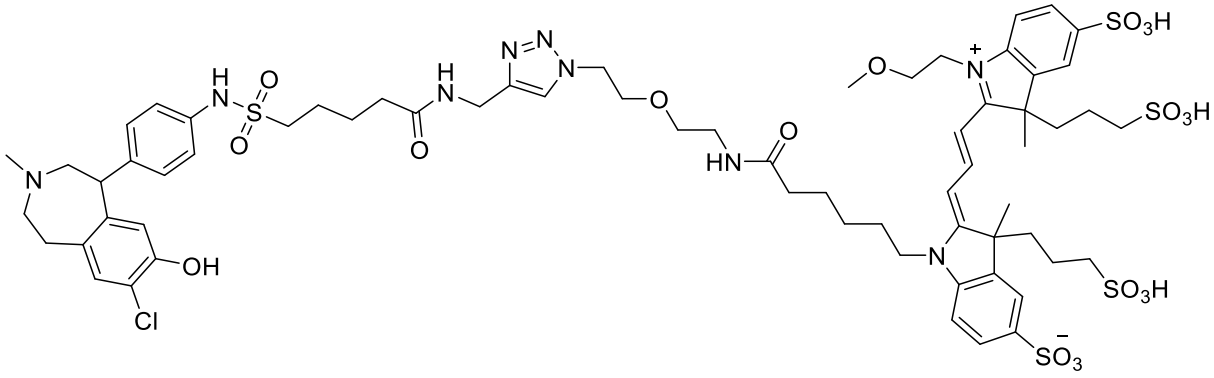

77
Chemical Formula: $C_{65}H_{86}ClN_9O_{19}S_5$
Exact Mass: 1491,4332

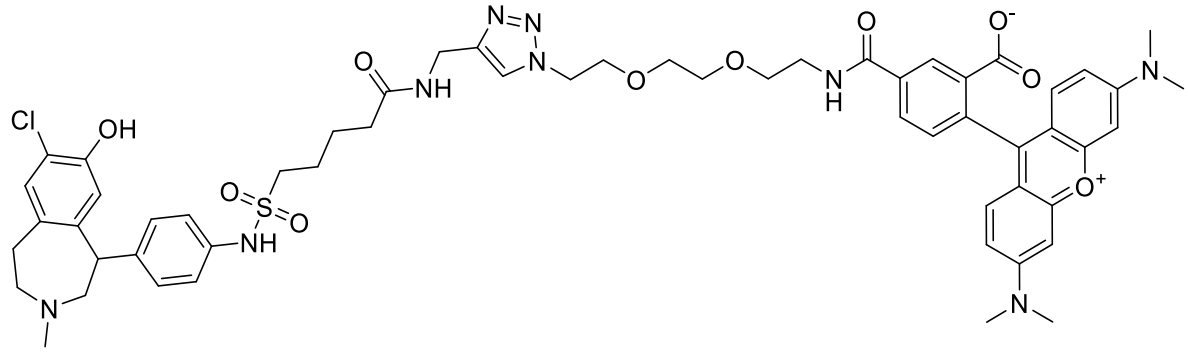

78
Chemical Formula: $C_{56}H_{64}ClN_9O_{10}S$
Exact Mass: 1089,4185

Figure 8.26: Chemical structures of fluorescent ligands **76**-**78**.

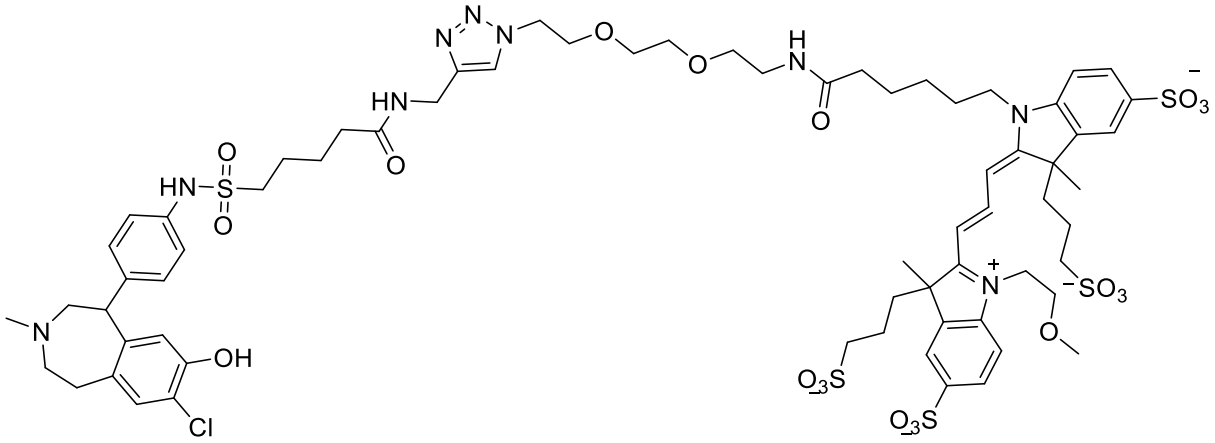

79

Chemical Formula: $C_{67}H_{87}ClN_9O_{20}S_5^{3-}$

Exact Mass: 1532,4376

Figure 8.27: Chemical structure of compound **79**.

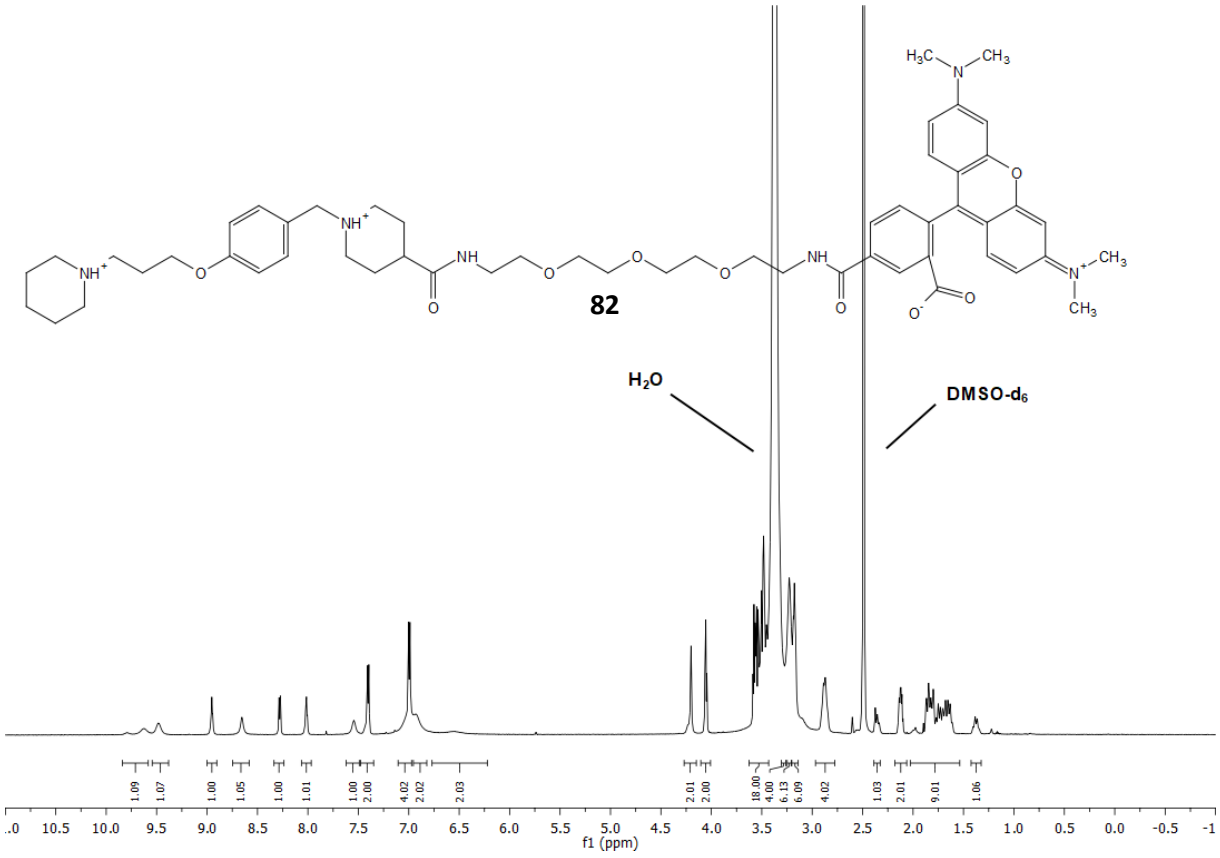

Figure 8.28: Chemical structure and ^{1}H NMR spectrum (600 MHz, DMSO-d_6) of fluorescent ligand **82**.

Eidesstattliche Erklärung

Ich erkläre hiermit an Eides statt, dass ich die vorliegende Arbeit ohne unzulässige Hilfe Dritter und ohne Benutzung anderer als der angegebenen Hilfsmittel angefertigt habe; die aus anderen Quellen direkt oder indirekt übernommenen Daten und Konzepte sind unter Angabe des Literaturzitats gekennzeichnet.

Teile der experimentellen Arbeiten wurden in Zusammenarbeit mit anderen Institutionen und Personen durchgeführt. Entsprechende Vermerke zu den Beiträgen der betreffenden Personen finden sich jeweils zu Beginn des entsprechenden Kapitels, in der „Experimental section“ und unter „Acknowledgements“.

Weitere Personen waren an der inhaltlich-materiellen Herstellung der vorliegenden Arbeit nicht beteiligt. Insbesondere habe ich hierfür nicht die entgeltliche Hilfe eines Promotionsberaters oder anderer Personen in Anspruch genommen. Niemand hat von mir weder unmittelbar noch mittelbar geldwerte Leistungen für Arbeiten erhalten, die im Zusammenhang mit dem Inhalt der vorgelegten Dissertation stehen.

Die vorliegende Arbeit wurde bisher weder im In- noch im Ausland in gleicher oder ähnlicher Form einer anderen Prüfungsbehörde vorgelegt.

Regensburg, den _____

Niklas Rosier